

**Novel Amorphous Silica and Silica Xerogels
for the Adsorption of Organic Pollutants
from Water**

Andrea Luca Tasca

Thesis submitted to the University of Strathclyde for the degree of Doctor
of Philosophy

Department of Chemical and Process Engineering
University of Strathclyde

2017

Copyright declaration

This thesis is the result of the author's original research. It has been composed by the author and has not been previously submitted for examination which has led to the award of a degree.

The copyright of this thesis belongs to the author under the terms of the United Kingdom Copyright Acts as qualified by University of Strathclyde Regulation 3.50. Due acknowledgement must always be made of the use of any material contained in, or derived from, this thesis.

Signed:

Dated:

Acknowledgments

The completion of this PhD would not have been possible without the contribution of a large number of people.

My greater thanks go to my supervisor, Dr Ashleigh Fletcher. Her support and guidance were fundamental for my development as a researcher and as a person. Three years later, I want to say thanks Ashleigh to believe in me at the beginning, because believing was probably the only option considering my initial confuse ideas expressed with horrible English.

Thanks also to my research group, especially to Ivan, Craig, Thomas and Stewart, who all provided me the support necessary to start and progress this PhD.

Thanks to Francesco, for making pleasant the office-time and amazing the last summer free time.

My gratitude goes to the laboratory technicians, with a special mention to Ian Airdrie and Mara Knapp. Their support allowed me to not exceed the threshold of madness too often throughout the instrumental troubleshooting.

Thanks to Dr Gemma Turnes and Dr Fernando Maya, for their choice to follow me during my last experimental activity and to Christer Sjöström and Farnaz Ghajeri, for their precious collaboration.

I would also like to thank all the Chemical and Process Engineering Department members and staff and the University of Strathclyde, for the magnificent opportunity.

Finally, to my family, to support my initial studies, but overall to never opposing the choices that from the end of the high school led me here.

Abstract

The demand on water supplies is becoming more intensive, thus the need for innovative and cost effective produced water treatment technologies is rising. Produced water is the largest by-product generated by oil and gas extraction, hence, there are significant quantities requiring remediation. Furthermore, over recent years, the presence of other organics known as Endocrine Disrupting Chemicals (EDCs) in various sewage discharges, fresh- and estuarine-waters, has been extensively reported, becoming an increasing source of concern.

Membranes are a promising technology for water remediation and the use of an adsorption media as a prior treatment could make them a potentially cost-effective option. Among solid sorbents, hydrophobic aerogels exhibit attractive properties for oil spill applications; however, very few studies have investigated their adsorption performance at low organic concentrations and the cost of functionalisation of these materials, hinder their use as sorbents in the final stages of produced water treatments.

This work studies the adsorption of benzene, toluene and the EDC 3,4-dichloroaniline (3,4-DCA) below their solubility limits on hydrophilic and hydrophobic samples of the novel amorphous silica Quartzene and on silica xerogels, synthesised by a low cost and environmentally friendly synthesis, inspired from the work of Bangi, Rao A.P., Hirashima and Rao A.V. [1]. All adsorbents used in this study were also characterised by SEM, FTIR and BET analysis.

The full adsorption capacity of hydrophilic Quartzene was achieved in less than 10 h, with 70-90% of uptake in the first 6 h. Adsorption capacities were found to be up to 264 mg/g for benzene and 78.8 mg/g for toluene. Hydrophobic Quartzene, demonstrated an equilibrium value four times higher that of the hydrophilic analogue, reached in less than 3 h at a concentration of 200 ppm benzene.

With regard to the synthesised xerogels, evaporation rates and the optimal combination of reactants were identified, in order to obtain the desired degree of hydrophobicity and a surface area mainly due to pores with sufficient dimension to allow pollutant penetration. The so synthesised xerogels adsorb dissolved benzene and 3,4-DCA from

water, showing no damage of the granules after days of rotary stirring, suggesting potential re-use. The adsorption behaviour is described by a two-step mechanism, with equilibrium times of ~24 h, with adsorption capacities up to 75 mg/g for benzene and 12.5 g for 3,4-DCA.

Micro Column Rapid Breakthrough tests coupled with Sequential Injection Analyses were also conducted, in order to obtain a preliminary evaluation of the adsorbents operative feasibility under conditions more similar to those typically used in water treatment facilities. Micro-columns were designed and 3D printed in methacrylate. Automated solid-phase extraction was used to verify desorption of the analytes by methanol injection.

The removal efficiency of the hydrophobic sample of Quartzene was found to be >5.85 mg/g of benzene, with an initial concentration of 73.3 mg/L. The removal efficiency of the silica xerogels was found to be >22.62 mg/g for benzene, with an initial concentration of 105.12 mg/L; the corresponding uptakes of 3,4-DCA were found to be >4.63 mg/g and >7.17 mg/g, respectively, at flowrates of 1.8 mL/min and 0.6 mL/min and with an initial concentration of 16-20 mg/L. Higher removal efficiencies coupled with higher rate of adsorption, which would lead to lower Empty Bed Contact Times (EBCTs), would be required for all the sorbents tested here to be used for treatment of produced water prior to a membrane configuration, especially in offshore facilities. The rate of adsorption of 3,4-DCA, and the related adsorption capacity of the silica xerogels studied here could be promising for large scale application to removal of pesticides and other organic micropollutants, as filling of filters, cartridges or permeable reactive barriers.

Table of contents

Copyright declaration.....	i
Acknowledgments.....	ii
Abstract	iii
Table of contents	v
List of Figures	xii
List of Tables.....	xix
List of Abbreviations.....	xxi
1 Water depletion and pollution.....	1
1.1 Water scarcity.....	1
1.2 Water pollution.....	5
1.2.1 Aromatic micropollutants: Endocrine Disrupting Chemicals (EDCs).....	5
1.2.1.1 3,4-dichloroaniline (3,4-DCA)	6
1.2.2 Produced water pollutants	13
1.2.2.1 Introduction.....	13
1.2.2.2 Produced water composition.....	14
1.2.2.3 Fate and impact of produced water discharge	15
1.2.2.4 Disposal standards	16
2 Technologies for organics removal from water	18
2.1 EDC removal technologies: focus on 3,4-dichloroaniline	18
2.1.1 Bioremediation.....	18
2.1.1.1 Bacteria	18
2.1.1.2 Uptake by fungi and cultivated plants	22
2.1.2 Adsorption and ligand exchange.....	23
2.1.3 Chlorination, ozonisation, precipitation and Fe ⁰ /H ₂ O ₂ System	23

2.1.4	Electrochemical and electrohydraulic methods	24
2.1.5	Final considerations	26
2.2	Produced water treatment	27
2.2.1	Offshore technologies for dissolved oil removal	28
2.2.1.1	Media filtration and adsorption.....	28
2.2.1.2	Macro-porous polymer extraction	32
2.2.1.3	Membranes.....	34
2.2.1.4	Looking ahead: electrochemistry	40
2.2.2	North Sea offshore Oil and Gas plants.....	41
3	Adsorption	44
3.1	Introduction	44
3.1.1	Adsorption from solution	44
3.1.2	Surface area and porosity	45
3.1.3	Physisorption and Chemisorption	46
3.1.4	First approaches to adsorption phenomena	47
3.1.4.1	Freundlich adsorption theory	48
3.1.4.2	Langmuir adsorption theory.....	50
3.1.4.3	Brunauer-Emmett-Teller (BET) adsorption theory	53
3.1.4.4	Polanyi adsorption potential theory	56
3.1.4.5	Dubinin's theory and its extension to the adsorption of aqueous organics on microporous materials	58
3.1.5	Surface energy and wetting.....	59
3.2	Porous materials for organics adsorption	62
3.2.1	Introduction	62
3.2.2	Activated carbons.....	62
3.2.2.1	Introduction.....	62

3.2.2.2	Organics adsorption	62
3.2.3	Clay minerals	67
3.2.3.1	Introduction.....	67
3.2.3.2	Organics adsorption	68
3.2.4	Periodic mesoporous organosilica.....	70
3.2.4.1	Introduction.....	70
3.2.4.2	Organics adsorption	70
3.2.5	Amorphous mesoporous silica-alumina.....	73
3.2.6	Silica aerogels	74
3.2.6.1	Properties and applications	74
3.2.6.2	Sol-gel synthesis	75
3.2.6.3	Ageing and drying	76
3.2.6.4	Surface chemical modification	77
3.2.6.5	Organics adsorption	77
3.2.7	Sodium silicate based xerogels	79
3.2.7.1	Introduction.....	79
3.2.7.2	The sol-gel route: neutralisation and condensation	80
3.2.7.3	Washing and solvent exchange.....	82
3.2.7.4	Functionalisation.....	83
3.2.7.5	Final drying.....	84
3.2.8	Promising low-cost, raw sorbents	84
3.2.9	Ligand exchange	84
4	Column adsorption tests.....	86
5	Research approach	89
5.1	Aims and objectives	89
5.2	Technological choices	89

5.3	Choice of the pollutants.....	93
5.4	Choice of the adsorbent: filling the gaps.....	93
5.5	Methodology	94
6	Experimental methods	95
6.1	Synthesis of the adsorbents	95
6.1.1	Amorphous silica Quartzene.....	95
6.1.2	Silica xerogels via Ambient Pressure Drying (APD) and low temperature synthesis.....	96
6.2	Characterisation.....	97
6.2.1	Surface area and porosity	97
6.2.1.1	Surface area: BET method.....	97
6.2.1.2	Total pore volume.....	100
6.2.1.3	Pore size distribution: Barrett Joyner and Halenda method	100
6.2.1.4	Microporosity.....	103
6.2.1.5	Methodology.....	107
6.2.2	Bonds: Fourier transform infrared spectroscopy (FTIR)	108
6.2.2.1	Introduction.....	108
6.2.2.2	Procedure	108
6.2.3	Surface topography: Scanning Electron Microscopy (SEM).....	110
6.2.3.1	Introduction.....	110
6.2.3.2	Procedure	110
6.3	Measure of the concentrations.....	111
6.3.1	Ultraviolet-visible spectroscopy (UV-Vis)	111
6.3.1.1	Introduction.....	111
6.3.1.2	Procedure	112
6.3.2	Gas chromatography (GC-MS and GC-FID).....	113

6.3.2.1	Introduction.....	113
6.3.2.2	Procedure	115
6.4	Adsorption Tests.....	116
6.4.1	Adsorptives	116
6.4.2	Batch tests	117
6.4.3	Microcolumn tests.....	119
6.4.3.1	3D printing of the column.....	119
6.4.3.2	Breakthrough curves	119
6.5	Membranes: preliminary evaluation of casting	120
7	Results and discussion	121
7.1	Synthesis of the silica xerogels.....	121
7.1.1	Effect of process parameters	121
7.1.1.1	Introduction.....	121
7.1.1.2	Water / Sodium Silicate ratio.....	122
7.1.1.3	Acid catalyst	125
7.1.1.4	Amount of Silylating agent.....	126
7.2	Characterisation.....	127
7.2.1	Granulometry	127
7.2.2	Surface area and porosity	129
7.2.2.1	Quartzene	129
7.2.2.2	Silica xerogels.....	131
7.2.3	Bonds	131
7.2.3.1	Quartzene	131
7.2.3.2	Silica xerogels.....	132
7.2.4	Surface topography and composition.....	133
7.3	Measure of organic concentrations.....	134

7.3.1	Ultraviolet-visible spectroscopy (UV-Vis)	134
7.3.2	Gas chromatography	135
7.3.2.1	GC-MS.....	135
7.3.2.2	GC-FID	136
7.4	Adsorption tests	139
7.4.1	Batch tests	139
7.4.1.1	Optimal methodology	139
7.4.1.2	Quartzene	140
7.4.1.3	Silica xerogels.....	146
7.4.2	Microcolumn tests.....	153
7.4.2.1	3D column printing.....	153
7.4.2.2	Breakthrough curves	156
7.5	Membrane: casting procedure	160
8	Conclusions.....	162
8.1	Introduction	162
8.2	Characterisation and measure of the concentrations	163
8.3	Sorbents: synthesis and characterisation	164
8.3.1	Amorphous silica Quartzene	164
8.3.2	Silica xerogels	164
8.4	Adsorption performance.....	165
8.4.1	Amorphous silica Quartzene	165
8.4.1	Silica xerogels	167
8.5	Application	169
9	Outcomes of the project.....	172
9.1	Publications	173
9.1.1	Published papers	173

9.1.2	Papers submitted	188
9.1.3	Invited papers	216
9.2	Pending patent of Quartzene	233
10	References	256

List of Figures

Figure 1.1: Total renewable water resources (cubic metres per capita per year), 2014 [5].	1
Figure 1.2: Percentage of renewable water resources withdrawn: Millennium Development Goal (MDG) water indicator [7].....	2
Figure 1.3: Annual average water stress based on the withdrawals-to-availability ratio 1981-2010 [6].....	2
Figure 1.4: Groundwater storage anomalies in millimetres per year, as averaged over the 2003-2013 base period [9].	3
Figure 1.5: Water quality risk index for major river basins during base period (2000-2005) compared to 2050 projections (Commonwealth Scientific and Industrial Research Organisation (CSIRO) -medium scenario*) [10] * This scenario takes into account a drier future (as projected by the CSIRO climate change model) and a medium level of socio-economic growth.	5
Figure 2.1: Degradation pathway of diuron by <i>Micrococcus</i> sp, confirmed by FTIR spectra and HPLC [124].....	20
Figure 2.2: Intermediates formed during photodegradation of 3,4-DCA using Ti-V (sol) catalyst, confirmed by HPLC and GC/MS analysis [32].	25
Figure 2.3: Diagram showing key steps involved in offshore produced water treatment [143].	27
Figure 2.4: Spectrum® filter oil droplet removal by size performance [147].....	31
Figure 2.5: Combined adsorption-coagulation-DAF process [148]	32
Figure 2.6: Macro-porous polymer extraction system [150].	33
Figure 2.7: Schematic representation of forward and reverse osmosis processes. In reverse osmosis, the pressure applied on the osmotic solution must overcome $\Delta\Pi$ (with $\Delta\Pi=P_2-P_1$).	37
Figure 2.8: Pilot membrane plant for the production of boiler feedwater from produced water [164]. Pump P-101 pumps the feed from tank TK-101 to the MF module. P-102 provides hot distilled water to backwash the MF membrane. MF permeate is supplied in TK-102 and P-101 pumps the feed from TK-102 to the bottom	

of the UF module. P-102 pumps the feed from TK-103 to P-103, which provides the high pressure necessary to feed the RO module. Tank 103 is also used for backwashing.

38

Figure 3.1: Cross section of a hypothetical porous grain with different pore types: closed (C), blind (B), through (T), interconnected (I) and together with some roughness (R) [175]. 45

Figure 3.2: Freundlich adsorption isotherms on powdered activated carbon. [176]. ..49

Figure 3.3: Linear plot of the Freundlich equation.....49

Figure 3.4: Langmuir adsorption isotherms of crystal violet (A) and methylene blue (B) dissolved in deionised water on mesoporous silica MCM-41.52

Figure 3.5: Characteristic point on a Type II adsorption isotherm [177].....54

Figure 3.6: Refined IUPAC classification of physisorption isotherms [179].....55

Figure 3.7: Balance of interfacial tensions at solid-liquid-air interface.61

Figure 3.8: Adsorption isotherms of dichloromethane (L) and toluene (R) on GAC at T:298 K, 303 K and 313 K [191]. Symbols = experimental data, line = model.65

Figure 3.9: Benzene and toluene sorption at 298 K [193].....65

Figure 3.10: Polanyi potential correlation plot for AC-F400. The experimental data closely fits the predicted curve reported from regression analysis by Sontheimer [193].

66

Figure 3.11: Kaolinite structure [195].67

Figure 3.12: Montmorillonite structure [195].....68

Figure 3.13: Adsorption isotherms of 3-chloroaniline (3-CA), 4-chloroaniline (4-CA) and 3,4-DCA on an acid activated halloysite, at 293 K and adsorption contact time of 24 h [24]. 69

Figure 3.14: X ray spectra of dehydrated systems (393 K): Na-montmorillonite (SWy-1), Na-montmorillonite/3-CA, Na-montmorillonite-3,4-DCA and Na-montmorillonite/ 2,4,6-trichloroaniline. The d-spacing of Na-montmorillonite, also in absence of water, increases to $\sim 1 \text{ \AA}$. The small peak ($2\theta \sim 5.1$) in the spectrum of Na-montmorillonite/3,4 DCA, suggests the presence of clay particles with a higher level of swelling due to pollutant intercalation [11].70

Figure 3.15: Kinetic plot showing equilibration time required for benzene adsorption on PMO [200]......71

Figure 3.16: Adsorption isotherms of (A) benzene and (B) toluene on PMO with experimental values and related fits of Langmuir, Freundlich, Redlich Peterson and Temkin models[200].	72
Figure 3.17: Adsorption isotherms of toluene (a) and benzene (b) on mesoporous silica-alumina [203].	73
Figure 3.18: Silica alkoxides used as common precursors of silica aerogels.	75
Figure 3.19: Polymerisation of silica alkoxides.	76
Figure 3.20: Hydrophobisation of a silica gel [210].	77
Figure 3.21: Comparison of isotherms obtained for benzene adsorption from aqueous solution onto aerogel materials, activated carbon (AC-F400) and a polymeric resin (XAD2). The concentration ranges used for the materials are similar (20-820 mg/L) [192, 217] and all below the solubility limit.	79
Figure 3.22: Hydrolysis and condensation of a waterglass solution, catalysed by acid addition.	81
Figure 3.23: Neutralisation of sodium silicate to silicic acid and subsequent reactions with (A) silicic acid or (B) sodium silicate [223].	82
Figure 3.24: Functionalisation of a silica xerogel with TMCS [223].	83
Figure 5.1: Diagram showing a typical North Sea process line up for produced water treatment [231].	90
Figure 6.1: Samples of diluted waterglass solution immediately after acid addition (left) and 15 min later (right), placed in oven at 323 K.	96
Figure 6.2: Silica gels during washing procedure (left) and after final drying in oven at 473 K.	97
Figure 6.3: Example plot obtained using the BET isotherm model.	99
Figure 6.4: N ₂ adsorption isotherm obtained at 77 K for an amorphous silica by Svenska AB. The plot shows the results directly displayed by the instrument software; the resulting BET analysis is always undertaken manually to correctly interpret the data.	100
Figure 6.5: t-Plot of adsorption data obtained for N ₂ adsorption on ND at 77 K. The intercept of the red straight line corresponds to the primary mesopore volume. The first linear trend, related to the total surface area, is not visible as a result of the low uptakes at low pressures. The microporosity of the material is negligible.	105

Figure 6.6: α_s -Plot of ND. The slope of the red straight line is related to the total surface area, while the slope of the blue straight line corresponds to the surface area external to primary mesopores. The intercept of the blue straight line is related to the primary mesopore volume.....	107
Figure 6.7: Micromeritics ASAP 2420. Degas ports (left) and N ₂ adsorption ports (right).	107
Figure 6.8: Diagram of a Mitchelson interferometer [239].	109
Figure 6.9: ABB MB 3000 spectrophotometer used for the FT-IR analysis.	109
Figure 6.10: Schematic of a scanning electron microscope (SEM) [240]. The position of the electron beam on the sample is controlled by scan coils situated above the objective lens.	110
Figure 6.11: Scanning Electron Microscope (SEM) HITACHI SU-6600. On the left side, samples CNF and CF148, gold coated, at the entrance of the instrument vacuum chamber.	111
Figure 6.12: UV-Vis spectrophotometer used for the analysis of benzene adsorption on silica xerogels synthesised in this study.	112
Figure 6.13: Schematic diagram of a gas chromatograph [241].	113
Figure 6.14: Shimadzu GC-FID 2014 (L) and Thermo Fisher GC-MS with autosampler (R).	115
Figure 6.15: Magnetic stirrers Hanna HI 190 used to aid dissolution of organics in this study.	118
Figure 6.16: Gerhardt® rotary stirrer used to ensure good contact for low density or high hydrophobicity samples used in this study.	118
Figure 6.17: Sequential injection analysis manifolds connected to the adsorption column and UV-Vis detector for adsorption tests on silica samples used in this study.	119
Figure 7.1: Citric acid catalysed water/Na ₂ SiO ₃ ratio VS gelation time for samples produced in this study.	123
Figure 7.2: Citric acid catalysis, full functionalisation: pore size distribution of water/Na ₂ SiO ₃ ratios 80 and 108.	124
Figure 7.3: Citric acid catalysis, full functionalisation: water/Na ₂ SiO ₃ ratio and pore size distribution.	125

Figure 7.4: Pore size distribution of silica xerogels samples synthesised with citric acid catalysis unfunctionalised (CNF148) and functionalised (CF148).	126
Figure 7.5: ND particle size distribution.	128
Figure 7.6: CMS particle size distribution.	128
Figure 7.7: α -Plot analysis of ND N ₂ adsorption isotherm measured at 77 K (solid line fit of low pressure data, dashed line fit of high pressure data).	130
Figure 7.8: FT-IR spectra of silica samples: Z1, ND and CMS.	131
Figure 7.9: Comparison between the FT-IR spectra of Z1 and hydrophobic Z1H, named Z1HPO.	132
Figure 7.10: FT-IR spectra of silica xerogels catalysed with citric acid.	132
Figure 7.11: FE-SEM analysis of Quartzene samples: CMS (a: x1k, b: x10k), ND (c: x1k, d: x 10k) and Z1 (e: x1k, f: x 10k).	133
Figure 7.13: FE-SEM analysis of functionalised xerogel sample CF148. Magnification: x1k.	134
Figure 7.14: Gas chromatograph analysis of aqueous benzene, with toluene as internal standard and methanol as solvent. x-axis: time/min; y axis: signal/ μ V*k, where k is the magnification factor.	137
Figure 7.15: Calibration curve used to relate the peak areas of the chromatograph to the benzene concentration in the aqueous solutions.	138
Figure 7.16: Gas chromatograph analysis of 3,4-DCA in water, with dimethyl phthalate as internal standard and methanol as solvent. x-axis: time/min; y axis: signal/ μ V*k, where k is the magnification factor.	139
Figure 7.17: Kinetic profiles of benzene adsorption on Z1, ND and CMS at 293 K.	141
Figure 7.18: Kinetic profiles of toluene adsorption on Z1, ND and CMS at 293 K.	141
Figure 7.19: Adsorption isotherms at 293 K for benzene on Z1, ND and CMS at 293 K.	142
Figure 7.20: Adsorption isotherms at 293 K for toluene on Z1, ND and CMS at 293 K.	143
Figure 7.21: Kinetics obtained for benzene adsorption by granular forms of Quartzene Z1 and Z1H at 293 K.	145

Figure 7.22: Adsorption isotherms comparison between hydrophilic and hydrophobic Quartzene: Z1 and Z1H.....	146
Figure 7.23: Adsorption isotherms comparison between hydrophilic and hydrophobic Quartzene: CMS and CMSH.....	146
Figure 7.24: Kinetic of adsorption of benzene on the xerogel sample CF148.	147
Figure 7.25: Adsorption of benzene on xerogel CF148. Data confirmed a change in the shape of the isotherm around 125 mg/L.....	148
Figure 7.26: Benzene adsorption on mesoporous silica alumina [203]. Data fitted by a model resulting from the combination of Langmuir and Langmuir-Freundlich equations (Equation 3.27).	150
Figure 7.27: Adsorption kinetics of 3,4-DCA by CF154, characterised as in Table 7.1, after 2 d rotary stirring at 20 rpm. Concentrations were determined by GC-FID analysis. 150	150
Figure 7.28: Isotherm of adsorption at 293 K of 3,4-DCA by CF154, characterised as in Table 7.1, after 2 d rotary stirring at 20 rpm. Concentrations were determined by GC-FID analysis. 151	151
Figure 7.29: Inner column (L) and its fitting into the external cylinder (R).....	154
Figure 7.30 : Models of the microcolumn and related supports, as shown by the software preForm (FormLabs).	155
Figure 7.31: LHS: printed column on Form1+ 3D printer (FormLabs). Printed column inner still contains resin that was deposited but not polymerised. RHS: printed column on its supports, prior to smoothing.....	155
Figure 7.32: Printed columns inside the CL-1000 ultraviolet crosslinker (L) and column smoothing (R).	156
Figure 7.33: Breakthrough curve of benzene solution, 73.3 mg/L, flowed through microcolumn packed with 230 mg of NDH at 1 mL/min.	157
Figure 7.34: Breakthrough curve of benzene 105.12 mg/L at 0.6 mL/min, flowed through a microcolumn packed with 110 mg of silica xerogels catalysed with citric acid and with H ₂ O/Na ₂ SiO ₃ ratio = 148.	159
Figure 7.35: Breakthrough curves of 3,4-DCA adsorption on 110 mg of silica xerogels catalysed with citric acid and with H ₂ O/Na ₂ SiO ₃ ratio = 148, 16 mg/L at 1.8 mL/min; 20 mg/L at 0.6 mL/min.	160

Figure 7.36: vacuum filtration system [248]..... 161

List of Tables

Table 1.1: Properties of 3,4-dichloroaniline.	9
Table 1.2: Summary of worldwide oilfield-produced water parameters [102].	14
Table 2.1: Characteristics of walnut shell media. pH, moisture content, porosity and surface obtained from tests conducted at the University of Regina; other values provided by USFilter, USA [144].	29
Table 2.2: Cost of adsorbents required to treat 100 m ³ /d of oily water, initial concentration = 200 mg/L; final concentration = 10 mg/L. Cost of walnut shell media provided by USFilter, USA. 2010 [145].	30
Table 2.3: Comparison of the efficiencies of different technologies in oil removal [152].	34
Table 2.4: Offshore produced water treatment technologies. Extract of Table 2 from Judd et al. [143].	42
Table 5.1: Data summary for single units for produced water treatment [143].	92
Table 6.1: Sigma Aldrich SPB®-5 Capillary GC column characteristics.	116
Table 7.1: Citric acid catalysis, full functionalisation: water/Na ₂ SiO ₃ ratio VS porosity.	124
Table 7.2: Hydrochloric acid VS citric acid catalysis.	126
Table 7.3: Characterisation of virgin silica xerogel and functionalised silica xerogel.	127
Table 7.4: Surface areas and porosities of Quartzene samples.	130
Table 7.5: Freundlich adsorption model parameters calculated using data obtained for adsorption of toluene and benzene of samples used in this study, measured at 293 K. Maximum uptakes are determined from extrapolative interpolation to either a benzene solubility of 1.763 g/L or a toluene solubility of 0.57 g/L [247].	144
Table 7.6: Parameters of models used to fit the adsorption data of benzene in water (Figure 7.26). Sample: CF148.	148
Table 7.7: Parameters of Langmuir-Freundlich fit of 3,4-DCA adsorption from water at 293 K by CF154 (Figure 7.28).	152

Table 7.8: Surface area, pore size and adsorption data of different material tested for the removal of 3,4-dichloroaniline from water. Parameters q_m and b refer to the Langmuir model (Equations 3.9 and 3.10).	153
Table 7.9 : Parameters related to microcolumn tests with sample NDH (average particle size R_{SC} assumed equal to 0.14 mm and assuming 0.5 mm as particle size of the large column).	158
Table 7.10: Parameters related to microcolumn tests using silica xerogels catalysed by citric acid (ratio $H_2O/acid = 148$), with average particle size R_{SC} of 0.1 mm and assuming 0.5 mm as particle size of large column.....	160

List of Abbreviations

AOP	Advanced Oxidation Process
BET	Brunauer Emmett and Teller
BJH	Barrett Joyner Halenda
BTEX	B enzene T oluene X ylene E thylbenzene
CMS	Quartzene sample with Calcium and Magnesium Sources
CMSH	hydrophobic Quartzene sample with Calcium and Magnesium Sources
CF	Citric acid catalyzed Functionalized silica xerogel sample
CNF	Citric acid catalyzed Non Functionalized silica xerogel sample
DBD	Dielectric Barrier Discharge
EBCT	Empty Bed Contact Time
EDC	Endocrine Disruptor Chemical
EHD	Electric Hydraulic Discharge
FTIR	Fourier Transform Infrared Spectroscopy
GAC	Granular Activated Carbon
GC-FID	Gas Chromatography - Flame Ionization Detector
GC-MS	Gas Chromatography - Mass Spectrophotometry
MCRB	Micro Column Rapid Breakthrough
HF	chloric acid catalysed functionalized silica xerogel sample
ND	Quartzene sample ($\text{SiO}_2:\text{Na}_2\text{O} = 3.35$)
NDH	hydrophobic Quartzene sample ($\text{SiO}_2:\text{Na}_2\text{O} = 3.35$)
RSSCT	Rapid Small Scale Column Test
SEM	Scanning Electron Microscope
UV-Vis	Ultraviolet-Visible spectroscopy
Z1	Quartzene sample with different level of activation than ND
Z1H	hydrophobic Quartzene sample with different level of activation than ND

1 Water depletion and pollution

1.1 Water scarcity

Less than 3% of water on our planet exists in a readily usable form for human activities [2]. Between 2011 and 2050, the world population is expected to increase by 33%, growing from 7 billion to 9.3 billion [3], hence, the pressure on water supplies is becoming intensive, and there is a rising need for innovative and cost effective produced water treatment technologies to be developed to help provide the resources that will be needed.

National water scarcity can be estimated by the use of the indicator: cubic meters of renewable water per capita per year [4], which first estimates the number of people that can reasonably live with a certain unit of water resources, before different levels of water stress are identified using the following threshold values of water supplies:

- 1,700 m³ per capita per year: the country is under regular water stress;
- 1,000 m³ per capita per year: chronic water scarcity;
- 500 m³ per capita per year: absolute scarcity.

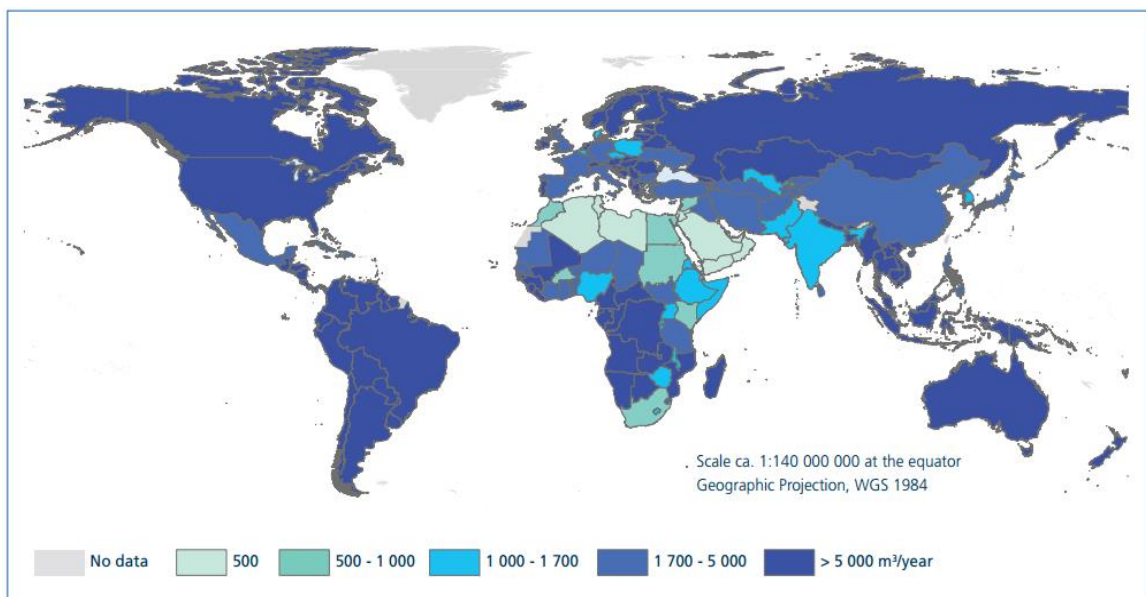


Figure 1.1: Total renewable water resources (cubic metres per capita per year), 2014 [5].

The Millennium Development Goal (MDG) Water Indicator estimates the level of human pressure placed on water resources, based on the ratio between water withdrawal by agriculture, municipalities, and industries, against total renewable water resources [6]. The disparities that exist between countries are graphically represented in Figure 1.2. The higher the ratio, the more difficult it will be to satisfy increasing water demands. For some larger countries, such as Australia, China, and USA, averaging water availability over their entire territory does not reflect in-country variability, as shown from the basin level analysis in Figure 1.3.

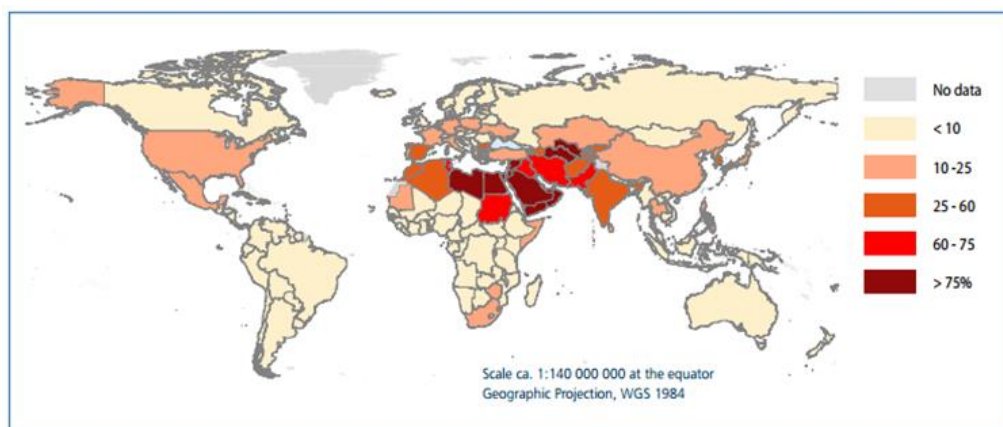


Figure 1.2: Percentage of renewable water resources withdrawn: Millennium Development Goal (MDG) water indicator [7].

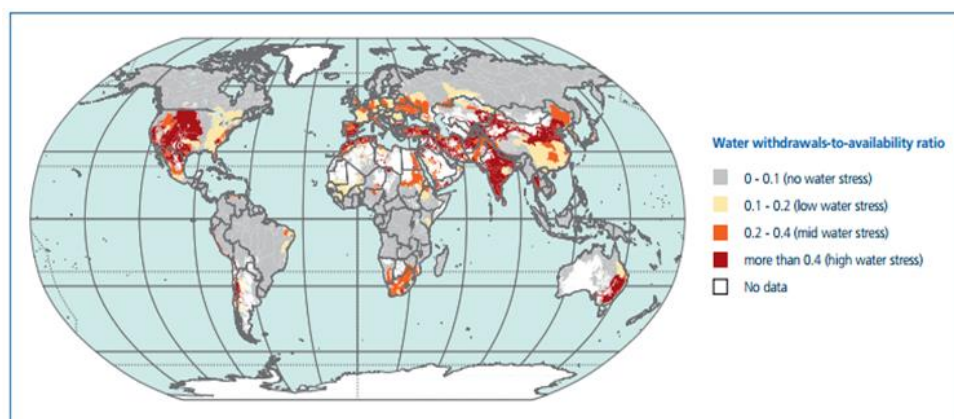


Figure 1.3: Annual average water stress based on the withdrawals-to-availability ratio 1981-2010 [6]

Climate change is reportedly responsible for recently observed increasing variability in precipitation and evaporation patterns; such trends enhance spatial and temporal variations in water availability and demand. The indicators described previously refer to physical water stress, but effective water scarcity results from physical, economic and institutional water scarcity. Economic water scarcity is due to a lack of infrastructure resulting from financial or technical constraints, while institutional water scarcity is determined by the failure of institutions to ensure reliable and equitable supply of water to users.

Areas subject to the most severe surface water stress are generally in regions where groundwater stress is also high. Groundwater provides opportunities for storage, acting as a buffer to compensate for seasonal variation of surface water availability, with the exception of fossil groundwater, which has been stored underground for hundreds or thousands of years, and is not naturally replenished. As can be seen from Figure 1.4, 21 of the World's 37 largest aquifers are over-exploited. Globally, the rate of groundwater abstraction is increasing by 1% to 2% per year [8].

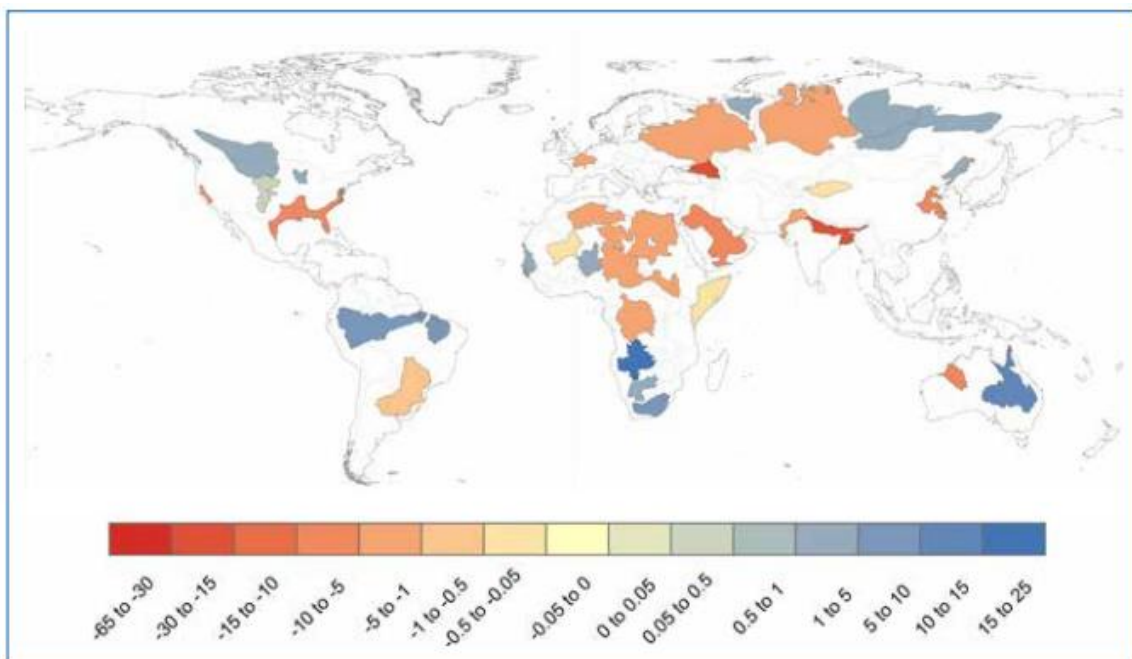


Figure 1.4: Groundwater storage anomalies in millimetres per year, as averaged over the 2003-2013 base period [9].

Water availability analysis should be coupled with an assessment of water quality; the lower the quality, the fewer possible uses that water may have and the associated cost of treatment is subsequently increased; water quality is expected to decrease in coming decades, as shown in Figure 1.5. Industrial production, untreated urban runoff, and wastewater that has been insufficiently purified, generate a wide spectrum of chemical pollutants, which is only expected to increase; and a similar trend is expected for chemicals and nutrients, such as nitrogen and phosphorous, which are related to eutrophication, from the massive use of phytosanitary products and fertilizers in agriculture. Significant increases in exposure to pollutants will occur where populations are greater and economic growth is expected i.e. low- and lower-middle income countries.

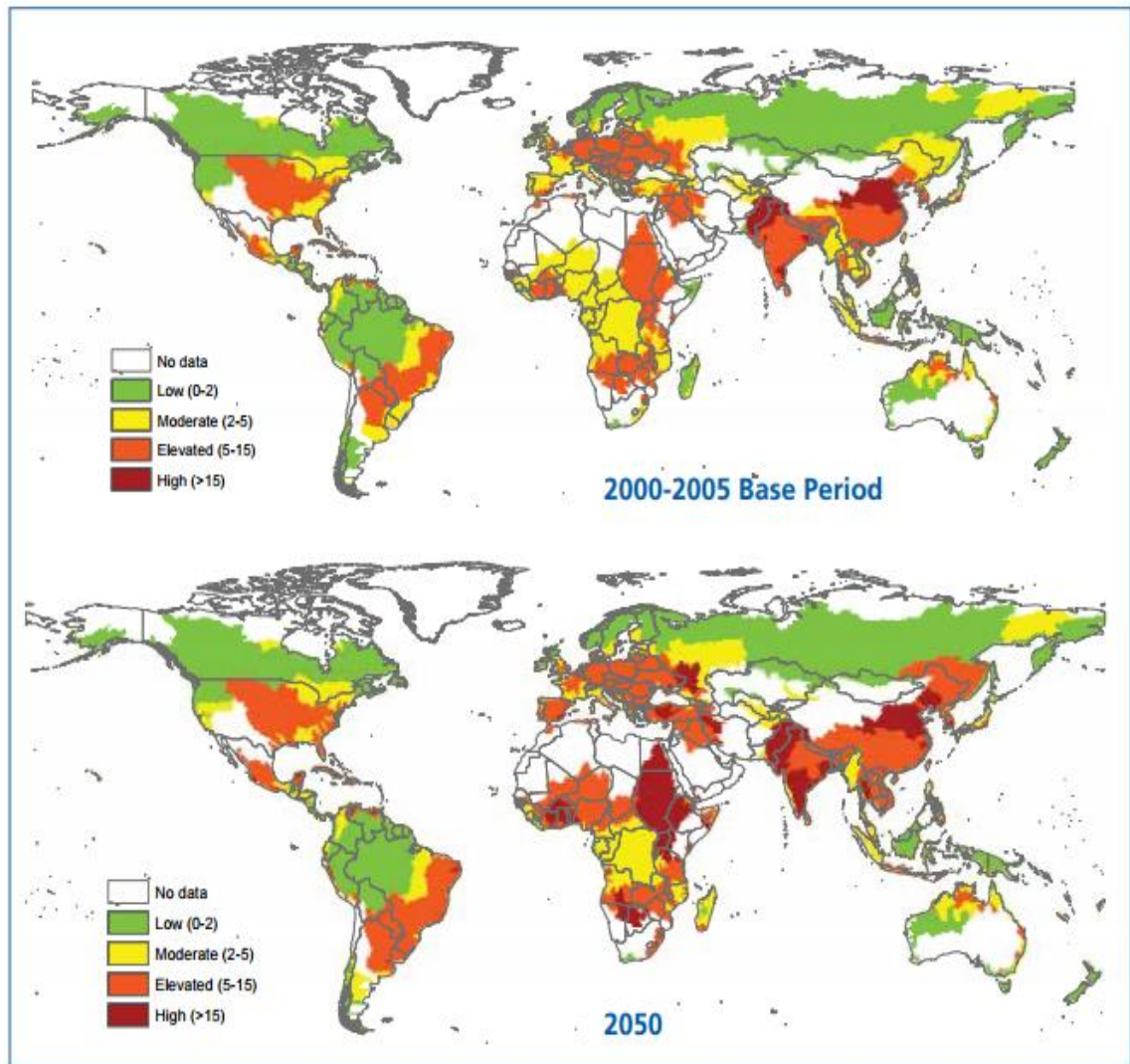


Figure 1.5: Water quality risk index for major river basins during base period (2000-2005) compared to 2050 projections (Commonwealth Scientific and Industrial Research Organisation (CSIRO) -medium scenario*) [10] * This scenario takes into account a drier future (as projected by the CSIRO climate change model) and a medium level of socio-economic growth.

1.2 Water pollution

1.2.1 Aromatic micropollutants: Endocrine Disrupting Chemicals (EDCs)

Some organic pollutants have become sources of high concern, not just for marine environments but also for drinking water supplies. In recent years, the presence of Endocrine Disrupting Chemicals (EDCs) in wastewater discharges from agricultural and industrial sources [11], in fresh- and estuarine-waters, and soils has been confirmed within the open literature [12]. Reports of adverse changes within wildlife populations,

linked to exposure to these substances in the environment, suggest that humans could be at a similar risk of adverse health effects [13, 14]; this increased concern has motivated a need for action to understand and reduce such risks.

EDCs affect male and female reproduction, thyroid metabolism [15-17], breast development and cancer rates (including prostate cancer), neuroendocrinology, obesity [18], and cardiovascular endocrinology [19]. The intricate mechanisms of action of these substances, and their physical and chemical diversity, suggest that many endocrine disrupting properties have yet to be assessed. Moreover, the importance of mixtures is acknowledged; effects of different EDCs can be additive or synergistic [19, 20], even when each chemical is present below the threshold of detectable effects [21]. The lack of knowledge regarding exposure scenarios is still an obstacle for significant human risk assessments [22]. An assessment of the adsorption performance of these pollutants would, therefore, make an important contribution in filling the current knowledge gap.

1.2.1.1 3,4-dichloroaniline (3,4-DCA)

1.2.1.1.1 Introduction

3,4-dichloroaniline (3,4-DCA) has been classified as an EDC, with reference to endocrine disruption data relevant to both wildlife and human health [23]. Dichloroanilines are used in the production of agricultural agents, rubber additives [24], polyurethane polymers [25, 26], pharmaceuticals, and pigments [11]. 3,4-DCA is found in the environment as a product of the biodegradation of phenylurea and phenylcarbamate pesticides [26, 27]; furthermore, it can be introduced via industrial and municipal wastewater that has been insufficiently purified, accidental spills, or illegal releases [28-30]. The concentration of 3,4-DCA in soil and water is, therefore, increasing as a result of such releases, and exacerbated by its high persistence, accumulation, and low biodegradability [24, 31, 32]. Thus, both soil and water remediation techniques need to be studied in more detail, considering the low levels of removal achievable by commonly used techniques, such as activated sludge treatment, and the generation of carcinogenic trihalomethanes as a consequence of the routine oxidation by chlorine [33].

1.2.1.1.2 Use and Exposure

The worldwide production of 3,4-DCA was ~42-47 kt/yr prior to 1986 [34], and, in the period 1996-1998, the EU's production volume was still 13.5-15.5 t/yr [35]. 3,4-DCA is a derivative of aniline, an intermediate for chemical synthesis used in the production of 3,4-dichlorophenylisocyanate, and phytosanitary products including propanil, linuron, diuron, and neburon [35-37], which are applied to treat a variety of crops including rice, potatoes, beans, or tobacco [38]. It is also employed in the synthesis of azo dyes for polyester fabrics [37] and pharmaceuticals [23]. There is no direct use of the chemical that denotes a risk for a vulnerable group, but exposure is expected indirectly through food (vegetables and fruit) [23]. It arises in the environment through hydrolysis and biological degradation of phenylurea, phenylcarbamates and acylchloroanilide pesticides in soil [39-47], field water, and by plant enzymes [48]. Furthermore, 3,4-DCA enters the environment via industrial wastewater [32], mainly from microbial conversion from 3,4-dichloro-1-nitrobenzol in water treatment plants [23, 48].

1.2.1.1.3 Toxicity

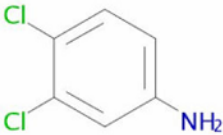
In soils, chloroanilines can negatively affect soil microflora; inhibition of nitrosomonads was detected in a study into the effects of phenylamide herbicide degradation products on soil nitrification [49]. Polar narcosis is generally recognised as the primary mode of action of 3,4-DCA against aquatic organisms [50, 51]; from short and long term toxicity data, fish and crustaceans seem the most sensitive organisms with respect to water column exposures of this pollutant, while annelids are the most sensitive to exposure in the sediment [37]. Tests on marine and fresh water animals and unicellular algae suggest that the acute toxicity of 3,4-DCA can be considered to be relatively low compared with the chronic effects [52, 53], and significant consequences for reproduction of the planktonic crustacean *Daphnia magna* were detected at 20 µg/L [54]. Concentrations of 200 µg/L 3,4-DCA have been observed in breeding male sticklebacks, where lower androgen synthesis was associated with changes in secondary sex characteristics [55]. Tests on rats have shown in vitro competition for binding sites on the androgen receptor [56]. In order to avoid chronic effects, Predicted No-Effect Concentrations (PNECs) of 0.2 µg/L for freshwater and seawater bodies and 0.1 mg/kg dw (0.04 mg/kg ww) have been suggested [37].

1.2.1.1.4 Environmental behaviour and fate

Chloroanilines are compounds with high levels of environmental diffusion [11, 24, 57]; 3,4-DCA is very difficult to remove from the environment and concentrations in soils and waters are increasing, due to its high persistence and accumulation, [24, 32] low biodegradation [58], and low leaching potential [59].

3,4-DCA has been detected in various surface waters in Germany [36], and in western Europe [60], but is barely measurable in water bodies [23]; however, it occurs in higher concentrations in water than its parent herbicide diuron [61]. The movement of 3,4-DCA into surface and ground waters is determined by transport and retention mechanisms [62]. Based on relatively low values of the Henry's law constant, 3,4-DCA is not expected to volatilise from a water column [37, 63]. Hydrolysis is not thought to be relevant due to covalent bonding of the substituent attached to the aromatic ring, in conjunction with the high negative charge-density of the aromatic nucleus [63]. As a result of the physical properties of this pollutant (Table 1.1), the losses of 3,4-DCA from natural waters are determined mainly by photochemical degradation, and adsorption on sediment and dissolved humic material [64]. Photo-transformation of 3,4-DCA has been suggested as the major degradation pathway in environmental waters [36], as confirmed via measurement of light absorption spectra, with a defined peak at ~300 nm, hence, within the solar spectrum at sea level [54].

Table 1.1: Properties of 3,4-dichloroaniline.

Property	Value	Ref.
Molecular formula	C ₆ H ₅ Cl ₂ N	[65]
Molecular structure		[35]
Appearance	Solid at 20 °C	[35]
Molecular weight	162 g/n	[35]
Molecular size	0.35 nm ²	[66]
Henry's law constant	0.05 Pa.m ³ /mol	[35]
Solubility in water	580 mg/L at 20 °C	[35]
Octanol-water partition coefficient (log K _{ow})	2.7 (shake flash method)	[23, 36]
Estimated surface waters half life	18 d	[35]
Measured rates of loss in outdoor water systems	0.11 - 0.17 d ⁻¹	[54]
	0.06 - 0.14 d ⁻¹	[64]
Estimated atmospheric half life	9 h	[35]
Estimated half-life in soil and sediment	470-1500 d	[67]

The mobility and bioavailability of pollutants, and their degradation products, in soils depend on a combination of adsorption and desorption processes by the soil components, and the leaching action of meteoric rain and snow [62]. The majority of 3,4-DCA released to the environment accumulates over time on the organic fraction of sediments and soils [35]. The binding effect of soil generally increases with time, leading to a decrease in pollutant bioavailability and toxicity, due to meteoric leaching

[68]; conversely, sorption onto dissolved macromolecules and colloidal particles promotes transport in subsurface environments [69].

When released to the soil with herbicides, only a small portion of chloroanilines are mineralised, and most persist for years [70], immobilised by interactions with humic substances [28, 39, 71, 72]. A small fraction of liberated chloroanilines undergo dimerisation or polymerisation via microbial oxidases and peroxidases, forming stable azo compounds [62, 73]. The soluble fraction of soil organic matter, fulvic and humic acids, plays a significant role in xenobiotics binding, due to substituents like hydroxyl and carboxylic acid groups, ketones, amino acids, saccharides and aminosaccharides [74, 75]. Surface adsorption, due to van der Waals forces or electrostatic interactions, is often the initial phase in binding pollutants and soil, while stronger bonds may arise over time [11]. Aniline sorption onto soil starts with hydrophobic partitioning and cation exchange, then continues with covalent bonding, due to the limited energy, or availability, of sorption sites. This initially reversible equilibrium is followed by a slower irreversible process, which is well described by a biphasic kinetic model [76, 77].

Information on the sorption mechanisms of 3,4-DCA is fundamental in developing remediation strategies. This compound adsorbs onto the sediment [64] and soil particles and builds stable, probably covalent, bonds with organic substances [36, 37]. In laboratory experiments more than 70% of radio labelled 3,4-DCA was determined as bound to sediment and suspended matter in the water column [78], while ~80% of the removal of the radioactivity from the water column was demonstrated after 8 d, rising to 99% after 90 d [79].

With regard to the soil environment, dissolved organic matter (DOM) and the interactions between DOM, organic contaminants, and other soil components strongly affect the fate of 3,4-DCA in soil and water systems [80-83]. Increasing soil organic carbon content, via through organic matter amendment, introduces DOM, enhances sorption and decreases leaching of pollutants [84, 85]. Improvements in the sorption capacity of 3-4-DCA were observed when increasing the organic carbon content in soil samples [64], as well through organic matter amendments in inorganic soils [30, 62].

During a study of the influence of different humic fractions on the herbicide diuron [86], the main degradation product, 3,4-DCA, was found irreversibly to be bound by humic acids days after formation. Hence, this pollutant is not expected to have a high risk of leaching in soils with significant humic acid (HA) or fulvic acid (FA) content. Ten times higher capacity of sorption was demonstrated for HA fractions compared with FA fractions.

The amino group of 3,4-DCA preferentially reacts with the carboxyl and carbonyl groups of soil HA, leading to the formation of soil bound residues [87, 88], as confirmed by its high adsorption and small desorption constants [64]. The sorption of this chemical in soil can be described as a physicochemical process in which a fraction of the pollutant is physically bound to organic and inorganic soil components, while another fraction strongly adsorbs on the organic component [58].

Soil samples agitated with solutions of 3,4-DCA revealed removal of the pollutant from solution after 15 min, while up to 70% equilibrium was reached after 50 h; physical interaction was seemingly followed by formation of a chemical bond between 3,4-DCA and the soil organic matter, giving biphasic kinetics with rate constants equal to 4.9 h^{-1} and 0.03 h^{-1} [64]. Similar kinetics were observed for aqueous samples of 3,4-DCA and various agricultural soils [58], with sorption equilibria reached within 48 h, regardless of the initial pollutant concentration, up to $16.2 \text{ } \mu\text{g/mL}$. The Freundlich equation fitted the data well:

$$C_s = K_f C_e^n \quad \text{Equation 1.1}$$

Where C_s is the concentration of 3,4-DCA sorbed ($\mu\text{g/g}$), C_e is the equilibrium solution concentration ($\mu\text{g/mL}$), and K_f (mL/g) expresses the soil sorption capacity. The exponent n is related to the degree of isotherm nonlinearity.

The amount sorbed was higher in sandy clay loam soil ($K_f = 52 \text{ mL/g}$), which had the highest organic matter content of the soils studied, and slightly acidic pH, while the lowest sorption was obtained for calcareous silty clay soil and sand.

The availability of adsorption sites decreases with increasing adsorbate concentration, as confirmed by n values < 1 . Such sorption behaviour exhibits L-type isotherms [89]. The K_{oc} values (sorption constant per gram of organic carbon in soil) suggests a high potential of 3,4-DCA for ground-water contamination in soils with lower sorption characteristics [59]. Sorption capacity also correlates more strongly with organic matter content than with clay content or cation exchange capacity. However, considering soil organic content alone is inadequate; less sorption of diuron should be expected on clay rich soils, probably as a result of the reduced availability of binding sites in humic substances (HS), due to the interaction between HS and clay [86]. Soil pH may be another factor relevant in the sorption of this pollutant, as demonstrated by the reduction of K_f values by $\sim 50\%$ after liming [58]. Such a reduction could be due to a shift in aniline changing from its protonated form in acidic soils to a neutral version with increasing pH [76, 90, 91].

In other work, a solution containing a sample of calcareous soil and 3,4-DCA was mixed until sorption equilibrium was reached [62]; the high value found for the Freundlich coefficient K_f , which signifies the dependency between adsorption and concentration [92], seems to validate the assumption that adsorption occurs mainly via hydrophobic interactions due to the presence of neutral aniline functional groups at high soil pH [88, 93]. This mechanism is confirmed by the high K_{ow} of 3,4-DCA [28, 94]. The value of $K_{oc} = K_d/OC \times 100$, where K_d reflects the distribution ratio of the organic molecules between the sorbed phase and the solution, was equal to 338.6 l kg^{-1} for 3,4-DCA. K_{oc} and K_{ow} values, together with low water solubility, suggest that this metabolite has a low potential for groundwater contamination in calcareous soils with sufficiently high organic matter content.

DOM has been observed to compete with organic pollutants for soil surface sorption sites [95, 96] or to build stable bonds with them [97], enhancing the apparent solubility of organic pollutants, reducing sorption, and increasing their mobility [83, 98]. In contrast, DOM applied in soils may be adsorbed to soil surfaces, enhancing sorption of hydrophobic organic compounds [99], especially when tannic acid is added [30]. Dissolved organic carbon extracts from a commercial peat (DOC-PE) and high-purity tannic acid (DOC-TA) were mixed with a soil sample and a solution of 3,4-DCA [62].

If the coefficient $K_{d,DOC}$ is defined as X_{doc}/C_{doc} , where X_{doc} is mg C/ L in the solution of DOC, and C_{doc} the corresponding equilibrium concentration, the consistently higher $K_{d,DOC}$ values compared with K_d confirm the influence of DOC on adsorption of the pollutant on soil. The increased sorption of 3,4-DCA due to the presence of DOC was confirmed by the use of an environmental matrix, with ions and organic matter, in place of pure water [100]. Sorption on sediment, placed in a sediment extract media, was found to be greater than using pure or run-off water, likely facilitated by previously sorbed DOC on the sediment surface through physical interactions [88].

1.2.2 Produced water pollutants

1.2.2.1 Introduction

Produced water is water trapped in underground formations, brought to the surface during the extraction of oil and gas. Underground formations are permeated by different fluids; before trapping hydrocarbon compounds within the rocks, they were saturated with saline water. As a consequence of their lower density, hydrocarbons migrate into the pores, expelling some of the saline water from the formation; thus, underground reservoirs store both water and hydrocarbons. During the extraction of oil and gas, water is injected underground to avoid decreasing the porous media pressure, and to improve oil recovery. Therefore, produced water is obtained from:

- hydrocarbon filled porous media;
- areas close to the hydrocarbon reserve;
- injected fluids.

Globally, ~250 million barrels of water are produced daily from both oil and gas fields, and more than 40% of this amount is discharged into the environment [101]. This water is the largest by-product generated by oil and gas extraction, and treatment on-site offers the potential of a source of fresh water for water-stressed oil-producing countries. Furthermore, environmental concerns, including the ever more severe regulations on produced water discharge into the environment and reservoir age (old reservoirs have high water/oil ratios), make produced water management an important part of the oil and gas business.

1.2.2.2 Produced water composition

Produced water is a slightly acidic mixture of different organic and inorganic compounds: dissolved and dispersed oils, grease, waxes, production chemicals, formation solids, dissolved formation minerals, salts, scale products (calcium carbonate and iron sulphide), dissolved gases and microorganisms (Table 1.2).

Table 1.2: Summary of worldwide oilfield-produced water parameters [102].

Parameter	Values	Heavy metal	Values (mg/L)
Density (kg/m ³)	1014–1140	Calcium	13–25800
Surface Tension (dynes/cm)	43–78	Sodium	132–97000
TOC (mg/L)	0–1500	Potassium	24–4300
COD (mg/L)	1220	Magnesium	8–6000
TSS (mg/L)	1.2–1000	Iron	<0.1–100
pH	4.3–10	Aluminum	310–410
Total oil (IR; mg/L)	2–565	Boron	5–95
Volatile (BTX; mg/L)	0.39–35	Barium	1.3–650
Base/ neutrals (mg/L)	<140	Cadmium ^a	<0.005–0.2
(Total non-volatile oil and grease by GLC/MS) base (µg/L)	275	Chromium	0.02–1.1
Chloride (mg/L)	80–200,000	Copper	<0.002–1.5
Bicarbonate (mg/L)	77–3990	Lithium	3–50
Sulfate (mg/L)	<2–1650	Manganese	<0.004–175
Ammoniacal nitrogen (mg/L)	10–300	Lead ^a	0.002–8.8
Sulfite (mg/L)	10	Strontium	0.02–1000
Total polar (mg/L)	9.7–600	Titanium	<0.01–0.7
Higher acids (mg/L)	<1–63	Zinc ^a	0.01–35
Phenols (mg/L)	0.009–23	Arsenic ^a	<0.005–0.3
VFA's (volatile fatty acids) (mg/L)	2–4900	Mercury	<0.001–0.002
		Silver ^{a,b}	<0.001–0.15
		Beryllium	<0.001–0.004

^a Analyzed by atomic absorption.

^b Value should be regarded as a minimum due to poor solubilities.

Produced water production and composition change as a function of: type of hydrocarbon extracted, the location of the reservoir, the method of drilling, water separation technologies used, the mechanical integrity of the holes, and underground

communications. Produced water discharged from gas platforms is ~10 times more toxic than water discharged from oil wells, but the volumes from gas production are much lower; hence, the total impact may be less [103]. It is notable that the volumes become higher with increasing reservoir lifetime.

Dissolved hydrocarbons are primarily low molecular weight aromatics, mainly the BTEX group (benzene, toluene, ethyl benzene, and xylene); the dispersed fraction of hydrocarbons includes PAH (polynuclear aromatic hydrocarbons) and alkylated phenols, due to their higher molecular weights and lower solubility. Dissolved formation minerals comprise heavy metals, other anions and cations, and naturally occurring radioactive materials (mainly ^{226}Ra and ^{228}Ra). Salinity is due to dissolved Na^+ and Cl^- ions, with smaller contributions from Ca^{2+} , Mg^{2+} , and K^+ ; the salt concentration of produced water can vary from a few ppm to ~300,000 mg/L [102]. The most common heavy metals are Cr, Hg, Cd, Cu, Pb, Ni and Zn, in concentrations dependent on the age of the wells and the formation history of the reservoirs. Dissolved gases in produced water include CO_2 , O_2 and H_2S . Production chemicals are compounds injected to enhance oil recovery and improve produced water management: surfactants, inhibitors of corrosion, hydrate formation, scale deposition, foam production, wax deposition, bacterial growth, and gas dehydration.

1.2.2.3 Fate and impact of produced water discharge

Produced water discharges from the offshore industry are a growing source of concern because of the continuous input of pollutants to the sea; the sources of contamination are large and widely dispersed. Moreover, the effects on populations and ecosystems are very difficult to define [104].

The impact of contaminants on environmental quality can be estimated by analysing the results of monitoring programs, carried out with increasingly advanced techniques, to satisfy more and more stringent regulations. Monitoring programmes provide data related to the distribution and fate of contaminants and an estimation of their ecotoxicological effects. The water column is monitored by passive samplers to quantify:

- aqueous concentrations of target contaminants;

- exposure of caged organisms;
- produced water dispersal (to validate dispersion models).

The actual reliability of the monitoring carried out by passive samplers need to be improved by extending the range of samplers used, and further clarifying the relationship between produced water discharge concentrations and observed ecotoxicological end points in organisms [105].

Studies related to the Norwegian continental shelf revealed accumulation of alkylphenols and PAH in cods and blue mussels caged near outlets, such chemicals are quickly metabolized in cods. Alkylphenols and PAHs may affect reproductive functions and chemical, biochemical and genetic indicators of the biological condition (biomarkers). Laboratory and field studies state that significant biological effects on marine organisms in a water column and on the seabed will be local, restricted to a distance of less than 2 km, due to rapid dilution and related brief exposure time. Hence, the risk of widespread, long term impact due to produced water discharges on the marine ecosystem is considered low; however, published literature is still insufficient to validate this assumption, because there are very few studies on the effects on populations. Only risk related modelling has been used to estimate potential effects at the population and ecosystem levels, therefore cumulative effects need to be measured on the populations, to effectively assess the long term impact of the discharges on the marine ecosystem [104].

1.2.2.4 Disposal standards

Countries all over the World are setting more stringent regulatory standards, focussing on dispersed and dissolved oil fractions of produced water. The monitoring of marine, coastal and transitional waters of the North-East Atlantic Ocean and its adjoining seas is governed by:

- the Oslo Paris Convention (OSPAR) Joint Assessment & Monitoring Programme (JAMP) [106];
- the EU Marine Strategy Framework Directive (MSFD; Directive 2008/56/EC) [107];

- the Water Framework Directive (WFD 2000/60/EC) with its directive on Environmental Quality Standards (EQS) related to transitional, coastal, and territorial waters [108].

The EU Water Framework Directive, adopted in 2000, is committed to ‘zero discharge’ in response to the need for a more protective system to tackle aquatic pollution [101]; however, it applies only to waters within one nautical mile from land [105]. Since 2005, the Norwegian Oil Industries Association also agreed to implement a zero environmental harmful discharge level; to attain this, the EIF (Environmental impact factor) was developed to take into account all of the pollutants in produced water [109]. In 2014 the dispersed oil average concentration before discharge in UK oil fields was ~14 ppm [110]. OSPAR agreed that the maximum discharge concentration was to be reduced to 30 ppm and, before 2020, overall oil discharges in produced water were to be reduced by 15% from what they were in 1999 [109]. The Republic of China recently set a monthly average limit of ‘oil and grease’ discharge at 10 ppm.

2 Technologies for organics removal from water

2.1 EDC removal technologies: focus on 3,4-dichloroaniline

Myriad remediation technologies have been developed for the destruction of chloroanilines in wastewaters. Methods for the treatment of 3,4 DCA could be classified as physicochemical, chemical (oxidation) and biological. Physicochemical methods include adsorption, ion exchange, electrolysis, and photodegradation, while biological degradation involves aerobic and anaerobic microorganisms.

2.1.1 Bioremediation

2.1.1.1 Bacteria

3,4-DCA is not readily biodegradable [37]; biodegradation is very slow in aquatic solutions. In a recent study, Erlenmeyer flasks were incubated in the dark with either pond water only or pond water with sewage sludge inoculum; 97% and 94%, respectively, of the added 3,4-DCA was recovered after 2 wk [111], while no biodegradation was reported in the same amount of time with an OECD 301 C test using activated sludge [112]. No degradation was observed after 28 d in an OECD 301 D test and <5% was reached in a 29 d OECD 303A test, both using activated sludge [37]. Again no removal was observed in a biodegradation study using North Sea water [113], while only primary degradation occurred after 1 mo. using river water as inoculum [114].

Usually, xenobiotics should be in solution to be degraded by bacteria. The bioaccessible fraction of the pollutant is given by the concentration in the pore water, the 'bioavailable fraction' plus the 'potentially available fraction', which is the one reversibly sorbed. Sorption on soil organic matter reduces the bioaccessibility; the addition of FA and HA to inoculated soils decreased the rate of diuron degradation, reducing bioavailability but not bioaccessibility; after 32 d all diuron was degraded to 3,4-DCA [86]. Hence, bioaccessibility is a better indicator of the long-term influence of humic substances on diuron degradation than bioavailability. The mineralisation rate of 3,4-DCA in soils is low and it decreases as the concentration of the pollutant increases [35]. Only 3.9-11.9% mineralisation of 1 mg/kg radio-labelled 3,4- DCA was recorded

after 16 wk in various soil types [67]. Degradation of 50% of 3,4-DCA was observed in soil slurries with indigenous soil populations and it was only slightly influenced by the addition of buffer, mineral salts and acetate [57]. In non-acclimated sediments, dechlorination of the applied 3,4-DCA started after 20 d and it was anaerobically converted into 3-chloroaniline (44%) and 4-chloroaniline (33%) in 2 mo. These metabolites were not further degraded [115].

The microbial strains *Pseudomonas acidovorans* [116] and *Pseudomonas diminuta* [117] are able to use chlorinated anilines as sole source of carbon and energy; the latter was able to grow on 3,4-DCA [118]. The addition of *Pseudomonas acidovorans* to 3,4-DCA enriched soil slurries enhanced mineralisation, leading to complete elimination of chloride after 10 d [57]. Up to 250 mg/L of the pollutant and its intermediates were anaerobically degraded in <7 d by the strain *Pseudomonas fluorescens* 26-K. Without added glucose and nitrogen sources, degradation was slower, with 40% of toxicant removal in the first 15 d at an initial concentration of 75 mg/L [119].

Pseudomonas diminuta was found to dechlorinate up to 50 µg/mL of 3,4-DCA during the growth process; this strain also increased the ratio of degradation in water samples from natural water reservoirs [120] and in fish ponds, where destruction of pollutant reversibly sorbed on the bottom ground was observed in the first 12 d. An appreciable decrease of the irreversibly sorbed fraction took place in the first 5 d [121].

Microorganisms from Cuban soils were grown in two culture media, using 3,4-DCA as (i) the sole source of carbon (ii) as sole source of carbon and nitrogen [122]. The pollutant disappeared within 3 wk and species of *Pseudomonas*, *Arthrobacter*, *Aspergillus*, *Penicillium*, and *Fusarium* were isolated in the first media, while species of *Bacillus*, *Arthrobacter*, *Cunninghamella*, *Trichoderma*, and *Fusarium* were isolated in the latter.

The biodegradation pathway of 3,4-DCA, and other substituted anilines, involves conversion by an oxygenase to the corresponding catechol, which is then metabolised via an ortho-cleavage pathway [123]. Two modes of dioxygenation were found when utilising degrading bacteria obtained by genetic exchange between two strains of *Pseudomonas*; this led to the formation of 3- and 4-chlorocatechol from 3-chloroaniline

(3-CA). Only 4-chlorocatechol was generated from the dioxygenation of 4-chloroaniline (4-CA) [117], and when bacterial strains of *Pseudomonas acidovorans* were used for the degradation of 3-CA and 4-CA, the rate-limiting degradation steps were found to be the first attack to the substrate and then conversion to chlorocatechols [116].

Research into 3,4-DCA degradation by *Pseudomonas* sp. showed the relevance of catechol 2,3-dioxygenase in the process [118]. The activities toward 4-methylcatechol, 3-methylcatechol and 4-chlorocatechol were found to be almost 60%, 27% and 13% that of catechol, respectively. The activity of catechol 2,3-dioxygenase was also confirmed in the degradation of 3,4-DCA by a strain of *Pseudomonas fluorescens*; the presence of 3-chloro-4-hydroxyaniline as a metabolite suggested a pathway including dehalogenation and hydroxylation of the aromatic ring, followed by cleavage via catechol 2,3-dioxygenase [119].

Shaken flasks experiments, with *Micrococcus* sp, demonstrated 96% of diuron degradation within 30 h of incubation, at a concentration of 250 ppm and with the addition of non-ionic detergent (0.01%) [124]. A hydrolysis step followed the removal of the $-CH_3$ group leading to the accumulation of 3,4-DCA, with conversion starting within 24 h to 4,5-DBD and further intermediates (Figure 2.1).

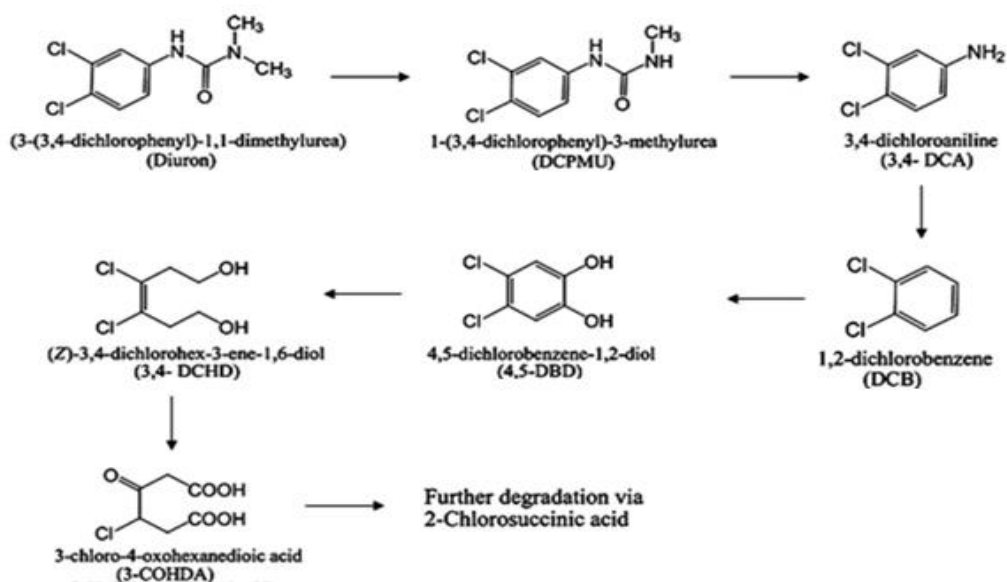


Figure 2.1: Degradation pathway of diuron by *Micrococcus* sp, confirmed by FTIR spectra and HPLC [124].

Diuron mineralisation was also confirmed by the metabolic cooperation of *Arthrobacter* sp. and *Achromobacter* sp., with CO₂ as only final product [125]. Strains of *Aquaspirillum itersonii* and sp. 2CA, as well as *Paracoccus denitrificans* were found able to utilise 3,4-DCA as the only source of carbon and nitrogen [126]. The latter could metabolize the pollutant at concentrations up to 150 mg/L, via oxidation to *o*-diphenol, intradiol cleavage of 4,5- dichloropyrocatechol and further stages of preparatory metabolism associated with dehalogenation.

Within a suite of microorganisms isolated from Kuban soils treated with Propanil, a *P. denitrificans* strain was found to be the most resistant to 3,4-DCA [66]. The cleavage of the aromatic ring via the ortho- or meta-pathway, following 4,5- dichloropyrocatechol activity allows full decomposition; hence, adsorptive bioremediation was successfully performed by introducing activated carbons and bacteria into polluted soils [127]. Activated carbon acts as a buffer, which keeps the pollutant concentration in the soil solution below the threshold of toxicity for the bacteria.

Three types of activated carbon were saturated with 3,4-DCA and placed in a mineral medium with a *Paracoccus denitrificans* strain [66]. The pollutant was reversibly sorbed and available for the bacterial population. Degradation rates varying from 2 to 10 wk suggested that easier desorption and quicker decomposition were linked to the minor micropore volume. *Paracoccus denitrificans* can only penetrate into the macropores, thus desorption of 3,4-DCA from smaller carbon pores is necessary; this bacterium seems able to accelerate desorption, either by acidifying the medium or through the excretion of surface-active substances.

A microbial consortium was successfully applied for the removal of propanil and 3,4-DCA in a repeated batch suspended cell culture [128], as well as in biofilm reactors for agricultural wastewater treatment [129]. In the latter case, the porous volcanic stone tezontle was used as a support for the biofilm in a continuous process able to degrade propanil and metabolic intermediates at rates up to 24.9 mg L⁻¹ h⁻¹, without any need for a co-substrate. *Pseudomonas* sp., *Acinetobacter calcoaceticus*, *Rhodococcus* sp., *Xanthomonas* sp. and *Koehleria* strains could grow individually in 3,4-DCA. Other strains found in the biofilm, but unable to degrade propanil metabolites, are probably

involved in the metabolism of herbicide adjuvants or in the maintenance of biofilm integrity.

The removal of chloroanilines in a sewage treatment plant could be improved by promoting the growth of indigenous communities of bacteria and by the introduction of adapted laboratory strains. The addition of readily degradable aniline and nontoxic haloaromatics may respectively improve the breakdown of chloroanilines and the chlorocatechol potential [117].

2.1.1.2 Uptake by fungi and cultivated plants

When free chloroanilines are released, as herbicide metabolites, they can be incorporated in the plant's 'insoluble' residue fraction, with degradation experiments proposing lignin as a primary binding site [130, 131].

The bivalve *Corbicula fluminea* was immersed in cages both upstream and downstream of conventional rice fields in the region of Camargue [43]. The concentration of 3,4-DCA measured downstream from rice plantations was approximately half that compared to *Corbicula* caged upstream, suggesting a partial bioaccumulation in rice plants. Tomato plants, oat, barley, and wheat were grown in nutrient solutions with 4-CA and 3,4-DCA; 90-95% of the chloroanilines incorporated were found in the roots and the uptake was proportional to the amount of chloroaniline applied. The distribution of the same chemicals in carrots was equally divided between the roots and the upper part of the vegetables [132], and these results suggest a potential risk of chronic toxicity due to the consumption of 3,4-DCA through food.

Some lignin degraders can metabolize chloroanilines and their lignin conjugates; experiments have shown that chloroanilines appear to be bioavailable to the white rot fungus *Phanerochaete chrysosporium*, once mineralised as lignin [133]. More than 50% of the free [ring-U-14C]-3,4-DCA was mineralised after 33 d of incubation of the samples studied, and free 3,4-DCA was a better substrate for mineralisation than free 4-CA. Different metabolites were formed, but chloroanilines or their azo- and azoxy-derivatives were not found. Hence, lignin incorporation and fungal oxidation can lead to a complete removal of 3,4-DCA from the environment. However, it has been shown that fungi adsorbed less chloro-substituted anilines per biomass unit than bacteria [14];

furthermore, the degradation pathway operated by white-rot fungi could lead to the formation of toxic tetrachloroazobenzenes [134].

2.1.2 Adsorption and ligand exchange

Adsorption technologies offer an effective method for removal of many organic pollutants from aqueous media [135], and different adsorbents have been studied for the removal of chloroanilines from wastewaters, as discussed in detail in Section 3.2. Furthermore, a comparison between different sorbents is presented in Table 7.8 in Section 7.4.1.

2.1.3 Chlorination, ozonisation, precipitation and Fe⁰/H₂O₂ System

A common sequence of operations adopted in many drinking water plants is preoxidation, adsorption, and coagulation. Preoxidation is carried out using aqueous sodium hypochlorite (NaClO), and 100% removal has been demonstrated for a concentration of 658 ng/L of 3,4-DCA [33]. The problem associated with use of NaClO is the production of carcinogenic trihalomethanes as by-products. The oxidation of a sample with the same concentration stated above, by ozone, shows 85% pollutant removal; subsequent coagulation and flocculation was found to be ineffective, while further adsorption treatment with activated carbons led to complete removal [33].

The oxidizing potential of Fe⁰ towards different organic compounds is well known [136]. Fe⁰/H₂O₂ systems can be used to reduce levels of diuron and other pesticides in polluted environments and agricultural waste. Fe⁰ promotes the reduction of H₂O₂ to hydroxyl radicals, generating Fe²⁺, which in turn produces more hydroxyl radicals via H₂O₂ reduction. The degradation of a 10 mg/L diuron solution containing 2 mmol L⁻¹ of H₂O₂ and H₃PO₄ that was flowed through a glass tube, filled with 2 g of iron wool, was seen to be strongly affected by pH. At pH 2.5 more than 99.9% of the pesticide was removed after 10 min, with only 1 ug/L of 3,4-DCA found in the effluent, while at higher pH the hydrolysis of iron ions and deposition of iron oxides on the Fe⁰ surface led to a significant decrease in the degradation efficiency [137].

2.1.4 Electrochemical and electrohydraulic methods

Electrohydraulic discharge (EHD) is a potential method for oxidative degradation of 3,4-DCA, achieved by exposing wastewaters to pulsed electrical discharges generated using submerged electrodes [138]. UV radiation is produced by the plasma channel created with EHD, generating a shockwave with its expansion against the water. The degradation rate is expressed by Equation 2.1:

$$\frac{dC}{dN} = -k_1 C_i - k_0 \quad \text{Equation 2.1}$$

where dC/dN is the change in concentration per discharge, C_i is the initial substrate concentration, k_0 is the zero-order term, expression of direct photolysis, and k_1 is the first-order term related to the oxidation in the plasma channel region.

As part of Advanced Oxidation Processes (AOP), photocatalysis can be employed for water treatment in (i) slurry reactors, where an additional step is required for the separation of the suspended catalysts, or (ii) into reactors in which the catalysts are immobilised on adsorbents or on membranes. Separate sols of vanadium pentoxide and cerium oxide were added to a titanium dioxide sol to prepare, respectively, Ti–V catalyst and Ti–Ce catalyst. 0.1 g L⁻¹ of powdered catalyst were added to 3,4-DCA solutions, stirred in an annular reactor with an internally integrated lamp. The irradiation power was set at 140 mW cm⁻². The Ti–V catalyst gave a higher level of degradation than the Ti–Ce catalyst, probably as a result of its band gap energy, which is more towards the visible region, and the smaller particle size. A plot of $\ln C_0/C$ against time indicates biphasic kinetics, with a sharp increase in rate after 45 min. Further experiments, using a bench scale reactor, showed 85% of degradation in 106 min [32]. The degradation pathway is shown in Figure 2.2.

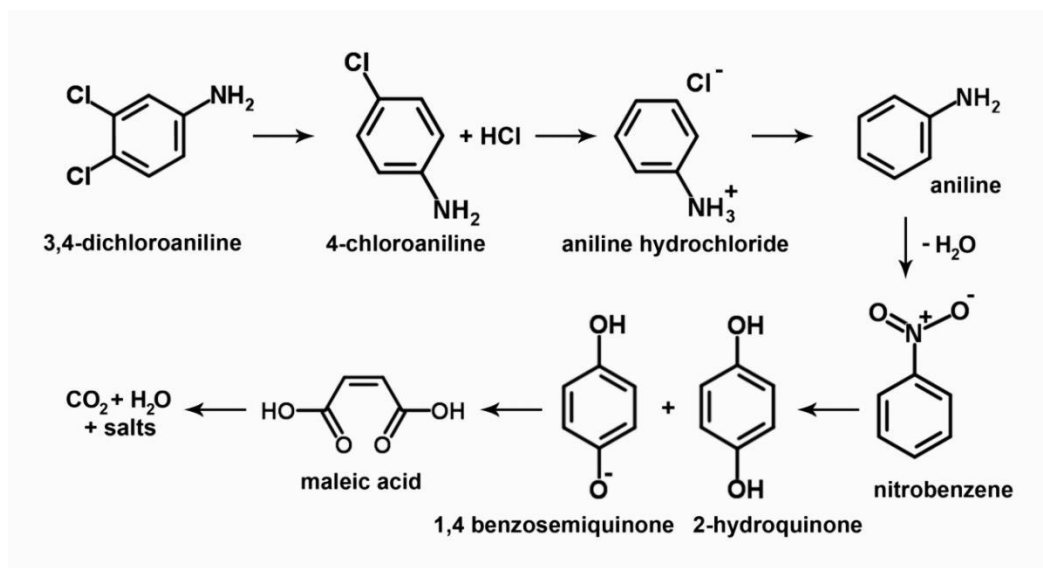


Figure 2.2: Intermediates formed during photodegradation of 3,4-DCA using Ti-V (sol) catalyst, confirmed by HPLC and GC/MS analysis [32].

Biphasic kinetics were also observed in the photocatalytic degradation of the same chemical using Ti-N and Ti-S catalysts [48]; the former showed higher surface area, lower particle size, and lower band-gap energy. Greater contact of the pollutant with the catalyst surface is achieved with a higher specific surface area. Smaller particle size means reduced degradation time, due to a shorter distance between the charge carrier and the surface, where the reaction takes place. 3,4-DCA was fully degraded using the Ti-N catalyst in 120 min; the highest level of degradation was observed at pH 6. At catalyst dosages higher than 0.1 g L^{-1} , the reaction rate was seen to decrease, as a consequence of the deactivation of molecules colliding with ground state molecules, and the agglomeration of catalyst particles. For 3,4-DCA concentrations higher than 10 mg/L , the degradation efficiency was seen to decrease, as the number of collisions between the 3,4-DCA molecules themselves increased, compared to collisions between pollutant molecules and $\cdot\text{OH}$ radicals [139].

Degradation of aqueous 3,4-DCA was recently performed using a dielectric barrier discharge (DBD) plasma reactor [140]. The ozone generated in the system interacts with the pollutant directly, or by via the formation of hydroxyl radicals, which form faster than the molecular ozone [141]. The process was carried out by flowing a water film

through the discharge zone generated between two aluminium electrodes. The degradation was well described by pseudo-first order kinetics and higher efficiencies were reached in acidic conditions, and by increasing the input power, and the addition of Fe^{2+} or Fe^{3+} . The main pathways involved were deamination, hydroxylation, dechlorination, and hydroxylation and oxidation, followed by the generation of organic acids, through the opening of the aromatic ring. Mineralisation into CO_2 and H_2O was only partial, as confirmed by the lower removal rate of total organic carbon than for DCA, and by the formation of degradation intermediates, identified using GC-MS analysis. The solution pH decreased during dichloroaniline degradation, as observed in a previous study [142], in which degradation of aqueous 3,4-DCA was carried out using a wire-cylinder DBD reactor. Here, the efficiency was observed to increase when the input power was increased to 90 W, but above this power a decrease was subsequently observed. The degradation rate was lower at neutral conditions than at either acidic or basic pH.

2.1.5 Final considerations

Lignin incorporation and fungal oxidation are able to attain a complete removal of 3,4-dichloroaniline from the environment [130]. The association of bacteria and porous materials can be successful in bioreactors as well as in-situ bioremediation technique. Bioremediation was successfully purposed, introducing activated carbons and bacteria in polluted soils [66]. The biological removal of 3,4-DCA in sewage can be enhanced through the growth of indigenous community and with the introduction of adapted laboratory strains [114]; however, the technical and economic feasibility of the process should be considered.

$\text{Fe}^0/\text{H}_2\text{O}_2$ systems could be developed for the degradation of this chemical in agricultural soils and waste [134], while photodegradation using doped TiO_2 was successfully carried out and degradation kinetics data are available for the scaling up of reactors [32]. Low toxicity and cost, chemical stability and high natural abundance [242] make this catalyst potentially suitable for an environmental friendly removal of this pollutant from water. Effective degradation is also observed by the use of dielectric

barrier discharge reactors, but further studies are required to reach the complete mineralization of 3,4-DCA [137].

2.2 Produced water treatment

The treatment and discharge of water, especially when related to offshore activities, is an environmental concern, but produced water can become a potential resource if treated in such a way as to allow its reuse. Usually, a single technology cannot provide suitable effluent characteristics; hence, many treatments are used in series operation (Figure 2.3). The choice of a suitable technology is based on the produced water composition, cost-effectiveness, space availability, and the fates of the water and any pollutants.

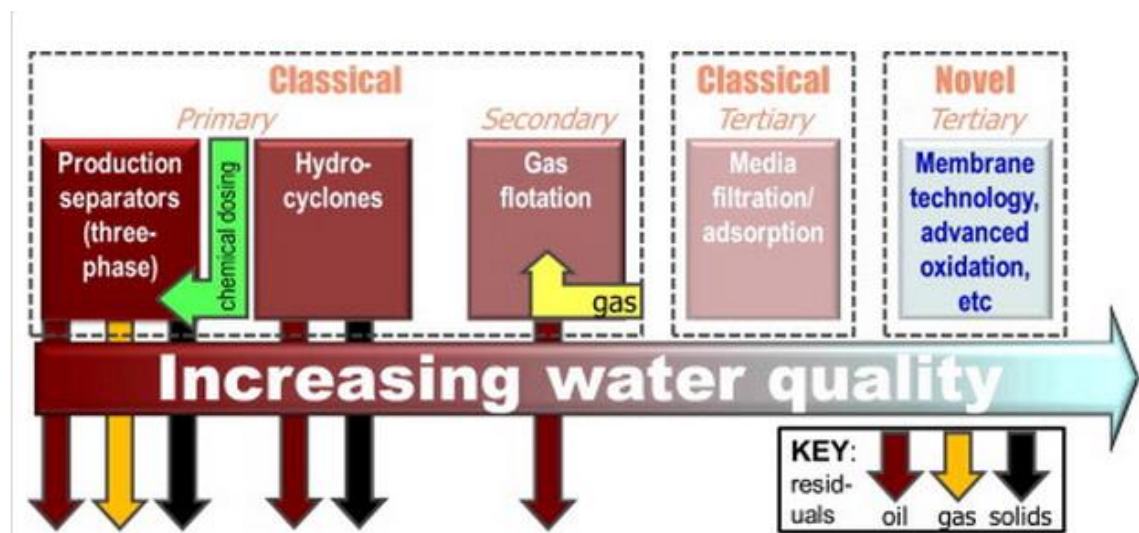


Figure 2.3: Diagram showing key steps involved in offshore produced water treatment [143].

Offshore platforms require compact units able to treat large fluxes in limited space. The range of treatment plants available is wide, and comparison can be based on robustness, reliability, mobility, flexibility, capital cost, as well as chemical and energy demands. Physical and chemical pre-treatments are always required, often followed by biological treatment in on-shore facilities, while lack of space and arduous management of streams seldom allows the implementation of bioreactors in offshore platforms due to processing limitations.

Managing produced water means the utilization of technologies to minimize its production, evaluation of reuse and recycling options, and finally actions to bring about its disposal. Best available preventive techniques are down-hole oil or gas water separation, and mechanical or chemical shut-off. The former is realised by separating the oily mixture with a hydrocyclone at the bottom of the production well, while the latter are achieved by installing either mechanical barriers in case of water breakthroughs, or a gel to block water cuts.

Reuse, recycling and disposal of produced water each require treatments to meet specific quality standards, and this generally implies:

- bulk de-oiling;
- removal of dispersed oils;
- removal of dissolved oils;
- removal of suspended particles;
- desalination;
- disinfection;
- softening (reducing water hardness);
- removal of radioactive particles;
- elimination of dissolved gas.

It is therefore crucial that complementary treatment methods are available, in tandem with water treatment, to optimise produced water processing.

2.2.1 Offshore technologies for dissolved oil removal

2.2.1.1 Media filtration and adsorption

2.2.1.1.1 Introduction

Filtration media are extensively employed for the removal of oil and grease from produced water. Water salinity does not affect the process and efficiency can be enhanced through the addition of coagulants prior to filtration, which can be accomplished using various types of media such as sand, gravel, anthracite, walnut shell and others. Regeneration of the filtration bed and solid waste disposal are the main operational costs; chemicals are often used to regenerate exhausted media, with

consequent liquid waste disposal, while media replacement results in solid waste management [101]. Different treatment options are discussed in detail below, including relevant conditions of operation.

2.2.1.1.2 Walnut shell filters

Crushed black walnut shell filters are widely used for produced water treatment; black walnut shells are also used ingredient to make and maintaining seals in fracture zones and unconsolidated formations. This media is effective for the removal of both fine solids and residual dispersed hydrocarbons.

Table 2.1: Characteristics of walnut shell media. pH, moisture content, porosity and surface obtained from tests conducted at the University of Regina; other values provided by USFilter, USA [144].

Parameters	Values	Chemical analysis	% by weight
pH	7.5	Nitrogen	0.1
Moisture content	1.97%	Sp. cellulose	40.6
Density	0.64 kg/L	Lignin	20.3
Specific gravity	1.2–1.4	Toluene solubility	0.5–1.0
Porosity	52%	Methoxyl	6.5
Surface area	0.1713 m ² /g	Chlorine	0.1
Colour	Light brown	Ash	1.5
Flash point	380 °F	Cutin	1

Crushed walnut shells are hydrophilic, hence binding to oils is weak, making mechanical backwashing (with mechanical agitation or walnut shells recirculation) suitable to recover full filter operation. Steam flood fields use water steam injection to improve oil recovery; the resulting produced water is hot so, in these facilities, periodic chemical cleaning of the filters is not required. The induced rubbing action of mechanical agitation, as used in the backwashing of this media, enhances the removal efficiency which, coupled with the very low amount of waste volume (no chemicals are

used), makes walnut shells optimal for the offshore sector. Reduction in backwash volume and footprint are the main challenges for further enhancing the efficiency of this technology.

Table 2.2: Cost of adsorbents required to treat 100 m³/d of oily water, initial concentration = 200 mg/L; final concentration = 10 mg/L. Cost of walnut shell media provided by USFilter, USA. 2010 [145].

Adsorption capacity (mg/g)	82.5
Mass of adsorbent required (kg/d)	230
Cost of adsorbent (\$/kg)	3.84
Cost of adsorbent required (\$/d)	884

2.2.1.1.3 Organoclay sorption media

Organoclays result from bonding an oleophilic surfactant to an inert mineral substrate, in order to attract oil into the large clay surface area [146]. Organoclays are well used in the Oil and Gas sector and they can remove highly emulsified and dissolved hydrocarbons including BTEX and phenols. The majority of these absorption media are based on bentonite, a sodium aluminium silicate clay consisting mostly of montmorillonite, that swells upon hydration, causing problems with handling and porosity.

PS85[®] is a different commercial technology which uses a non-swelling, magnesium aluminium silicate as the clay substrate; hence, it can be packaged differently than traditional organoclays [146]. Traditional media are used in deep beds with an EBCT (empty bed contact time) longer than 5 min, due to grain sizes of 1-3 mm. PS85 has a grain size of 0.5 mm, allowing efficient absorption with a bed depth of few centimetres and residence times < 1 min. In 2010, Weatherford Asia Pacific ran a well test in the Northwest Palawan Basin, during which produced water oil content needed to be reduced below 15 mg/L for overboard discharge. Two vertical cartridge filter vessels of PS85 adsorption media, able to operate in parallel thereby allowing continuous flow, were placed successfully downstream of conventional hydrocyclones and degassing vessels. The cartridge configuration is compact and has low capital cost, easy start up,

and is very efficient for moderate flow rates. For larger installations, the operating cost of cartridges becomes prohibitive and the traditional deep bed granular filter is more suitable; grain size >2 mm was tested for 2 yr in the Malampaya platform of the South China Sea with vessels containing each 2.1 tons of PS85 [146].

2.2.1.1.4 Multilayer filters

Multi-media beds comprise different grades of media, with a decrease in porosity with increasing depth. Common media types used are garnet (a vitreous silicate mineral) and anthracite, used for the removal of suspended soils, oils, or both; notably walnut shell filters are more commonly utilised for oil removal due to their higher efficiency. Multilayer filters can typically remove ~95% of 5 µm particles and ~90% of 2 µm particles from a produced water stream, making the effluent suitable for membrane treatment. The filter developed by Spectrum[®], has an upper layer of nutshells or anthracite, while the lower layer is of a finer particle size but higher density than the one above. This configuration ensures the maintenance of the filter structure with either high pressure or frequent backwashing. Furthermore, this filter can work with inlet oil concentrations of 20 to 50 ppm, and can sometimes be positioned directly downstream of a skim tank, with no previous induced gas flotation. Oil droplet removal by size is shown in Figure 2.4.

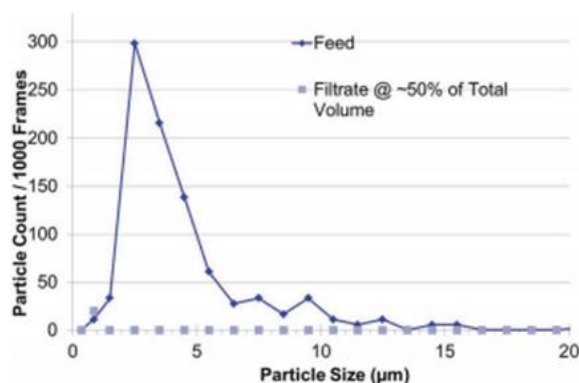


Figure 2.4: Spectrum[®] filter oil droplet removal by size performance [147].

2.2.1.1.5 Adsorbent media into combined processes

Chemical coagulation with ferric chloride (FeCl_3) coupled with adsorption by organoclay was previously investigated in a continuous stirred tank reactor (CSTR).

The outgoing flow was required to be suitable as the inlet for a dissolved air flotation unit (DAF), as shown in Figure 2.5. The initial concentration of dispersed and dissolved oil was 100 mg/L and it dropped to 10 ± 1.6 mg/L after coagulation with FeCl_3 only, to 15 ± 1.2 mg/L after adsorption with OC (OC-DAF) alone, and to 7 ± 1.4 mg/L after the integrated process (OC- FeCl_3 -DAF) [148].

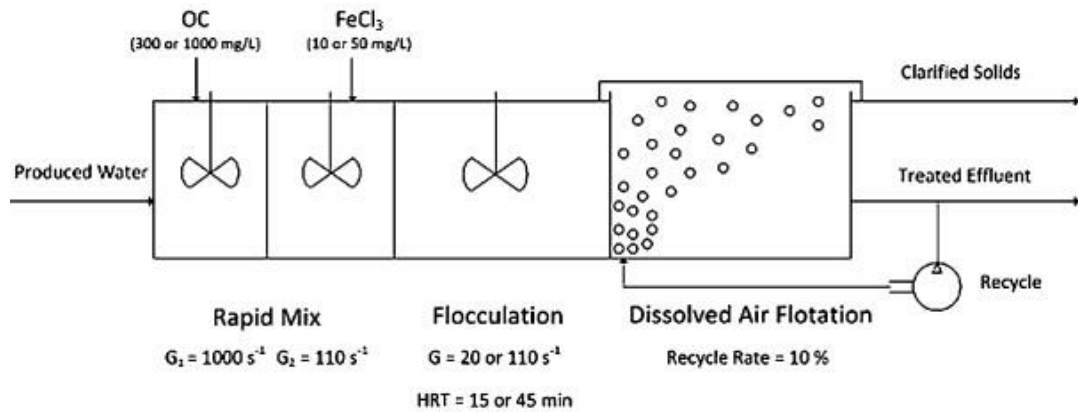


Figure 2.5: Combined adsorption-coagulation-DAF process [148]

A combination of filtration, coalescence and gravity separation was tested with North Sea produced water, downstream of hydrocyclones. The oily water flowed through different vessels containing media cartridges and finally passed into a recovery chamber. The oleophilic adsorbent material in the cartridges was polyurethane-based and it can continuously adsorb the oil emulsions; coalescing and desorbing them into larger oil droplets, which float to the top once in the recovery chamber. Inside the top of the vessel, the final separation occurs between the oil, gas and water. The oil and gas are retrieved for re-use. Solutions suitable for different produced water properties were developed and tested, through both field trials and laboratory experimental simulations. The results demonstrate that the technology is successful in the treatment of produced water oil concentrations below 10 mg/L [149].

2.2.1.2 Macro-porous polymer extraction

Macro-porous polymer extraction (MPPE) is one of the best available technologies, and best environmental practices, for produced water management in offshore oil and gas platforms [101]. The process, patented by Veolia®, is a fully automated, remote controlled liquid-liquid extraction system. Water containing hydrocarbons is passed

through a column packed with particles containing an extraction liquid, which removes the hydrocarbons from the water. Periodic in-situ regeneration of the extraction liquid is realised by hydrocarbons stripping using low-pressure steam. The so-obtained vapour is then condensed and the hydrocarbons are separated from the water phase by gravity (Figure 2.6). Almost 100% of the dissolved hydrocarbons are recovered and available for reuse, while the aqueous phase (condensed steam) is recirculated into the system [150].

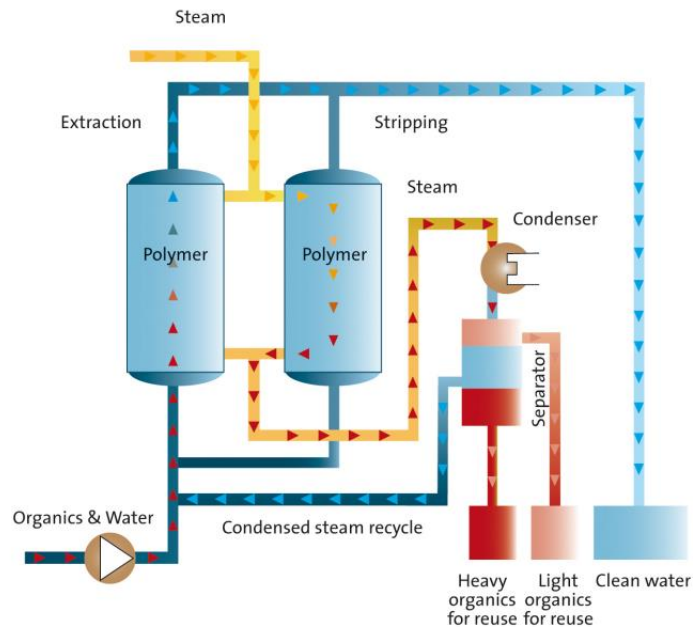


Figure 2.6: Macro-porous polymer extraction system [150].

The use of two columns allows simultaneous extraction and regeneration, typically extraction and regeneration require 1 h each of operating time. Gas flotation or hydrocyclones are required as pre-treatment. The cost of the unit actually still limits its wide application, but considering international legislation, with ‘zero discharge’ limits, MPPE is likely to become a major produced water treatment technology in the near future.

2.2.1.3 Membranes

2.2.1.3.1 Introduction

Membrane technology is one of the best available techniques for produced water treatment [151] and its use is expected to become more prevalent in the petroleum industry [152]. The demand for membranes in post-treatment downstream of dissolved air flotation or hydrocyclones in petroleum facilities, especially those offshore, will likely increase with the increasingly stringent discharge standards.

Offshore platforms have two options for produced water disposal: dumping into the sea or re-injection into reservoirs; oil removal and suspended solids removal are mainly required, respectively. Dissolved gas floatators and hydrocyclones experience difficulties in reaching water quality requirements for reinjection in very restrictive reservoirs, whereas membranes can almost completely remove both oils and fine suspended solids (Table 2.3).

An ideal membrane should [153]:

- be mechanically resistant;
- have high permeate flowrate;
- have high selectivity for target substances.

Table 2.3: Comparison of the efficiencies of different technologies in oil removal [152].

Rate of oil removal by technology	Min size of particles (μm)
API gravity separator	150
Corrugated plate separator	40
Induced gas flotation (without flocculants)	25
Induced gas floatation (with flocculants)	3–5
Hydrocyclone	10–15
Media filter	5
Centrifuge	2
Membrane filter	0.01

Membrane fouling, with related lower flux and lower membrane lifetime, is the major drawback of this technology, and the majority of recent studies focus on fouling reduction coupled with increasing flow to as high as possible, lower frequency of backwashing, and longer lifetimes. All of these targets require an accurate evaluation of optimum pre-treatments. Hydrophilic membranes, which adsorb less hydrocarbons than their hydrophobic counterparts, are expected to have lower fouling potential, but exceptions are reported in literature [154]. With regard to membrane permeability and other surface membrane properties, greater improvements have been observed when blending with organic materials as opposed to simple adoption of organic materials [155, 156].

2.2.1.3.2 Microfiltration, ultrafiltration, nanofiltration and reverse osmosis

Membranes have been applied for the treatment of produced water via microfiltration (MF), ultra-filtration (UF), reverse osmosis (RO) and, recently, by forward osmosis (FO). MF and UF operate at low transmembrane pressures (1–30 psi), achieving high water permeability and efficiency in oil rejection, while the high pressure of nanofiltration and RO membranes is more effective in the removal of dissolved ions and small organic particulates. RO membranes are able to achieve oil contaminant rejection rates > 99.9%, but they have high energy requirements and require expensive pre-treatments to avoid shorter lifetimes due to fouling. [157] Indeed, as a consequence of the hydraulic pressure applied, the compacted fouling layer on the membrane surface is not easy to remove [158].

Polymeric membranes are most commonly prepared from polyacrylonitrile (PAN) and Polyvinylidenedifluoride (PVDF) and they are cheaper than inorganic membranes. Inorganic membranes, like ceramic and zeolite membranes, generally offer improved chemical and thermal stability than polymeric ones, thus extending membrane lifetime. Ceramic membranes incur higher capital costs than polymeric membranes, and suffer some problems related to module housing. They are made from nitrides, oxides, or carbides of metals including zirconium, titanium, and aluminium. Tubular modules, in which the feed flows through the membrane channel, are the most used configuration

[153]; they consist of a porous support layer (usually α -alumina), decreasing pore diameter layers and an active layer. Ceramic membranes show greater removal of particles at higher flux than polymeric membranes, due to their well-defined pore size distribution, lower energy requirement and longer life cycle than inorganic membranes. Their thermal and chemical stabilities also permit chemical and thermal cleaning, ensuring longer lifetimes.

In composite zeolite membranes, an active layer of zeolite is supported by a porous material, e.g. porous alumina. In 2008, the high efficiency and stability of a zeolite-ceramic membrane was demonstrated, obtaining 99% of oil rejection with an inlet oil concentration of 100 mg/L and a flux of 85 L/(m² h). Backwashing with hot water and alkali solution did not lower membrane performance [159]. Zeolite-coated mesh films for gravity-driven oil-water separation was first tested in 2013 [160]; high oil separations could be obtained as a result of the superoleophobicity of the zeolite surface, which also explains its remarkable resistance to corrosion when used in underwater applications. Notably, it is also possible to achieve a desired flux by tuning the pore size, and by altering the crystallisation time of the zeolite crystals.

2.2.1.3.3 Forward osmosis

Nanofiltration and RO have high energy requirements, due to the required high pressures. Instead of using an external hydraulic pressure, FO allows separation of clean water from contaminated sources through a semi-permeable membrane by using the osmotic gradient between the feed and draw solutions. Hence, when seawater is available as the source of draw solution, FO may require very little energy input [161], and it can produce clean water with a quality comparable to a RO process. FO offers also easy cleaning, as the low pressures hinder compact fouling formation on the support [162]. Thus, FO may be a promising technology for the removal of dissolved oil from produced water [161], allowing effective and economic recycle of the water effluent [157]. FO processes require constant recycling of draw solutions, hence, the main challenge is regeneration of the diluted draw solution for reuse options.

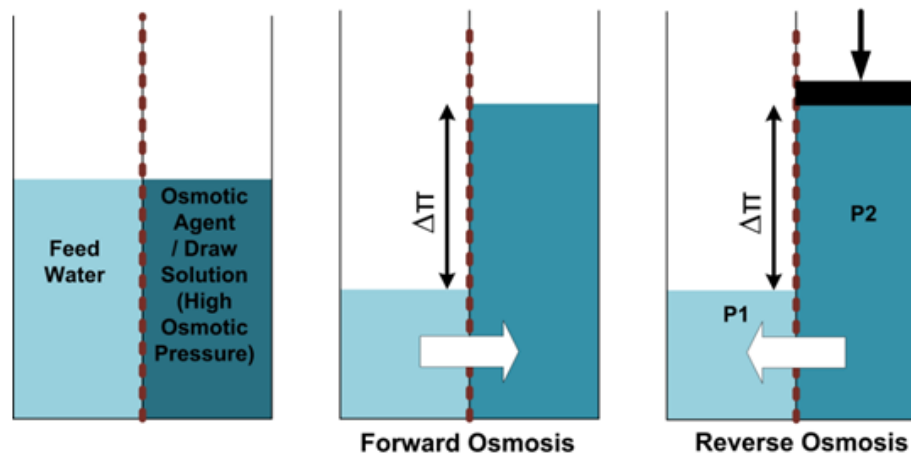


Figure 2.7: Schematic representation of forward and reverse osmosis processes. In reverse osmosis, the pressure applied on the osmotic solution must overcome $\Delta\Pi$ (with $\Delta\Pi=P_2-P_1$).

2.2.1.3.4 Integrated layout for re-use purpose

Previous work reports a polyetherimide hollow fibre MF module that was recently placed downstream of a coalescer bed (bed height 5 cm), formed by cationic exchange resins. [163]. The submerged membrane unit had a permeation area of 0.5 m² and the transmembrane pressure was varied from 12 to 30 kPa. Synthetic produced water, with oil concentrations between 200 and 400 mg/L, was used, with oil droplet diameters ranging from 3 to 8 μm . The fluid velocity through the coalescer bed ranged from 4.4 to 17.4 m/h and the water recovery rate in MF was: 0.75–0.90. The overall efficiency of the integrated process reached 93–100%, with oil concentrations from 0.1 to 14.8 mg/L, making the outgoing stream suitable for reuse purposes.

A tubular ceramic MF ($\alpha\text{-Al}_2\text{O}_3$) membrane unit was recently reported; fed with produced water from the Tehran refinery effluent, high in oil and grease, total organic carbon and dissolved solids [164], the unit reduced turbidity and solids content for a spiral wound polyacrylonitrile UF module, which further reduced turbidity and oil/grease content prior to the final spiral wound Polyamide RO unit (Figure 2.8). The optimum operating conditions for MF, UF and RO modules were respectively found to be:

- transmembrane pressure: 1.25, 2 and 15 bar;

- flowrate: 32.5, 12 and 10 L/min.

The MF-UF-RO integrated membrane system exhibited > 99.4% reduction of oil, and suspended solids, providing an effluent suitable to be used as boiler feedwater.

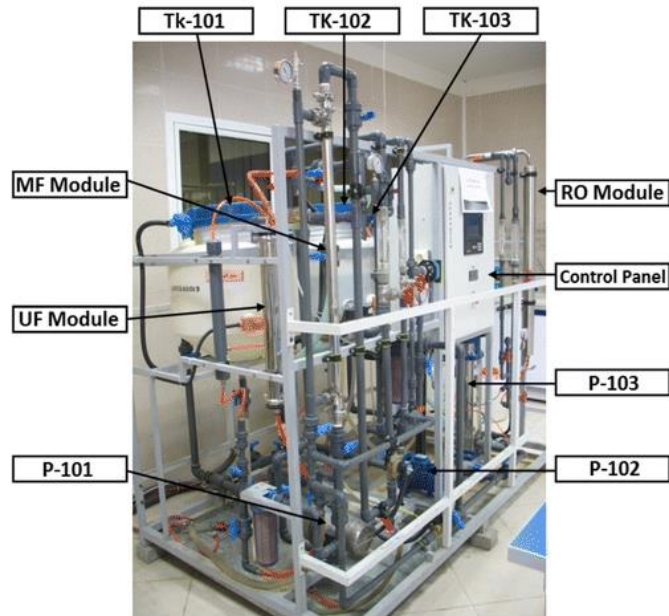


Figure 2.8: Pilot membrane plant for the production of boiler feedwater from produced water [164]. Pump P-101 pumps the feed from tank TK-101 to the MF module. P-102 provides hot distilled water to backwash the MF membrane. MF permeate is supplied in TK-102 and P-101 pumps the feed from TK-102 to the bottom of the UF module. P-102 pumps the feed from TK-103 to P-103, which provides the high pressure necessary to feed the RO module. Tank 103 is also used for backwashing.

2.2.1.3.5 Recent breakthroughs

Wettable materials, with superhydrophilic and superoleophobic properties, can separate water from oil and water mixtures. Compared with the ‘oil-removing’ type, i.e. superoleophilic sorbents, the ‘water removing’ materials are not so easily fouled by oils and are suitable for gravity-driven oil/water separation, as the density of water is greater than that of most organic pollutants [165].

Superoleophobic materials must have surface energies greater than that of water and smaller than that of oil. In recent years, important results have been achieved by chemical combination of superhydrophilic and superoleophobic molecules. In 2009, a

hydrophilic and oleophobic surface was created by modifying fritted glass membranes with perfluorinated end-capped polyethylene glycol surfactants; the hydrophilic polyethylene glycol component allowed easy penetration of water through the membrane, while hexadecane was retained thanks to the oleophobicity of the perfluoro-component [166]. Later a 'water-removing type of material was obtained by spraying poly(diallyldimethylammonium chloride) (PDDA) with sodium perfluorooctanoate (PFO) onto a steel mesh. When water was applied on the PDDA–PFO film, the fluorinated moieties were found able to reorganize and rearrange to allow the penetration of water molecules into the hydrophilic subsurface, while oil droplets could roll off the surface at low tilt angles [167].

Recent development of Smart separation (pH-responsive and electro-responsive surfaces) offers materials with surfaces with controllable oil wettability. A block copolymer comprising pH-responsive poly(2-vinylpyridine) and oleophilic/hydrophobic polydimethylsiloxane units was recently demonstrated to be able to switch its wettability and its conformation via protonation and deprotonation, depending on the pH of the solution [168]. The as-prepared material was coated onto porous non-woven textiles, fixed between two glass tubes and tested with a gasoline-water mixture (pH 6.5) introduced from the upper tube. Gasoline passed through the textile, while water was kept in the upper tube, but when the textile was rendered first wet with acidic water (pH 2.0) the opposite separation was observed, due to the fact that the textile became superhydrophilic and, when underwater, superoleophobic. Thus, the permeability for oil or water of such pH-responsive membrane can be switched on demand.

If a voltage is applied between a liquid droplet and an underlying solid substrate, charge will build up, both on the liquid side and on the solid electrode; the interfacial energy is lowered and the wettability of the substrate changes, switching from hydrophobicity to hydrophilicity. The contact angle for hexadecane (72°) was found to be independent of voltage, while the water contact angle decreased from 115° to 56° , as the voltage was increased from 0 to 1.5 kV [169]. Based on this measure, Kwon and co-workers sealed a stack of three nylon membranes coated with fluorodecylheptafluorodecyl polyhedral oligomeric silsesquioxane (fluorodecyl POSS) polydimethylsiloxane (-PDMS) between two vertical glass tubes [170]. Stainless steel mesh was used as one

electrode, a copper wire immersed in water served as the counter electrode, and a water-hexadecane mixture was poured into the upper tube. The mixture was entirely retained in the upper tube. After applying a voltage of 2 kV, the membrane became hydrophilic and water flowed through the membrane. The wettability of hexadecane was unchanged with voltage; thus, hexadecane was retained in the upper tube. This work showed the potential of electro-responsive surfaces for the controllable and remote operation of oil removal from water.

2.2.1.3.6 Final considerations

Membrane processes can achieve the highest water quality parameters. Most of the research previously conducted has been focused on membrane design, and the understanding of how oil droplets demulsify and coalesce together at membrane surfaces is providing the fundamentals for high performance membranes. More research is required to extend the lifetime of some modules and to reduce associated energy requirements.

2.2.1.4 Looking ahead: electrochemistry

A cost-effective technology with zero pollutant discharge represents the idealised future management of produced water; this target can be potentially achieved by using electrochemistry, as produced water is a prospective electrolyte as a result of its relatively good conductivity. The chemical breaking down of molecules into smaller units by light is known as photoelectrolysis; such technology has already been applied for hydrogen production and organics removal from wastewater. The photocatalytic decomposition of water on TiO₂ electrodes has also been investigated for the removal of organics from water. Photodegradation of organics can be increased with the addition of oxidants such peroxymonosulphate, peroxydisulphate and hydrogen peroxide, but the latter may induce corrosion processes [171]. 90% removal of total hydrocarbon content of produced water has been demonstrated, within 10 min, by semiconductor photocatalysis [172].

Electrochemical technologies can possibly generate and storage energy, remove organics, produce water suitable for re-use purposes and eventually recover valuable materials, without the use of additional chemicals and without any secondary waste

output. This engineering challenge may be achievable with the combination of photoelectrochemistry (photoelectrolysis, photocatalysis or photoelectrocatalysis), water electrolysis, fuel cell, electrodeposition and other electrochemical techniques into a single electrochemical process technology [101].

2.2.2 North Sea offshore Oil and Gas plants

There are physical, chemical and biological methods available to handle produced water, prior to reuse or discharge. Biological treatments are unsuitable for the majority of offshore platforms, due to high surface occupancy, long retention time and big fluxes of waste, while for onshore plants, biological pretreatment and refining is a cost-effective option. The initial step of the treatment of produced water is always the separation of bulk fluids and solids, followed by one or more polishing steps to remove dispersed and dissolved oils. Current generation in-line hydrocyclones and microbubbles gas flotation processes offer an ability to meet the actual stringent standards required for discharge. In hydrocyclones, pressurised produced water is injected tangentially, the shape of the cyclone increases the speed of the mixture and the centrifugal force splits the flow into two fluxes: the heavier water goes directly to the exit of the vessel, while the oil is directed to the centre. In-line hydrocyclones can separate oil and water, requiring only pre-treatment with a bulk de-oiler; they are suitable for offshore facilities as a consequence of their compact and flexible design and high efficiencies. There is no removal of dissolved oils; however, this can be achieved with the introduction of gas flotation, where small bubbles are generated within the produced water, either through pumps or mechanical rotating systems. Some flotation units have a striker plate to reduce the bubble size, other units are equipped with eductors that are able to generate bubbles in the range of 50-100 μm ; the smaller the bubbles, the higher the collision frequency, capture frequency and, thus, the separation efficiency of oil from water.

Discharging water means meeting stringent environmental regulations; the most common method of managing produced water is its re-injection into wells and this option is possible only after the removal of suspended solids, to avoid solids plugging, as this reduces injection volumes, increases energy requirements and can cause fractures in the reservoir media. Suspended solids can be naturally occurring, or formed

as products of corrosion, or generated by biological activities. Precipitation of dissolved solids is also called scaling and it is due to changes in temperature, pressure or pH; dissolved gases play a fundamental role in these processes and their removal is often realised in conjunction with suspended solids treatments.

Treatment options for re-injection in the North Sea offshore fields are hydrocyclones, induced gas flotation, filtration media and membrane filtration. The efficiency of these treatment processes can be compared in terms of area occupancy, evaluating the capacity by area ($F_A = \text{flow/area}$) and the capacity by volume ($F_V = \text{flow/volume}$). Judd *et al.* recently reported that hydrocyclones have the smallest area footprint, less than a half of an induced air flotation vessel, while cross flow membrane filtration has less than half the volumetric footprint of a nutshell filter, if the requirement for back flushing is considered. An individual hydrocyclone vessel can treat $> 440 \text{ m}^3/\text{h}$ of water per m^2 ($F_A = 440 \text{ m/h}$). Further improvements of the associated footprint can be realised by using modular hydrocyclones or cross flow membranes as a skid [143].

Table 2.4: Offshore produced water treatment technologies. Extract of Table 2 from Judd et al. [143]

Technology	F_A	F_V	C_{in}	C_{out}	% rem	Min. drop diam.
	m/h	h^{-1}	mg/L	mg/L	/	Mm
Hydrocyclone	100–440	450	–	20–80	90–95	12–20
Induced gas flotation	2.4–16	4–15	200–500	25–50	90–95	10–25
Compact flotation unit	45–90	–	200–500	15–25	90–95	10–25
Nutshell filter	27–37	13–24	20–50	2–5	99	2
Crossflow membrane filter	312	136	20–50	~0	99	< 1

Re-injection of produced water is a common practice. In terms of footprint and removal efficiency, cross flow microfiltration shows better results than the more diffuse nutshell filters. Recent improvements in hydrocyclones make this technology, preceded only by a bulk de-oiler, a promising technology for the treatment of produced water to allow its re-injection. It is not always possible to re-inject produced water, at which point it must be discharged; the most common option in North Sea offshore facilities is the use of multiple stages of three-phase separators, followed by dedicated hydrocyclone units. The flow from the hydrocyclones goes to a common degasser vessel and afterwards is dumped overboard or conveyed in flotation units or, in some cases, undergoes physical or chemical tertiary treatments. The degasser vessel can also act as a gas flotation system, with no need for other treatments prior to discharge [143].

3 Adsorption

3.1 Introduction

The phenomenon of adsorption occurs in both solid state reactions and biological mechanisms. It is defined as the enrichment of material or an increase in the density of a fluid near an interface, and occurs whenever a solid surface is exposed to a gas or liquid. The so described enrichment of one or more of the components in the region between a solid and a fluid phase is dependent on the extent of the interfacial area. With some systems, the adsorption process is accompanied by absorption, i.e. the penetration of the fluid into the solid phase (molecules are taken up by the volume, not by the surface). The term sorption is used to embrace both phenomena. The adsorbent is the solid material on which adsorption occurs, the adsorbable substance in the fluid phase is named adsorptive, while the substance in the adsorbed state is called adsorbate. Adsorption and desorption distinguish the direction from which the equilibrium states have been approached. Hysteresis arises when the amount adsorbed is not brought to the same level by the adsorption and desorption approaches at the same 'equilibrium' pressure or bulk concentration. The adsorption isotherm relates the amount adsorbed and the equilibrium pressure, at constant temperature [173].

3.1.1 Adsorption from solution

Adsorption from solution always involves the competition between solvent and solute. In the case of adsorption from solution, the adsorption of a solute at the liquid/solid interface can be evaluated by measuring the decrease in its concentration after defined contact time with the adsorbent. The adsorption isotherm is then represented as the adsorption of the solute against the equilibrium concentration.

At low concentrations, isotherms for adsorption from solution mainly fall into one of two main types among those listed by Giles and Smith [89]: the Type L (Langmuir isotherm) is concave to the concentration axis (Type I of the IUPAC classification) and the Type S is first convex and then concave to the concentration axis (IUPAC Types III or V). A Type L isotherm with a long plateau is associated with monolayer adsorption of the solute and minimal competition from the solvent. A Type S isotherm is due to strong adsorbate–adsorbate interactions, which are thought to generate a 'cooperative'

mechanism producing a vertical orientation of the molecules on the surface and a consequent upward swing over the first part of the adsorption isotherm [173].

3.1.2 Surface area and porosity

Porous adsorbents are solids with cavities or channels that are deeper than they are wide. The term surface area is generally used to indicate the experimentally accessible surface area, which is the surface available for the adsorption of certain adsorptives. The pore size is generally specified as the pore width, i.e. the available distance between two opposite pore walls; hence, pore size is related to the geometrical shape of the pore and the limiting size is that of the smallest dimension, and this should be used to represent the effective pore size. Pores can be open or close, blind (or dead-end pores) or interconnected (Figure 3.1). Pores which are open at both sides of a membrane or porous plug are named through pores [174].

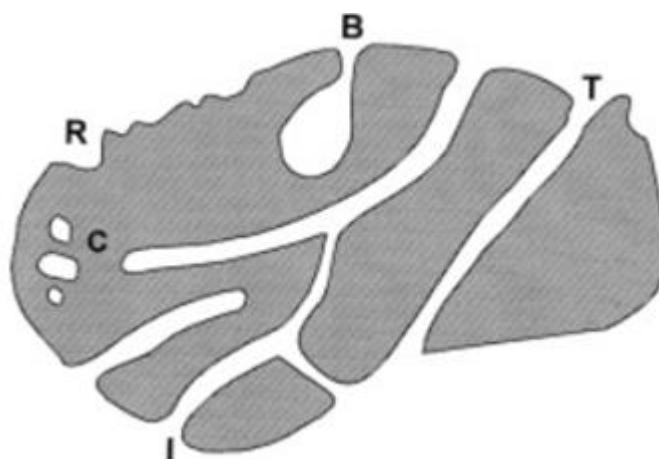


Figure 3.1: Cross section of a hypothetical porous grain with different pore types: closed (C), blind (B), through (T), interconnected (I) and together with some roughness (R) [175].

The pore volume denotes the volume of open pores. Porosity is the ratio of the volume of pores and voids to the volume occupied by the solid, where voids are the spaces between particles, which are dependent on the conditions of packing. The roughness includes all surface irregularities that are wider than they are deep. It is possible to distinguish between:

- Micropore Pore of internal width < 2 nm;

- Mesopore Pore of internal width between 2 and 50 nm;
- Macropore Pore of internal width > 50 nm.

The external surface area of a solid is expressed either as the area including roughness but not pores, or as the area outside the micropores. The pore shape is often assumed to be cylindrical but, for some materials, the pores are slits or interstices between spheroidal particles.

Pore structures can be created in different ways. Intra-crystalline pores are an inherent part of certain crystalline structures, for example zeolites, certain clays and Metal Organic Frameworks (MOFs). These pores are of molecular dimensions and are arranged as regular networks. Xerogel materials are composed of an assemblage of small particles in which the pore structure of the consolidated system is mainly dependent on the size and packing density of the primary particles; the synthesis process is thus constitutive. A third route is subtractive, where inherent parts of the original structure are removed to create pores, akin to the leaching process to produce porous glass.

3.1.3 Physisorption and Chemisorption

During the early 1930s, adsorption began to be sub-categorised into physisorption and chemisorption. Physical adsorption involves van der Waals interactions, and the forces implied are the same as those responsible for the condensation of vapours and deviations from ideal gas behaviour. Chemical adsorption interactions are essentially those responsible for the formation of chemical compounds; the adsorbed molecules are attached by chemical bonding. In 1932, Taylor introduced the concept of ‘activated adsorption’, i.e. the idea that activation energy in chemical kinetics expressed the marked increase of the adsorption rate with a rise in temperature, in terms of surface bond formation.

The most important distinguishing features between the two types of adsorption may be summarised as follows [173]:

- Physisorption is a phenomenon with a low degree of specificity.

- Chemisorbed molecules are linked to reactive parts of the surface, confined to a monolayer whereas, at high relative pressures, physisorption generally occurs as a multilayer.
- A desorbed physisorbed molecule returns to the fluid phase in its original form, while a chemisorbed molecule undergoes reaction or dissociation, thereby losing its identity and cannot be wholly recovered by desorption.
- Activation energy is often required for chemisorption and, at low temperature, the system may have insufficient thermal energy to achieve thermodynamic equilibrium. Physisorption systems generally reach equilibrium rapidly, but equilibration could be slow if the transport process is rate-determining.
- The energy of chemisorption is of the same order of magnitude as the energy change in a comparable chemical reaction. Physisorption is an exothermic process, but the energy involved is generally not much larger than the energy of condensation of the adsorptive, appreciably increased only when physisorption takes place in very narrow pores.

3.1.4 First approaches to adsorption phenomena

The exothermic nature of gas adsorption was firstly observed by de Saussure in 1814. Later, Mitscherlich suggested that the amount of gas adsorbed in a porous carbon was such that it was probably in the liquid state, while Favre showed, by adsorption calorimetry, that the heat of adsorption of various gases on charcoal was larger than the heat of liquefaction; he proposed that this was due to a higher density near the pore walls. Around 1880, Kayser related the amount of gas adsorbed to applied pressure and in 1881 he coined the term adsorption. The terms isotherm and isothermal-curve started to be used to define the results of adsorption measurements made at constant temperature. The first recorded isotherms of adsorption from solution are those reported by van Bemmelen in 1881, as a result of investigations on the final state (i.e. equilibrium concentration) of a solution in contact with soil.

Until 1907, it was generally believed that adsorption processes involved penetration into the solid structure, when Freundlich stated the role of the solid surface. He proposed a mathematical relation to express the isotherm, now commonly known as the Freundlich adsorption equation (Equation 3.1). Two years later McBain identified two stages in the

uptake of hydrogen by carbon: a rapid adsorption followed by a slower absorption into the interior of the solid and introduced the term sorption to cover both phenomena. In 1911, observing the large uptake of water vapour by silica gel, Zsigmondy proposed that the condensation of a vapour can occur in very narrow pores at pressures well below the normal vapour pressure of the bulk liquid. It is now recognised that capillary condensation plays an important role in physisorption by porous solids. Lord Rayleigh's earlier conclusion that certain films of polar oils on water were one molecule thick had not received attention until 1916, when Langmuir suggested that adsorption on both liquid and solid surfaces involved the formation of a monomolecular layer. This assumption underpinned future progress in the interpretation of adsorption from solution data. In light of Langmuir's theory, the plateau of a solute isotherm represents monolayer completion and the monolayer capacity can be determined by applying the Langmuir equation (Equation 3.8). Langmuir also stated that it is not possible to apply equations derived for planar surfaces with highly porous adsorbents and it is not possible to know exactly the area on which the adsorption takes place. This postulation was appreciated later by Dubinin and co-workers, who showed that the mechanism of physisorption in very narrow pores (micropores) is different from that in the wider pores (mesopores) or on an open surface.

3.1.4.1 Freundlich adsorption theory

The Freundlich adsorption isotherm (Figure 3.2), expressed in Equation 3.1, represents the isothermal variation of adsorption of a quantity of gas by unit mass of solid adsorbent with pressure:

$$\frac{x}{m} = kp^{1/n} \quad \text{Equation 3.1}$$

where x is the mass of the gas adsorbed on mass m of the adsorbent at pressure p ; k and n are constants whose values depend upon the adsorbent and gas at a particular temperature.

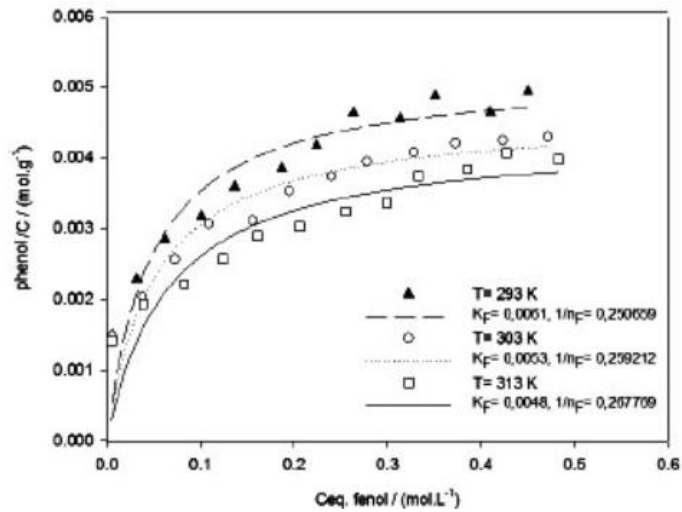


Figure 3.2: Freundlich adsorption isotherms on powdered activated carbon. [176].

At low pressure, extent of adsorption is directly proportional to pressure, which means: $x/m \propto p^1$. At high pressure, extent of adsorption is independent of pressure, i.e.: $x/m \propto p^0$. Hence at intermediate values of pressure, adsorption is directly proportional to $p^{1/n}$. Using a constant of proportionality (k) gives the Freundlich adsorption equation (Equation 3.1).

Taking logs of both sides of Equation 3.1, the resulting equation can be plotted as the equation of a straight line, allowing determination of k and n , as shown in Figure 3.3.

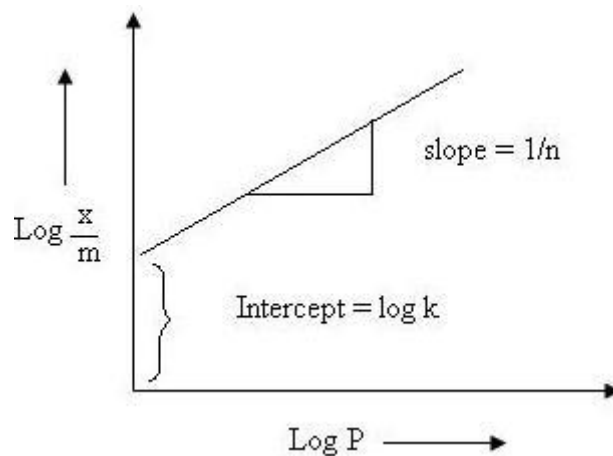


Figure 3.3: Linear plot of the Freundlich equation

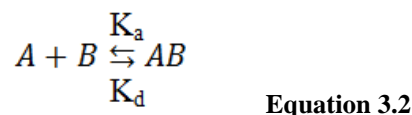
The extent of adsorption varies directly with pressure until the saturation pressure, then the rate of adsorption saturates also after applying higher pressure. Consequently, the Freundlich adsorption isotherm fails at higher pressure.

3.1.4.2 Langmuir adsorption theory

In 1916, Langmuir proposed an equation that explains the variation of adsorption with pressure, based on a relationship between the number of active sites of the surface undergoing adsorption and pressure. Langmuir proposed his theory by making the following assumptions:

- Fixed number of adsorption sites are available on the solid surface.
- All vacant sites are of equal size and shape on the adsorbent surface.
- Each site can hold a maximum of one molecule of gas and a constant amount of heat energy is released during this process.
- Dynamic equilibrium, which involves adsorption and desorption, exists between adsorbed gaseous molecules and the free gaseous molecules.
- Adsorption occurs as a monolayer process.

The dynamic equilibrium existing between adsorbed gaseous molecules and the free gaseous molecules can be expressed as:



where K_a and K_d are the equilibrium constants that govern the forward and reverse reactions, respectively. According to kinetic theory, at equilibrium, the rate of the forward reaction is equal to rate of the reverse reaction :

$$K_a[A][B] = K_d[AB] \quad \text{Equation 3.3}$$

$$K = \frac{K_a}{K_d} = [AB]/[A][B] \quad \text{Equation 3.4}$$

Equation 3.4 represents the equilibrium constant for distribution of adsorbate between the surface and the gas phase. If θ is defined as the fraction of surface sites covered by gaseous molecules, the fraction of surface free from gaseous molecules will be $(1 - \theta)$.

Now, the rate of the forward reaction (i.e. rate of adsorption) is directly proportional to the number of free sites available on the adsorbent surface $(1 - \theta)$ and pressure, P:

$$\text{Rate of adsorption} = K_a p(1 - \theta) \quad \text{Equation 3.5}$$

Similarly, the rate of the reverse reaction, or rate of desorption, depends on the number of sites occupied by the gaseous molecules on the adsorbent surface.

$$\text{Rate of desorption} = K_d(\theta) \quad \text{Equation 3.6}$$

At equilibrium, the rate of adsorption is equal to the rate of desorption:

$$K_a p(1 - \theta) = K_d(\theta) \quad \text{Equation 3.7}$$

Solving Equation 3.7, in terms of θ , gives:

$$\theta = Kp/(1 + Kp) \quad \text{Equation 3.8}$$

This is the Langmuir adsorption equation, and the Freundlich adsorption equation can be viewed as a special case of the Langmuir equation.

Equation 3.8 can be also written in terms of volume of gas adsorbed, redefining θ as the ratio between the volume of gas adsorbed under given sets of temperature and pressure and the volume of gas adsorbed at high pressure conditions required to cover the surface with a monolayer of gaseous molecules.

The main limitations of the Langmuir adsorption equation are:

- The adsorbed gas must behave ideally in the vapour phase, which is a condition that can be fulfilled at low pressure conditions only. Moreover, the Langmuir Equation assumes that adsorption leads to monolayer formation, which is possible only under low pressure conditions, as at higher pressure adsorbed gas molecules attract more adsorptive molecules and a multilayer process is more

realistic (as explained from Brunauer Emmett and Teller theory). Hence, the Langmuir Equation is valid under low pressure only.

- All sites on the solid surface are assumed to be equal in size and shape and have equal affinity for adsorbate molecules (i.e. the solid surface is homogeneous), but real solid surfaces are generally heterogeneous.
- Langmuir Equation assumes no interaction between molecules, while weak forces of attraction exist even between molecules of same type.
- The adsorbed molecules must be localised, thus the decrease in randomness must be zero ($\Delta S = 0$). This is not possible, as the condensation of gases via adsorption does result in a decrease in randomness but its value is not zero.

The Langmuir model can also be applied to adsorption of substances dissolved in aqueous solutions:

$$q = q_{max}bC_e/(1 + bC_e) \quad \text{Equation 3.9}$$

where q (mg/g) is the amount of adsorbate adsorbed per unit mass of adsorbent, C_e (mg/L) is the corresponding adsorbate concentration at equilibrium. q_{max} (mg/g) is the maximum amount of adsorbate per unit mass of adsorbent required to form a monolayer on the adsorbent surface, b (L/mg) is a constant proportional to the affinity of the binding sites.

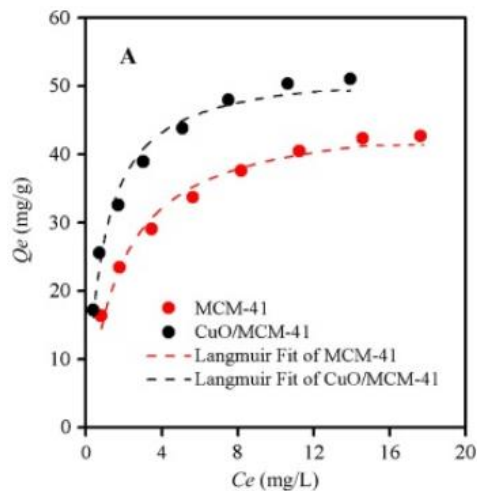


Figure 3.4: Langmuir adsorption isotherms of crystal violet (A) and methylene blue (B) dissolved in deionised water on mesoporous silica MCM-41.

Equation 3.9 can be re-written in the linearised form:

$$\frac{1}{q} = 1/(q_{max} b C_e) + 1/q_{max} \quad \text{Equation 3.10}$$

The parameters q_{max} and b can be determined from the slope and intercept of the subsequent plot.

3.1.4.3 Brunauer-Emmett-Teller (BET) adsorption theory

In 1934, Emmett and Brunauer used low-temperature adsorption of nitrogen to determine the surface area of an iron synthetic ammonia catalyst. They observed that adsorption isotherms of some gases, measured at temperatures as close as possible to their respective boiling points, were all S-shaped with distinctive features. Others, including Langmuir, had already suggested that this type of adsorption was not always characterised as a monolayer coverage process. An empirical approach was then adopted by Emmett and Brunauer to assess the stage at which multilayer adsorption begins. The theory is an extension of Langmuir theory applied to a multilayer adsorption process, with the following hypotheses:

- molecules of gas physically adsorb on the solid in infinite layers;
- there is no interaction between each adsorption layer;
- Langmuir theory can be applied to every layer.

The Brunauer, Emmett and Teller (BET) adsorption isotherm equation is so defined [177]:

$$p/[v_a(p_0/p)] = 1/(v_m/c) + (c - 1)/(v_m/c) \cdot p/p_0 \quad \text{Equation 3.11}$$

where:

- p is the partial vapour pressure of adsorbate gas in equilibrium with the surface at 77.4 K, which is the boiling point of the gas when nitrogen is used (Pa);
- p_0 is the saturated pressure of adsorbate gas (Pa);
- v_a is the specific volume of gas adsorbed (mm^3/mm^2) at standard temperature and pressure (STP), hence at 273.15 K and atmospheric pressure (1.013×10^5 Pa);

- v_m is the specific volume of gas adsorbed (mm^3/mm^2) at STP to produce an apparent monolayer on the sample surface;
- c is a dimensionless quantity related to the enthalpy of adsorption of the adsorbate gas on the adsorbent.

The completion of a monolayer is assumed to be characterised by the beginning of the nearly linear section of the adsorption isotherm, which corresponds to Point B in Figure 3.5. The surface area is determined from the amount adsorbed at Point B, assuming that the completed monolayer is in a close-packed state. In 1938, the publication of the BET theory identified Point B as the stage of monolayer completion and the beginning of multilayer adsorption.

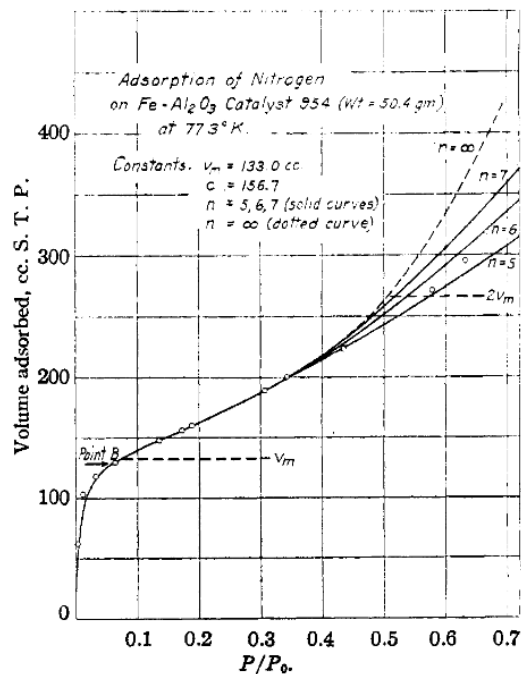


Figure 3.5: Characteristic point on a Type II adsorption isotherm [177]

This theory has become a standard procedure for the determination of the surface area of numerous fine powders and porous materials [178]. The BET model gives a simplified description of monolayer–multilayer physisorption, as an extension of the simple Langmuir mechanism of localised monolayer adsorption on a uniform surface. What it is unaccounted for are the effects produced by adsorbate–adsorbate interactions on different surface structures (degrees of heterogeneity). Low c value and indistinct

Point B are associated with the overlap of monolayer formation and multilayer development, due to weak adsorbent–adsorbate interactions or configurational entropy effects like those observed for *n*-hydrocarbons on silica. Hence, if $c < \sim 50$, the transition from the first to the next layer occurs over a wide range of coverage. Isotherms of benzene on some non-porous and mesoporous silica are typical examples of this shape, with gradual curvature and no sign of a Point B, with values of $c \sim 10$. Similarly, for nitrogen isotherms at 77 K, surface modification of mesoporous silica exhibits an appreciable change in isotherm shape and a reduction in c from ~ 110 to ~ 20 . BET theory is unable to account for the Type VI isotherm, shown in Figure 3.6.

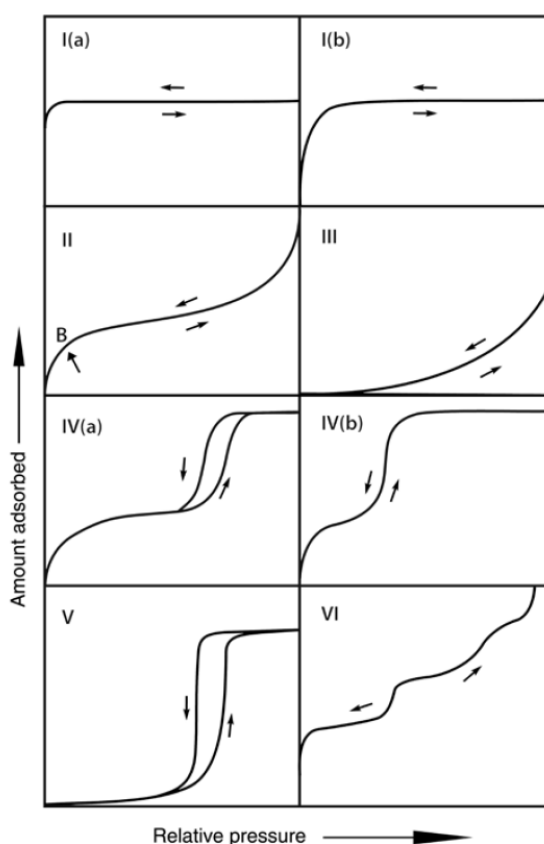


Figure 3.6: Refined IUPAC classification of physisorption isotherms [179].

It is inappropriate to apply the BET equation to Type III or Type V isotherms, but in the absence of microporosity or highly active sites, the BET plot of Type II or Type IV isotherms generally provides a fairly reliable assessment of monolayer capacity, when the knee of the isotherm is sufficiently sharp with a clearly identifiable Point B. Caution

should also be exercised when interpreting BET monolayer capacities derived from Type II or Type IV isotherms giving c values lower than ~ 50 or higher than ~ 200 [180].

3.1.4.4 Polanyi adsorption potential theory

The adsorption potential theory proposed by Polanyi in 1914 was developed from an older idea of attractive forces emanating from a solid surface. The adsorbed layer is described as a compressed film of decreasing density with increasing distance from the surface. This theory relates the amount adsorbed to the adsorption potential, exhibiting a characteristic curve, but some of its underlying principles were inconsistent with the then emerging treatment of intermolecular forces [173]. Despite this, the Polanyi concept of characteristic curves was later adjusted and adopted by Dubinin and his co-workers in their theory of micropore filling.

In his theory, Polanyi assumed that the attraction, largely due to van der Waals forces of the gas to the surface, is determined by the distance of the gas particle from the surface, and that the gas acts ideally until condensation, where it exceeds its equilibrium vapour pressure. While Henry's adsorption theory is applicable at low pressure and the BET equation is more useful between 0.05 and 0.35 p/p_0 , the Polanyi potential theory is suitable across a wide range of pressures ($p/p_0 \sim 0.1-0.8$). The main assumption made by Polanyi is that, at a constant temperature, the molecules near a surface move according to a potential, similar to that of gravity or electric fields. Gas molecules move closer to that surface when the pressure is higher than the equilibrium vapour pressure. The change in potential relative to the distance from the surface can be written using the formula for the difference in chemical potential:

$$d\mu = -S_m dT + V_m dP + dU_m \quad \text{Equation 3.12}$$

where μ ($\text{J}\cdot\text{mol}^{-1}$) is the chemical potential, S_m ($\text{J}\cdot\text{K}^{-1}\cdot\text{mol}^{-1}$) the molar entropy, V_m ($\text{m}^3\cdot\text{mol}^{-1}$) the molar volume and U_m ($\text{J}\cdot\text{mol}^{-1}$) the molar internal energy. At equilibrium, the chemical potential of the gas, at both a distance x from the surface and an infinitely large distance from the surface, denoted as $\mu(x, p_x)$ and $\mu(\infty, p)$, respectively, are equal. Thus, integration from an infinite distance to x from the surface is written as:

$$\int_{\infty, p}^{x, p_x} \mu = \mu(x, p_x) - \mu(\infty, p) = 0 \quad \text{Equation 3.13}$$

where p_x and p are the partial pressures of the gas at x and infinite distance from the surface, respectively. Since the temperature remains constant:

$$\int_p^{p_x} V_m dp + U_m(x) - U_m(\infty) = 0 \quad \text{Equation 3.14}$$

Setting $U_m(\infty) = 0$ and using the ideal gas law $PV_m = RT$, Equation 3.14 becomes:

$$-U_m(x) = \int_p^{p_x} \left(\frac{RT}{p}\right) dp = RT \ln(p_x/p) \quad \text{Equation 3.15}$$

Gas condenses into a liquid film of thickness x_f on a surface when the pressure of the gas exceeds the equilibrium vapour pressure p_0 ; the energy at p_0 is:

$$U_m(x_f) = -RT \ln(p_0/p) \quad \text{Equation 3.16}$$

Considering the partial pressure of the gases relates to the concentration, the adsorption potential \mathcal{E} is defined as:

$$\mathcal{E} = -RT \ln(C_s/C) \quad \text{Equation 3.17}$$

where C_s and C are the saturated concentration and the equilibrium concentration of the adsorbent, respectively.

The adsorption space in the vicinity of the solid is characterised by a series of equipotential surfaces, each contributing a specific value of the adsorption potential \mathcal{E} , which represents the energy of adsorption, i.e. the work needed to transfer a molecule from the gas phase at equilibrium with the solid at defined pressure. The characteristic equation of adsorption relates the distribution of the degree of filling of the volume of the adsorption space (i.e. the micropores volume) to the differential molar work of adsorption, identified as adsorption potential.

3.1.4.5 Dubinin's theory and its extension to the adsorption of aqueous organics on microporous materials

The Dubinin and Astakhov theory on volume filling of micropores is also based on the temperature invariance of the characteristic equation of adsorption but, in contrast with Polanyi, the molar work of adsorption is not identified as adsorption potential, but as the loss of Gibbs free energy A , also known as free enthalpy, which is the maximum reversible work that may be performed by a thermodynamic system at a constant temperature and pressure:

$$A = -\Delta G = 2.303RT \ln(p_0/p) \quad \text{Equation 3.18}$$

Using the adsorption potential, the degree of filling of the adsorption space is defined as N_a/N_{a0} , where N_a is the amount adsorbed (usually given in mol/g) at relative pressure p/p_0 and temperature T , and N_{a0} is the limiting amount filling the micropores. Then, the Dubinin–Astakhov equation is defined as [181]:

$$\frac{N_a}{N_{a0}} = \exp\left[-\left(\frac{A}{E}\right)^n\right] \quad \text{Equation 3.19}$$

where E is the characteristic energy of adsorption (Kj/n), depending on the solid and the adsorbate. The volume filled by the adsorbate can be defined as the product of N_{a0} and its molar volume (V_m) in the condensed state at the corresponding temperature.

Dubinin's theory requires that the temperature invariance of parameter E over a minimum reasonable temperature range to be used to predict adsorption equilibria of vapours, including water. The effect of the adsorbate itself is expressed by the affinity coefficient β , which comes from a comparison of the vapour under consideration and a standard vapour, usually benzene for activated charcoals. Under these circumstances, $E = \beta E_0$, where E_0 is the characteristic energy of adsorption of a standard vapour, again usually benzene. For activated carbons, the power n varies from ~ 1.5 to 3, and the most frequent case is $n = 2$ (which is the case of Equation 3.20).

Dubinin's theory can be extended to the adsorption of vapours on certain nonporous surfaces such as graphitised carbons blacks, and the Dubinin-Radushkevich equation then takes the form of the so-called Dubinin–Radushkevich–Kaganer (DRK) equation:

$$\frac{N_a}{N_{a,0}}(DRK) = \exp\left[-\left(\frac{A}{E}\right)^2\right] \quad \text{Equation 3.20}$$

The limiting amount $N_{a,0}(DRK)$ represents the monolayer capacity of the surface, which is close to $N_{am}(BET)$, the BET monolayer capacity obtained from the same isotherm at higher relative pressures ($0.05 < p/p_0 < 0.30-0.35$). It has been shown that the preferential adsorption of various compounds from aqueous solutions, by activated carbons, follows an equation of the DRK type [182]. Indeed, the equation above can be rewritten as:

$$N_a = N_{am} \exp\left\{-\left[\frac{RT \ln\left(\frac{C_s}{C_{eq}}\right)}{E_s}\right]^2\right\} \quad \text{Equation 3.21}$$

In this expression, the vapour–solid adsorption potential $A = RT \ln(p_0/p)$ is replaced by a new thermodynamic potential, $RT \ln(C_s/C_{eq})$, where C_s is the saturation concentration of the adsorbed species and C_{eq} is the concentration at equilibrium, which corresponds to the amount adsorbed, N_a . If the adsorbate is a sparingly soluble species, such as phenol, N_{am} is the monolayer capacity of the micropore walls and not filling of the micropores, as for the vapour phase. Furthermore, Equation 3.21 is similar to Equation 3.20, however, as adsorption takes place from an aqueous solution, there is no reason to relate E_s to the characteristic energy E_0 . The equation above does not imply a specific model for adsorption from a solution.

Due to the fact that the adsorption isotherms for phenol and related compounds show a plateau, the majority of authors use Langmuir's equation adapted to solution work, or also the Freundlich equation, but both suffer from the drawback that the thermal variation of their main parameters cannot be predicted in a simple fashion, as opposed to Dubinin's equation [182].

3.1.5 Surface energy and wetting

At a molecular level the thickness of the interfacial region is not zero. The electronic structure of a heterogeneous interface makes the properties of this region different from

the properties of the involved bulk materials. Indeed, when an interface is formed between two materials, there is a structural rearrangement of nuclei and electrons in the interfacial region in order to reduce the total energy of the system, with the formation of an interface dipole.

The surface, or interfacial, energy, is the excess energy at the surface of a material compared to the bulk; it quantifies the disruption of intermolecular bonds occurring when a surface is formed [183]. There is a higher energy density at the liquid surface than in the bulk, as the molecules at the surface cohere more strongly to those directly associated with them on the surface as they all have neighbouring molecules that are absent. Furthermore, at liquid-air interfaces, liquid molecules have greater attraction to each other than to the air molecules. As a consequence, a 'film' is formed on the liquid surface, which makes it more difficult to move an object through the surface than to move it once it is underwater. The surface energy density of a liquid is equivalent to its surface tension. The surface tension is the elastic tendency of a fluid surface, which makes it acquire the least surface area possible. It is expressed as force per unit area (J/m^2) and can also be defined as the energy required to increase the surface isothermally and reversibly by a unit amount [184].

When two liquids are mixed, forming a solution, the surface tension of the primary liquid can deviate from corresponding pure liquid values, as described by the Gibbs isotherm, which relates changes in concentration of a component in contact with a surface with changes in surface tension. Surface energy plays a fundamental role in wetting phenomena, which can be defined as the ability of a liquid to maintain contact with a solid surface. If the surface energy of a solid substrate changes with the addition of a liquid drop, the substrate is said to be wetting. High energy substrates are kept together by bonds, while low energy substrates are kept together by forces. Covalent, ionic, and metallic bonds are much stronger than forces such as van der Waals and hydrogen bonding. High energy substrates are more easily wet than low energy substrates, much more so if the substrate has a higher surface energy than the liquid [185]. The hood of a car is easily wet by water, as water has a lower surface energy than the car hood, but when the latter is covered with wax, water beads on the surface rather than wet out. This results from the fact that the waxed hood of the car has a lower

surface energy than water. A liquid drop, immobile on a solid surface, is in equilibrium through the balance of the interfacial tensions between solid and liquid (γ_{SL}), between solid and vapor (γ_{SV}) and between liquid and vapor (γ_{LV}), as shown in Figure 3.7. The angle formed by the liquid drop at the three-phase boundary, included between the plane tangential to the surface of the liquid and the plane tangential to the surface of the solid, is called the contact angle (θ), a quantitative measure of the wetting of a solid by a liquid. Similarly, the hydrophobic degree of an adsorbent material can be defined by measuring the contact angle of a fixed drop of water on its surface.

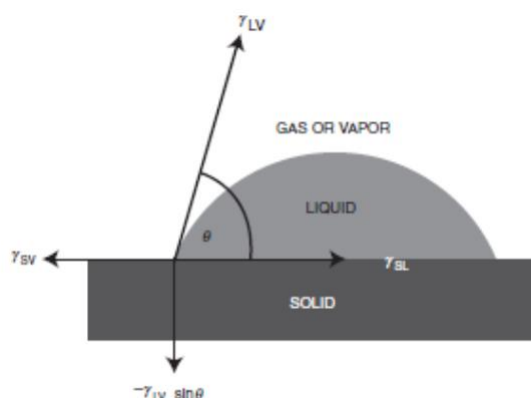


Figure 3.7: Balance of interfacial tensions at solid-liquid-air interface.

Organic liquids easily wet the surfaces of a porous material and then are preferentially drawn into the pores by capillary action, but since water also fills the available pores of a sorbent, it competes with the organics for the available surface sites. Hence, to increase the efficiency of organics separation from water it is fundamental to inhibit liquid water from entering the pores. Hydrophobicity is the key property of porous materials that inhibits wetting by liquid water. This property is inherent for polymers, e.g. polytetrafluoroethylene (Teflon), while carbons and aerogels generally have low liquid–solid interfacial energies and only through chemical modification they can be tuned as hydrophobic materials, enhancing the separation efficiency.

3.2 Porous materials for organics adsorption

3.2.1 Introduction

A common approach to organic solvent pollutant removal from water is via the use of highly porous filtration media, due to their high specific surface area and adsorption capacity. The adsorbent properties of clay, sand and wood charcoal were known by the ancient Egyptians, Greeks and Romans: these materials were used for the desalination of water, removal of oils and the treatment of diseases. Adsorbents are widely used as desiccants, catalysts or catalyst supports, for the separation or storage of gases, the purification of liquids, and for controlled drug delivery [173].

3.2.2 Activated carbons

3.2.2.1 Introduction

Granulated activated carbon (GAC) is widely used as a filter medium, due to its high surface area, often high microporosity, and low-cost synthesis. Activated carbon is produced from a carbon-rich precursor through chemical or physical activation. Some commercial grades of activated carbon have disordered micropore structures, while carbon-based adsorbents and catalyst supports are available in the form of activated carbon fibres and cloth, monoliths, gels and membranes.

3.2.2.2 Organics adsorption

The potential use of activated carbons for the removal of a wide range of pollutants such as aromatic hydrocarbons, humic acids and heavy metal ions is widely assessed.

Adsorption from solution is generally more complex than physisorption at the gas-solid interface. The measured adsorption is plotted against the equilibrium concentration, giving isotherms with characteristic shapes. Some activated carbons give isotherms of L type, but a well-defined plateau (corresponding to the monolayer completion or the micropore capacity) is not usually obtained. A simple or binary form of the Langmuir equation or the Langmuir–Freundlich relation is often applied, which take into account energetic heterogeneity [186].

The role of microporosity of activated carbons, in the adsorption of phenol and 4-chlorophenol, before and after surface oxidation, from aqueous solution was recently

found to be more important than the polar nature of the carbon surface [187]. Research into the adsorption of nitrophenols and chlorophenols showed a more complex behaviour, dependent on the adsorptive, the adsorbent and temperature [188]. Oxidation of the carbon surface decreases the density of π electrons, reducing the π - π interactions with the phenol ring and thus the adsorption capacity. Adsorption on activated carbon materials is then a function of the surface area of the adsorbent, oxygen surface functionalities and surface charge, the electron-donating or withdrawing properties of the adsorbate and of the pH of the solution [189]. This was also confirmed by analysis of adsorption of the herbicide Amitrole from aqueous solution by activated carbon, which is highly dependent on surface chemistry and on solution pH [190].

Theoretical models, like Langmuir or Freundlich equations, accurately reproduce the experimental data of the removal of sparingly soluble organics from aqueous solution, but predictions are difficult, due to the complexity of some parameters used in these expressions. Dubinin's theory (Chapter 3.1.4), can be applied to the adsorption of several solutes from aqueous solutions, often making quantitative predictions feasible for these filtration technologies.

For relative concentrations of $C/C_{sat} < 0.01$ – 0.05 (submonolayer conditions), adsorption of sparingly soluble species such as phenol and its derivatives from aqueous solution, by activated carbons, can be described by a modified Dubinin–Radushkevich–Kaganer (DRK) equation (Equation 3.20), replacing relative pressures with relative concentrations and the exponent n set to ~ 3 – 4 . Phenol and 3-chlorophenol are adsorbed as monolayers by both porous and nonporous carbons, displaying basic surface properties at pH lower than that for dissociation of any individual compound. In the case of sparingly soluble species, N_{am} (Equation 3.21) is related to the monolayer capacity of the walls of the micropores and not to the filling of them, as opposed to adsorption from the vapour phase. Indeed, the sorptive capacity of a microporous carbon is usually smaller from dilute aqueous solutions, than from the vapour phase. The principle of temperature invariance, assumed by Dubinin, for micropore filling also applies for adsorption from dilute solutions, as the parameters of n and E_s were observed as constant over a range of 293–303 K for single adsorption of a variety of organics. Hence, in comparison with the Langmuir model and other theoretical

expressions, this approach allows predictions for a range of concentrations and temperatures on the basis of simple physico-chemical properties of the adsorbent and the adsorbate.

Chlorinated hydrocarbons and aromatics are the major volatile organic compounds (VOCs) that contaminate groundwater and industrial wastewaters; adsorption of dichloromethane, as representative of VOCs, and toluene, as a typical aromatic volatile organic compound, was recently tested on a commercial GAC [191]. The adsorption isotherms were measured at different temperatures and below the organics species solubility in water. The maximum adsorption capacities of dichloromethane and toluene by GAC were 4 and 0.2 mol/kg, respectively. Organics removal from the solution was fast in the first 30 min and then very slow, for both the compounds; the uptake increased with increasing temperature, which confirms the sorption of dichloromethane and toluene to be an endothermic process. The experimental data obtained were compared with different equilibrium isotherm equations, with the Langmuir isotherm (Equation 3.9) found most suitable to represent dichloromethane uptake, while the Langmuir-BET hybrid isotherm (Equation 3.22) better fits the toluene data.

$$q = \frac{q_m b C_e}{1 + b C_e} + q_{max} K_{BET} C_s C_e / ((C_s - C_e) [C_s + (K_{BET} - 1) C_s]) \quad \text{Equation 3.22}$$

where C_e is the equilibrium concentration of the adsorbate (mol/L), q_e is the amount of adsorbate adsorbed per unit weight of the adsorbent (mol/kg), q_{max} and b are the Langmuir isotherm constants related respectively to maximum adsorption capacity and energy of adsorption, K_{BET} is the BET isotherm model parameter and C_s is the saturated solubility of the compound in water. Matlab 7.5 was employed to obtain isotherm equation parameters through a nonlinear fit of the experimental data (Figure 3.8).

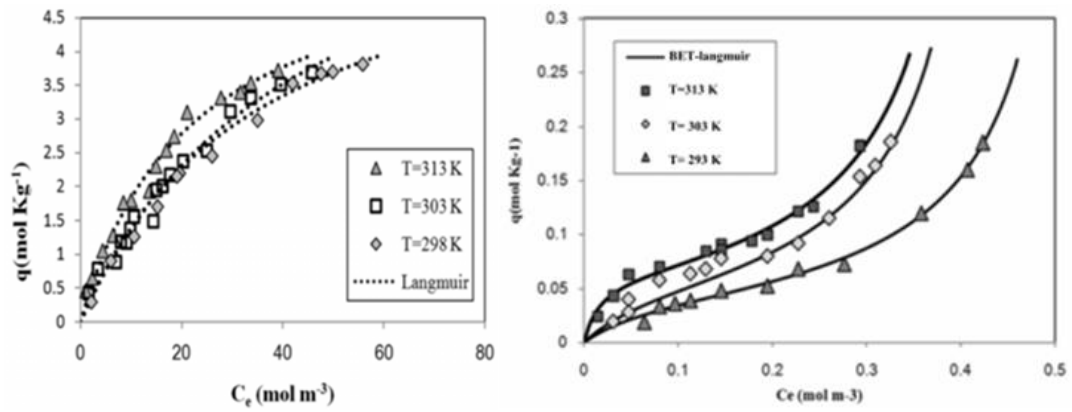


Figure 3.8: Adsorption isotherms of dichloromethane (L) and toluene (R) on GAC at T:298 K, 303 K and 313 K [191]. Symbols = experimental data, line = model.

For solution concentrations $< 25\%$ of the aqueous solubility of benzene and toluene, activated carbon AC-F400 demonstrated higher sorption capacity than polymeric resins XAD4, XAD2 and solid poly(styrene/divinylbenzene) copolymer microspheres [192]. The AC-F400 isotherms are characterised by a sharp initial trend, followed by a nearly constant adsorption level (Figure 3.9).

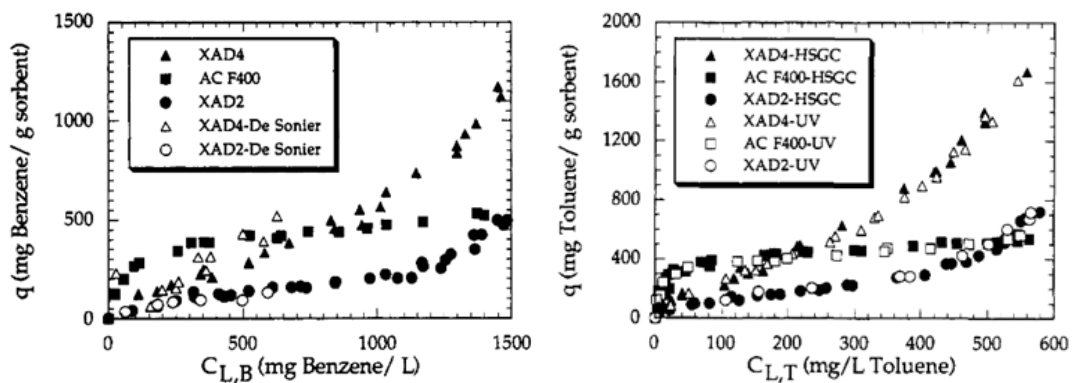


Figure 3.9: Benzene and toluene sorption at 298 K [193].

Sorption capacities q of benzene and toluene at: $C_{eq} = 0.1 C_{sat}$ were determined experimentally as 320 and 340 mg/g, respectively. The Polanyi potential correlation plot, shown in Figure 3.10, predicts the ‘adsorption volume’, as the potential tends to zero (i.e. $C_{eq} \rightarrow C_{sat}$), to be $0.62 \text{ cm}^3/\text{g}$, which is close to the total pore volume for AC-F400.

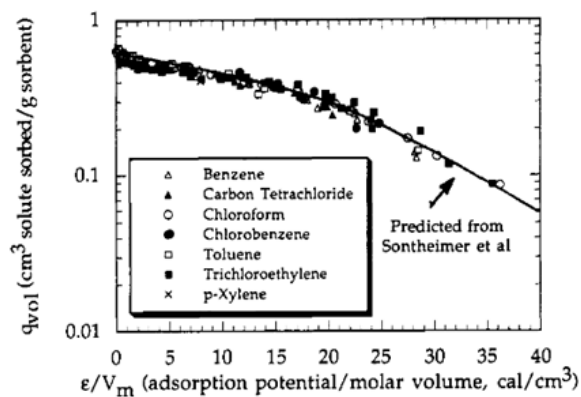


Figure 3.10: Polanyi potential correlation plot for AC-F400. The experimental data closely fits the predicted curve reported from regression analysis by Sontheimer [193].

The data also fitted the Freundlich isotherm, splitting the concentration ranges in different regions, a behaviour that is sometimes observed when a wide concentration range is analysed [193]; a Langmuir plot was also found to provide a good fit to the data over the entire concentration range ($R^2 = 0.984-0.988$). The monomolecular coverage (q_{\max}) was estimated for benzene, assuming a maximum radius of 3 \AA /molecule and circular coverage area, as 492 mg/g , quite close to q_m found from the Langmuir fit (528 mg/g).

The main surface area of activated carbons is due to microporous structure; the surface hydrophobicity determines their sorptive capacity towards many organic molecules and, thus, also of some EDCs, those with molecular size small enough to penetrate the micropores. Fine pore activated carbons, obtained from coal and peat, were confirmed as better sorbents than mesoporous carbons obtained from raw plant material. Increased contents of iron and other ash elements may have a positive influence on the maximum uptake, through enhanced chemisorption of active organic compounds like 3,4-DCA [66]. An aqueous solution of different pesticides and 10 mg L^{-1} of powdered activated carbon, with surface area $\sim 1000 \text{ m}^2/\text{g}$ and particle size $40 \text{ }\mu\text{m}$, was shaken for 5 min. The removal efficiency of 3,4-DCA (initial concentration 658 ng/L) was 70%, while complete removal could be obtained with preoxidation with ozone. [126]. To determine sorption isotherms, suspensions of activated carbon in aqueous 3,4-DCA were stirred at room temperature [66]. The Langmuir equation (Equation 3.9), indicative of monolayer

filling of the sorptive surface, adequately described the sorption isotherms, belonging to the 'L-type'[194].

3.2.3 Clay minerals

3.2.3.1 Introduction

Clay consists of crystalline particles, each of them constituted by aluminosilicates with eventual iron and magnesium substitutions by earth elements. Kaolinite and montmorillonite are clay minerals, part of the phyllosilicate group of minerals. Kaolinite: $\text{Al}_2\text{Si}_2\text{O}_5(\text{OH})_2$ is a layered silicate mineral, with a tetrahedral sheet of silica (SiO_4) linked by oxygen atoms to a sheet of alumina octahedra (AlO_6). The structure is shown in Figure 3.11.

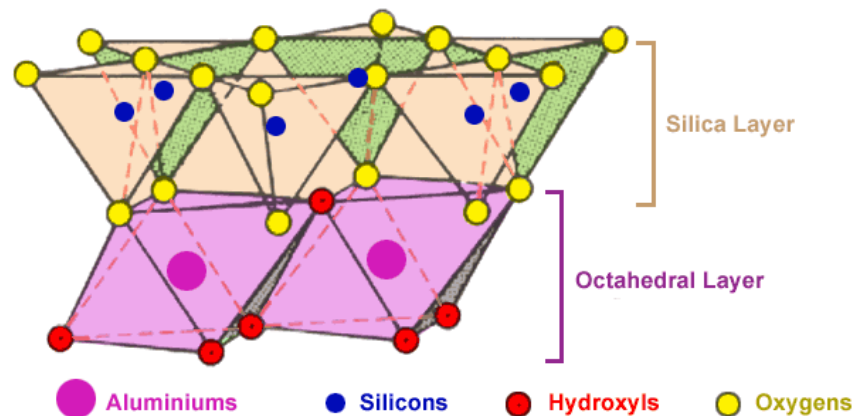


Figure 3.11: Kaolinite structure [195].

Montmorillonite structure consists of two sheets of tetrahedral silica with an interposed sheet of octahedral alumina (Figure 3.12). Its chemical formula is: $\text{Al}_2\text{Si}_4\text{O}_{10}(\text{OH})_2 \cdot n\text{H}_2\text{O}$. Montmorillonite can be transformed to halloysite under acidic conditions.

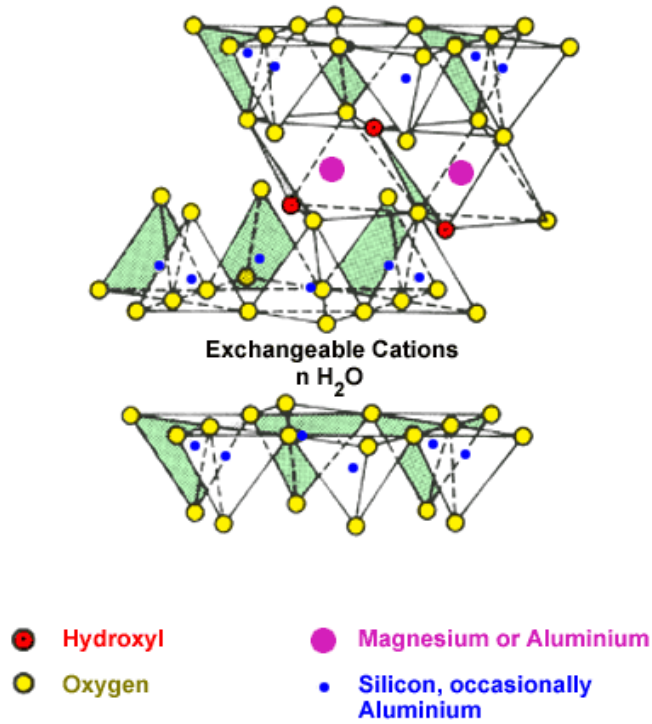


Figure 3.12: Montmorillonite structure [195].

3.2.3.2 Organics adsorption

Results for previous batch adsorption experiments in aqueous solutions of chloroanilines, conducted at pH ~5 with an acid activated halloysite [24], are shown in Figure 3.13. The experimental data were adequately fitted by a pseudo-second order kinetic model [196]:

$$\frac{t}{q_t} = \frac{1}{k_2 q_e^2} + \frac{1}{q_e} t \quad \text{Equation 3.23}$$

where: q_t (mg g^{-1}) is the amount of chloroaniline adsorbed at time, t ; k_2 ($\text{g mg}^{-1} \text{min}^{-1}$) is rate constant of the pseudo-second order adsorption and q_e (mg g^{-1}) is the amount of chloroaniline adsorbed at equilibrium.

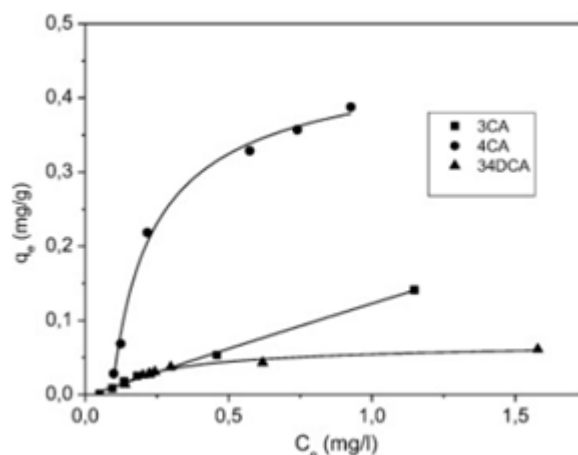


Figure 3.13: Adsorption isotherms of 3-chloroaniline (3-CA), 4-chloroaniline (4-CA) and 3,4-DCA on an acid activated halloysite, at 293 K and adsorption contact time of 24 h [24].

A ‘Weber–Morris’ plot: q_t versus $t^{0.5}$ confirmed that removal occurred via the fast diffusion of 3,4-DCA to the surface of the clay mineral in the first 180 min, before continuing as slower interparticle diffusion. The adsorption capacity of halloysite was lower for 3,4-DCA than for 3-DCA or 4-DCA. A semi-empirical Langmuir equation also effectively described the adsorption data (Equation 3.9). Additional adsorption experiments have been carried out with kaolinite (KGa-1) and montmorillonite (SWy-1) and standard solutions of 3,4-DCA, as well as other chloroanilines, at pH \sim 5 and \sim 9, respectively [11, 90]. At both these pH values, the organic pollutants are present as neutral species. Kinetic studies indicate an initial, rapid increase in chloroaniline retention and equilibrium was established in $<$ 4 d. Langmuir and Freundlich equations fitted the data appropriately [90]; however, the Langmuir plot showed a slightly better fit for montmorillonite, hence, the adsorption on this clay probably decreases as the surface sorption sites are saturated.

The chloroanilines studied in these previous works are mainly sorbed on the mineral surface of kaolinite, while the structure of montmorillonite allows swelling with sorption in the interlayer [197], as confirmed by studying the dehydrated clay [11]; after heating the distance between equivalent atomic planes d_{001} collapsed from 11 to 9.7 Å. X-ray diffraction results confirmed that chloroanilines can be adsorbed in the interlayer region of the mineral, with further evidence from X-ray analysis of the montmorillonite/3,4 DCA system (Figure 3.14). It was observed that kaolinite did not

release the pollutant during desorption experiments, while montmorillonite showed higher levels of desorption when the amount previously adsorbed was lower [90].

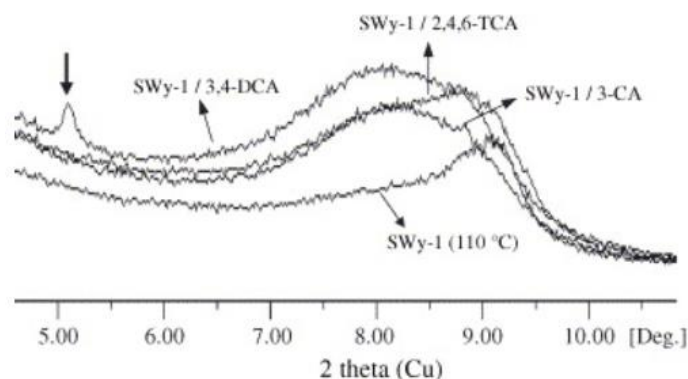


Figure 3.14: X ray spectra of dehydrated systems (393 K): Na-montmorillonite (SWy-1), Na-montmorillonite/3-CA, Na-montmorillonite-3,4-DCA and Na-montmorillonite/ 2,4,6-trichloroaniline. The d-spacing of Na-montmorillonite, also in absence of water, increases to ~ 1 Å. The small peak ($2\theta \sim 5.1$) in the spectrum of Na-montmorillonite/3,4 DCA, suggests the presence of clay particles with a higher level of swelling due to pollutant intercalation [11].

3.2.4 Periodic mesoporous organosilica

3.2.4.1 Introduction

Periodic Mesoporous Organosilica (PMO) are synthesised via a sol-gel process from organo-bridged alkoxy silanes with the support of structure-directing agents. The porous structures of PMOs consist of organic functional groups covalently bonded to siloxane groups (Si-O-Si) [198]. PMO development has attracted growing attention in recent years due to their ordered mesoporous frameworks, hybridised structures consisting of organic and inorganic fragments, and their varied morphologies, which can be selected to suit specific practical applications [199].

3.2.4.2 Organics adsorption

A PMO synthesised by condensation of 1,4 bis(triethoxysilyl)benzene under acidic conditions with a structure-directing agent (Pluronic P123), in the presence of KCl, has crystalline structure with hexagonally-ordered cylindrical mesopores. Adsorption tests were conducted [200], using 200 mg of adsorbent, 50 mL of aqueous solution

containing benzene, toluene and xylene (10 mg L⁻¹ each), stirred 24 h for adsorption batch tests by an orbital shaker device (200 rpm) at 295 K, gave data that was most appropriately fitted by a pseudo-first order kinetic model, which may be related mainly to physical adsorption [201]:

$$\log(q_e - q_t) = \log q_e - \left(\frac{k_1}{2.302}\right) t \quad \text{Equation 3.24}$$

where q_e and q_t are the amounts of BTX adsorbed (mg g⁻¹) at equilibrium and at any time t (min), respectively; k_1 (min⁻¹) is the rate constant of the process.

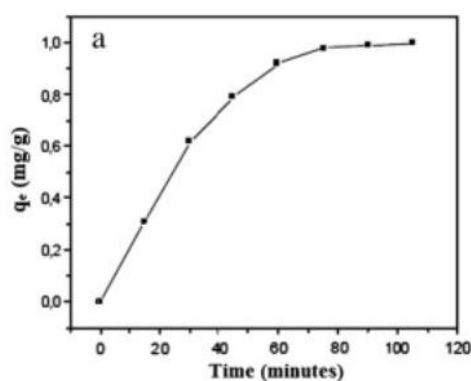


Figure 3.15: Kinetic plot showing equilibration time required for benzene adsorption on PMO [200].

Removal efficiencies were > 60%, except for benzene, where the adsorption efficiency was 44%. In all cases, removal efficiency was inversely related to solubility of the organic species in water, what may reflect the influence of this property on adsorption capacity, since the solvent attracts and surrounds the solute molecules, preventing them from being adsorbed [201]. In addition to high surface areas and large pore diameters, van der Waals interactions have a fundamental role in the adsorption of BTX onto PMO, mainly due to the displacement of electrons in the aromatic ring of the organic molecules, which may result in intense London dispersion forces between the solute and the adsorbent surface. Both Langmuir and Temkin models gave appropriate fits for adsorption isotherms of toluene; while Langmuir and Redlich–Peterson models adequately represented the data obtained for benzene (Figure 3.16).

The Redlich–Peterson equation is expressed as follows:

$$q_e = k_{rp}C_e/(1 + C_e^b a_{rp}) \quad \text{Equation 3.25}$$

where K_{RP} ($L\ mg^{-1}$), a_{RP} ($L\ mg^{-1}$) and b are the Redlich–Peterson parameters. This model incorporates the characteristics of Langmuir and Freundlich isotherms into a single equation (the Freundlich isotherm model takes into account both multilayer and heterogeneous adsorption).

The Temkin model accounts for the effects of indirect adsorbate–adsorbate interactions, which cause the heats of adsorption to more often decrease than increase with increasing coverage [202]. The Temkin model is based on the assumption that the decline of the heat of sorption is a function of temperature and not logarithmic, as assumed in the Freundlich equation.

The Temkin equation has the form:

$$q_e = B \ln(aC_e) \quad \text{Equation 3.26}$$

where the term B corresponds to RT/b ; T is absolute temperature (K), R is the gas constant, b is the Temkin constant related to the heat of sorption ($kJ\ mol^{-1}$), and a is the Temkin isotherm constant ($L\ g^{-1}$).

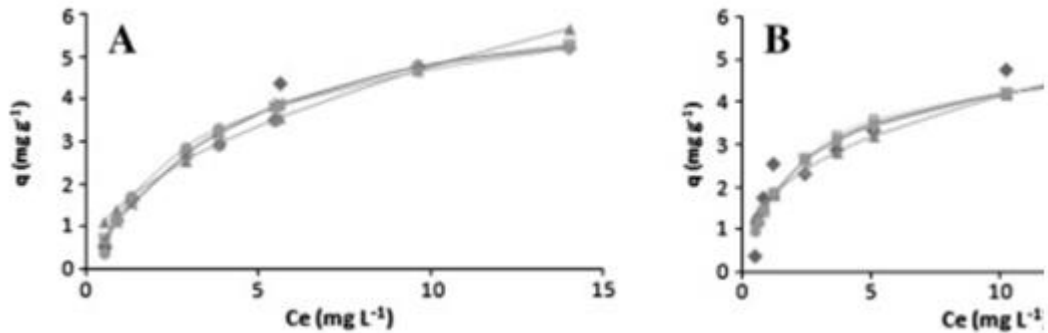


Figure 3.16: Adsorption isotherms of (A) benzene and (B) toluene on PMO with experimental values and related fits of Langmuir, Freundlich, Redlich Peterson and Temkin models[200].

The calculated values of q_{\max} , from Langmuir analysis, varied according to removal efficiency, with the exception of benzene, which had a higher q_{\max} and lower efficiency of removal at a concentration of 10 mg/L.

3.2.5 Amorphous mesoporous silica-alumina

Amorphous silica-alumina covers a wide range of synthetic amorphous molecular sieve materials; mainly used as catalysts or catalyst supports, they have also been successfully tested for the adsorption of non-dissociated contaminants with high molecular size, as a consequence of their wide pore openings, high pore volumes and large surface areas [203]. An amorphous mesoporous siliceous material, with narrow pore size distribution and a disordered arrangement of pores, was synthesised according to the procedure of Carati *et al.* [204] and tested for adsorption of benzene and toluene from water [203]. $\text{Al}(\text{iso-OC}_3\text{H}_7)_3$ was dissolved in an aqueous solution of tetrapropylammonium hydroxide, prior to the addition of $\text{Si}(\text{OC}_2\text{H}_5)_4$, the resulting sol was kept at 358 K for 3 h and the subsequent clear sol was transformed to an opalescent homogeneous gel by solvent evaporation. The so-synthesised material was extruded into a cylindrical shape, using alumina (Al_2O_3) as a binder. The characterisation of this material yielded a BET surface of $487 \text{ m}^2/\text{g}$, a pore volume of $1.04 \text{ cm}^3/\text{g}$ and an average pore diameter of 50 nm. Equilibria were established within 24 h for all batch tests; from the experimental data obtained (Figure 3.17), it is evident that a two-step adsorptive mechanism exists, with a change in the shape of the isotherms after Langmuir-type behaviour for concentrations $< 5\%$ of the solubility limit.

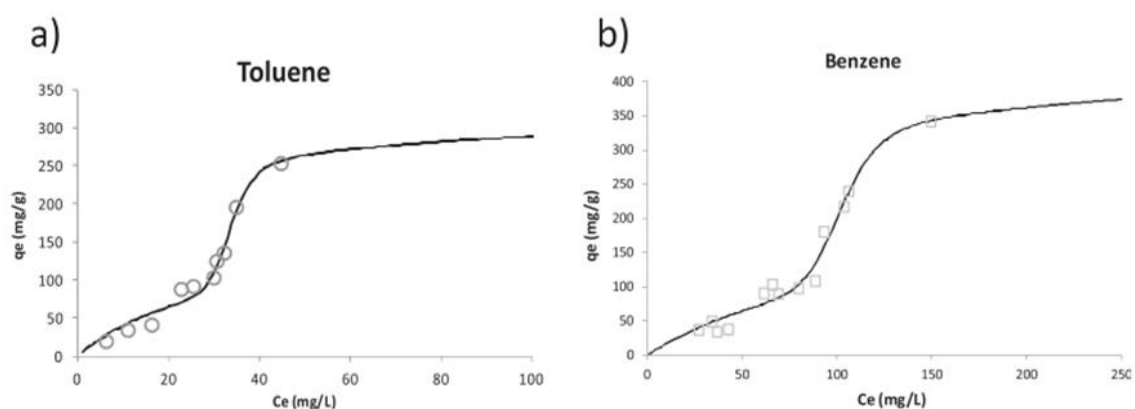


Figure 3.17: Adsorption isotherms of toluene (a) and benzene (b) on mesoporous silica-alumina [203].

The experimental isotherms were described using the hybrid model proposed by the Lee *et al.* [205], which is a combination of the Langmuir and Langmuir-Freundlich models (Equation 3.27); the Langmuir-Freundlich isotherm described the adsorption trend at higher concentrations.

$$q_e = q_{max} \left(\frac{k_1 C_e}{1+k_1 C_e} + \frac{k_s C_e^n}{1+k_s C_e^n} \right) \quad \text{Equation 3.27}$$

where q_e is the quantity of toluene (or benzene) adsorbed (mg/g), q_{max} is the maximum adsorbable quantity of the given species (mg/g), C_e is the equilibrium solution concentration (mg/L), k_1 is the Langmuir constant (L/g), k_s is the Langmuir-Freundlich constant (L/g) and n is a generic parameter related to the heterogeneity of the adsorption mechanism. The first step is related to adsorption of a complete monolayer on the mesoporous walls, in agreement with the Langmuir model, then adsorption continues with the formation of successive layers, until filling of the entire mesoporous channel is complete. Toluene exhibited the highest affinity in terms of kinetic constants, in both the Langmuir and Langmuir-Freundlich domains, which is probably due to the hindrance of free rotation of the toluene molecule by the substituent methyl group; benzene, by contrast, is more mobile molecule and, therefore, exhibits slower adsorption [206]. The maximum adsorption capacity (q_{max}) was, conversely, greater for benzene (450 mg/g) than for toluene (330 mg/g), which is likely due to the smaller molecular dimensions of benzene, which allows a greater number of molecules to adsorb within the pores of the material.

3.2.6 Silica aerogels

3.2.6.1 Properties and applications

Silica aerogels are amorphous materials with large surface areas (typically 250-800 m²/g), high porosities, low densities and conductivities, which can be successfully used as thermal insulators, catalyst supports, adsorbents, and in many other scientific and commercial applications [207]. Thanks to their very low thermal conductivities, of the order of 0.015 W m⁻¹K⁻¹ [208], they are already used as thermal insulators in the aeronautical and aerospace industries. The transparency and the transmittance of visible light by silica aerogels can be high and the scatter of transmitted light is low, resulting

in remarkable optical properties. With regard to mechanical properties, ageing and post-treatments can strengthen these materials, but compressive and tensile strengths, as well as elastic moduli, are generally very low.

The average pore diameter of these materials is usually between 20 and 40 nm, pore volume > 90% of their monolith volume, and densities < 2 g/cm³. Significant micropore volumes can be obtained by acid catalysis; by tuning porosity and hydrophilicity, silica aerogels can be used to adsorb gases or compounds dispersed and dissolved in water. They can also be used for the controlled release of medical drugs, fertilizers and phytosanitary products [209].

3.2.6.2 Sol-gel synthesis

Silica gels are synthesised by hydrolysing silicon alkoxide precursors (Figure 3.18), employing either acidic or basic catalyst [210]. The nanostructured solid network of SiO₂ aerogels is formed from a liquid solution (i.e. sol) as a consequence of a polymerisation process, with the creation of siloxane bridges between Si atoms [211]. Initially dispersed nanoparticles (size < 1 μm) or linear oligomers are formed, and these elements subsequently interlink, generating a 3D open network structure, called a ‘gel’. The transformation from sol to gel is known as the ‘gelation’ process and the reactions involved are hydrolysis and condensation. Different precursors can be used as the silica source; tetramethoxysilane (TMOS), tetraethoxysilane (TEOS) and methyltrimethoxysilane (MTMS) (Figure 3.18) have all been used as precursors of materials that have been tested for organics adsorption from water.

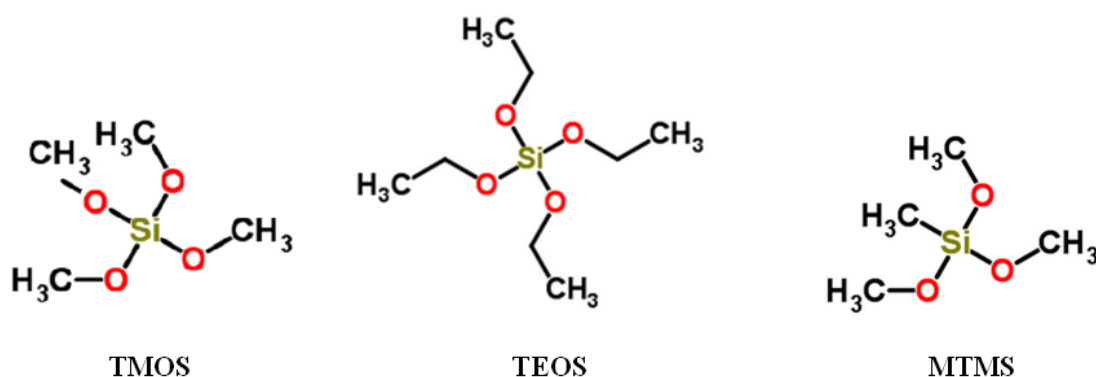


Figure 3.18: Silica alkoxides used as common precursors of silica aerogels.

Silica aerogels, with a texture similar to organic aerogels are obtained only if the hydrolysis rate is faster than the condensation rate; this can be guaranteed by the use of acid catalysis. Conversely, proton acceptors (bases) increase the condensation rate leading to the formation of denser gels. Variation of synthesis parameters can, thus, be used to tune particle size, pore size and distribution and density of the final product. Silica alkoxides are available as complexes in alcoholic solution; polymerisation is obtained by the use of an organic solvent with simultaneous hydrolysis, polycondensation of water and polycondensation of the alcohol (Figure 3.19). Hydrolysis starts with a nucleophilic attack of an oxygen lone pair (i.e. the pair of valence electrons of the oxygen not shared with other atoms) of a water molecule on a silicon atom. The existing Si-O bond is polarised, thus the silicon atom holds a partial positive electronic charge, which determines the rate of nucleophilic attack and kinetics of the entire hydrolysis step [211].

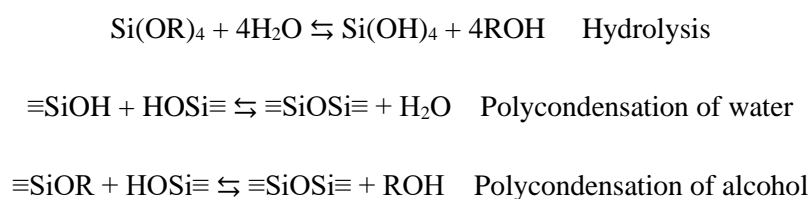


Figure 3.19: Polymerisation of silica alkoxides.

3.2.6.3 Ageing and drying

The aim of an ageing step is to reinforce the solid skeleton obtained during the gelation process, through the modification of the liquid phase present in the pores. The average pore size and the apparent density both increase during the ageing phase; furthermore, supplementary condensation and dissolution, or re-precipitation, of silica may occur. The kinetics of ageing are determined mainly by pH and the nature of the solvent [211].

Si-O bonds are usually 50% ionic and 50% covalent; the covalent character makes silica gels more resistant to evaporative effects than other oxide gels. However, capillary stress is expected to occur during pore liquid evaporation, when gas-liquid menisci are present at the pore boundaries. Capillary stress and consequent shrinkage or cracking of the gel structure can be avoided by the use of supercritical drying, which is developed in organic solvents at their supercritical state or in supercritical CO₂. The former case

requires high temperatures, while the use of CO₂ to exchange the liquid in the wet gel pores (usually methanol or ethanol) is named as ‘cold supercritical drying route’, as the temperature used is slightly above 304 K.

3.2.6.4 Surface chemical modification

Further treatments can be applied to increase aerogel performance in the desired field of application. The network of silica aerogels is tailored mainly in the sol-gel step, but further post-treatments also determine their final properties. If untreated, silica aerogels are slightly hydrophilic, due to surface silanol groups ($\equiv\text{Si-OH}$) formed by residual alkoxy (RO-) and hydroxyl (OH-) groups. When applications require materials that do not absorb water vapour, hydrophobic silica aerogels are synthesised to incorporate nonpolar side functions, like $\equiv\text{Si-CH}_3$, into the gel surface (Figure 3.20).

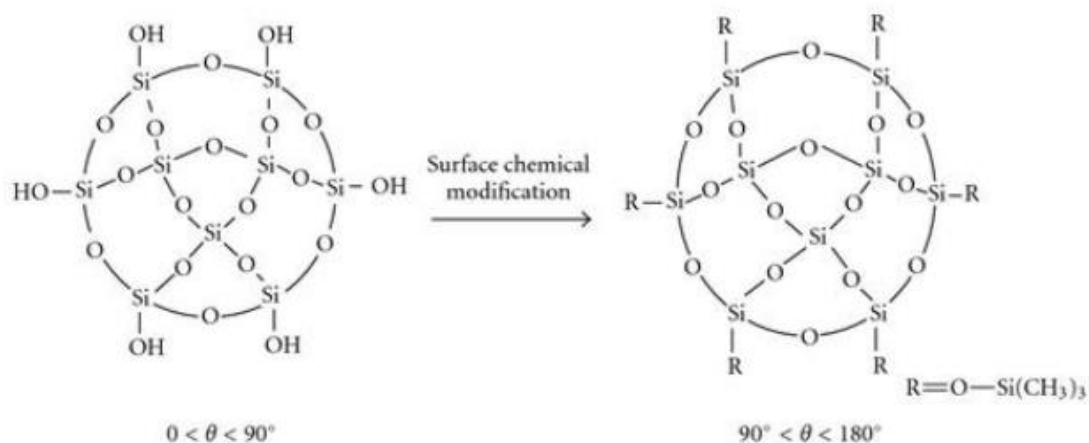


Figure 3.20: Hydrophobisation of a silica gel [210].

3.2.6.5 Organics adsorption

Aerogels have been studied extensively for the absorption of oil spills [212-215]; however, despite their adsorption potential for organic species, they have not been used in water treatment plants for the separation of organic pollutants. Some researchers tested these sorbents on crude oil-water mixtures and showed that functionalisation with fluorinated organic groups allows the highest levels of hydrophobicity to be achieved, hence, the best performance in terms of organic adsorption from pure oil or oil-water mixtures [212, 216]. Silica aerogels have been shown to absorb pure organic

compounds, such as benzene and toluene, to levels in excess of 13 g/g aerogel [217]. These high uptakes are mainly due to the resulting swelling of the adsorbent. Researchers reported a $\text{CF}_3(\text{CH}_2)_2$ - functionalised aerogel powder capable of absorbing up than 230 times its weight in oil [213], while further studies showed that such doped hydrophobic materials can adsorb > 30 times the volume of toluene compared with Granular Activated Carbon (GAC) [216].

Other authors verified the performance of aerogels for the adsorption of the most representative dissolved organics in produced water. Silica gels, synthesised using TMOS as the precursor, were modified by replacing the Si-OH groups, responsible for the adsorption of water, with Si-CH₃ groups via addition of MTMS and trimethylethoxysilane (TMES). Adsorption tests on the subsequent gels revealed maximum benzene adsorption capacities 300 times higher than GAC [218], with equilibrium established in < 30 min. The solvent fills the available volume of the adsorbent, which swells, leading to a volume larger than that of the original aerogel.

An issue with these past studies is that many work at excessive concentrations of organic species within the aqueous phase; whereas produced water, at the refining stage, contains only low concentrations of dissolved oil droplets, mainly part of the BTEX group (benzene, toluene, ethylbenzene and xylene). There have been limited studies into the adsorption behaviour of hydrophobic and hydrophilic silica materials towards trace quantities of aqueous phase organic species, presenting a gap in the current knowledge base.

It has been proven that for aqueous solutions of benzene and toluene, activated carbon and polymeric resins give better performance than functionalised aerogels [217]. Previous work compared benzene adsorption isotherms, using aerogel materials, an activated carbon and a polymeric resin, at similar concentrations, and no free oil phase present in the batch tests; the results, presented in Figure 3.21, showed that greater amounts of benzene and toluene were adsorbed from aqueous solution using activated carbons or polymeric resins rather than functionalised aerogels [217]. At aqueous concentrations of benzene at one tenth of its solubility limit, polymeric resin XAD2 and activated carbon ACF400 were shown to adsorb more than 60 mg/g and 300 mg/g of benzene, respectively [192, 217], as shown in Figure 3.21.

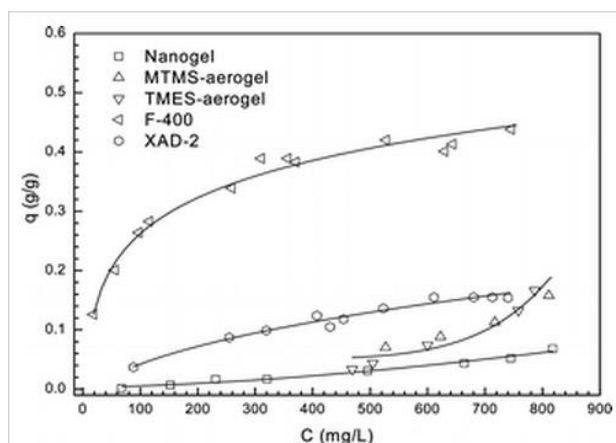


Figure 3.21: Comparison of isotherms obtained for benzene adsorption from aqueous solution onto aerogel materials, activated carbon (AC-F400) and a polymeric resin (XAD2). The concentration ranges used for the materials are similar (20-820 mg/L) [192, 217] and all below the solubility limit.

Hydrophobic silica aerogel ‘Nanogel’ TLD 301 with trimethyl-silyl ($-\text{Si}(\text{CH}_3)_3$) surface functionalities, was tested by Standeker *et al.* for the adsorption of organic compounds from solution phases, with adsorbate concentrations in water below the solubility limit. Equilibrium was reached in < 20 min and the adsorption capacities, derived from Freundlich isotherms, were 87 mg/g for benzene and 223 mg/g for toluene [217]. Recently, aerogels, obtained using MTMS as a precursor and dried supercritically, were shown to adsorb > 50 mg/g of benzene at an aqueous concentration of 50 mg/L, which is actually the most significant result at such a low concentration [219].

3.2.7 Sodium silicate based xerogels

3.2.7.1 Introduction

When the liquid from the gel is removed by evaporative drying, the solid material remaining is called a xerogel. Common precursors of silica gels, like TEOS and TMOS, are costly. Moreover, supercritical is a drying procedure with high energy requirements. The use of sodium silicate, also known as ‘waterglass’, as a precursor and ambient pressure drying (APD) is the most promising route for the production of cheaper xerogels with porosities and surface areas comparable to silica aerogels. Sodium silicate is synthesised from quartz sand and sodium hydroxide or sodium carbonate, reactants with high abundance in nature; it is the cheapest industrial silica source. It easily

dissolves in water, thanks to its polarity, which is due to Si-O^- and Na^+ ion pairs, it has no flammability hazard as is the case for TEOS and TMOS, and its stability allows long-term storage. Another cheaper precursor could potentially be rice husks from agricultural waste; silica gels were successfully prepared from this source both by supercritical drying [220] and evaporative drying at atmospheric pressure [221, 222].

Ambient dried silica gels can be obtained by:

- gelation, solvent exchange and hydrophobisation;
- co-precursor method: the functionalisation agent is introduced with the waterglass during gelation.

The rate of synthesis can be increased by:

- combined solvent exchange and hydrophobisation;
- ageing undertaken in a water/alcohol mixture.

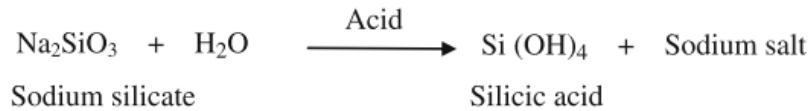
3.2.7.2 The sol-gel route: neutralisation and condensation

The gelation of a waterglass solution can be induced by:

- use of an ion exchange resin and addition of a base;
- addition of an acid.

The first method employs an ion exchange resin to replace sodium ions (Na^+) with protons (H^+); gelation is then induced with the addition of a base. The addition of a Brønsted acid, able to donate an H^+ to a base, modifies the pH of the solution, lowered to a range from 5 to 9. The so-called ‘acid catalysis’ is a single step process, with partial neutralisation of the sodium silicate. The silica gel is formed through neutralisation and condensation. When sodium silicate is used as precursor, the addition of H^+ by acid catalysis leads to a partial protonation of Si-O^- centres and the partial neutralisation of sodium silicate initiates the condensation of the solution. Larger silica polycondensates or colloidal silicate particles form and the 3D-gel network can grow only after the formation of free Si-OH and by overcoming the electrostatic repulsive interactions amongst silica species.

Hydrolysis



Condensation

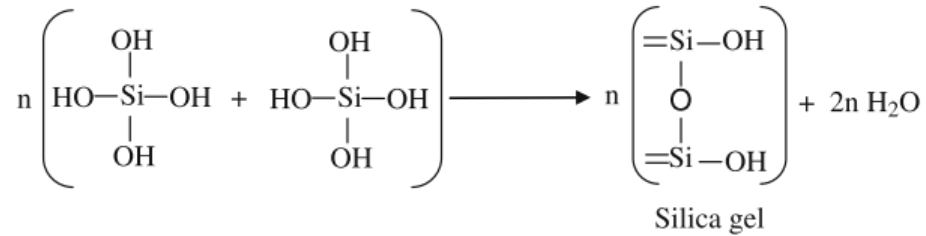


Figure 3.22: Hydrolysis and condensation of a waterglass solution, catalysed by acid addition.

At $\text{pH} > 10$, where sodium silicate is the prevalent species, the negative charges of Si-O^- groups prevent the coming together of silicate ions; furthermore, there is strong competition between condensation and dissolution. Condensation amongst Na_2SiO_3 molecules, or between Na_2SiO_3 molecules and free silicic acid molecules (Fig 3.23 B), is also not favourable from an entropic perspective (two molecules forming one species). On the other hand, at low pH , the rate of polycondensation slows as a result of the lack of Si-O^- groups, primarily a consequence of the fact that they are better nucleophiles than free Si-OH . For these reasons, condensation and, thus, gelation of silica happen most likely at pH values between 5 and 9 [211].

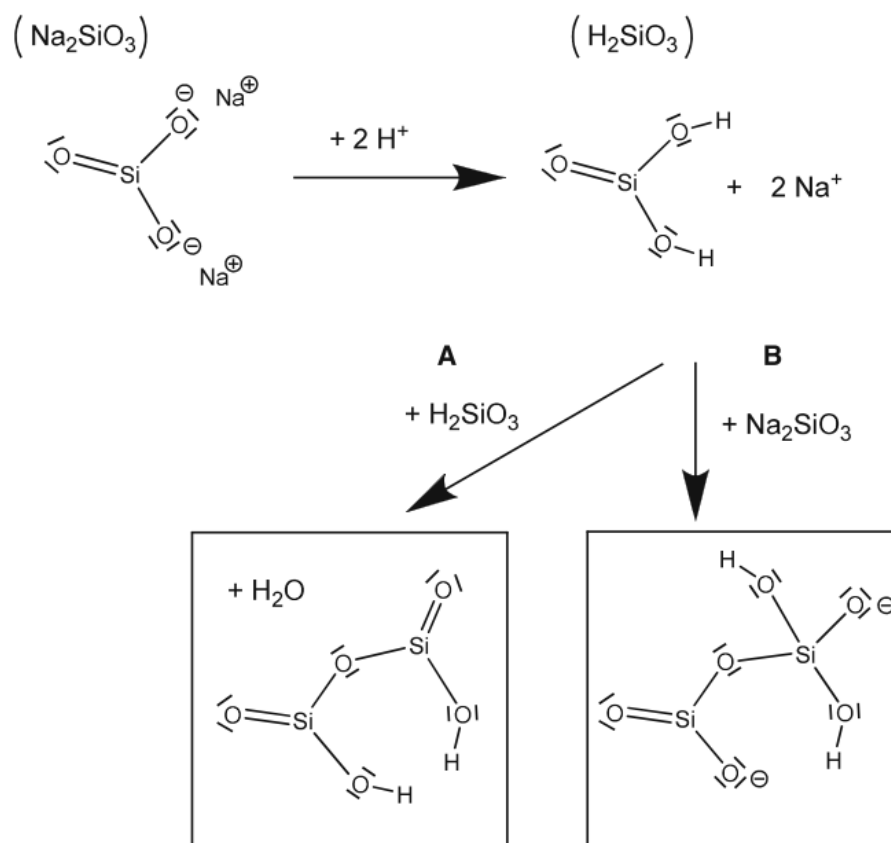


Figure 3.23: Neutralisation of sodium silicate to silicic acid and subsequent reactions with (A) silicic acid or (B) sodium silicate [223].

3.2.7.3 Washing and solvent exchange

Sodium silicate xerogels are synthesised in aqueous solution, while alkoxy-derived silicate gels are synthesised in alcoholic media. The former gels are washed with water, to remove Na^+ ions to strengthen the structure, and then water is exchanged with an alcohol prior to functionalisation. Washing, solvent exchange and functionalisation can be combined in a single step, which is less time consuming than the three procedures in series. However, due to the reactivity of functionalising agents like trimethylchlorosilane (TMCS, shown in Figure 3.24) or hexamethyldisilazane (HMDS) with free hydroxyl groups, large amounts of functionalised agents are consumed by reaction with water or alcohol [223]. Hence, combined procedures can be advantageous at laboratory-scale, but not for industrial processes.

3.2.7.4 Functionalisation

During evaporative drying (the last step of xerogel synthesis) most silanol groups condense, due to the presence of residual alkoxy and hydroxyl groups, but a silanol surface coverage is still present at the end of the drying procedure, making untreated xerogels slightly hydrophilic. The networks of untreated silica aerogels and xerogels collapse during drying, due to capillary pressure related to surface tension and viscosity of the pore liquid, drying rate and wet gel permeability [211]; this can be controlled through hydrophobisation, for both alkoxide silica aerogels and waterglass-derived xerogels. Surface modification of sodium silicate xerogels introduces non-polar alkyl groups, which replace silanol groups on the gel surface, as shown in Figure 3.24. Alkyl groups interact with the organic solvents used during the ambient drying procedure, reducing capillary stresses.

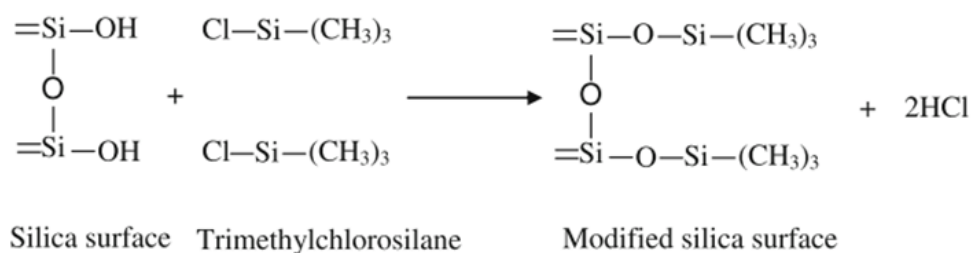


Figure 3.24: Functionalisation of a silica xerogel with TMCS [223].

Functionalisation consists of grafting silylating agents, such as TMCS or HMDS onto surface hydroxyl groups of the wet gel, introducing hydrophobic chemical moieties. These organosilane compounds are immiscible with water. Furthermore, they tend to react with water, consuming the functionalization agent. Thus, if water is present in the aerogel pores, functionalisation of the silica surface is impossible. For this reason, water must be exchanged with an organic solvent prior to any functionalisation procedure.

Furthermore, hydrophobisation is fundamental in preventing the deterioration of these materials if exposed to humid air or immersed in water. Indeed, if the pores of the virgin aerogel or xerogel are filled with water, the evaporation of water corresponds to a second drying cycle with consequent partial collapse of the structure.

3.2.7.5 Final drying

Drying of gels from the organic solvent phase is first performed at a temperature of 293-323 K, up to 2 d. The gels are further dried for 1-2 h at temperatures ranging from 423 K to 473 K. This step, consequently, incurs higher energy penalties.

3.2.8 Promising low-cost, raw sorbents

Sugar beet pulp, corncob, corncob char, perlite, vermiculite and sand have been recently studied for the sorption of 3,4-DCA from aqueous solutions at pH 4.8 [100]. These sorbents may be used in field conditions, so it is fundamental to understand the sorption behaviour in different matrices. Liquid matrices contain cations and organic matter but, except for corncob, no significant differences were observed in the maximum uptake of 3,4-DCA between pure water and run off water. The mechanism of sorption was satisfactorily described by the Freundlich isotherm model, with highest sorption obtained for corncob char (99% removal) and sand (86% removal). Further investigations are required to verify the adsorption capacity of low cost materials in field conditions, encouraged by the discovery that sorbents such as sand could offer > 50% removal of 3,4-DCA even in sediment extract media.

3.2.9 Ligand exchange

With regard to ligand exchange processes, polymeric chelating resins can selectively remove target contaminants but eluate recycle, regeneration of depleted adsorbent, and the high cost of transition metals used as complexing ions in the ligand are still significant obstacles to commercial applications in wastewater treatment. The possibility of recovery of aromatic amines at low concentration from water has already been demonstrated with chelating resin-bound cobalt ions [224]. A mini-column apparatus with Co(II)-CDAE-sporopollenin resin was also tested for adsorption of chlorinated anilines and the Langmuir model was found to effectively describe adsorption of 2-chloroaniline, 4-chloroaniline and 2,5-dichloroaniline [26]. The lower, similar values of the maximum adsorption capacity (q_m) for the binding of 2-chloroaniline and 4-chloroaniline, compared with 3-DCA and 2,5-DCA, onto the Co²⁺ matrix raise the hypothesis that both electrical forces and steric hindrance are involved. This conclusion is supported by the inductive effects of *o*-Cl and *p*-Cl atoms

and by the nature of these ligands, which contain sterically hindered and charged groups. Moreover, steric hindrance around the amino nitrogen weakens binding to the metal ions and causes a faster migration of these pollutants [225]. The adsorption of 3-chloroaniline was better represented by the Freundlich model, probably due to a more complex type of binding than the independent and univalent binding described in the Langmuir model.

4 Column adsorption tests

It is notable that the majority of previous work on adsorption of organics from aqueous phase has been limited to batch tests, which fails to fully assess the feasibility of the materials developed as sorbents in the type of apparatus commonly used in water treatment plants.

Column breakthrough experiments are crucial in identifying sorbent capacity, allowing estimation of material utilisation rate and treatment costs. The first recorded breakthrough experiments employed non-sieved sorbents and high flow rates in order to guarantee the same empty bed contact times (EBCT) employed in treatment facilities, where long exposure times and large sample volumes are required. Such experimental regimes have not always been practicable, hence, advanced studies were subsequently performed using small (>100 g), mini (>5 g) and then micro (<2 g) columns. [226], while Rapid Small Scale Column Tests (RSSCT) were specifically developed to provide an estimate of the operative capacities of granular activated carbons [227]. The underlying theory behind RSSCT and all Micro-Column Breakthrough (MCRB) techniques is the appropriate scaling of hydrodynamic and mass transfer characteristics to small scale flow test column dimensions, assuming that the breakthrough curves would be similar to those of a pilot scale plant. Such tests mean that only minimal quantities of water and time are required to simulate pilot scale studies.

Similarity of operation to that of full-scale filters is assumed by the proper selection of particle size, hydraulic loading and empty bed contact time (EBCT) to be used in the small scale test. Hydraulic loading, or linear velocity, is the ratio between the flowrate applied (Q) and the cross-sectional area. The EBCT is defined as V/Q, where V is the volume of the adsorption bed. EBCT of RSSCT is determined by intraparticle mass transfer resistances; Equation 4.1 allows scaling between small and large column EBCTs [228]:

$$\frac{EBCT_S}{EBCT_L} = \left(\frac{R_S}{R_L}\right)^{(2-x)} = \frac{t_{SC}}{t_{LC}} \quad \text{Equation 4.1}$$

Where:

- $EBCT_S = EBCT$ small column;
- $EBCT_L = EBCT$ large column;
- $R_S =$ adsorbent particle size for small column;
- $R_L =$ adsorbent particle size for large column;
- $x =$ coefficient relating intraparticle diffusion to particle size;
- $t_{SC} =$ time required for small column to reach breakthrough (elapsed time);
- $t_{LC} =$ elapsed time large column.

If intraparticle diffusivities are assumed to be constant irrespective of particle size, i.e. the degree of spread of the breakthrough curve, which results from intraparticle mass transfer resistance in the small and the large column, are identical in relation to the column length, then x can be set as 0. The Reynolds number is used to predict the transition from laminar to turbulent flow; it is function of channel diameter, velocity, density and viscosity of the fluid, and it is used to scale similar but different-sized flow situations. The condition of constant diffusivity requires that the Reynolds numbers for the RSSCT and large-column be equal. The condition of constant diffusivity within a GAC column does not apply for the adsorption of large molecules, like humic and fulvic acids [228], and the minimum column diameter required to avoid channelling is 50 particle diameters [227].

$EBCT_{SC}$ can be determined from Equation 4.1, once the desired $EBCT_{LC}$ and R_{LC} are fixed; height and sectional area of the large column, as well as flowrate applied can be determined from the $EBCT_{LC}$ selected, once the desired hydraulic loading is established, usually between 5 to 20 m/h for full scale carbon adsorbers [229]. As a result of this scaled design, the number of bed volumes treated by the large scale column is assumed equal to the number of the bed volumes treated by the small column, which is given by the ratio between the elapsed time (i.e. bed life) t_{SC} of the small column and the $EBCT_{SC}$. The specific throughput of the full scale system is assumed to be equal to that of the small scale system, which is determined using the ratio of volume of water fed to the small column and the mass of adsorbent packed in the small column.

Additional improvements to MCRB methods have recently been proposed by Chang *et al.*, who simplified the procedure by using a low cost sampler, piping, fittings, and

pumps, to obtain data on the adsorption of phenol, methyl tert-butyl ether, and other organic pollutants on carbon [226]. In tandem with these improvements, sequential-injection analysis (SIA) has been shown to overcome the major disadvantages of flow-injection analysis (FIA), mainly related to complex manifold operations [230].

5 Research approach

5.1 Aims and objectives

This project aims to develop a sorbent suitable for the removal of organic pollutants from water. The use of such a sorbent will be investigated for the treatment of the outgoing flow from secondary treatment of produced water, focused on removal of dispersed hydrocarbons, mainly part of the BTEX group. Due to molecular similarities with the BTEX group, the developed sorbent will also be tested using selected Endocrine Disrupting Chemicals, to evaluate its application within drinking water plants and as a remediation technology for polluted groundwater.

The suitability of a material for water treatment would require:

- good uptake;
- low cost and environmentally friendly synthesis;
- easy regeneration options;
- suitability for use with existing remediation technologies.

The overarching aims of the project are:

- develop adsorbents by low cost and environmentally friendly synthesis;
- characterize the sorbents developed;
- verify the resistance of produced materials under stirring conditions;
- measure the uptake and rate of uptake of organics from water;
- evaluate the benefits of functionalising the materials produced;
- suggest promising fields of application for the sorbents studied;
- identify strengths and weaknesses of the experimental techniques used.

5.2 Technological choices

Chapter 2.1.7 reviews the current ‘state of the art’ of North Sea produced water treatments; in a separate literature review all of the technologies used in other countries were also explored to inform this work. In many areas, tertiary treatments are already a common feature within treatment plants, either providing water suitable for re-use options, or to comply with stringent requirements for re-injection or discharge. As

shown by Figure 5.1, the standard layout of North Sea plants does not include tertiary treatments, but future legislation will likely require some developments.

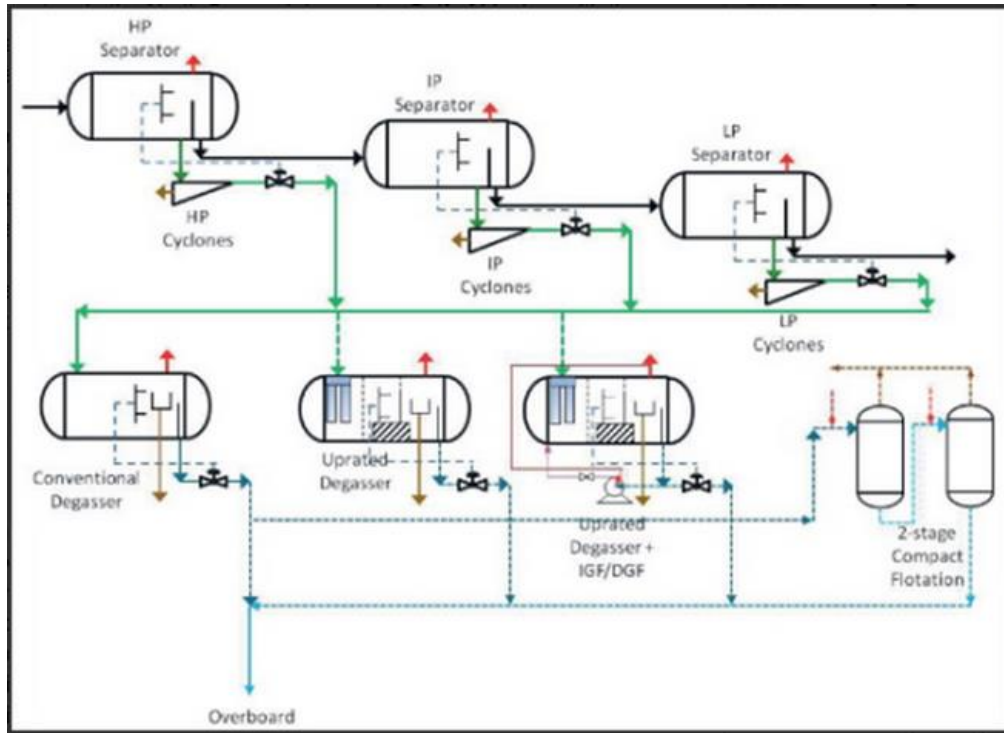


Figure 5.1: Diagram showing a typical North Sea process line up for produced water treatment [231].

Re-use is most common on-shore and in water-stressed countries, but there is debate over whether re-use on-board offshore facilities is an option. Produced water volumes are at least four times those of the oil extracted, so water always requires re-injection and/or discharge. North Sea fields need to purify the water before discharge or reinjection; they also have the option to update hydrocyclones and flotation units to satisfy European standards. Nutshell filters or membranes are the best available tertiary treatment options if re-injection must be made in hard reservoirs. Concentration limits will undoubtedly be reduced further in future, hence, plants may choose to adopt the same technologies that they use for the re-injection for refining treatment, with membranes shaped not for the separation of suspended solids but rather to achieve enhanced removal of dissolved oils. Based on analyses of North Sea plants and by comparison of the technologies examined in Chapters 2.1.6 and 2.1.7, it can be

concluded that, where tertiary technologies are applied, filters, membranes and electrochemistry are the most promising methods.

With regards to membranes, it has been proven that ceramic membranes are more advantageous than polymeric ones (as discussed in Chapter 2.1.6.3). Recent studies on membranes have focused on improving their wettability, creating superhydrophilic and superoleophobic surfaces, as hydrophilic surfaces are less prone to fouling than hydrophobic layers. This raises the issue of where to position membranes within a treatment system and the answer, within a typical North Sea configuration, is after the hydrocyclones and flotation units. In comparison with nutshell filters, treating the same input concentration, the advantages of membranes are lower oil output and greater fluxes treated in the same space. Disadvantages are high capital costs and energy requirements to produce the operating pressure and for cleaning. Hence, research projects related to membranes in the final treatment of produced water could be based on the following targets:

- low cost material;
- low fouling;
- low pressure treatment;
- long life cycle;
- tests with real produced water under similar process conditions (this represents a significant gap in the literature).

With uses in filtration and as adsorption media, nutshell filters have had the greatest diffusion into offshore fields in recent years; they can reduce the concentration of dispersed oil from 20-50 ppm to 2-5 ppm. Proposing other media in place of nutshell filters, to treat the output of gas flotators and meet actual standards of discharge or to re-injection in the reservoirs, is inconvenient. Nutshell filters dominate over other adsorption technologies, at the tertiary step of treatment, due to their simplicity and low cost, as discussed in Chapter 2.1.6.1. The cost to reduce concentration to < 10 mg/L using organoclay is prohibitive. Activated carbon is typically employed in large pressurised vessels; compared to organoclay, it does not adsorb as much organic material per unit volume. GACs exhibit disadvantages including slow kinetics and < 100% working capacity [218]. This means that larger volumes of activated carbon are

needed to remove the same amounts of organic materials removable with organoclay. As a consequence of the stringent space requirements of offshore platforms, activated carbon is rarely used and does not guarantee better efficiency than nutshell filter.

Table 5.1: Data summary for single units for produced water treatment [143].

Technology	F_d (m/h)	F_r (h ⁻¹)	C_{in} (mg/L)	C_{out} (mg/L)	% (rem)	Min. drop dia. (µm)	No. data
<i>Onshore</i>							
API gravity separator	4.4	1.1	5000–20,000	50–100	80–90	150	1
Corrugated plate interceptor (CPI)	6.5–14	3.2	5000–20,000	40	90–98	20–40	2
<i>Offshore</i>							
Hydrocyclone (HC)	100–440	450	–	20–80	90–95	12–20	4
Induced gas flotation (IGF)	2.4–16	4–15	200–500	25–50	90–95	10–25	21
Compact flotation unit (CFU)	45–90	–	200–500	15–25	90–95	10–25	2
<i>Onshore/offshore</i>							
Nutshell filter (NSF)	27–37	13–24	20–50	2–5	99	2	2
Crossflow membrane filter (CMF)	312	136	20–50	~0	99	<1	3

Proposal of an adsorption based technology to completely replace combined hydrocyclones and gas flotators is inadvisable, due to the high efficiency and small footprint of the latter; however, it should be possible to propose an adsorbent media that is able to act as a tertiary treatment downstream to hydrocyclones, replacing induced gas flotators to guarantee an outflow concentration < 10 ppm. Such technology could act as a pre-treatment for a final membrane configuration, to reach the ‘zero discharge prospective’. This material could work in a single bed reactor or in a filter configuration (with other layers or filters in series of sand, gravel and nutshell).

Referring to Table 5.1, the ‘window of feasibility’ of the proposed technology should be: ~80-10 ppm. The developed material could significantly lower the amount of energy

required to run the hydrocyclones to reach the best removal efficiency. At the same time, it could provide an oil concentration input to a cross-flow membrane, which is less than half of the maximum acceptability, reducing the fouling problem and the energy requirements for the backwashing of the membrane. This would result in an extended lifetime of the membrane, providing justification of the high capital cost of its installation to meet ‘zero discharge standards’.

5.3 Choice of the pollutants

Benzene and toluene were selected as the most representative of the dissolved hydrocarbons still present in the final stages of produced water treatments. Moreover, benzene is the lightest and, hence, the most difficult organic to adsorb amongst the soluble monoaromatics that are part of the BTEX group; this results from the fact that the solubility of the BTEX group decreases with molecular weight so, conversely, their adsorption potential increases with molecular weight [217].

A review of the presence and associated risks of Endocrine Disruptor Chemicals (EDCs) in water was conducted, and fewer than ten, from > 300 substances were judged worthy of consideration for batch adsorption tests with the synthesised aerogels; this selection was based on of the following factors:

- production and emission in the environment;
- toxicity;
- risk (hazard, vulnerability and exposure) for humans and aquatic environment;
- structural similarity with BTEX molecules (to permit interpretation of results compared to structural analogues);
- solubility and persistence.

Between the few substances identified from the criteria stated above, 3,4-DCA was selected as the representative EDC for study.

5.4 Choice of the adsorbent: filling the gaps

Aerogels and xerogels have previously been studied for absorption of oil spills, and these materials could find application as adsorbent materials in filter or membrane configurations for the removal of dispersed hydrocarbons. The adsorption of pure oils

by hydrophobic silica aerogels has already shown the suitability of these sorbents in oil spills. Only few studies have investigated the adsorption of organics from water below the solubility limit. No previous studies were identified that investigated:

- hydrophilic silica gels behaviour in the adsorption of BTEX in water below the solubility limit;
- application of hydrophobic silica gels from cheap precursor, room ambient pressure and low temperature synthesis in the removal of BTEX from water below the solubility limit;
- adsorption of EDCs from water by silica gels;
- with the exception of the Wang's work on Nanogel [217], all adsorption experiments related to the application of silica gels for organics removal from water were performed with powdered sorbents, so there is a lack of information with regards to kinetics and behaviour of the material in treatment plants (in which materials are expected to be employed in granular form);
- experiments on silica gel behaviour in a system closer to a filter or membrane application than a batch test on dissolved organics removal, e.g. microcolumn tests.

5.5 Methodology

This work focuses on adsorption of single aromatics from oil-water mixtures on synthetic amorphous silica, changing the synthesis parameters and verifying their influence on the materials developed by characterisation techniques. Once evaluated, appropriate concentrations for input and output of an application in produced water treatments can be used to test adsorption and mechanical performance via adsorption experiments in batch configuration. Moreover, breakthrough experiments will be conducted using 3D printed microcolumns fed by oil emulsion at constant flow rate, measuring the concentration of oil in the effluent at various time intervals using the analytic technique determined to be most reliable from a review of the literature.

6 Experimental methods

6.1 Synthesis of the adsorbents

6.1.1 Amorphous silica Quartzene

The adsorbent material initially tested was Quartzene, a synthetic amorphous silica provided by Svenska Aerogel AB. Six Quartzene based sorbents were used in the study, namely: ND, CMS Z1 and their methylated analogous NDH, CMSH and Z1H. The structure and the properties of these sorbents are comparable to silica aerogels: both have skeletal structures composed of porous silica, very low densities, and very low thermal conductivities. The only significant physical difference is that Quartzene is produced as a powder, not as a gel from a sol-gel process. Its chemical properties, in terms of hydrophilicity/hydrophobicity, can be tailored to fit a specific application and the porous structure can also be controlled, notably without the need of a surfactant. Unlike traditional aerogels, Quartzene is an environmentally friendly material, which is significantly cheaper to produce, as a result of the ambient pressure and temperature conditions used in its manufacture.

ND type Quartzene was prepared via the precipitation of sodium silicate with sodium chloride at ambient temperature. A defined amount of dilute active aqueous sodium silicate solution ($\text{SiO}_2:\text{Na}_2\text{O} = 3.35$) was prepared, representing solution A, while solution B was composed of aqueous sodium chloride (NaCl). Solutions A and B were mixed under rapid stirring and the resulting precipitate mixed with a defined amount of tap water, before vacuum filtration through a filter paper until a paste, comprising up to 85% water, was obtained and dried via spray drying. Z1 type samples were prepared using a method analogous to that for ND but with a different level of activation of the silica source [232].

CMS type Quartzene was prepared by adding calcium and magnesium sources at concentrations of 1:2 to the silica source (Waterglass $\text{SiO}_2/\text{Na}_2\text{O} = 3.35$). A 500 mL salt solution, consisting of MgCl_2 hexahydrate and CaCl_2 dihydrate was prepared at a ratio of 68 mol% Mg and 32 mol% Ca; 500 mL salt solution, was poured onto 1.5 M (with respect to SiO_2) sodium silicate solution (500 mL), and the resulting mixture agitated at

room temperature. Subsequent coagulation occurred, as previously described [233], and the obtained gel was washed, filtered and dried in the same manner as ND.

Furthermore, methylated versions of Quartzene, were developed by Svenska Aerogel AB, allowing direct comparison of adsorption uptakes and kinetics between hydrophilic and hydrophobic versions of the same base material.

6.1.2 Silica xerogels via Ambient Pressure Drying (APD) and low temperature synthesis

Silica xerogels were synthesised from diluted solution of sodium metasilicate, also known as waterglass (Na_2SiO_3). The commercial solution has the following formulation: $(\text{NaOH})_x(\text{Na}_2\text{SiO}_3)_y \cdot z\text{H}_2\text{O}$, $\geq 10\% \text{NaOH}$ basis and $\geq 27\% \text{SiO}_2$ basis. Commercial solution was diluted with distilled water to obtaining molar ratio $\text{H}_2\text{O}:\text{Na}_2\text{SiO}_3$ ranging from 80 to 130. Acid catalysis was performed by dropwise addition of citric acid 3M, 10% vol in 40 mL of diluted sodium silicate solution placed in 400 mL glass containers, manually stirred during the addition. Acid catalysis was also performed with HCl 3 M. The containers were then placed at room temperature or in oven at 323 K, covered or partially covered, for gelation and a first drying phase.



Figure 6.1: Samples of diluted waterglass solution immediately after acid addition (left) and 15 min later (right), placed in oven at 323 K.

Consecutive washing, solvent exchange and hydrophobisation were chosen to minimize the consumption of hydrophobisation agent (as explained in Chapter 3.2.7). 22-24 h after the acid addition, the dried gels were cut into small pieces (cubes of ~1 cm

dimensions) to speed up the exchange of sodium ions with distilled water; they were washed three times in 24 h (Figure 6.2, left). Water was then exchanged with methanol prior to functionalisation with a mixture 1:1:1 volume of hexane, trimethylchlorosilane and methanol, as reported by Uzma Bangi *et al.* [223]. Samples were placed in the oven at 323 K during washing, methanol exchanging and functionalisation; each of these procedures lasted ~24 h. Finally, curing for 1 d at room temperature and 1 h in the oven at 473 K completed the synthesis. Similar gels were then synthesised without functionalisation.

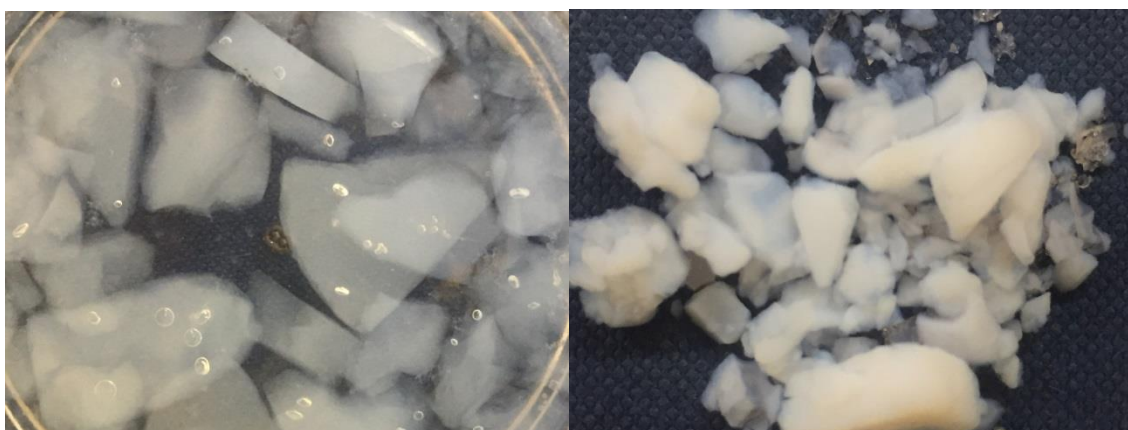


Figure 6.2: Silica gels during washing procedure (left) and after final drying in oven at 473 K.

The exchange procedures and discharge of the functionalisation mixture were performed in a fume cupboard. All reactants were purchased from Sigma Aldrich Ltd. The purity of the citric acid used was $\geq 99.5\%$, while chloric acid was bought as reagent grade, assay 37%. Methanol, hexane and TMCS used were all HPLC grade, $\geq 99.9\%$.

6.2 Characterisation

6.2.1 Surface area and porosity

6.2.1.1 Surface area: BET method

The BET method is commonly used to determine surface areas of adsorbents based on multilayer adsorption; it is based on the Brunauer –Emmett–Teller (BET) theory, introduced in Chapter 3.1.4.3, which describes the physical adsorption of gas molecules

on the surfaces of solids. The theory is an extension of Langmuir theory, moving from monolayer adsorption to a multilayer process, with the following hypotheses:

- the molecules of the gas physically adsorb on the solid in infinite layers;
- there are no interactions between the layers;
- the uppermost layer is in equilibrium with the gas phase, with similar adsorption and desorption rates;
- Langmuir theory is applicable to every layer.

The specific surface area of a material is evaluated by physical adsorption (van der Waals forces) of a gas, such as N₂, Ar or CO₂, on the surface of the material, followed by the determination of the gas amount related to a single monomolecular layer. BET experiments in this study were conducted using N₂ at 77 K.

The BET equation is expressed by:

$$\frac{p}{[n_a(p_0-p)]} = \frac{1}{n_m C} + \frac{C-1}{(n_m C) p_0} p \quad \text{Equation 6.1}$$

where:

- p and p_0 are the equilibrium and saturation pressures of the adsorbate, respectively, at 77.4 K, expressed in Pa;
- n_a is the amount of gas adsorbed (mol) at 273.15 K (standard temperature) and atmospheric pressure (1.013×10^5 Pa), which is equal to the volume of gas adsorbed divided by the molar volume of the gas (22.4×10^3 cm³/mol);
- n_m is the amount of gas adsorbed (mol) at 273.15 K that corresponds to monolayer coverage of the surface;
- C is the BET dimensionless constant, which is a function of the enthalpy of adsorption of the gas.

The BET value $p/[n_a*(p_0-p)]$ is plotted against p/p_0 to linearize the data (Figure 6.3); non-linearity is often obtained at p/p_0 values lower than 0.05 and close to and higher than 0.3, so the relative pressure range initially selected for the analysis is: 0.05-0.3.

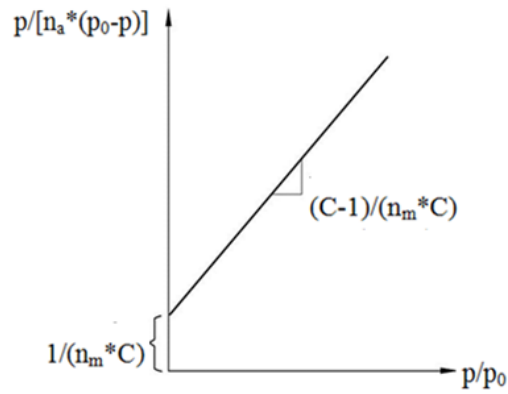


Figure 6.3: Example plot obtained using the BET isotherm model.

A linear regression analysis evaluates the slope and intercept:

- $n_m = 1/(\text{slope} + \text{intercept});$
- $C = (\text{slope}/\text{intercept}) + 1.$

The BET surface area is defined by:

$$S_{BET} = n_m N s / m \quad \text{Equation 6.2}$$

where:

- $N = \text{Avogadro's number } (6.023 \times 10^{23} \text{ molecules/mole});$
- $s = \text{adsorption cross section of the adsorbing species } (\text{cm}^2/\text{molecule});$
- $m = \text{mass of the adsorbent tested } (\text{g}).$

Small pores are filled more easily than larger pores, which are filled by increasing the pressure until the saturation point; a sample plot is shown in Figure 6.4.

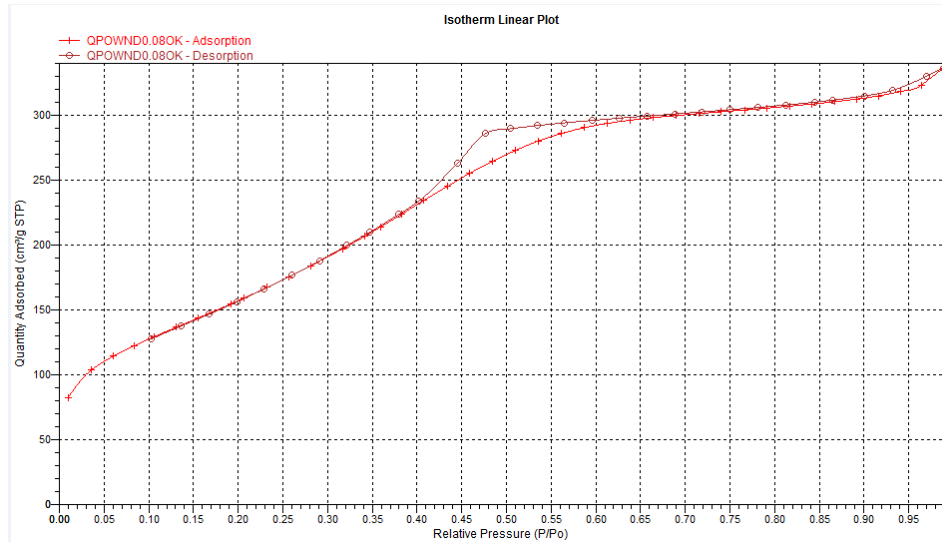


Figure 6.4: N₂ adsorption isotherm obtained at 77 K for an amorphous silica by Svenska AB. The plot shows the results directly displayed by the instrument software; the resulting BET analysis is always undertaken manually to correctly interpret the data.

6.2.1.2 Total pore volume

Once a N₂ monolayer is formed on the solid, by continuously increasing the relative pressure, capillary condensation occurs in the mesopores and, when p/p_0 is close to 1, the pores effectively contain liquid nitrogen. Hence:

$$TPV = \left(\frac{MQA}{V} * mw\right) / d_n \quad \text{Equation 6.3}$$

where:

- TPV = Total Pore Volume (cm³/g);
- MQA (cm³/g STP) = maximum quantity of N₂ adsorbed (at p/p_0 close to 1);
- V = molar volume of the gas at STP (22414 cm³/mol);
- mw = molecular weight of nitrogen (g/mol);
- d_N = bulk liquid nitrogen density (0.8081 g/cm³).

6.2.1.3 Pore size distribution: Barrett Joyner and Halenda method

The algorithm of the software of the Accelerated Surface Area and Porosimetry System (ASAP) 2020 used for the pore size distribution determination is an implementation of the Barrett, Joyner, and Halenda method [234], also known as the BJH method. The

desorption branch of the isotherm is used to relate the amount of adsorbate removed from the adsorbed core in a desorption step to the average size of pores emptied during that step. The dataset is then composed of relative pressure (p/p_0) and volume adsorbed (V_a) pairs from $((p/p_0)_1, V_{a,1})$ to $((p/p_0)_n, V_{a,n})$. Each data pair represents a desorption step boundary for intervals i to $i+1$, where n = total number of $((p/p_0)_i, V_{a,i})$ pairs. The BJH model applies only to the mesopore and small macropore size range and it considers a system of open ended, cylindrical pores that respond in the same way to changes in relative pressure of the adsorptive. At relative pressure $(p/p_0)_1$, equal to unity, all pores are filled with liquid. A first reduction in relative pressure will result in emptying the largest pore of its capillary condensate and in a reduction of the thickness of the physically adsorbed layer. The relationship between the pore volume of the largest pore P_1 ($V_{p,1}$) and the observed volume of gas desorbed lowering the relative pressure from $(p/p_0)_1$ to $(p/p_0)_2$, denoted as ΔV_1 , is:

$$V_{p1} = r_{p1}^2 / (r_{k1} + \Delta t_1)^2 \Delta V \quad \text{Equation 6.4}$$

where:

- r_{p1} is the radius of the largest pore;
- r_{k1} is the radius of the inner capillary;
- Δt_1 is the reduction of the thickness of the physically adsorbed layer.

Lowering $(p/p_0)_2$ to $(p/p_0)_3$ the volume of liquid desorbed comes from the smaller pore, denoted as P_2 and from a further thinning of the physically adsorbed layer left behind in the pore P_1 , denoted as $V_{\Delta t2}$:

$$V_{p2} = r_{p2}^2 / (r_{k2} + \Delta t_2)^2 (\Delta V_2 - V_{\Delta t2}) \quad \text{Equation 6.5}$$

$$V_{\Delta t2} = V \Delta t_2 A c_1 \quad \text{Equation 6.6}$$

where $A c_1$ is the average area from which the gas is desorbed. The same argument applies from $(p/p_0)_i$ to $(p/p_0)_{i+1}$ and the formula above can be generalised to represent each one of the desorption steps as:

$$V_{\Delta t_n} = \Delta t_n * \sum_{j=1}^{n-1} A c_j \quad \text{Equation 6.7}$$

where $A c_j$ is the area of each pore of size j (A_{pj}) multiplied by a coefficient c_j .

Generalizing the equation for V_{p2} above and substituting the previous equation for $V_{\Delta t_n}$ yields [234]:

$$V_{p,n} = \frac{r_n^2}{(r_{k_n} + \Delta t_n)^2} (\Delta V_n - \Delta t_n * \sum_{j=1}^{n-1} A_{pj} c_j) \quad \text{Equation 6.8}$$

It is probable that a very close approximation to the correct pore size distribution can be obtained by using a constant c value for any one adsorbent [234]. The formula above can then be re-written as:

$$V_{p,n} = \frac{r_n^2}{(r_{k_n} + \Delta t_n)^2} (\Delta V_n - c \Delta t * \sum_{j=1}^{n-1} A_{pj}) \quad \text{Equation 6.9}$$

The relationship between (p/p_0) and Δt was obtained from a plot of experimental data, but to make the Equation 6.9 useful, it is also necessary to adopt a relationship that relates p/p_0 to r_k and this is possible by computing values from the Kelvin equation [234]:

$$\log \left(\frac{p}{p_0} \right) = - \frac{2\sigma V}{8.316 \cdot 10^7 * 2.303 T r_k} = -4.14 / r_k \quad \text{Equation 6.10}$$

where:

- σ = surface tension of liquid nitrogen (erg/cm^2);
- V = molar volume of liquid nitrogen (cm^3);
- $8.316 \cdot 10^7$ = gas constant (erg/K)
- r_k = radius of capillary (cm);
- T = absolute temperature (K).

6.2.1.4 Microporosity

6.2.1.4.1 V-t curves

An adsorbate film covers an adsorbent with a defined density profile, but assuming that the film thickness is uniform, it is possible to obtain a statistical thickness t from gas adsorption isotherms. The thickness is expressed by curves obtained by plotting the ratio of the weight of gas adsorbed W_A on some non-porous adsorbents to the weight W_M corresponding to a monolayer formation, versus relative pressure values. Considering the monolayer as one molecule in depth, a t-profile is given from W_A/W_M (equal to the number of monolayers) multiplied by the adsorbate molecular diameter. With regard to nitrogen adsorption:

$$t = 3.54W_A/W_M (\text{\AA}) \quad \text{Equation 6.11}$$

where 3.54 Å is the monolayer depth, assuming that the film structure is close packed hexagonal [235]. The same equation can be re-written as a function of the volume of gas adsorbed V_{liq} and the total surface area S :

$$t = V_{liq}/S \quad \text{Equation 6.12}$$

where, with regard to nitrogen density ρ at standard pressure:

$$V_{liq} = V_{ads}(STP)\rho_{273\text{ K}}/\rho_{77\text{ K}} \quad \text{Equation 6.13}$$

Equation 6.12 for some nonporous adsorbents is represented by a straight line which intercepts the origin of the axes. Lippens and De Boer showed that for different non-porous siliceous materials the thickness of the adsorbed nitrogen layer at 77 K is independent of the sample [236]. From the Harkins-Jura equation they defined the following [237]:

$$t = \left[\frac{13.99}{0.034 - \log\left(\frac{p}{p_0}\right)} \right]^{0.5} \quad \text{Equation 6.14}$$

The thickness equation can be employed as a reference to estimate surface area, average pore size and pore volume of a material with similar composition and BET C constant. A plot of thickness versus volume of gas adsorbed, for the reference material, shows non-linear regions and a non-zero intercept, which results from differences between the isotherms obtained for the reference and sample. Where the t-plot is linear, the equation fits the experimental isotherm, but with a different slope, because the surface area is different; if the intercept is positive, it means that the tested sample is microporous. From Equation 6.12, using the slope (s) of the t-plot of the tested material:

$$S = s\rho_{273\text{ K}}/\rho_{77\text{ K}} \quad \text{Equation 6.15}$$

In the case of pure mesoporous materials, the gas is initially adsorbed on the internal surface of the mesopores and on the external surface, while after capillary condensation on the mesopores occurs the gas is adsorbed only on the external surface. The fit of the first regime of the t-plot is a straight line with an intercept at the origin; the slope of this regime gives S , the total surface area as a sum of the mesoporous and external surface area. The external surface area S_{ext} is given by the slope of the linear t-plot trend after condensation and the mesoporous area S_{meso} results from the difference between S_t and S_{ext} . The intercept of the linear t-plot regime after condensation or the first point of the linear regime after condensation can be used to determine the mesopore volume (Figure 6.5); the former is more accurate than the latter if the mesopores have pore diameter < 3.6 nm [238].

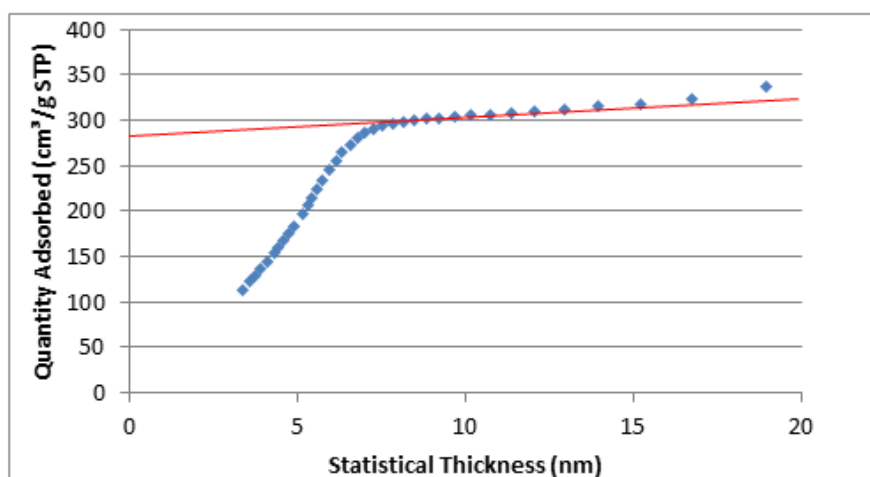


Figure 6.5: t-Plot of adsorption data obtained for N₂ adsorption on ND at 77 K. The intercept of the red straight line corresponds to the primary mesopore volume. The first linear trend, related to the total surface area, is not visible as a result of the low uptakes at low pressures. The microporosity of the material is negligible.

With regard to materials with both micropores and mesopores, the slope of the first linear trend corresponds to S , then after a sharp change, due to condensation in the micropores, a second linear trend is observed, with a slope corresponding to the surface area external to micropores; S_{ext} . S_{micro} is given by $S - S_{ext}$. Often the first linear trend is not visible or indeterminable, then the BET surface area (Equation 6.2) is used as S . The positive intercept (i) of the extrapolation of the thickness linear regime after capillary condensation in the micropores is related to the micropore volume (MPV):

$$MPV = i\rho_{273 K}/\rho_{77 K} \quad \text{Equation 6.16}$$

The intercept of the linear t-plot regime, after condensation in the mesopores or the first point of this linear regime, can be used to determine the total pore volume (TPV) and the mesoporous volume in absence of macroporosity is given by $TPV - MPV$.

As previously mentioned, an assumption of the t-plot method is the uniformity of the thickness of the adsorbed layer, so adsorption on mesoporous surfaces is considered similar to adsorption on a flat surface; but the thickness on small mesopores is not constant, but rather a function of pore diameter. This method, with regard to N₂ adsorption, should be used with caution in the presence of mesopore diameters < 3.6 nm

[238], as for QND. For this reason, the decision was made to estimate the porosity using the α_s plot method (Chapter 6.2.1.4.2).

6.2.1.4.2 α_s plot

The α_s method is based on the comparison of the selected adsorption data with a reference isotherm of a non-porous sorbent; the chemical and structural characteristics of the non-porous material are similar to those of the tested material; the equation of the α_s plot is [235]:

$$a(x) = a + k_{st} S_{ext} \alpha_s \left(\frac{p}{p_0} \right) \quad \text{Equation 6.17}$$

where:

- $a(x)$ is the quantity adsorbed;
- a is the intercept with the y-axis, related to the adsorption in saturated micropores;
- $k_{st} = a_{st}(x=0.4) / S_{st}$, where S_{st} is the specific surface area of the reference material (or: ‘standard material’);
- $\alpha_s = a_{st}(p/p_0) / a_{st}(p/p_0 = 0.4)$;
- S_{ext} = external surface area of the adsorbent analysed.

At low-pressures, the presence of micropores determines an initial sharp slope of the plot followed by a levelling at higher relative pressures, after filling of the micropores by the condensed gas. If the solid under study does not contain micropores, adsorption in mesopores initially proceeds, as on the macroporous/non-porous reference, via multilayer formation and it defines a linear plot. After capillary condensation of the adsorbate in the mesopores the plot levels off.

Porosity is calculated in the same way as described in chapter 6.2.1.4.1; in a material with different ranges of porosity, differences of y-intercepts of plots of linear regimes of the α_s plot give an estimation of the volume of last filled pores.

S_{ext} is derived from Equation 6.17 and the slope s of the α_s plot as:

$$S_{ext} = s/k_{st} \quad \text{Equation 6.18}$$

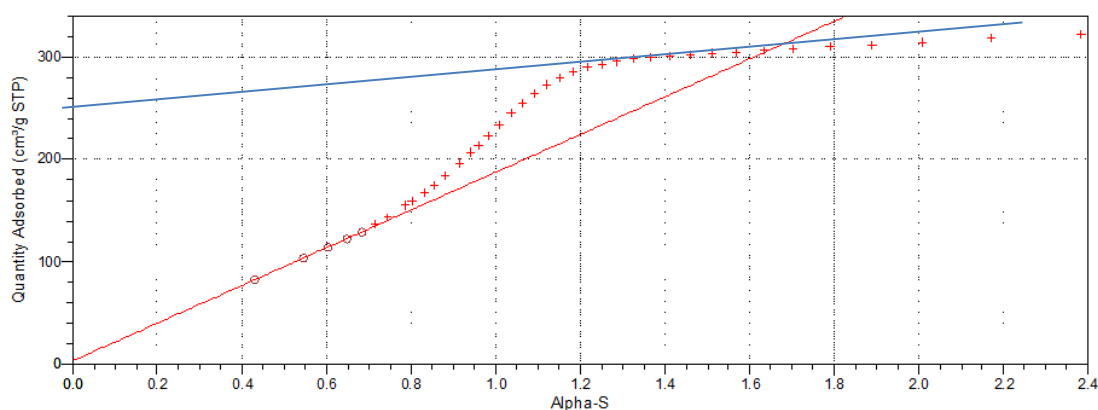


Figure 6.6: α_s -Plot of ND. The slope of the red straight line is related to the total surface area, while the slope of the blue straight line corresponds to the surface area external to primary mesopores. The intercept of the blue straight line is related to the primary mesopore volume.

6.2.1.5 Methodology

N_2 adsorption and desorption procedures were carried out at 77 K, using a Micromeritics ASAP 2420 (Figure 6.7), after drying the sample by degas at 393 K. Increasing and then decreasing the relative pressure p/p_0 , allowed 40 adsorption points and 30 desorption points to be determined. The degas procedure requires less time at higher temperatures, but the thermal regime selected was to ensure that it did not affect the structure of the material. The amount of sample analysed ranged from 0.1 to 0.5 g, depending on the surface area available for adsorption.



Figure 6.7: Micromeritics ASAP 2420. Degas ports (left) and N_2 adsorption ports (right).

After sorption is complete, the software provides the data in an electronic form and calculates several parameters automatically. The data were re-analysed manually to obtain surface area and total pore volume using BET theory. t-Plot analysis was performed by applying the Harkins-Jura equation derived from Lippens and De Boer for non-porous siliceous materials and nitrogen adsorption at 77 K (Equation 6.14) to the desorption branch. An estimation of the micropore volume, external surface area and micropore area was obtained by linear regression of different regions of the t-plot, after capillary condensation of the gas in the micropores. α -Plot analysis was also performed.

6.2.2 Bonds: Fourier transform infrared spectroscopy (FTIR)

6.2.2.1 Introduction

FTIR analysis allows structural information of the sample surface functionalities to be obtained, providing details of the functional groups and their density on the material surface. Infrared absorption spectroscopy is a method used to determine the structures of molecules based on their characteristic absorption of infrared radiation. Once exposed to infrared radiation, a molecule absorbs radiation of specific wavelengths and its vibrational energy level transfers from ground state to the excited state. The frequency of the absorption peak is related to the molecule vibrational energy gap. The number of absorption peaks is determined by the number of vibrational freedom of the molecule, while their intensity depends on the change of dipole moment and the possibility of the transition of energy levels. The absorption radiation of the majority of organic compounds and inorganic ions is between $\sim 4000\text{ cm}^{-1}$ and $\sim 400\text{ cm}^{-1}$.

6.2.2.2 Procedure

An FTIR spectrometer consists of a source of radiation that is incident on the sample and then passes through a Michelson interferometer, which consists of two perpendicular mirrors and a beamsplitter (Figure 6.8). The beamsplitter transmits half of the light and it reflects the other half; the transmitted light hits the stationary mirror, while the reflected light strikes the movable mirror. The two beams of light reflected by the mirrors are recombined with each other at the beamsplitter and the resulting signal reaches the detector. An amplifier provides to amplify the signal, converted from the analogic form to the digital one by the converter. The signal is then usually transferred

to a computer that carries out the Fourier transform, decomposing the signal (function of time) into the frequencies that make it up.

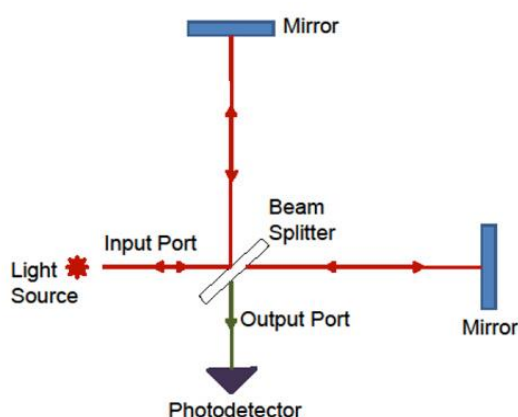


Figure 6.8: Diagram of a Michelson interferometer [239].

FT-IR analysis was performed using an ABB MB 3000 spectrophotometer with Horizon MB™ FTIR software (Figure 6.9). Materials were dried at 323 K for 2 h prior to analysis. Once the sample was placed on the analysis port, a background spectra was first collected. The test spectrum, which has a background spectrum subtracted from it, is subsequently obtained as an absorption spectrum, showing peaks with intensity proportional to the concentration of different bonds. This provides a measure of concentration of the various functional groups, as each absorbs infrared radiation within a specific wavelength interval.



Figure 6.9: ABB MB 3000 spectrophotometer used for the FT-IR analysis.

6.2.3 Surface topography: Scanning Electron Microscopy (SEM)

6.2.3.1 Introduction

A Scanning Electron Microscope scans a focused electron beam across the surface of a sample; electrons from the beam interact with the sample surface and the resulting signals are converted into an image, which provides information related to the surface topography and composition of the material analysed.

Defining the resolution as the smaller distance that can be distinguished between two points, the lenses of a microscope can magnify this distance to allow the human eye to distinguish points closer together than 0.2 mm. The maximum magnification of optical (i.e. light) microscopes is ~1000x. White light used by these instruments has an average wavelength of 550 nm and the related limit of resolution (i.e. visibility) in white light is > 200 nm. Electrons have much shorter wavelengths; hence, an electron microscope allows better resolution.

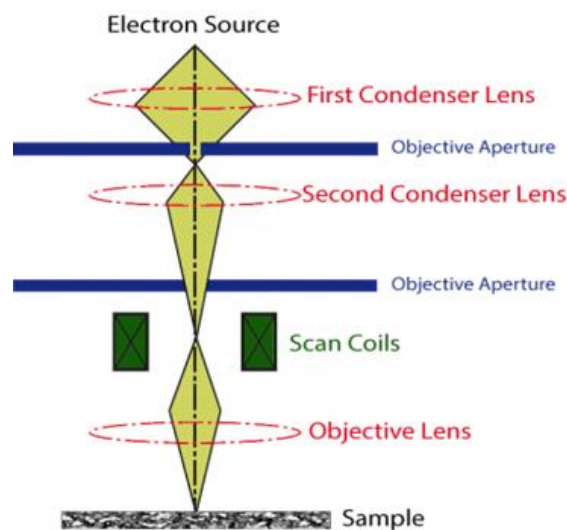


Figure 6.10: Schematic of a scanning electron microscope (SEM) [240]. The position of the electron beam on the sample is controlled by scan coils situated above the objective lens.

6.2.3.2 Procedure

The HITACHI SU-6600 (2010) Field Emission Scanning Electron Microscope used in this study is shown in Figure 6.11. The instrument is equipped with Energy Dispersive Spectroscopy (EDS), Oxford Inca 350 with 20 mm X-Max detector and Wavelength

Dispersive Spectroscopy (WDS), and uses Oxford Inca Wave 700 Microanalysis System with Energy + Software. Samples were initially dried for 2 h at 358 K prior to coating with a thin layer (~1.5 nm) of gold. Samples were then placed on a platform in a chamber area (Figure 6.11, RHS) and the SEM column and chamber were evacuated by pumps to produce a vacuum. Electrons are produced at the top of the SEM column, accelerated down and transmitted through a combination of lenses. The so focused beam of electrons then strikes the sample surface. Coils above of the objective lenses enable the beam to be scanned over the sample surface. The signals resulting from the interaction between the beam electrons and the sample surface are collected by detectors and finally converted to images on a computer screen.

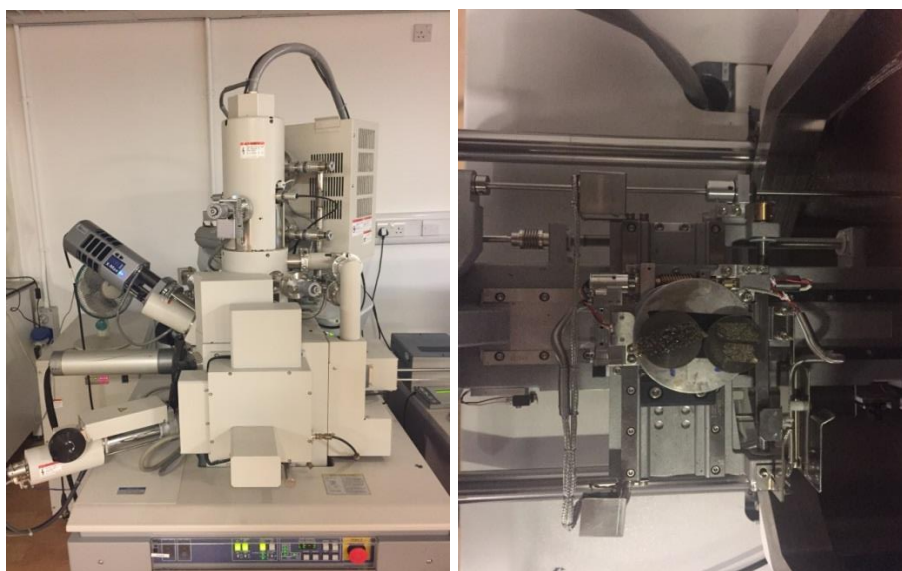


Figure 6.11: Scanning Electron Microscope (SEM) HITACHI SU-6600. On the left side, samples CNF and CF148, gold coated, at the entrance of the instrument vacuum chamber.

6.3 Measure of the concentrations

6.3.1 Ultraviolet-visible spectroscopy (UV-Vis)

6.3.1.1 Introduction

Sunlight (or white light) is made of a broad range of radiation wavelengths in the ultraviolet (UV), visible and infrared portions of the spectrum. If sunlight is passed through a prism, it bends the light in vary degrees according to wavelength and so the

component colours of the visible portion can be separated. Visible light can be viewed as a wave, with related wavelength, defined as the distance between adjacent peaks, and frequency (number of wave cycles travelling past a fixed point per unit of time). Visible wavelengths range from ~400 to ~800 nm, while UV wavelength is between ~10 and ~400 nm, but only the region > 200 nm is usually scanned from UV-Visible (UV-Vis) spectrophotometers. In a UV-Vis spectrophotometer a beam of light from a visible and/or UV light source (a lamp) is separated into its component wavelengths through a prism or other optical component able to diffract the light. Each monochromatic (single wavelength) beam in turn is divided in two beams with same intensity by a half-mirrored device. One beam passes through the cuvette containing the sample, while a reference beam, passes through the cuvette containing only the solvent, which was distilled water in the present study. Electronic detectors measure the intensities of the light beams travelled through the cuvettes allowing comparison of the intensities. The intensity of the reference beam, which only undergoes absorption due to the container and the solvent, is defined as I_0 , while I is the intensity of the sample beam (absorbed by cuvette, solvent and organic dissolved into the solvent). The spectrometer automatically scans all the component wavelengths in the wavelengths region selected. Absorption can then be presented as Transmittance: $T = I/I_0$, or Absorbance: $A = \log I_0/I$. The absorbance of the solution into the sample cuvette is expected to be proportional to the molar concentration of the organic dissolved.

6.3.1.2 Procedure

Helios Omega UV-Vis spectrophotometer, equipped with a deuterium lamp, was used to test organics concentrations in water before and after adsorption tests (Figure 6.12).



Figure 6.12: UV-Vis spectrophotometer used for the analysis of benzene adsorption on silica xerogels synthesised in this study.

Two cuvettes were first filled with distilled water and scanned to fix the baseline, one was retained to act as reference, while the other was washed with acetone and distilled water and dried. 1.2 mL of sample was taken out from the test container under stirring and immediately placed into the cleaned cuvette for the analysis. Benzene exhibits strong light absorption near 180 nm and weak absorption at 200 nm, but as it is said above only the region > 200 nm can be scanned successfully from the majority of UV-Vis spectrophotometers. Benzene exhibits a weak absorption peak at ~ 254 nm; hence, single beam mode was selected, and the region between 251 and 257 nm was investigated, confirming 254 nm as the wavelength with the strongest adsorption of those measurable by the instrument. Multiple analyses were performed on the same cuvette, to verify instrument precision. Different depths of sampling from the containers used for the adsorption test were also investigated to preclude any effects from a concentration gradient within the bulk.

6.3.2 Gas chromatography (GC-MS and GC-FID)

6.3.2.1 Introduction

Gas chromatography is an experimental technique used for the separation and analysis of substances after vaporisation. A gas chromatograph consists of an injection port, an oven into which is placed a column, gas flow control devices, heaters for the injection port and column, a detector and a recorder (Figure 6.13).

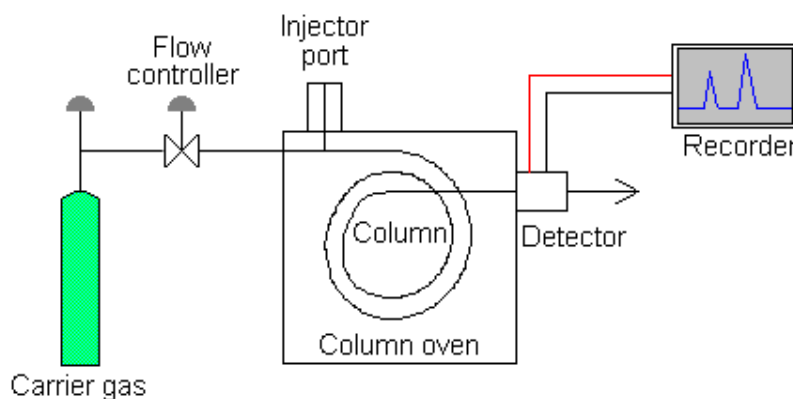


Figure 6.13: Schematic diagram of a gas chromatograph [241].

The sample to be analysed is injected into the sample port with a calibrated microsyringe, piercing a rubber septum. A septum purge gas flow carries away any bleed of plasticisers from the septum, to avoid unknown peaks in the final results. The sample is vaporised in a liner placed on a heated chamber and then forced into the column by the carrier gas flow. In 'split' mode, only a proportion of the mixture of sample and carrier gas passes into the column, while in splitless mode all of the sample is fed to the column. The sample travels into the column within the gas flow. The carrier gas is the mobile phase: it has to be chemically inert to not interact with the compounds, and also dry and free of oxygen to avoid damage of the column. The carrier gas is stored in a pressurised tank, as well as the air and hydrogen required for the detector. Helium and hydrogen both give good resolution, but the former is most often used as a carrier gas as it is less dangerous than the latter. The flow - and thus the pressure - of the gas can be regulated by valves placed on the tanks and by the GC software. The column has to be chemically inert, to avoid any alteration of the sample; it can be packed or capillary. Capillary columns have an internal diameter < 1 mm and length between 30 and 100 m. The tubing phase is made of stainless steel or fused silica and the walls of the tube are coated with a layer, which supports the liquid phase (the stationary phase). The compounds of the gaseous flux interact with the stationary phase of the column and this leads to different retention times for different compounds, so they will elute separately. The detector is the device placed at the end of the column. Different types of detectors can be used; in a Flame Ionisation Detector (FID), which requires a flammable gas, the sample is mixed with hydrogen and air and is then combusted. Ions released by pyrolysis from the C atoms of the compounds carry current through the flame. Above the flame there is a collector electrode; the number of ions that hit the detector in a unit of time gives the response. The current is measured by a sensor and the analogue signal is converted by another device to a digital signal, suitable for software analysis.

In gas chromatography mass spectrometry (GC/MS) the gas chromatograph (GC) is coupled to a mass spectrometer (MS). Electron ionisation is used for ion production, where a beam of electrons ionises the molecules of the sample, resulting in the loss of electrons, hence, formation of radical cations. When the resulting peak from these ions is seen in a mass spectrum, it gives the molecular weight of the compound; a mass

analyser (filter) then separates the positively charged ions according to various mass related properties. Different types of analyser exist: the most common are quadrupoles and ion traps. After the ions are separated they enter a detector, the output from which is amplified to boost the signal. The information collected from the detector is finally sent to a computer that converts the electrical impulses into visual displays.

6.3.2.2 Procedure

Gas chromatography, using a Shimadzu GC 2014 gas chromatograph equipped with FID detectors, was used to measure the concentrations of organic species in the aqueous systems studied (Figure 6.14, left side).



Figure 6.14: Shimadzu GC-FID 2014 (L) and Thermo Fisher GC-MS with autosampler (R).

Samples were extracted with a micropipette and placed in sealed vials, to which the solvent (methanol) and internal standard were also added; from these vials, 1 μL was removed, by microsyringe, and injected into the chromatograph sample port, piercing a rubber septum. The construction of a calibration curve allowed direct comparison of peak ratios, thus, the determination of the concentration of the organic species in the test system. The chromatographic column used was purchased from Sigma Aldrich and conditioned at 553 K for 3 h before first use (column characteristics are shown in Table 6.1).

Table 6.1: Sigma Aldrich SPB®-5 Capillary GC column characteristics.

material	fused silica
L × I.D.	25 m × 0.32 mm
matrix active group	Bonded; poly(5% diphenyl/95% dimethyl siloxane) phase
column type	capillary non-polar

The same procedure was followed for analyses with GC-MS, with the exception of the injection, which was made automatically from the vials to the column through an autosampler. The instrument is shown in Figure 6.14, right side. A capillary column Zebron ZB semivolatile, equivalent to the SPB-5 used for the GC-FID analyses, was used. Sample analyses were repeated to be sure of instrument precision, while tests were performed with both GC-FID and GC/MS on the same sample to allow method comparison.

6.4 Adsorption Tests

6.4.1 Adsorptives

Benzene and toluene were used in this study as representative components of dissolved oils in produced water from the BTEX family; the organics were purchased from Sigma Aldrich® as chromatography grade reagents (HPLC, ≥ 99.9%). Benzene is the most representative of dissolved oils contained in produced water. Furthermore, is the most difficult of the BTEX group to adsorb from solution, due to the fact that the adsorption potential of the solute in the liquid carrier decreases with increasing solubility of the adsorbate. The solubility of the monoaromatics in the BTEX group decreases with molecular weight, while their adsorption potential increases with the molecular weight [217]; hence, the lowest molecular weight species (benzene) is the most difficult to adsorb.

3,4- dichloroaniline (3,4-DCA) was selected as a representative endocrine disruptor chemical for adsorption tests within this work, due to its structural similarity with the BTEX molecules and its continued high levels of production and emission into the

environment, as well as its high solubility, persistence, and related toxicity risk for humans and wildlife.

6.4.2 Batch tests

Different borosilicate containers were used for all adsorption studies, and bottle volumes were selected in order to reduce headspace within the vessel. Pre-determined amounts of adsorbent were added to prepared bottles of aqueous phase organics to study adsorption characteristics; kinetic tests were conducted at pre-determined intervals, over 24 h, to determine times for maximum equilibrium to be achieved for each sample. Mixtures of water and the target pollutant were stirred in filled bottles to solubilize the organic. All measurements were conducted at 293 K. Lower temperatures were not investigated, as the reduction in temperature significantly impacts on kinetic performance by increasing the time required for equilibration and making kinetic measurements impractical.

Adsorption tests involved the addition of benzene, at concentrations in the range 0-1.1 g/L, to 110 mL of distilled water mixed with 100-500 mg of adsorbent, equilibrated for 3-24 h before analysis. An analogous procedure was used for toluene and 3,4-DCA, but using different aqueous concentrations. 3,4-DCA was weighed, while benzene and toluene were added by micropipette, or microsyringe for the smallest amounts. Isotherms and kinetics were determined, placing the adsorbents in glass bottles continuously stirred, to assure maintenance of the emulsion. Magnetic stirrers (Hanna® HI 190M) were used to assist dissolution of organics in water (Figure 6.15), when the density or the hydrophilicity of the sorbent allowed optimal contact between sorbent and adsorbate.



Figure 6.15: Magnetic stirrers Hanna HI 190 used to aid dissolution of organics in this study.

When the density or the hydrophobicity of the sorbents tested did not allow good contact with the adsorbate, a Gerhardt® rotary stirrer (Figure 6.16) was used, with a fixed speed of 20 rpm. The stirring rate was sufficient to guarantee good mixing of the sorbent and also eliminate any concentration gradient in the bulk, as revealed by multiple sampling along the bottle height.



Figure 6.16: Gerhardt® rotary stirrer used to ensure good contact for low density or high hydrophobicity samples used in this study.

6.4.3 Microcolumn tests

6.4.3.1 3D printing of the column

Column design was undertaken using the Rhinoceros 5 3D modelling tool for designers, developed by Robert McNeel & Associates. The internal components of the column were created individually and combined using Boolean operators. The model of the column was subsequently extracted as a Stereolithography file (.STL file) and loaded in the software preForm, provided by FormLabs. A Form1+ 3D printer from FormLabs (tech specs) was used to print the model on clear methacrylate photopolymer, while a CL-1000 ultraviolet crosslinker was adopted to perform the curing process.

6.4.3.2 Breakthrough curves

Samples were ground so as to obtain a particle size suitable for adsorption studies, allowing a range of particle sizes and different cylindrical microcolumns to be tested. Microcolumns were filled with adsorbent material and stoppered with glass fibre disks (max pore dimension: 10 nm). Benzene and 3,4-DCA stock solutions were previously solubilized in methanol (1:10), before 0.5 mL of the resulting solutions were added to 50 mL distilled water in 55 mL sample containers.

UV-vis spectrophotometry was used for species detection. The adsorption apparatus was positioned between a rotary valve and a UV-Vis detector, as presented in Figure 6.17.

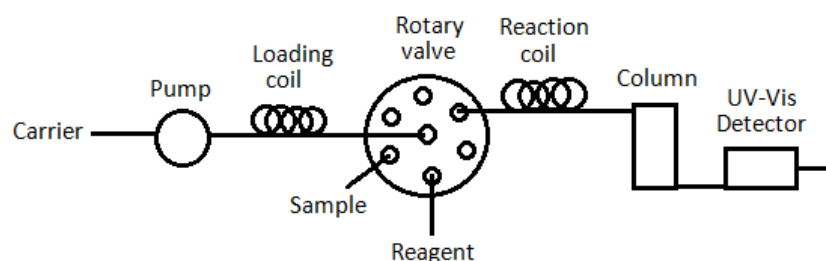


Figure 6.17: Sequential injection analysis manifolds connected to the adsorption column and UV-Vis detector for adsorption tests on silica samples used in this study.

Compared to flow-injection analysis (FIA), sequential-injection analysis (SIA) employs a simpler, single-channel manifold for sample introduction, even with multi-component

chemical systems; additionally, more accurate, robust syringe pumps are used in place of multi-channel peristaltic pumps. Through single-channel operation, the same manifold can be used to implement a wide range of assays and the rotary valve enables automated calibration. Moreover, sample and reagent use are significantly reduced [230]. In this study, using the aforementioned valve and a bidirectional syringe pump, water samples containing the target analyte were inserted into a loading coil (between the syringe and the central port of the valve), and subsequently injected towards the column. At the same time the detector began recording the signal, in order to determine whether the analyte was fully retained in the column. Breakthrough curves were thus obtained, in order to establish both the volume and capacity of saturation. Prior to sample injection, the column was packed and conditioned by flowing with methanol, and subsequently washing with distilled water.

Automated solid-phase extraction was used to test the regeneration of exhausted adsorbents; whereby the procedure outlined above to obtain breakthrough curves was modified slightly, such that instead of loading a sample, methanol was loaded to promote desorption of the analyte once it was known to have been retained within the column.

6.5 Membranes: preliminary evaluation of casting

NDH, CMSH and Z1H samples, and silica xerogels functionalized with citric acid, were tested individually, following an analogous procedure, and different particle sizes were tested. 100 mg of silica powder was dispersed in 3 mL acetone through bath sonication for 15 min in a scintillation vial. 1 g of PVDF solution (7.5% wt in DMF) was added to the silica suspension, which was again sonicated for 15 min. The acetone was removed with nitrogen, by rotary evaporation, leaving a silica 'ink'. The ink was cast onto nylon disks and the coated surfaces were then placed in an oven to remove any solvent.

7 Results and discussion

7.1 Synthesis of the silica xerogels

7.1.1 Effect of process parameters

7.1.1.1 Introduction

Methanol and isopropanol are already used in solvent exchange methods to produce higher porosities and lower densities for silica xerogels [223]. Ageing and washing periods, as well as synthesis temperatures, were selected as described by Bangi *et al.* Different containers and sealing methods were investigated. If the amount of the silica solution is fixed, different sizes of the containers correspond to different heights of the solution contained, with significant differences in the gelation times and on the density and homogeneity of the gel obtained. Same applies to the sealing method chosen, as it defines the evaporation ratio. With reference to the amount of silica solution used for each sample (Chapter 6.1.2), cylindrical containers with diameter of 10 cm were finally chosen and covered with aluminium foil with three holes of ~0.5 cm diameter during gelation and drying phases, while the containers were sealed with caps during washing and functionalization.

The steps of the synthesis can be summarized as follow:

- preparation of the diluted sodium silicate solution with the desired $\text{H}_2\text{O}:\text{Na}_2\text{SiO}_3$ ratio;
- addition of acid 3M, 10%vol in 40 mL of diluted sodium solution placed in 400 mL glass container;
- container covered with pierced aluminium foil and placed in oven at 323 K for three hours after gelation is occurred;
- gel cut in small pieces, distilled water addition and exchange of the water three times in 24 hours. Container sealed with cup and placed in the oven at 323 K every time after water exchange, until the next exchange;
- water exchanged with methanol, container sealed with cup and placed in the oven at 323 K for 24 hours;

- methanol exchanged with a mixture of methanol, hexane and TMCS. Container sealed with cup and placed in the oven at 323 K for 24 Hours. This step is absent if the final material is not functionalized;
- discharge of the solvents and drying at room temperature for 24 hours;
- container covered with pierced aluminium foil and placed in the oven at 473 K for 1 hours.

The effect of $\text{H}_2\text{O}/\text{Na}_2\text{SiO}_3$ ratio, acid catalysis and amount of silylating agent were investigated and are discussed below, with reference to the characterisation results obtained.

7.1.1.2 Water / Sodium Silicate ratio

The diluted sodium silicate solution was stirred vigorously during dropwise addition of citric acid; otherwise partial instant gelation was observed. Instant gelation, during acid addition, was always observed for ratios < 110 . No gelation was observed within 24 h for ratios > 200 , and only partial gelation was observed after a few days. Gels obtained with high ratios, were cut into pieces of ~ 1 cm for the first washing, however, they became fine particles during the washing procedure. If too little silica is present within the solution, the network created is thin and fragile. Hence, gels catalysed by citric acid addition with ratios ≥ 175 , were confirmed as too weak to undergo the washing procedure, as they dissolved in water. By increasing the dilution of waterglass, the collision frequency between condensing silica species is reduced, as the distance between particles increases. Hence, increasing gelation time is expected for increased $\text{H}_2\text{O}/\text{Na}_2\text{SiO}_3$ ratios. Such behaviour, confirmed in the present study for xerogels catalysed with citric acid (Figure 7.1), was also observed with sodium silicate xerogels catalysed with acetic acid [242].

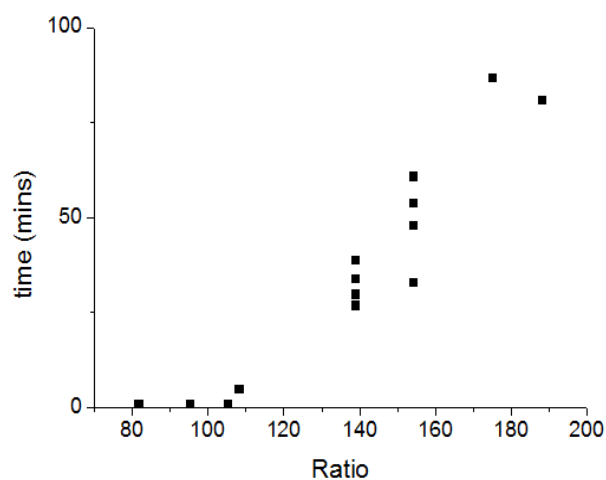


Figure 7.1: Citric acid catalysed water/ Na_2SiO_3 ratio VS gelation time for samples produced in this study.

With regard to bulk density, it is already known to first decrease and then increase with increasing $\text{H}_2\text{O}/\text{Na}_2\text{SiO}_3$ ratios (> 150) and acetic acid catalysis [232], with the lightest xerogel obtained at ratios between 130 and 160. Direct measurement of density was not performed in this work, however, containers with known volume were filled by samples crushed to the same mesh and it was evident, from the volume obtained and the weight measured, that the xerogels with the lowest density between those catalysed with citric acid were those for ratios of 138 and 154. For xerogels catalysed with HCl, the lowest density was observed for a ratio of 108.

With regard to the influence of the $\text{H}_2\text{O}/\text{Na}_2\text{SiO}_3$ ratio on material texture, average pore diameters, pore volumes and surface areas were found to increase in gels obtained from citric acid catalysis with increasing ratio (80 to 138-154). The lower porosity of sample CF148 in comparison with gels CF138 and CF154 is likely due to a shorter cooling period after the last hour of oven drying (Table 7.1). Indeed, the oven temperature was set to decrease at 10 K/min from 473 K to 323 K before the dried CF148 was removed from the oven, while for samples CF138 and CF154 the gradient was fixed at 1 K/min, to investigate the effect of a longer cooling time.

Table 7.1: Citric acid catalysis, full functionalisation: water/ Na_2SiO_3 ratio VS porosity.

Sample	Ratio $n \text{ H}_2\text{O}/n \text{ Si}_2\text{O}_3$	Surface Area m^2/g	Pore Volume cm^3/g	Pore Size nm	Pore size distribution (90%) nm
CF10/05	80	449.53	1.22	10.77	6.4-18
CF10/05	108	473.47	2.16	17.98	8.1-65
CF13827/6 *	138	654.04	3.27	16.80	7-70
CF148	148	648.20	2.96	15.57	5.9-70
CF15427/6 *	154	669.40	3.24	15.65	6.5-70

* Longer cooling time (3 h)

It is also notable that the main pore size distribution is considerably narrower for the lower ratio examined (Figure 7.2). As can be seen in Figures 7.2 and 7.3, from ratios 108 to 154 the distribution is centred on the same value, but ratios 148 and 154 show sharper peaks than the lower ratios.

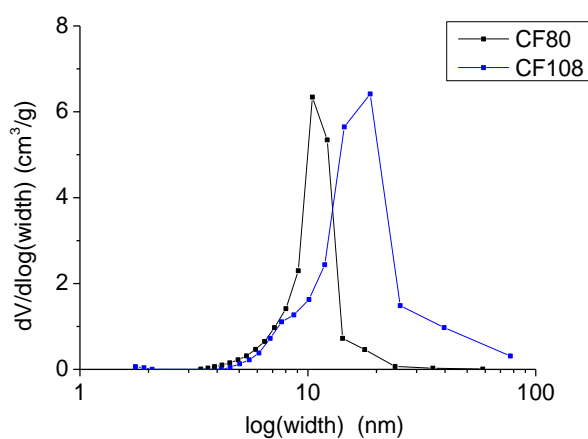


Figure 7.2: Citric acid catalysis, full functionalisation: pore size distribution of water/ Na_2SiO_3 ratios 80 and 108.

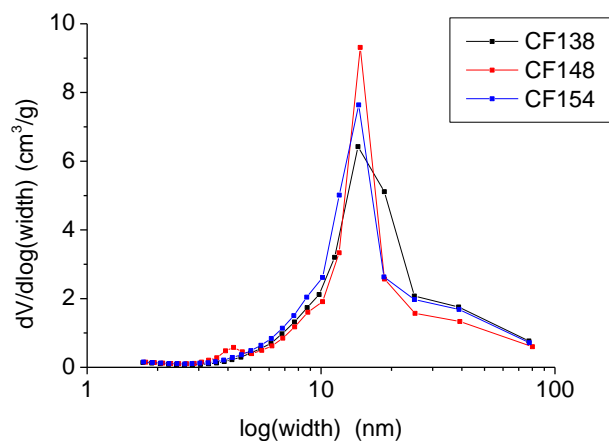


Figure 7.3: Citric acid catalysis, full functionalisation: water/ Na_2SiO_3 ratio and pore size distribution.

7.1.1.3 Acid catalyst

Citric acid (3 M) was added 10% v/v to the diluted Na_2SiO_3 solution for sol-gel catalysis. Acid catalysis was also performed using HCl; all materials produced for different $\text{H}_2\text{O}/\text{Na}_2\text{SiO}_3$ ratios were weighed; a much greater yield was always obtained through citric acid catalysis compared with HCl catalysis. Density was not directly measured, but weighing the samples and placing them in containers of equal volume was sufficient to identify xerogels with ratio 108 catalysed with HCl (named HF108) and with ratios between 138 and 154 catalysed with citric acid as those with significantly higher yields (g) and lower densities than any other sample. These results are in agreement with the work of Bangi *et al.* [1], and their xerogels produced with a $\text{H}_2\text{O}/\text{Na}_2\text{SiO}_3$ ratio of 146.67. Samples HF108 and HF130 revealed the highest specific surface area and specific pore volume between those catalysed with the same acid, but both these parameters were found to be lower than for any the of samples obtained by citric acid catalysis, with the exception of sample CF80. Moreover, the yields of samples CF138 and CF154 were more than double any of the samples catalysed with HCl. Hence, focussing on a use of such materials as sorbents, catalysis with citric acid was determined to be the most promising choice between the two alternatives analysed. This choice was also supported by the results for preliminary adsorption tests discussed in Chapter 7.4.1.3.

Table 7.2: Hydrochloric acid VS citric acid catalysis.

Sample	Acid	Ratio	Yield g	Surface area m ² /g	Pore volume cm ³ /g	Pore size nm	Pore size distribution (90%) nm
HF10/05	HCl	108	0.77	325.80	1.55	20.99	9.0-27
CF10/05	C ₆ H ₈ O ₇	108	1.76	473.47	2.16	17.98	8.1- 65

7.1.1.4 Amount of Silylating agent

The role of trichloromethylsilane chosen for the functionalisation process was investigated using gels synthesised by citric acid catalysis. It was found to strongly affect pore volume, pore size distribution (Figure 7.4) and the strength of the silica network.

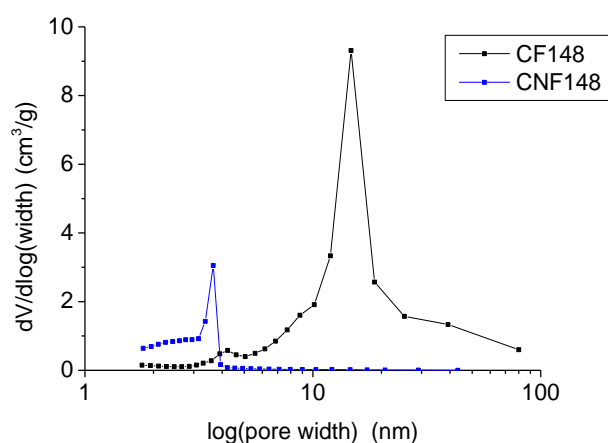


Figure 7.4: Pore size distribution of silica xerogels samples synthesised with citric acid catalysis unfunctionalised (CNF148) and functionalised (CF148).

Analysis of samples with the same H₂O/Na₂SiO₃ ratio reveals that unfunctionalised CNF148 has a lower pore volume and smaller average pore size than functionalised CF148. However, CNF148 has a higher surface area; this is due to the smaller pores of the virgin xerogel, which shows a micropore volume from α -plot analysis equal to 0.41 cm³/g.

Table 7.3: Characterisation of virgin silica xerogel and functionalised silica xerogel.

Sample	Ratio	Yield	Surface area	Pore volume	Pore diameter	Pore size distribution (90%)
		g	m²/g	cm³/g	nm	nm
CNF148	148	1.33	707.13	0.48	2.89	1.9-4.5
CF148	148	1.61	648.20	2.96	15.57	5.9-70

Virgin (unfunctionalised) fully functionalised and half-functionalised xerogels were placed in water and stirred using a rotary stirrer (20 rpm) for 3 d. They were all initially granular, with particle sizes between 0.5 and 1.4 μm . After the first day, the virgin and half-functionalised samples were all recovered as powder; however, even after 3 d, fully functionalised xerogels were recovered as granules, with no visible deterioration, and the water in which they were immersed was completely clear. Functionalisation is, therefore, confirmed as fundamental in the production of xerogel materials for cyclic use in water based applications.

7.2 Characterisation

7.2.1 Granulometry

The ND and CMS types of Quartzene were provided by Svenska AB, as powders with particle sizes between 2 and 150 μm , and Dv90 (i.e. 90% of particles below the stated diameter), of 46 and 75 μm , respectively. Measurements were carried using a SvAAB with a Malvern Hydro 2000S (Figures 7.5 and 7.6). CMSH and NDH were provided as powders, with a particle size between 75 and 200 μm , while Z1 and Z1H samples had particle sizes between 1 and 1.5 μm .

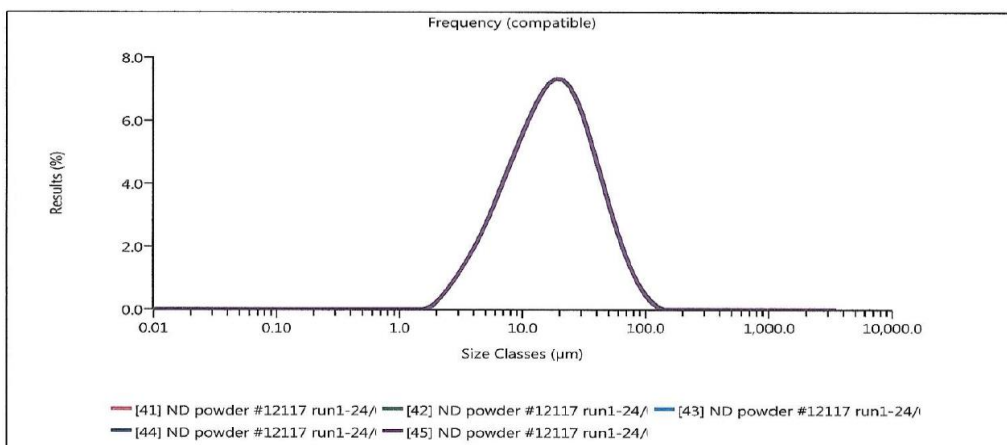


Figure 7.5: ND particle size distribution.

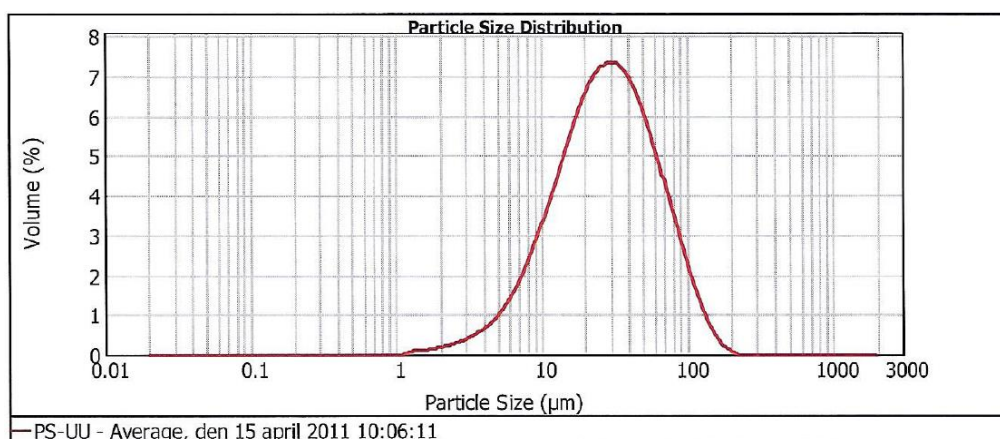


Figure 7.6: CMS particle size distribution.

Xerogels synthesised at low temperature and ambient pressure were obtained as monoliths and cut into pieces of ~1 cm size before washing, and subsequent manual grinding and sieving to obtain particles with a main size between 0.5 and 1.4 mm. Sorbents are usually tested as fine particles, to verify their maximum adsorption capacity in a shorter time. However, whenever is possible, the use of sorbents in granular form is here assumed to be more representative of the material behaviour in a filter configuration; furthermore, it makes it easier to verify resistance to stress induced by immersion and stirring in water.

7.2.2 Surface area and porosity

7.2.2.1 Quartzene

N₂ sorption measurements were performed at 77 K using a Micromeritics ASAP 2420, on samples accurately weighed between 0.15 and 0.5 g and degassed at 393 K. 40 adsorption points and 30 desorption points were collected per isotherm, spanning the relative pressure range 0 - 0.99. Degassing at low temperatures requires longer treatment times but has the benefit that the structure of the material is preserved. BET analysis [177] was used to interpret the data obtained.

The Harkins-Jura thickness equation, derived from Lippens and De Boer's analysis for non-porous siliceous materials characterised by N₂ adsorption at 77 K [236], can be employed as a reference, to determine 'statistical thickness' (t), and to estimate surface area, average pore size and pore volume of materials with similar composition and BET C constants, using the t -plot analysis method. An assumption of the t -plot method is the uniformity of the thickness of the adsorbent layer, hence, adsorption on a mesoporous surface is considered similar to adsorption on a flat surface; however, the adsorbed thickness on small mesopores is not constant, but it varies as a function of the pore diameter. Consequently, this method, when applied to nitrogen adsorption, should be used with caution in the presence of mesopores with diameters < 3.6 nm [238], which, in this study, includes ND samples. Furthermore, it is essential that the reference surface should be energetically and structurally similar to the porous solid surface under analysis, as both factors affect the level of adsorbate loading at a given relative pressure; however, the BET C value does not guarantee a similar surface structure, so it is not sufficient basis for selection of a reference isotherm [243]. For these reasons, surface areas and pore volumes of Quartzene were estimated also using α -plot analysis. Parameters of the reference adsorbent Lichrospher-1000 were applied in the equation 6.17. Figure 7.7 shows the α -plot analysis of the N₂ adsorption isotherm obtained at 77 K for Quartzene ND. The slope of the first region of the α -plot (solid line in Figure 7.7) provides an estimate of the surface area, while the gradient of the upper dashed line corresponds to the surface area external to the primary mesopores, which is ascribed as the surface area of any large mesopores and macropores present in the material. The

intercept of the dashed line provides an evaluation of the already filled small mesopores, i.e. the small mesopore volume.

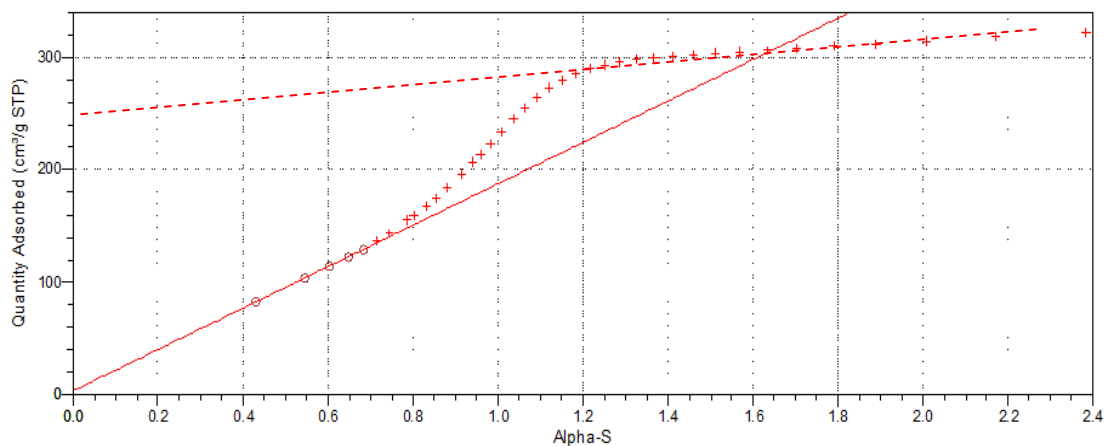


Figure 7.7: α -Plot analysis of ND N₂ adsorption isotherm measured at 77 K (solid line fit of low pressure data, dashed line fit of high pressure data).

Surface areas obtained for the four samples studied here show good agreement between the two methods (BET and α_s), except in the case of ND, which exhibits small mesopores, thereby suggesting the value obtained using the α -plot method would be more accurate. Pore sizes determined for CMS, Z1 and Z1H samples are widely distributed between 2 and 80 nm, while ND exhibits a discrete pore size distribution centred around 3.3 nm (Table 7.4). Consequently, ND is the only material with a small mesopore contribution but it is notable that all samples exhibit significant total pore volume.

Table 7.4: Surface areas and porosities of Quartzene samples.

Sample Name	S_{BET} m ² /g [†]	S_{α_s} m ² /g	Average pore width nm	Total pore volume cm ³ /g	Small mesopore volume cm ³ /g [‡]	Meso- and macro-pore volume cm ³ /g [‡]
Z1	325	331	20.3	1.03	/	1.03
Z1H	186	186	17.4	0.97	/	0.97
CMS	158	161	14.6	0.50	/	0.50
ND [§]	597	546	3.3	0.54	0.40	0.14

[†] BET linearisation ($p/[n_a \cdot (p^0 - p)]$ vs. p/p^0) was performed over the relative pressure range 0.05-0.3.

[‡] Pore volume contributions were determined using the α_s method.

§ α -plot for ND exhibits two ranges of mesoporosity (Figure 7.7); surface area of small mesopores is estimated as 524 m²/g.

7.2.2.2 Silica xerogels

Surface area, average pore size and pore size distribution are presented and discussed in Chapter 7.1.1: ‘Effect of process parameters’. Materials, with the exception of the virgin xerogel sample catalysed with citric acid, were found to be mesoporous, with pore size > 3 nm. Hence, with the exception of CNF148, the t-plot method was considered reliable for the xerogels studied here. The silica alumina used as reference sorbent for the thickness method is compatible with the xerogels analysed, but the t-plot is not reliable once part of the pore volume corresponds to pores with size around 2-2.5 nm. For this reason, α -plot was performed for sample CNF148.

7.2.3 Bonds

7.2.3.1 Quartzene

Surface chemical functionalities of adsorbents are known to determine the hydrophilic or hydrophobic nature of a material, and this is also true of silica [244]. FT-IR analysis was used to determine surface functionalities of samples prepared as hydrophilic. The obtained spectra (Figure 7.8) shows the presence of silanol polar groups (Si–OH), in the range 2700-3650 cm⁻¹, for all materials studied, with Z1 and ND showing similar surface chemistries, while CMS exhibits more refined Si-OH bond peaks; consequently, these Quartzene materials can be categorised as hydrophilic in nature.

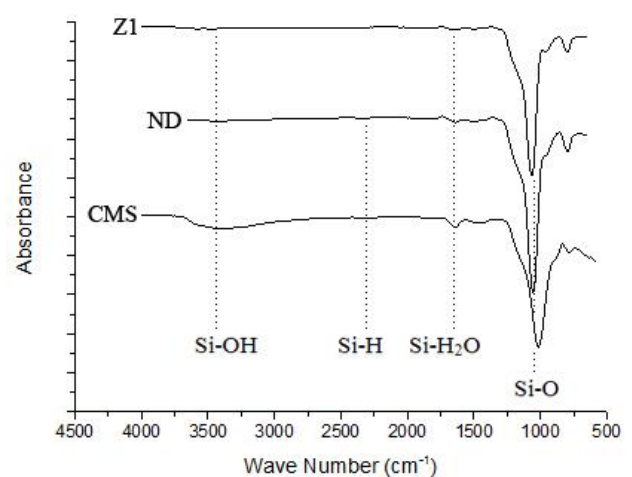


Figure 7.8: FT-IR spectra of silica samples: Z1, ND and CMS.

FTIR spectra of Z1H, shows a small peak around 1250 cm^{-1} (Figure 7.9), attributed to the Si-CH₃ bonds, formed as consequence of the functionalisation process. The presence of CO₂ can produce an absorption peak at $\sim 2300\text{ cm}^{-1}$, however, immediately prior background measurements were used to account for its atmospheric presence.

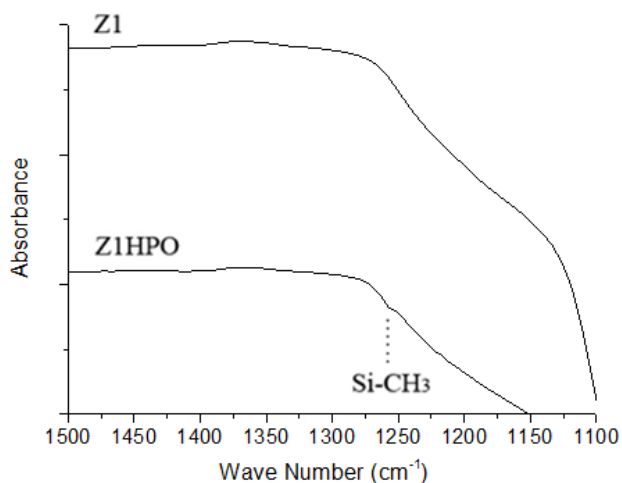


Figure 7.9: Comparison between the FT-IR spectra of Z1 and hydrophobic Z1H, named Z1HPO.

7.2.3.2 Silica xerogels

The FTIR spectrum for silica xerogel catalysed with citric acid and fully functionalised is shown in Figure 7.10. Functionalization with TMCS results in the formation of Si-CH₃ bonds, which are visible at 1250 cm^{-1} .

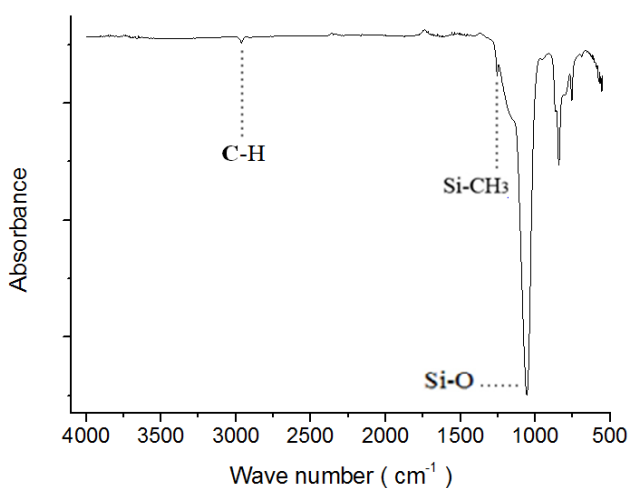


Figure 7.10: FT-IR spectra of silica xerogels catalysed with citric acid.

7.2.4 Surface topography and composition

Results of SEM analyses on Quartzene hydrophilic samples are presented in Figure 7.11; the observed networks reflect the difference of the CMS synthetic process, indeed the CMS sample is the only exhibiting spherical particles.

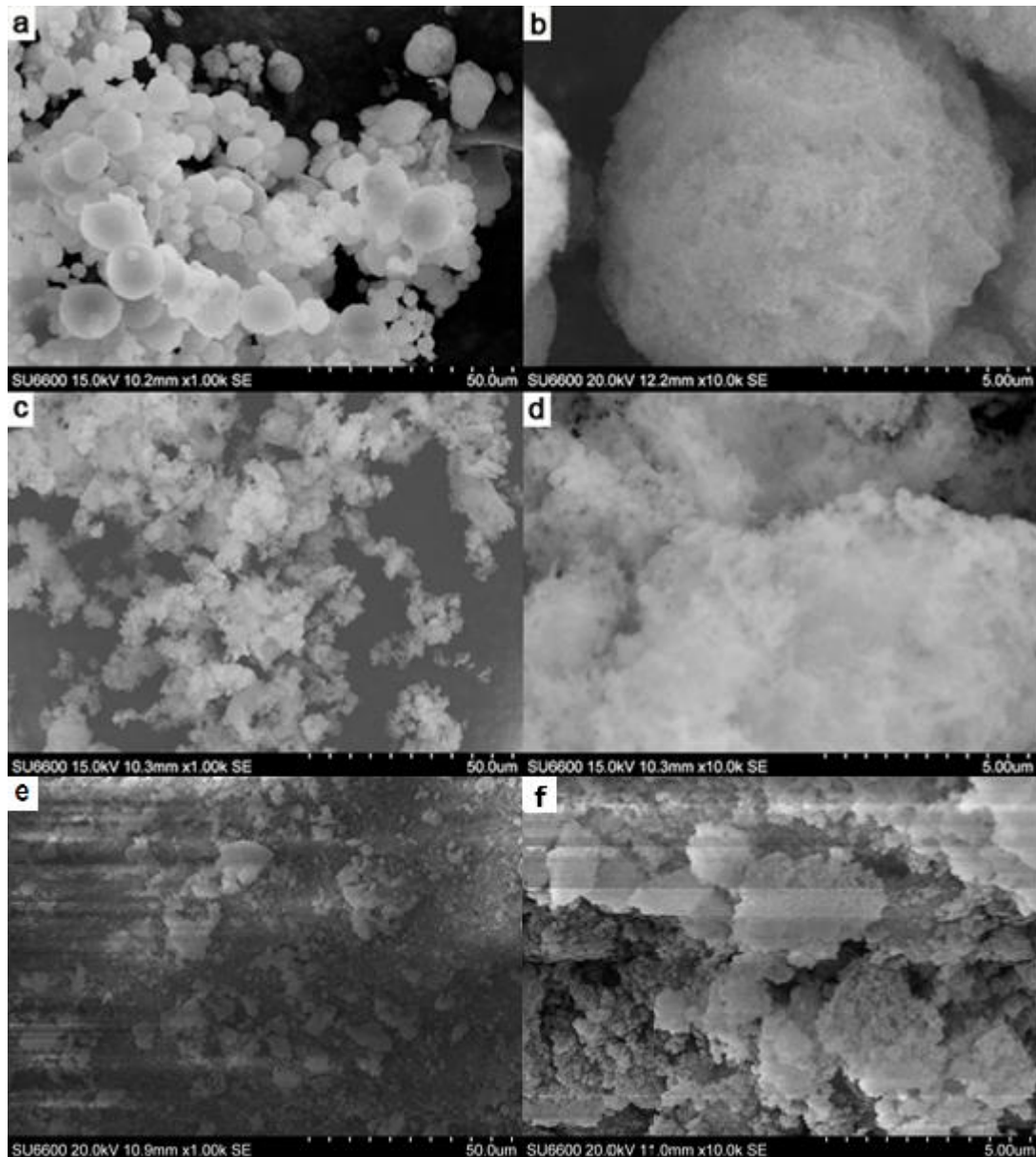


Figure 7.11: FE-SEM analysis of Quartzene samples: CMS (a: x1k, b: x10k), ND (c: x1k, d: x 10k) and Z1 (e: x1k, f: x 10k).

Figures 7.12 and 7.13 show the SEM analysis of the citric acid catalysed materials. The differences between Figures 7.12 and 7.13 can be attributed to the functionalisation step, which results in discrete particles at the magnification level probed.



Figure 7.12: FE-SEM analysis of virgin xerogel sample CNF148. Magnification: x1k.

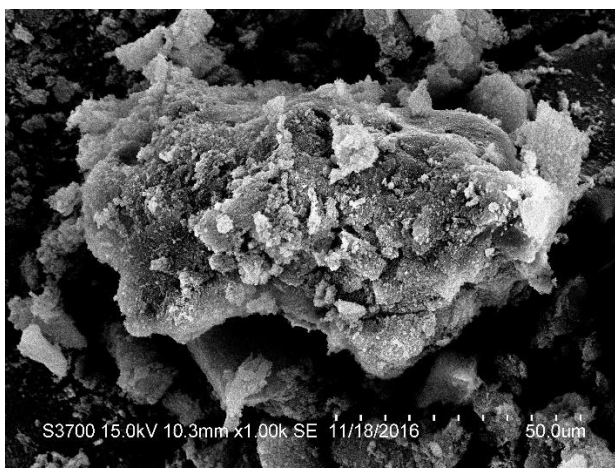


Figure 7.13: FE-SEM analysis of functionalised xerogel sample CF148. Magnification: x1k.

7.3 Measure of organic concentrations

7.3.1 Ultraviolet-visible spectroscopy (UV-Vis)

UV-Vis spectroscopic analysis should be easier and faster than gas-chromatography, as it does not require the solution to be mixed with other substances prior to analysis, and the analysis time is < 1 min, compared to 10-20 min for GC-FID or GC-MS. Quartz cuvettes are required for UV-Vis studies, due to the low wavelength used to measure

benzene absorbance in solution. Despite ultraviolet-visible spectroscopy already being used for similar analyses [219], this method, tested only for the xerogel samples, was found to be unreliable. The precision of the instrument was high, with repetitive analyses on the same cuvette giving variations below 0.6%. The adsorption of benzene estimated from UV-Vis spectroscopy was found to be lower than the uptake measured by GC-FID analysis on the same sample. New sets of UV-Vis analyses were performed after rotary stirring, using same adsorbent, pollutant concentration and stirring time but the values of absorbance obtained were not close to the value obtained with the previous tests, a few were even higher than the initial concentrations. The poor accuracy of this method was ascribed to the presence of fine particles in the solution (invisible to the naked eye), due to minimal erosion of the sample during stirring.

7.3.2 Gas chromatography

7.3.2.1 GC-MS

Flow rates between 1.8 mL/min and 1.2 mL/min, different temperature programmes and split ratios from 0 to 20 were evaluated. The optimal program, able to allow the best separation between peaks in the shortest time, was finally identified as:

- Carrier gas: He;
- flow rate: 1.5 mL/min;
- split ratio: 1:10;
- 323 K, holding time 1.80 min, ramp to 553 K at 20 K/min.

Between each analysis, a cleaning run was made using methanol injection and by increasing the temperature from 323 K to 553 K, at 25 K/min.

The precision of the instrument was found to be lower than that obtained with GC-FID, due to unexpected outliers for analyses on the same vial, thus only GC-FID analysis was used for further adsorption data interpretation. The reason of the lower accuracy of GC-MS has not been clarified, but due to the suitability of the technique for the desired measurements and the carefully selected conditions of the column, the reduced performance is probably a result of non-optimal operative conditions for the instrument connections and valves (i.e.: the split valve).

7.3.2.2 GC-FID

7.3.2.2.1 Benzene and toluene

Samples were introduced into the gas chromatograph by piercing the rubber septum on the injector port with a microsyringe. The capillary column was purchased from Sigma Aldrich and conditioned at 553 K for > 3 h. Low temperatures of the injector port can result in the incomplete volatilisation of the sample and residues can contaminate the following analysis; conversely, too high temperatures can destroy the analytes. Minimal temperatures of the oven and thus of the column, provides good resolution, but longer elution times than higher temperatures. The samples analysed had a wide boiling range (due to the presence of dimethyl phthalate as internal standard), hence, temperature programming, in which the temperature is increased as the separation advances, was selected. Column flows between 3 to 1.3 mL/min, different oven temperature programs, and different detector temperatures were evaluated and the program found to give the best resolution was:

- carrier gas: He;
- injection: splitless;
- injector temperature: 523 K;
- detector temperature: 523 K;
- column flow: 1.5 mL/min;
- purge flow: 2.5 mL/min;
- oven program:
4 min at 323 K, ramp to 353 K at 5 K/min, holding time 1.5 min, ramp to 453 K at 15 K/min, with final holding time of 10 min.

Such a low flow, which results in a long program to obtain elution of the internal standard, was found indispensable to allow the separation of the solvent peak and benzene peak. The long elution time of dimethyl phthalate was found to affect the reproducibility of the results, so toluene was finally selected as an internal standard for benzene and vice-versa. The reproducibility was significantly improved and the total time of analysis decreased without any effect on peak resolution, as can be seen in Figure 7.14. Column flows, oven and detector temperatures evaluated to optimise peak resolution resulted in the following program:

- carrier gas: He;
- injection: splitless;
- injector temperature: 523 K;
- detector temperature: 523 K;
- column flow: 1.5 mL/min;
- purge flow: 2.5 mL/min;
- oven program: 4 min at 323 K, ramp to 453°K at 10 K/min, ramp to 553 K at 10 K/min, with final holding time of 5 min.

The low flow used was imperative to allow separation of the solvent and benzene peaks. The last ramp to 553 K was adopted to avoid any residues in the column during the next analysis; this choice is faster than the alternative procedure of methanol cleaning between analyses. Referring to Figure 7.14: the larger peak, beginning at 4.3 min, is due to the solvent (methanol), followed by the benzene peak (elution time: 6.5 min) and finally the toluene peak (elution time: 8.3 min).

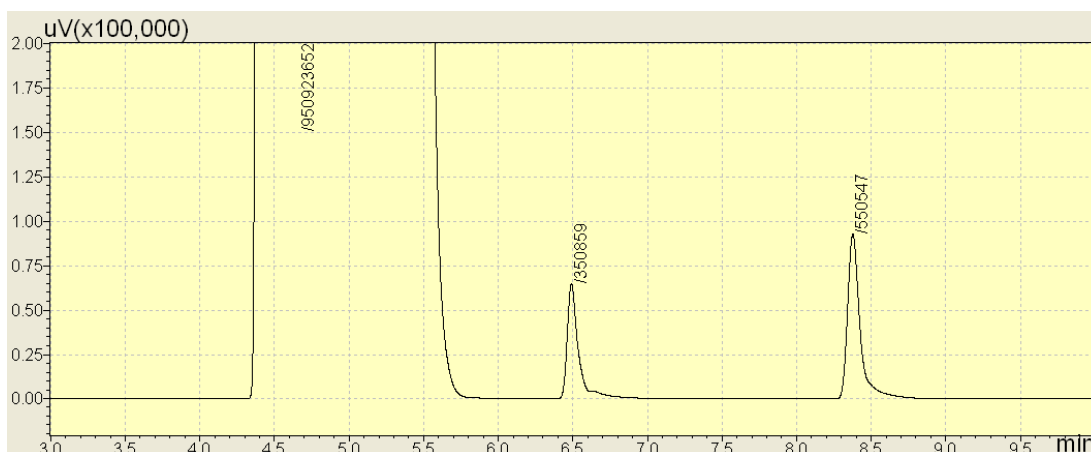


Figure 7.14: Gas chromatograph analysis of aqueous benzene, with toluene as internal standard and methanol as solvent. x-axis: time/min; y axis: signal/ $\mu\text{V} \cdot \text{k}$, where k is the magnification factor.

Repetitive analyses on the same sample were conducted to ensure gas chromatograph precision. The same sample was also tested on two separate occasions, in order to verify the reproducibility of the results, once by conducting routine analysis and the other involved shutting down and restarting the instrument; this was to rule out effects from

inadequate run times or too low temperatures after final elution, which can lead to accumulation of reactants in the column that are released later as ghost peaks or excessive concentrations.

Calibration solutions of benzene in water with concentrations ranging from 5 to 200 ppm were put in glass bottles with sealed caps, allowing the minimum possible headspace and stirred for 1 h. A calibration curve was thus defined by GC injection of samples from the calibration solutions with toluene (internal standard) 110 ppm in methanol and plotting the ratio for benzene and toluene areas (obtained from GC analyses) versus the corresponding concentration of benzene added (Figure 7.15). This curve was then utilised to determine the concentration of benzene after the adsorption tests. A calibration curve was also created using benzene, as internal standard to verify adsorption of toluene.

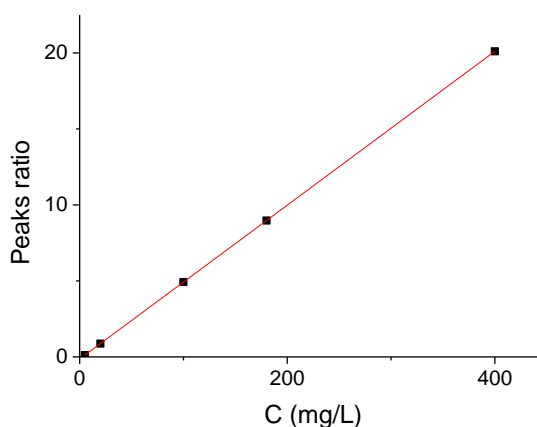


Figure 7.15: Calibration curve used to relate the peak areas of the chromatograph to the benzene concentration in the aqueous solutions.

7.3.2.2.2 3,4-dichloroaniline

Dimethyl phthalate 25 ppm in methanol was used as internal standard. The choice was made to avoid longer elution times between analyte and internal standard. The instrument program which gives best results was evaluated as:

- carrier gas: He;
- injection: splitless;
- injector temperature: 523 K;

- detector temperature: 583 K;
- column flow: 6.4 mL/min;
- purge flow: 2.5 mL/min;
- oven program: 2 min at 343K, ramp to 563 K at 10 K/min.

A calibration curve was obtained for 3,4-DCA aqueous concentrations ranging from 40 mg/L to 200 mg/L. A sample analysis is shown in Figure 7.16.

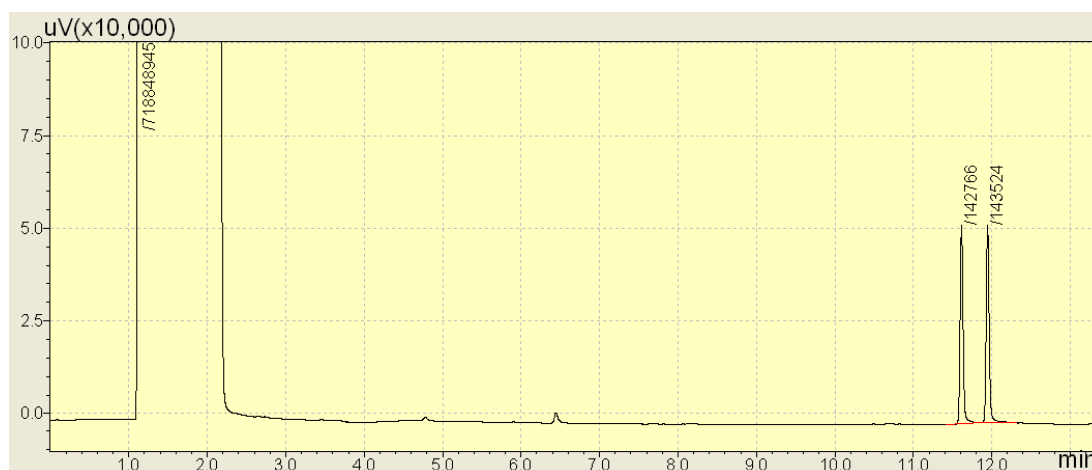


Figure 7.16: Gas chromatograph analysis of 3,4-DCA in water, with dimethyl phthalate as internal standard and methanol as solvent. x-axis: time/min; y axis: signal/ $\mu\text{V} \cdot \text{k}$, where k is the magnification factor.

7.4 Adsorption tests

7.4.1 Batch tests

7.4.1.1 Optimal methodology

Adsorption batch tests were carried out only after verifying the absence of volatilisation and gradient of concentration in the containers. First choice were 112 mL flasks, with a bulk space of 109.5 mL and a neck space of 1.5 mL leaving only 1.5 mL of headspace, following the procedure described by Wang *et al.* [217]. The bottles were filled with 110.5 mL of distilled water, and 40 microliters of benzene were added using a micropipette and the containers were immediately sealed. Concentration gradients along the length of the round bottom flasks were measured after 30 min stirring by an orbital agitator, and the test was repeated using magnetic stirrers. Differences in the initial

concentrations measured in different bottles could not be ascribed purely to evaporate losses; alternatively, benzene could stick on the surface of the bottles or be adsorbed by the porous or dirty glass and caps, or the concentration of benzene in the bulk could be inhomogeneous, due to the shape of the flask. New cylindrical bottles were thus used and the weight was measured before and after mixing to be sure that losses were due only to volatilisation. The stirring procedure was conducted with magnetic stirrers and no gradient of concentration was observed after half an hour; the bottles were opened and closed in < 3 s during sampling and the concentration of benzene was lower than its solubility, so the volatilisation rate was found to be negligible.

The adsorption behaviour of hydrophobic Z1H was only tested using aqueous benzene, agitated using a rotary shaker to guarantee sorbent contact with the aqueous phase, which could not be guaranteed by use of a magnetic stirrer, as used for the hydrophilic materials, due to the fact that the light hydrophobic material floats in water. Blank tests, conducted without sorbent, demonstrated negligible volatilisation rates for both kinetic and adsorption standard tests. Stirring rates used were constant: 200 rpm for magnetic stirring and 20 rpm for rotary stirring. Sampling was also performed at various depths within a selected test vessel to verify the absence of concentration gradients within the bulk.

During kinetic tests, each time that a sample was taken, a small amount of benzene would be lost by volatilisation, but these amounts were found to be negligible and, therefore, had no effect on the kinetic curves obtained.

7.4.1.2 Quartzene

7.4.1.2.1 Hydrophilic ND, CMS and Z1

Kinetic data were obtained as outlined above and in Chapter 6.4.2. Results show a logarithmic relationship for the first 6 h of data, in which 84-90% of adsorption occurred on CMS and ND samples. The full equilibration time was < 24 h, for both benzene and toluene uptakes (Figures 7.17 and 7.18).

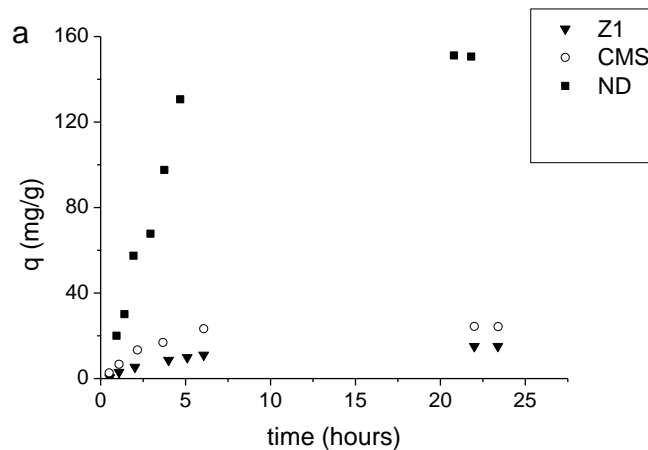


Figure 7.17: Kinetic profiles of benzene adsorption on Z1, ND and CMS at 293 K.

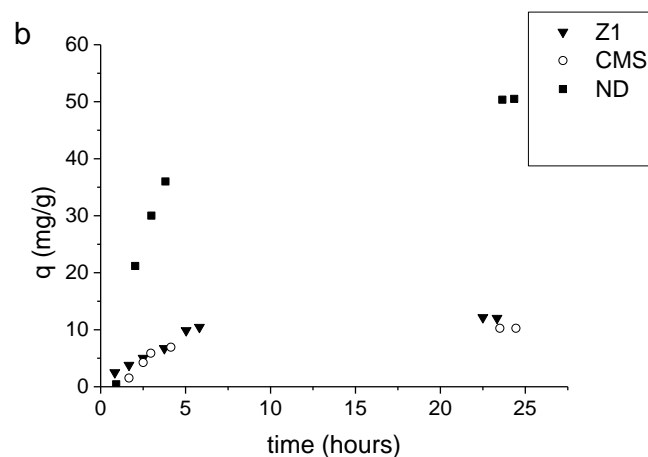


Figure 7.18: Kinetic profiles of toluene adsorption on Z1, ND and CMS at 293 K.

Quartzene Z1 showed slower kinetics, with < 80% of toluene and < 70% of benzene adsorbed after 24 h. Hydrophobic silica aerogels have been shown to reach their full adsorption capacities in < 1 h [219] or even < 30 min [218]; the materials tested here show good short time performance but it should be noted that full equilibration takes several hours.

The Freundlich adsorption model [245] has been used extensively to determine adsorption capacities, mainly due to the fact that it considers the heterogeneity of real surfaces. It is described by Equation 3.1 for the adsorption of gas, while by Equation 1.1 and by the following analogue for adsorption in aqueous solution:

$$q = kC_e^{1/n} \quad \text{Equation 7.1}$$

where:

- q = mg adsorbate/g adsorbent;
- C_e = equilibrium concentration of the solute (mg/L);
- k = constant, indicator of adsorption capacity (L/g);
- $1/n$ = constant, related to the intensity of the adsorption.

Higher values of k indicate higher maximum adsorption capacities; while higher $1/n$ values (> 1) denote favourable adsorption. The $1/n$ values obtained in this study are all > 1 , hence, adsorption for all materials with both adsorbates is dominated by physical sorption, as opposed to chemical sorption [246]. The Freundlich model was found to fit the data well for benzene and toluene adsorption on all the hydrophilic amorphous silica tested (Figures 7.19 and 7.20).

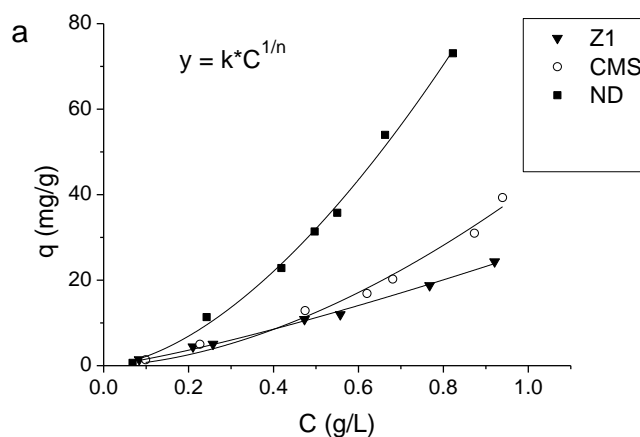


Figure 7.19: Adsorption isotherms at 293 K for benzene on Z1, ND and CMS at 293 K.

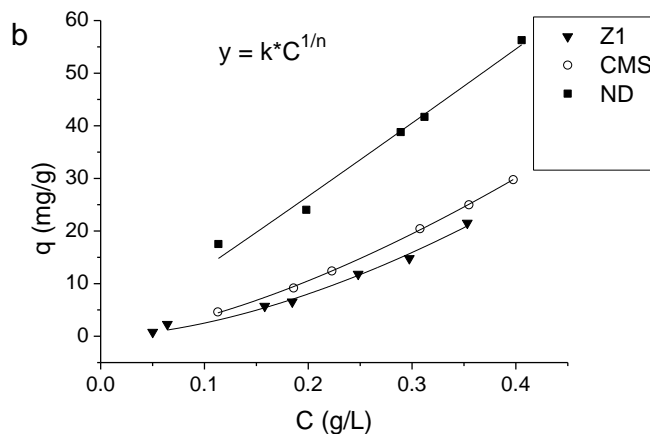


Figure 7.20: Adsorption isotherms at 293 K for toluene on Z1, ND and CMS at 293 K.

Aerogels studied previously show higher uptakes for toluene compared to benzene, however, it is important to note that such results are based on adsorption isotherms obtained for two adsorptives with disparate solubility limits; consideration of the parameters obtained by Freundlich analysis show that, while k values support this observation, the $1/n$ values demonstrate the theoretical maxima would be greater for benzene, in agreement with previous findings [217, 218]. Such high concentration behaviour is observed as a possible consequence of the delocalisation of the ring in benzene, which is reduced for toluene; also, the functional group of toluene may cause associated packing effects, reducing the effective adsorption capacity, hence the maximum adsorption uptake, but only at high theoretical maximum concentrations. It can be seen, from Table 7.5, that the ND and CMS samples perform best from the three sorbents studied in the range of concentrations used, as supported by the k values obtained from Freundlich analysis, with maximum adsorption capacities for ND estimated as close to the adsorbate solubility limits: 78.8 mg/g and 264 mg/g for toluene and benzene, respectively. The higher adsorption of Quartzene ND is ascribed, not only to the comparatively high surface area of this material but also, to its discrete pore size distribution centred around 3.3 nm, which provides good access for the organic molecules of interest while also being sufficiently narrow to prevent the molecular repulsion that can be observed with large adsorbate clusters. The results obtained for Z1 show a greater $1/n$ value for toluene compared to benzene, which is contrary to previous findings and the other data reported here. Z1, which was the only original material used

in granular form, underwent significant mechanical degradation during stirred reaction experiments.

Table 7.5: Freundlich adsorption model parameters calculated using data obtained for adsorption of toluene and benzene of samples used in this study, measured at 293 K. Maximum uptakes are determined from extrapolative interpolation to either a benzene solubility of 1.763 g/L or a toluene solubility of 0.57 g/L [247].

Sample	Adsorbate	K (L/g)	1/n	Adj. R ²	Max uptake (mg/g)
Z1	benzene	26.44	1.23	0.9954	53.25
	toluene	120.81	1.68	0.9861	46.91
CMS	benzene	41.42	1.73	0.9820	110.48
	toluene	120.09	1.51	0.9995	51.36
ND	benzene	102.23	1.67	0.9950	264.03
	toluene	141.15	1.04	0.9890	78.82

The theoretical amount of benzene corresponding to a monolayer coverage can be calculated from the surface area obtained from alpha-plot analysis and the molecular size of benzene ($\sim 0.5 \text{ nm}^2$). Such amount corresponds to 85.87, 41.77 and 141.64 mg/g, respectively, for Z1, CMS and ND samples. The surface of Z1 samples is then likely only partially covered by benzene molecules, while the adsorption on samples CMS and ND likely involves both surface coverage and pore-filling.

7.4.1.2.2 Comparison of hydrophilic and hydrophobic version of Z1 and CMS

Only aqueous benzene concentrations below 0.25 g/L were explored in the comparison of adsorption characteristics the hydrophilic and hydrophobic versions of Quartzene. Adsorption was faster and a higher quantity of benzene was adsorbed from the hydrophobic materials (Figures 7.21, 7.22 and 7.23). Notwithstanding the fact that the stirring rate was faster for the hydrophilic samples (200 rpm with magnetic stirrer, versus 20 rpm for the rotary stirrer adopted for hydrophobic silica), hydrophobic

Quartzene demonstrates quicker adsorption, as can be seen in Figure 7.21. Furthermore, no significant mechanical degradation and absolutely no degradation were observed for Z1H and CMSH, respectively, even after 5 d of rotary stirring at 20 rpm. Equilibrium was reached in < 3 h for Z1H, while previously studied hydrophobic aerogels, particle size < 250 μm , were found to reach full adsorption capacity in < 1 h, adopting a similar method and rate of stirring [219]; this difference is likely due to differences in particle size, with a much larger particle size studied here. Testing the granular form of sorbents, as opposed to powders, provides greater insight in to material performance within a filter configuration, which is the most probable layout in a tertiary process dedicated to organics separation from water. The comparison of adsorption behaviour for hydrophilic and hydrophobic amorphous silica confirms that hydrophobisation is fundamental to multiple cyclic use of a material.

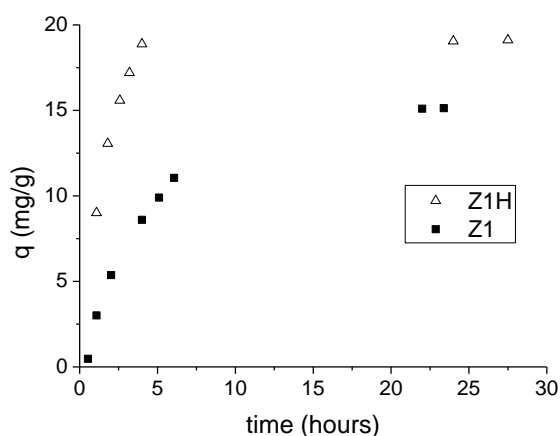


Figure 7.21: Kinetics obtained for benzene adsorption by granular forms of Quartzene Z1 and Z1H at 293 K.

At concentrations of ~ 200 ppm, benzene adsorption on Z1H is 4 times higher than for Z1, but the difference in terms of uptake between the two adsorbents is reduced with decreasing organic concentration (Figure 7.22). Same behaviour was observed for the comparative analysis between CMS and CMSH (Figure 7.23). Hence, at very low aqueous concentrations of organics, hydrophobisation may have negligible effect on pollutant access to the internal porosity of the material. This finding suggests a necessity to test adsorption performances of both hydrophilic and hydrophobic

materials, especially when target organic pollutant concentrations are low enough as to make the economic profitability of cyclic use, and associated regeneration costs, questionable given the expense of sorbent functionalisation.

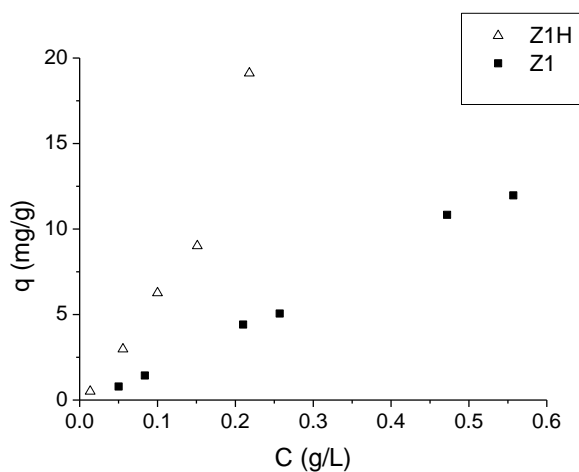


Figure 7.22: Adsorption isotherms comparison between hydrophilic and hydrophobic Quartzene: Z1 and Z1H.

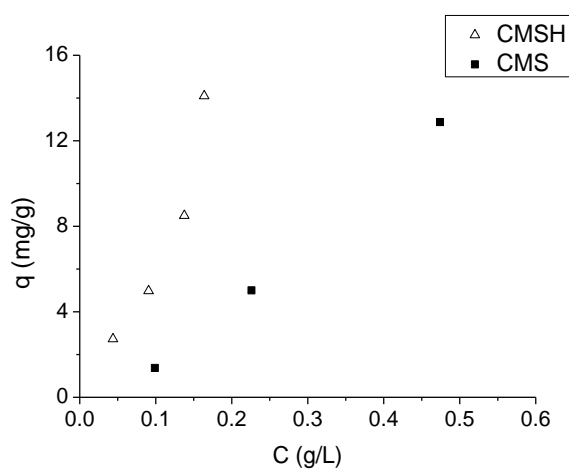


Figure 7.23: Adsorption isotherms comparison between hydrophilic and hydrophobic Quartzene: CMS and CMSH.

7.4.1.3 Silica xerogels

7.4.1.3.1 Benzene

Preliminary tests were conducted to evaluate differences in terms of adsorption capacity between gels obtained by HCl catalysis, named HF, and by citric acid catalysis, named

CF or CNF (if unfunctionalised). A sample of HF108, evaluated as the most promising between gels obtained with HCl, by surface area and pore size analyses, was immersed in an aqueous solution of 250 ppm of benzene in water. The uptake was found to be less than that obtained in analogous conditions with sample CF148. The higher yield of the latter, double that for HF108 obtained from the same quantity of precursor, encouraged the decision to focus further adsorption tests only on xerogels obtained by citric acid addition.

100 mg of xerogel sample CF148 were ground to obtain particles with main dimensions between 0.5 and 1.4 mm. They were then placed in glass bottles containing an aqueous solution of benzene (250 mg/L) previously equilibrated for 3 h with magnetic stirring. Kinetic tests using a rotary stirrer showed a long equilibration time (Figure 7.24); 50% of adsorption capacity was measured in 5 h, while full equilibrium was reached within 2 d.

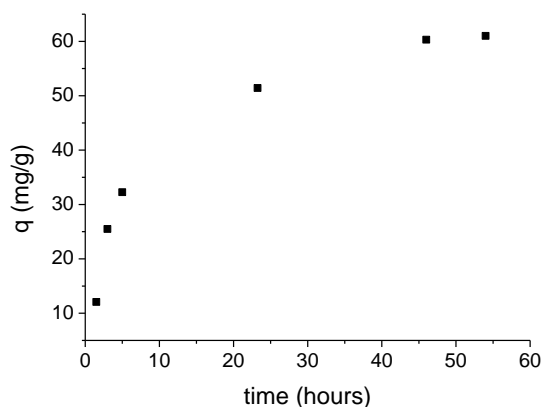


Figure 7.24: Kinetic of adsorption of benzene on the xerogel sample CF148.

Unfunctionalised samples of xerogel catalysed with citric acid showed insufficient mechanical resistance during the rotary stirrer tests, and were recovered as powder after 1 d of mixing. The same result was obtained with samples catalysed with half TMCS/sodium silicate ratios with respect to the full functionalised samples. It can be concluded that materials which are not fully functionalised, synthesised by APD and low temperature, cannot be used for the uptake of organics from water in a filter configuration.

First adsorption tests with benzene on xerogel samples followed Langmuir-Freundlich behaviour, but the position of the point obtained at concentrations < 100 mg/L suggested a different behaviour at low concentrations. Indeed, the inclusion of that point in the plot would give an x-axis intercept far from 0 g/L. However, it was impossible to validate this assumption without the determination of more points. Hence, a lower range of concentrations was investigated using the xerogel sample CF148 and a two-step adsorptive mechanism was confirmed. The Langmuir-Freundlich behaviour was again confirmed at concentrations > 125 mg/L, while a Langmuir trend could describe the first adsorption points (Figure 7.25).

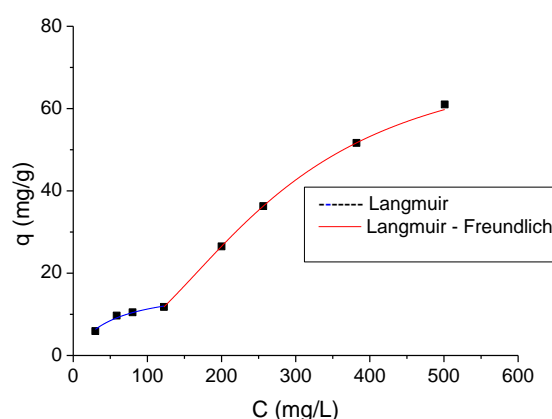


Figure 7.25: Adsorption of benzene on xerogel CF148. Data confirmed a change in the shape of the isotherm around 125 mg/L.

Table 7.6: Parameters of models used to fit the adsorption data of benzene in water (Figure 7.26). Sample: CF148.

Langmuir			
q_{\max} (mg/g)	b (L/g)	R^2	
19.41	0.0155	0.9823	
Langmuir-Freundlich			
q_{\max} (mg/g)	k_s (L/g)	n	R^2
74.03	0.0038	2.1956	0.9997

A similar adsorption isotherm was recently observed on mesoporous silica by Maretto *et al.* [203], who suggested a hybrid isotherm model (Equation 3.27) similar to that obtained by Lee for adsorption of gaseous hydrocarbons on mesoporous silica MCM-48 [205]. In Maretto's work, the organic uptake at low concentrations is described by the Langmuir model and shifts to Langmuir-Freundlich behaviour at concentrations > 75 mg/L. Similarly, to gas adsorption, the first step is related to adsorption on the wall of the mesoporous channel until a monolayer is formed, in agreement with the Langmuir model, then the adsorption continues with the formation of successive layers in agreement with the Langmuir-Freundlich model, until the filling of the entire mesoporous channel. The theoretical amount of benzene corresponding to a monolayer coverage calculated as described in Chapter 7.4.1.2 would be ~ 168.1 mg/g, significantly greater than the value given from Langmuir analysis. The reason could be attributed to the fact that hydrophobization of the surface is only partial, i.e. only a fraction of the hydroxyl groups is replaced by methyl functional groups. Surface coverage would be then only partial and only a fraction of the pores would be interested by the micropore-filling process. In the plot used by Maretto *et al.* (Figure 7.26) no experimental values were obtained > 150 mg/L and the model probably underestimates the adsorption of benzene at concentrations over this value. This hypothesis is supported by the results obtained in the present work and by the work of Simpson *et al.* [192] and Wang *et al.* [217].

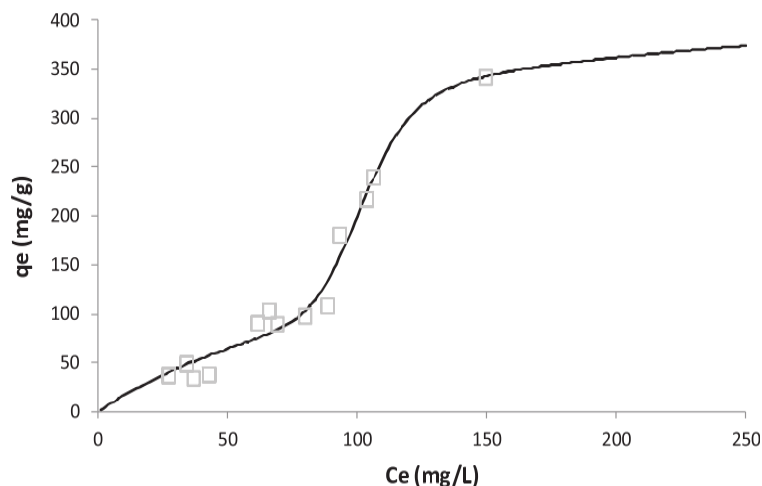


Figure 7.26: Benzene adsorption on mesoporous silica alumina [203]. Data fitted by a model resulting from the combination of Langmuir and Langmuir-Freundlich equations (Equation 3.27).

7.4.1.3.2 3,4-dichloroaniline

Kinetic tests using a rotary stirrer revealed an equilibration time of ~24 h, with 75% of the sorption capacity reached within the first 6 h, as can be seen in Figure 7.27.

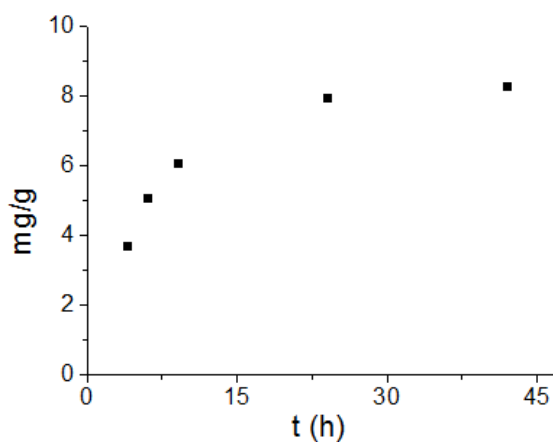


Figure 7.27: Adsorption kinetics of 3,4-DCA by CF154, characterised as in Table 7.1, after 2 d rotary stirring at 20 rpm. Concentrations were determined by GC-FID analysis.

Adsorption tests confirmed Langmuir-Freundlich behaviour for concentrations > 40 mg/L (Figure 7.28). The adsorption capacity of 3,4-DCA was found to be similar to benzene uptake at a concentration of 130 mg/L (12 mg/L), but lower than benzene uptake for lower concentrations (Figure 7.25). Considering the solubility of 3,4-DCA

and benzene at 293 K (0.58 g/L and 1.77 g/L, respectively), it can be concluded that the adsorption trend of 3,4-DCA it is similar to that obtained for benzene at concentrations between 125-600 mg/L, shifted to a lower range of concentrations (40-125 mg/L), as the solubility limit of 3,4-DCA is lower. Indeed, 90% of the estimated q_{\max} is reached at ~125 mg/L for 3,4-DCA and at 600 mg/L for benzene, following the same adsorption trend from concentrations above ~8% of their solubility limits. The x-axis intercept of the Langmuir-Freundlich plot for 3,4-DCA would again be far from zero (Figure 7.29), as observed for the adsorption of benzene on silica xerogels. Thus, further analyses could be useful to verify the presence of a two-step adsorption mechanism for the uptake of 3,4-DCA, as the one observed for benzene adsorption. However, such tests have not been conducted here due to difficulties in working at the low concentrations required. Indeed, the GC-FID, which was the instrument giving the most reliable results during the adsorption tests carried out in batch, could not provide good quality peaks with sufficient resolution at low concentration. This was not due to the capillary column, but likely to the noise from the FID detector, despite a careful cleaning procedure. This issue could not be resolved, hence, the results presented here are subject to the region afforded by the instrument used.

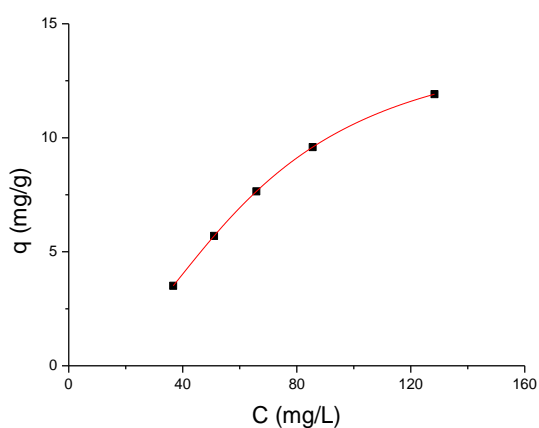


Figure 7.28: Isotherm of adsorption at 293 K of 3,4-DCA by CF154, characterised as in Table 7.1, after 2 d rotary stirring at 20 rpm. Concentrations were determined by GC-FID analysis.

Table 7.7: Parameters of Langmuir-Freundlich fit of 3,4-DCA adsorption from water at 293 K by CF154 (Figure 7.28).

Langmuir-Freundlich			
$q_{\max}(\text{mg/g})$	$k_s (\text{L/g})$	n	R^2
14.4340	0.00161	2.1462	0.999

Adsorption capacities for silica xerogels were found to be greater than those determined for silicate minerals in previous studies; adsorption on silicate like halloysite, kaolinite and montmorillonite is presented in Table 7.8. Differences are likely to be related to the greater pore volume of xerogels and to the role of this parameter in the physical adsorption mechanism.

With regard to the adsorption mechanism, 3,4-DCA removal from water by halloysite was described as occurring via the fast diffusion of 3,4-DCA to the surface of the clay mineral in the first 180 min, and continues as slower interparticle diffusion [24]. Chloroanilines are mainly sorbed on the mineral surface of kaolinite, while the structure of montmorillonite allows swelling with sorption in the interlayer [11]. Here, mesoporosity is assumed to play the main role in the adsorption process. If the double-step mechanism observed for benzene is assumed to also occur for 3,4-DCA uptake, the first step may be related to adsorption on the wall of the mesoporous channel until the achievement of a monolayer, while the second step could correspond to the formation of successive layers in agreement with the Langmuir-Freundlich model, until complete filling of the mesoporous channel.

Table 7.8: Surface area, pore size and adsorption data of different material tested for the removal of 3,4-dichloroaniline from water. Parameters q_m and b refer to the Langmuir model (Equations 3.9 and 3.10).

Adsorbent	Surface area	Pore volume	q_m	b	Equil. time	Stirrer type	Ref
	(m^2/g)	(cm^3/g)	(mg/g)	(L/g)	(h)		
Halloysite	76.6	0.039	0.078	0.0027	> 3	rotary	[24]
Kaolinite	/	/	0.311	0.009	> 96	electrom.	[90]
Montmorillonite	/	/	0.077	0.023	> 96	electrom.	[90]

7.4.2 Microcolumn tests

7.4.2.1 3D column printing

7.4.2.1.1 Model design

All internal components of the column were individually created using the 3D modelling tool specified in Chapter 6.4.3. Working from the top of the column to the bottom they comprise:

- a 7 mm diameter cylinder of 7 mm length;
- a 1 mm diameter cylinder of 1 mm length;
- a truncated cone with 1 mm diameter top (to fit the previous tube) and 12.5 mm diameter base, with 5.75 mm height (to obtain the required 45° angle);
- a 12.5 mm diameter cylinder of 40 mm length (the inner column);
- a reverse truncated cone with 12.5 mm diameter base, height of 1 mm (to obtain the 20° angle) and 7 mm diameter base;
- a 7 mm diameter cylinder of 7 mm length.

A Boolean union was used to combine the objects listed above into one solid piece; this command trims the shared areas of selected surfaces, creating a single polysurface from the unshared areas. The so-created inner part of the column (Figure 7.29, LHS) was then fitted into a cylinder of 25 mm diameter and height equal to the sum of the heights of the previous parts (Figure 7.29, RHS).

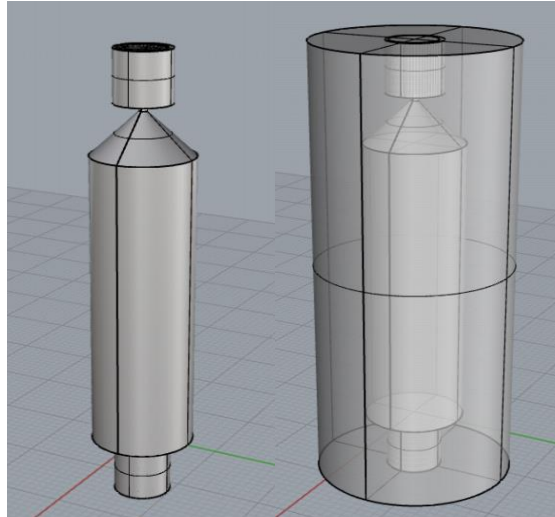


Figure 7.29: Inner column (L) and its fitting into the external cylinder (R).

Using a Boolean difference, which trims the shared areas of selected polysurfaces with another set of polysurfaces, the volume of the inside part of the model was extracted from the outside cylinder. Spirals were then designed in the inner part of the upper and lower cylinders of 7 mm diameter and 7 mm height, to permit fitting of the required connections. Once complete, the model was extracted as a .STL file, which stands for Stereolithography file, and sent to the 3D printer.

7.4.2.1.2 Printing the model

The .STL file created as described in Chapter 7.4.2.1.1 was loaded in the software preForm, provided by FormLabs. The model was then 3D printed on clear methacrylate photopolymer resin. After loading, two different orientations of the model, horizontal and inclined at 45°, were chosen, and related supports were designed for correct printing. Figure 7.30 shows the model in both orientations ready for printing:

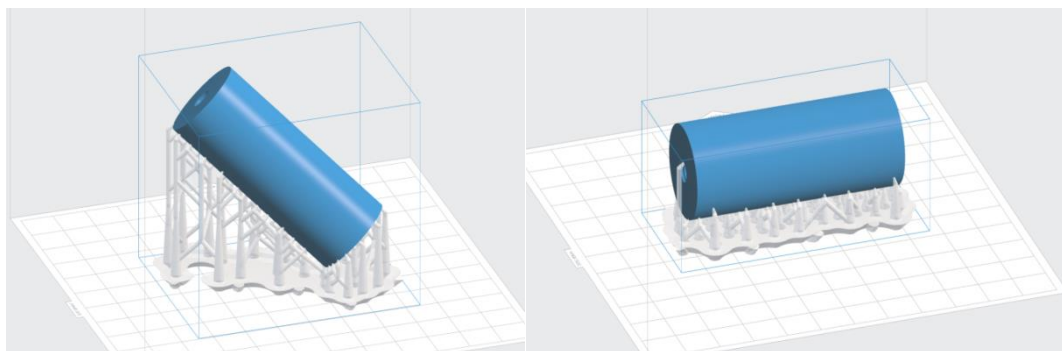


Figure 7.30 : Models of the microcolumn and related supports, as shown by the software preForm (FormLabs).

The printing time for the model on the RHS of Figure 7.30 was 4 h, requiring 31.41 ml of resin, while the model on the LHS required 1 h 38 min and 30.99 ml of resin due to the lower number of layers used in the print. The thickness of each layer was 0.1 mm. When each print was complete, the model was taken out of the printer, the supports were removed with a cutting tool, and the column was washed in isopropyl alcohol to eliminate any remaining liquid resin.

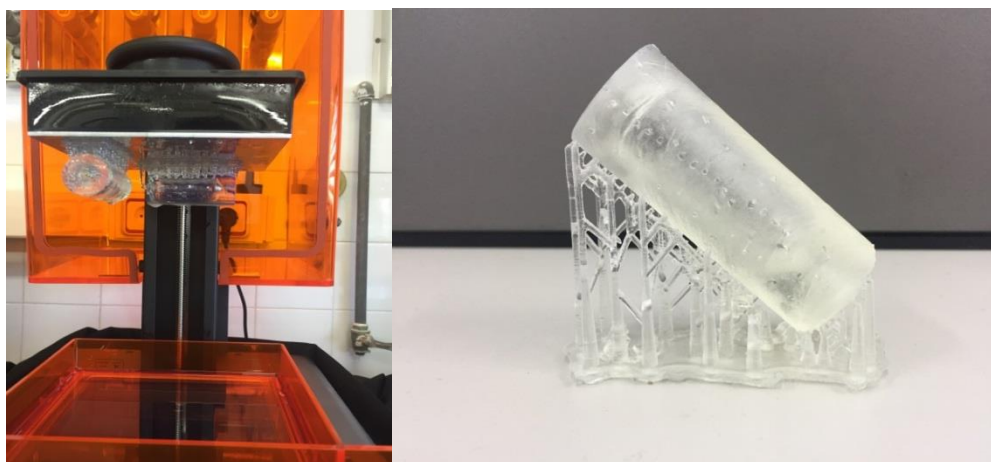


Figure 7.31: LHS: printed column on Form1+ 3D printer (FormLabs). Printed column inner still contains resin that was deposited but not polymerised. RHS: printed column on its supports, prior to smoothing.

The penultimate processing step involved a CL-1000 ultraviolet crosslinker, used to cure the resin and remove the residual surface residue of methacrylate photopolymer

and the associated ‘tacky’ sensation (Figure 7.32, LHS); finally a lathe was used to smooth the surface of the model (Figure 7.32, RHS).



Figure 7.32: Printed columns inside the CL-1000 ultraviolet crosslinker (L) and column smoothing (R).

7.4.2.2 Breakthrough curves

30 mm x 7 mm and 40 mm x 10 mm columns were used and preliminary tests were conducted to evaluate the flowrate applicable without incurring overpressure (with consequent partial return of the flow in the sample container). Overpressure problems were experienced with the smaller column. Furthermore, channelling was less likely in the larger column, so the data reported here refer to the 3D printed 40 mm x 10 mm column. The materials were slightly swollen after flowing with methanol, with the increased volume notably maintained after washing with water. The sample solution organic concentration was determined, both during and at the end of the test, to confirm the absence of losses. For the same reason, the sample was flowed through the system after disconnecting the column and again no significant losses were recorded. Hence, it can be assumed that the difference between the concentration of the organic in the solution before and after passing through the column it is due to adsorption on the packed material. Adsorption capacities were estimated by excluding the first 2 mL of sample flowed to wash the column from the water previously introduced and were limited to the uptake corresponding to the last point measured, so ~90% of the ratio C/C_0 , where C_0 is the initial concentration of the organic in the solution flowed and C is the concentration of the organic in the solution leaving the column.

7.4.2.2.1 Quartzene

230 mg of NDH, provided with a particle size between 75 and 200 μm , were packed into the fabricated microcolumn, and a solution of 73.3 mg/g benzene in water was flowed through it at 1 mL/min. The flowrate selected equates to an EBCT_s of 1.47 min and EBCT_L of 19.5 min, for a particle size of 0.5 mm to be employed in the bench scale reactor. The removal efficiency at $0.9 \cdot C/C_0$ was found to be 5.85 mg/g, i.e. insufficient to support scale up of the reactor.

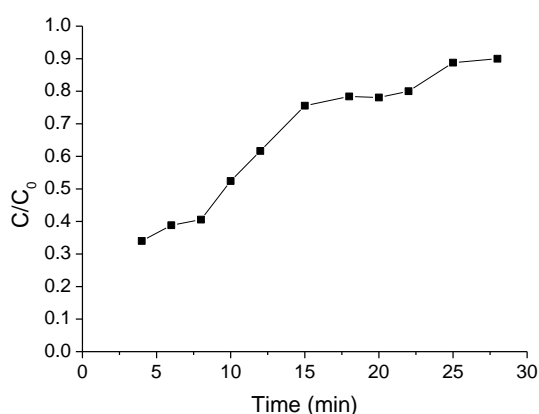


Figure 7.33: Breakthrough curve of benzene solution, 73.3 mg/L, flowed through microcolumn packed with 230 mg of NDH at 1 mL/min.

The analyte was successfully desorbed by the use of automated solid-phase extraction. Higher flowrates were not investigated, as even lower adsorption capacities would be expected, as contact time would be reduced. Higher removal efficiencies, coupled with no increase in EBCT_L would be required for the adsorbent tested to be used for treatment of produced water prior to a membrane configuration, especially in offshore facilities.

Table 7.9 : Parameters related to microcolumn tests with sample NDH (average particle size R_{sc} assumed equal to 0.14 mm and assuming 0.5 mm as particle size of the large column).

Adsorbent	Pollutant	Concentration	R_{sc}	EBCT _{sc}	EBCT _{LC}	Flowrate	Uptake
		mg/L	mm	min	min	mL/min	mg/g
NDH	Benzene	73.3	0.14	1.47	19.5	1	5.85

7.4.2.2.2 Silica xerogels

110 mg of silica xerogel, catalysed with citric acid and with H_2O/Na_2SiO_3 ratio = 148, were packed into a capillary microcolumn. The material was crushed and sieved to obtain particle sizes between 60 and 140 μm . A 105.12 mg/L benzene solution was flowed into the column at 0.6 mL/min; the related breakthrough curve is shown in Figure 7.34. The column was then packed with the same amount of adsorbent and solutions of 20 mg/L and 16 mg/L of 3,4-DCA were flowed at rates of 0.6 mL/min and 1.8 mL/min, respectively. Both the analytes were then successfully desorbed by the use of automated solid-phase extraction.

The uptake of benzene at $0.9 \cdot C/C_0$ was 22.62 mg/g, and this significant removal efficiency is related to long EBCT_s, thus, long EBCT_L, during flow. Benzene adsorption was tested at selected concentrations, which were higher than those used for 3,4-DCA and in keeping with the range of interest for the offshore oil & gas sector probed in the present work. As described in Chapter 5.2, the sorbents studied here would not be competitive with hydrocyclones or flotators at concentrations of BTEX >100 mg/L, nor would they be competitive with nutshell or membrane for BTEX concentrations <20 mg/L.

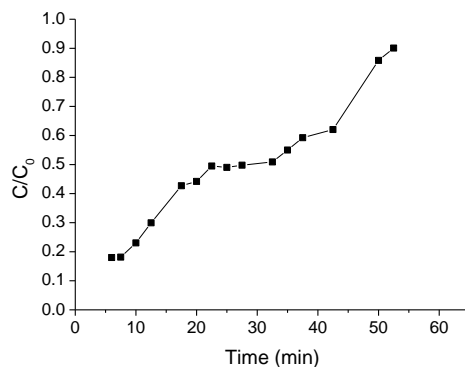


Figure 7.34: Breakthrough curve of benzene 105.12 mg/L at 0.6 mL/min, flowed through a microcolumn packed with 110 mg of silica xerogels catalysed with citric acid and with H₂O/Na₂SiO₃ ratio = 148.

Greater flowrates, despite the corresponding reduction in adsorption capacity, could lead to a positive evaluation of the material for the use in a bench scale reactor; 1.8 mL/min was tested, but was judged unsuitable, as breakthrough curves started with values of 0.5 C/C₀. Silica xerogels synthesized here could then find an application for the adsorption of benzene, but only in systems for which fast adsorption rate is not a priority.

The uptake of 3,4-DCA was found to be >4.63 mg/g and >7.17 mg/g at flowrates of 1.8 mL/min and 0.6 mL/min, respectively; the breakthrough curves of the two runs are shown in Figure 7.34. The flowrate of 1.8 mL/min gives an EBCT_L of 20.7 min, considering 0.5 mm particles to be employed in the full scale reactor. The rate of adsorption, and the adsorption capacity of these silica xerogels, could be promising for a large scale application, as filling of filters, cartridges or permeable reactive barriers.

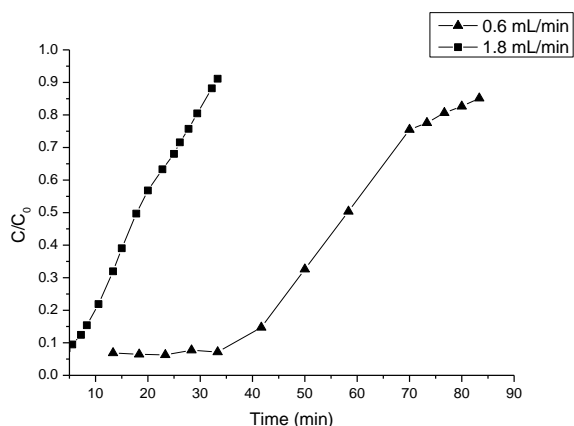


Figure 7.35: Breakthrough curves of 3,4-DCA adsorption on 110 mg of silica xerogels catalysed with citric acid and with H₂O/Na₂SiO₃ ratio = 148, 16 mg/L at 1.8 mL/min; 20 mg/L at 0.6 mL/min.

It is interesting to note that both the adsorption capacities obtained with column tests exceed those verified through batch test (Chapter 7.4.1). This could be due to interparticle retention of the organic molecules and/or methanol conditioning prior to column packing.

Table 7.10: Parameters related to microcolumn tests using silica xerogels catalysed by citric acid (ratio H₂O/acid =148), with average particle size R_{sc} of 0.1 mm and assuming 0.5 mm as particle size of large column.

Adsorbent	Pollutant	Conc. mg/L	R _{sc} mm	EBCT _{sc} min	EBCT _{LC} min	Flowrate mL/min	Uptake mg/g
Silica xerogel	benzene	105.1	0.1	2.44	61	0.6	22.62
	3,4-DCA	20	0.1	2.44	61	0.6	7.17
	3,4-DCA	16	0.1	0.83	20.7	1.8	4.63

7.5 Membrane: casting procedure

Silica xerogels failed to adhere to the nylon disks, while all Quartzene samples crushed to a particle size <75 µm were cast successfully. The oven temperature was initially set at 90 °C but the silica particles did not adhere to the surfaces, hence the temperature was

lowered to 70 °C. The coated surfaces were found to dry within 50 min, before testing in a vacuum filtration manifold system (similar to the one shown in Figure 7.35) for the separation of aqueous rhodamine and benzene. However, the results were not recorded because of the large amount of benzene stripped by the vacuum (about 30% of the initial concentration at 75 mg/L, as verified by a test with a non-covered nylon disk). The disks were recovered after testing with no evidence of material removal from their surface, hence, the casting procedure is considered successful. Future work could involve the testing of a system able to assess the adsorption performance of the material casted on nylon disks (thus avoiding large amounts of losses of the analyte due to vacuum) as preliminary evaluation of his suitability to be used for a membrane process.



Figure 7.36: vacuum filtration system [248].

8 Conclusions

8.1 Introduction

Produced water is the largest by-product generated by oil and gas extraction, hence, there are significant quantities requiring remediation, of which the removal of dissolved oils is the final step. Legislation on water discharge is becoming increasingly stringent; moreover, many water-stressed countries with oilfields are searching for ways to supplement their limited fresh water resources. Focusing on efficient methods to treat produced water will make its channelisation to agricultural and industrial uses a real option. Furthermore, some organic pollutants named Endocrine Disrupting Chemicals (EDCs) have become a source of high concern, not just for marine environments but also for drinking water treatment plants. Reports of adverse changes in wildlife exposed to these substances, and the suggestion that humans could also be at similar risk of adverse health effects [13, 14], have raised concerns about the urgent need for action to understand and reduce such risks. Many technologies have been developed for the degradation of pesticides; however, attention should be given to the fate of metabolites. EDC 3,4-DCA is a degradation product generally more toxic than the parent substances, and with high persistence. If it is covalently bound to humic substances in the soil, the risk of groundwater contamination through leaching is low, but this also lowers the rate of mineralisation [86].

Solid sorbents are among the technologies used for removal of organic pollutants from water. While hydrophobic aerogels and xerogels exhibit very attractive properties for oil spill applications, very few studies have investigated their adsorption performance with low organic concentrations. Authors verified the performance of aerogels for the adsorption of the most representative dissolved organics in produced water. Silica gels were synthesised using tetramethoxysilane (TMOS) as precursor and replacing the Si-OH groups, responsible for adsorption of water, with Si-CH₃ groups by addition of MTMS and TMES. Adsorption tests revealed an adsorption capacity of benzene 300 times higher than GAC [218], with equilibration time reached in < 30 min. The increased capacity is due to the fact that the solvent fills the available volume of the adsorbent, which swells, leading to a larger volume of the aerogel than the initial

volume. An issue with these past studies is that many work at excessive concentrations of organic species within the aqueous phase; whereas produced water, at the refining stage, contains only low concentrations of dissolved oil droplets, mainly part of the BTEX group. Hence, it is fundamental to evaluate adsorption performance with concentrations of these pollutants well under the solubility limit. In addition, the cost of the precursors and functionalisation, in conjunction with the lower uptakes observed for systems where oils are well dispersed in solution, hinder the use of these materials as sorbents in the final stages of produced water treatments. Furthermore, it has been recently hypothesised that aqueous solutions of organic compounds cannot fill the interior pores of functionalised silica aerogels, owing to the hydrophobicity of the material; hence, only the external space is available for adsorption [249]. Hydrophilic silica could then be promising for the adsorption of organics from very dilute solutions, but there have been limited studies into the adsorption behaviour of hydrophilic silica materials towards trace quantities of aqueous phase organic species, presenting a gap in the current knowledge base. Reviewing the literature, there appears to have been no research related to the uptake of organics in water by hydrophilic aerogels and xerogels, most likely as a result of the initial attention that these materials received as adsorbents for application to oil spills, hence, the focus was previously on increasing their hydrophobicity.

8.2 Characterisation and measure of the concentrations

UV-Vis analysis were investigated in this study for batch adsorption samples testing, as it has been used previously for similar analyses [219], however, it was deemed to be inaccurate, due to the presence of fine particles in the solution after the stirring test. Hence, gas chromatography was used for all concentration analyses of the batch samples. GC programs were optimised for analyses and, due to issues related to the long elution time of dimethyl phthalate, toluene was selected as internal standard for benzene and vice-versa; dimethyl phthalate was used as internal standard for 3,4-DCA, and repetitive analyses on the same sample were conducted to ensure gas chromatograph precision. UV-Vis technique was found reliable for the analysis of the microcolumn eluate, thanks to the glass fibre disk placed at the bottom of the column, which avoided any contamination of the outgoing flow from silica particles.

8.3 Sorbents: synthesis and characterisation

8.3.1 Amorphous silica Quartzene

The novel amorphous silica Quartzene was synthesised by Svenska Aerogel AB at low temperature and ambient pressure. Various Quartzene based sorbents were used in the study, namely: ND, Z1, CMS and the hydrophobic analogues NDH, CMSH and Z1H prepared by varying the level of activation of the silica source [232] and the addition of co-precursors. FT-IR spectra of hydrophilic Quartzene showed the presence of silanol polar groups, with Z1 and ND showing similar surface chemistries, while CMS exhibits more refined Si-OH bond peaks; consequently, these Quartzene materials can be confirmed as hydrophilic in nature. Z1H shows hydrophobic character, attributed to the Si-CH₃ bonds incorporated during the functionalisation process. ND have the highest surface area (597 m²/g) mainly due to the smallest pore size. All Quartzene samples exhibit significant total pore volumes and pore sizes determined for CMS, Z1, Z1H and CMS HPO samples were found to be distributed between 2 and 80 nm, while ND exhibited a sharp pore size distribution centred around 3.3 nm.

8.3.2 Silica xerogels

Several silica xerogels were synthesised using methods outlined in Chapters 6.1.2 and 7.1. Within the protocol used for citric acid catalysis, stirring was found to be critical for low concentrations of silicate due to partial instant gelation, while anyway instant gelation was always observed for H₂O/Na₂SiO₃ ratios < 110, which contrasts with higher ratios, as samples with ratios > 200 did not form a gel within 24 h. Increasing H₂O/Na₂SiO₃ ratio, increases dilution of the waterglass, thereby increasing gelation time, as a result of decreased collision frequency between condensing silica species. Once too small amount of silica is contained in the solution, the network created is thin and fragile. Hence, gels catalysed by citric acid addition with ratios ≥ 175, were confirmed too weak to overcome the washing procedure and they dissolved in water. With regard to the bulk density, it is already known to first decrease and then increase with increasing H₂O/Na₂SiO₃ ratios > 150 and acetic catalysis [232]; the least dense xerogels here catalysed with citric acid were those obtained between ratio 138 and ratio 154. Between xerogels catalysed by HCl addition, the lowest density was observed for a

ratio of 108. The amount of trimethylchlorosilane chosen for the functionalisation process was investigated on gels synthesised by citric acid catalysis. It was found strongly affecting pore volume, pore size and strength of the silica network.

Average pore diameter, pore volume and surface area were found to increase in gels from citric acid catalysis from ratio equal to 80 to ratios between 138 and 154. Longer time of cooling of the samples are likely related to major pore volume of xerogels obtained. The main pore size distribution is considerably narrower for the lower ratio examined. From ratios 108 to ratio 154 the distribution is centred on the same value, but ratios 148 and 154 showed sharper peaks than the lower ratios.

Xerogels with ratio 108 catalysed with HCl (HF108) and xerogels catalysed with citric acid (CF138, CF148 and CF154) gave significantly higher yields and lower densities than any other samples, and the latter results are in agreement with the work of Bangi *et al.* [1]. Sample HF108 exhibited the highest surface area and pore volume of those catalysed with HCl, but both parameters were lower than any samples obtained by citric acid catalysis, with the exception of CF80. Moreover, the yield of samples CF138 and CF154 was more than double any sample catalysed with HCl. Hence, when focussing on a such materials as sorbents, catalysis with citric acid was evaluated as the most promising choice between the two alternatives studied.

The analysis of two samples catalysed with citric acid with same $\text{H}_2\text{O}/\text{Na}_2\text{SiO}_3$ ratio revealed that the unfunctionalised CNF148 has lower pore volume ($0.48 \text{ cm}^3/\text{g}$) and lower average pore size than the functionalised CF148, which revealed a pore volume of $2.96 \text{ cm}^3/\text{g}$. However, CNF148 has a higher surface area ($707 \text{ m}^2/\text{g}$ VS $648 \text{ m}^2/\text{g}$); this is due to the significant micropore volume of the virgin xerogel ($0.41 \text{ cm}^3/\text{g}$ from α -plot analysis).

8.4 Adsorption performance

8.4.1 Amorphous silica Quartzene

Quartzene samples were tested for the adsorption of aqueous phase benzene and toluene, at concentrations below their solubility limits. Kinetics and isotherms were

determined by batch test. Direct comparison was made with the analogous hydrophobic version of samples Z1 and CMS.

Hydrophilic silica equilibrium was reached in < 10 h, with 70-90% of uptake in the first 6 h. Kinetic tests reveal up to 90% of benzene and toluene is adsorbed in the first 6 h of treatment, and up to 50% in the first 2 h. There were no significant differences between the rates of adsorption for either benzene or toluene. The adsorption mechanism is described fully by the Freundlich model, with $1/n > 1$, while the adsorption capacity, at low concentrations, is higher for toluene, as expected from the literature [218, 250]. Quartzene ND outperforms the other hydrophilic materials tests and shows adsorption capacities of 264 mg/g for benzene (solution concentration of 1.76 g/L) and 78 mg/g for toluene (solution concentration of 0.57 g/L), demonstrating the potential of these materials for produced water remediation.

Hydrophobic silica used in this study, demonstrated an equilibrium value four times higher than that of the hydrophilic analogues, reached in < 3 h at a concentration of 200 ppm benzene. A rotary shaker was used to stir hydrophobic materials, as magnetic stirring was found not able to guarantee optimum contact between sorbents and adsorbates. The comparison between hydrophilic Z1, CMS and hydrophobic Z1H, CMSH confirmed that hydrophobisation is required to impart the mechanical longevity for cyclic use, and leads to increased adsorption of benzene from aqueous phase concentrations > 50 ppm. It is notable that the observed differences in uptake between the two forms of Z1 and CMS are reduced as organic concentration decreases. This finding supports the hypothesis that at very low aqueous phase organic concentrations, hydrophobisation has no discernible effect on access of the pollutants to the internal porosity of the material. Possible explanation of this phenomenon was recently given only by Shi *et al.* [249]; aqueous solution of organic compounds cannot fill the interior pores of functionalised silica aerogel, owing to the hydrophobicity of the material. Thus, only the external space is available for adsorption. Hence, tuning the hydrophobicity of sorbents to perform multiple adsorption cycles with the added costs of regeneration, should be fully evaluated via a cost analysis to determine whether the actual pollutant concentrations are significantly high to justify the expense of a functionalisation process.

The removal efficiency of Quartzene NDH tested in the 3D printed microcolumn was found to be 5.85 mg/g of benzene at $0.9 \cdot C/C_0$, with an initial concentration of 73.3 mg/L, i.e. not sufficient to encourage the scale up of the reactor for produced water treatment facilities. Indeed, higher removal would be required for this scope, in light of a proven adsorption capacity of walnut shells media greater than 80 mg/g [145].

8.4.1 Silica xerogels

Sodium silicate xerogels synthesised by low temperature and room pressure methods were tested for adsorption of benzene and 3,4-DCA in water, using granular form to provide a clearer indication of how the material can be expected to perform in a filter configuration. The use of granules in places of powder allowed verifying the resistance to the stress induced by the immersion and stirring in water. The low density and hydrophobic character of these materials required the use of a rotary shaker to guarantee sorbent contact with the aqueous phase, which was not achieved by conventional magnetic stirring.

At the end of preliminary stirring test in water, only fully functionalised xerogels were recovered as granules, with no visible deterioration, confirming that functionalisation is required for cyclic use of sodium silicate based xerogels for water remediation. The uptake of HF108 was found to be less than that obtained in analogous conditions with CF148. The higher yield of the latter further encourages future focus on adsorption tests using xerogels obtained by citric acid addition.

Kinetic tests carried out for benzene adsorption on silica xerogels obtained by citric acid catalysis showed a long equilibration time, 50% adsorption capacity within 5 h and full equilibrium within 2 d. Adsorption tests confirmed a two-step adsorptive mechanism, where a Langmuir-Freundlich model was confirmed at concentrations > 125 mg/L, while a Langmuir trend described adsorption at concentrations < 125 mg/L. Similar results were recently observed on mesoporous silica by Maretto *et al.* [203]. As proposed in Langmuir's original model, the first step can be ascribed to adsorption on the mesopore walls until monolayer formation, whereafter formation of successive layers is in agreement with the Langmuir-Freundlich model, until complete pore filling. Despite the similar results obtained by Maretto *et al.* they used only experimental values

< 150 mg/L, hence, their model probably underestimates benzene adsorption at higher concentrations. The greater adsorption at higher benzene concentrations is not only supported by the results presented here but also the work of Simpson *et al.* [192] and Wang *et al.* [217].

With regards to 3,4-DCA sorption on xerogels catalysed with citric acid, kinetic tests showed an equilibration time of ~24 h, with 75% sorption capacity reached within the first 6 h. Adsorption tests confirmed Langmuir-Freundlich behaviour for concentrations > 40 mg/L, similar to the behaviour observed for benzene at concentrations > 130 mg/L. It is proposed that the Langmuir-Freundlich multilayer formation occurs at different concentrations for the two species, shifted due to their relative solubilities (0.58 g/L for 3,4-DCA and 1.77 g/L for benzene). The x-axis intercept of the Langmuir-Freundlich plot for 3,4-DCA would be far from zero, as observed for adsorption of benzene; hence, further analyses would be required to verify the presence of a two-step adsorption mechanism for 3,4-DCA. In such a case, the first step could be related to the adsorption on the wall of the mesoporous channel until the achievement of a monolayer, while the second step could correspond to the formation of successive layers in agreement with the Langmuir-Freundlich model, until the filling of the entire mesoporous channel.

3,4-DCA removal from water by halloysite occurs through rapid diffusion to the surface of the clay mineral in the first 3 h, and continues as slower interparticle diffusion [24], while chloroanilines are mainly sorbed on the surface of kaolinite, and sorption in interlayers has been observed in montmorillonite [11]. By contrast, adsorption of 3,4-DCA on silica xerogels was found to be greater than for silicate minerals as outlined above, for the xerogel materials the difference is ascribed to their greater pore volume and its main role in the physical adsorption mechanism.

Microcolumn tests made possible a preliminary evaluation of the suitability of the application of the silica xerogels tested in water treatment plants. The removal efficiency tested with the microcolumn apparatus was found greater than 22.62 mg/g for benzene at flowrate of 0.6 mL/min. This great removal efficiency is related to long EBCT_s, thus, long EBCT_L, during flow, making not advisable the use of these materials in offshore produced water treatment facilities. Indeed, the resulting EBCT_L would be

greater than 40 minutes, while for the large vessels of walnut shells typically employed is expected to be minor than 20 minutes. The uptake of 3,4-DCA was found >4,63 mg/g and >7,17 mg/g, respectively at flowrates of 1,8 mL/min and 0,6 mL/min, encouraging the scale up of an adsorption technology dedicated to groundwater in-situ remediation.

8.5 Application

Walnut shells can cost less than 4 \$/kg and are capable to adsorb oil up to 82.5 mg/g [145], so the development of competitive materials for the adsorption of soluble hydrocarbons from water has necessary to focus on cheaper precursors and synthesis, to obtain materials able to work within a range of concentrations greater than those usually treated by walnut shells in offshore facilities (as explained on Chapter 5).

The structure and the properties of Quartzene are comparable to silica aerogels: both have skeletal structures composed of porous silica, very low densities and thermal conductivities. A significant physical difference is that Quartzene is produced as a powder, not as a gel from a sol-gel process. Its chemical properties, in terms of hydrophilicity/hydrophobicity, can be tailored to fit the desired application and the porous structure can also be controlled, without the need of any surfactant. Unlike traditional aerogels, Quartzene is cheaper, environmentally friendly material, as a result of the ambient pressure and temperature conditions used in its manufacture and same consideration applies to silica xerogels here synthesised by the cheapest silica source available (sodium silicate) at room pressure and low temperature.

Micro Column Rapid Breakthrough tests coupled with Sequential Injection Analyses demonstrated that higher removal efficiencies coupled with lower Empty Bed Contact Times (EBCTs) would be required for all the adsorbent tested to be used for treatment of produced water prior to a membrane configuration, especially in offshore facilities. Notwithstanding the use of Quartzene based materials and hydrophobic sodium silicate based xerogels in offshore facilities for the treatment of produced water seems not advisable, the materials studied here are promising sorbents for the removal of organic pollutants from water. Adsorption capacity of Quartzene based sorbents on benzene

and toluene and the uptake of benzene of silica xerogels reveal their potential for the removal of these pollutants in any application which is not required the fast flowrates demanded from the offshore oil&gas sector. The rate of adsorption of 3,4-DCA, and the related adsorption capacity of the functionalised sodium silicate based xerogels tested demonstrate their potential for the removal of 3,4-DCA and other organic endocrine disruptors for the in-situ remediation of pesticides-polluted groundwater as part of permeable reactive barriers. With regard to the application in drinking water treatment plants, the performance of the sorbents need to be previously tested on a lower range of concentrations. All the sorbents studied here need to be tested on a wider range of organic pollutants to prove their potential in other applications. In order to establish their full capabilities, defined ranges of pollutant concentration should be identified to allow selection of the most appropriate hydrophilic or hydrophobic material type, with additional lifetime cycling measurements to assess the economic feasibility of their use in water treatments plants. An assessment of the performance of any proposed technology, based on five steps, would be fundamental to understand the potential of development. These steps are: i) the ability to remove selected contaminants; ii) associated energy requirements; iii) necessity for pre-treatments; iv) durability of the technology and v) mobility of the technology. Furthermore, a comparison with adsorbents currently used could be made, evaluating adsorption performance; cost of the material; breakthrough time; pre-treatment needed; and regeneration options available.

The comparison could be extended to alternative technologies, performing Life Cycle Assessment (LCA) analysis, and it would be useful to understand the relative positioning of such proposed adsorption technologies in the actual layout of a water treatments plant. Performance and flexibility are key targets; performance in organics removal requires reduced environmental impact, particularly energy consumption during adsorption and material regeneration, while flexibility is fundamental to the ongoing operation of each plant, limiting dead time. This second target is usually satisfied by using in series-reactors, allowing split flow from the exhausted reactor to another, until regeneration (or substitution) of the media in the exhausted reactor is complete. Ideally, such a plant would also be flexible in terms of water composition, suitable for different areas of the World.

9 Outcomes of the project

Within this PhD, the following article has been published:

Novel hydrophilic and hydrophobic amorphous silica: Characterization and adsorption of aqueous phase organic compounds. Andrea Luca Tasca, Farnaz Ghajeri, Ashleigh Flecher, *Adsorption Science & Technology*, 2017.

The following have been invited for the submission at the end of the present year as part of special issues:

- Organics adsorption on novel amorphous silica and silica xerogels: Micro Column Rapid Breakthrough test coupled with Sequential Injection Analysis and automated solid-phase extraction. Andrea Luca Tasca, Fernando Maya Alejandro, Ashleigh Flecher, Gemma Turnes. *Journal of Porous media*.
- Quartzene® process: From synthesis to commercial scale of a green nanoporous silica material. Farnaz Ghajeri, Andrea Tasca, Hassan Jafri, Klaus Leifer, Ashleigh Fletcher, Christer Söjstrom. *Current Opinion in Green and Sustainable Chemistry*.

Furthermore, awaiting acceptance from the *Journal of Environmental Science and Health*:

State of the Art of the Environmental Behaviour and Removal Techniques of the Endocrine Disruptor 3,4-dichloroaniline. Andrea Luca Tasca, Ashleigh Fletcher.

Moreover, a patent is pending:

A filter apparatus and a method for removing dissolved organic compounds from a water based liquid. Swedish pending patent application No. 1750086-9.

9.1 Publications

9.1.1 Published papers

Adsorption
Science &
Technology

Research Article

Novel hydrophilic and hydrophobic amorphous silica: Characterization and adsorption of aqueous phase organic compounds

Adsorption Science &
Technology

0(0) 1–16

! The
Author(s) 2017 DOI:
10.1177/0263617417692339

journals.sagepub.com/home/a



Andrea Luca Tasca

Department of Chemical and Process Engineering,
University of Strathclyde, UK

Farnaz Ghajeri

Department of Engineering Sciences, Applied Materials Science, Uppsala University, Sweden

Ashleigh J Fletcher

Department of Chemical and Process Engineering, University of Strathclyde, UK

Abstract

Very few studies have investigated the adsorption performance of hydrophobic and hydrophilic silicas with dissolved organics in water, which is a required final step during produced water treatment. The cost of functionalization also hinders the use of hydrophobic materials as sorbents. Novel hydrophilic silicas, prepared at low temperature and ambient pressure, were characterised by SEM, FTIR and BET analysis, and studied for the adsorption of aqueous phase organic compounds at concentrations below their solubility limits. Adsorption capacities were found to be up to 264 mg/g for benzene and 78.8 mg/g for toluene. Direct comparison is made with the analogous hydrophobic version of one of the silica materials, demonstrating comparable uptakes for benzene concentrations lower than 50 mg/L. This finding supports the hypothesis that, at very low aqueous phase organic concentrations, hydrophobicization has no discernible effect on access of the pollutants to the internal porosity of the material.

Keywords

Quartzene, benzene, toluene, produced water, GC

Corresponding author:

Andrea Luca Tasca, University of Strathclyde, James Weir Building, 75 Montrose Street, Glasgow G1 1XJ, UK. Email: andrea.tasca@strath.ac.uk

Creative Commons CC-BY: This article is distributed under the terms of the Creative Commons Attribution 3.0 License (<http://www.creativecommons.org/licenses/by/3.0/>) which permits any use, reproduction and distribution of the work without further permission provided the original work is attributed as specified on the SAGE and Open Access pages (<https://us.sagepub.com/en-us/nam/open-access-at-sage>).

Introduction

Silica aerogels are materials with large surface areas, high porosities, low densities and conductivities, which can be successfully used as thermal insulators, catalyst supports, adsorbents, and in many other scientific and commercial applications (Wang et al., 2015). Researchers reported a $\text{CF}_3(\text{CH}_2)_2$ -functionalized aerogel powder capable of absorbing up than 230 times its weight in oil (Reynolds et al., 2001), while further studies showed that such doped hydrophobic materials can adsorb more than 30 times the volume of toluene compared with Granular Activated Carbon (GAC) (Hrubesh et al., 2001). Silica gels, synthesised using tetramethoxysilane (TMOS) as the precursor, were modified by replacing the Si-OH groups, responsible for the adsorption of water, with S- CH_3 groups via addition of methyltrimethoxysilane (MTMS) and trimethylethoxysilane (TMES). Adsorption tests on the subsequent gels revealed maximum benzene adsorption capacities 300 times higher than GAC (Standeker et al., 2007), with equilibrium established in less than 30 min. Silica aerogels have been shown to uptake pure organic compounds, such as benzene and toluene, to levels in excess of 13g/g aerogel (Wang et al., 2011). The high uptakes are mainly due to the resulting swelling of the adsorbent.

Consequently, aerogels have been studied extensively for the absorption of oil spills (Adebajo et al., 2003; Olalekan et al., 2014; Reynolds et al., 2001; Wang et al., 2012); however, despite their adsorption potential for organic species, they have not been used in water treatment plants for the separation of petroleum hydrocarbons. Several researchers have previously tested aerogels on crude oil-water mixtures, and it has been proven that functionalization with fluorinated organic groups, which maximises hydrophobicity, gives the best performance in terms of organic adsorption from pure oil or oil-water mixtures (Hrubesh et al., 2001; Wang et al., 2012).

An issue with these past studies is that many work at excessive concentrations of organic species within the aqueous phase; whereas produced water, at the refining stage, contains only low concentrations of dissolved oil droplets, mainly part of the BTEX group (benzene, toluene, ethylbenzene and xylene). Hence, it is essential to evaluate the adsorption performance of potential sorbent materials with concentrations of these pollutants well below the solubility limits. Previous work compared benzene adsorption isotherms, using aerogel materials, an activated carbon and a polymeric resin, at similar concentrations, and no free oil phase present in the batch tests; the results showed that greater amounts of benzene and toluene were adsorbed from aqueous solution using activated carbons or polymeric resins rather than functionalized aerogels (Wang et al., 2011). Using aqueous concentrations of selected organic pollutants at one-tenth of their solubility limits, polymeric resin XAD4 and activated carbon AC F400 were shown to respectively adsorb 150 mg/g and 320 mg/g of benzene, 180 mg/g and 340 mg/g of toluene (Simpson et al., 1993; Wang et al., 2011). Hydrophobic silica aerogel 'Nanogel' TLD 301, the surface of which is decorated with trimethyl-silyl groups ($-\text{Si}(\text{CH}_3)_3$), was recently tested for the adsorption of organic compounds from aqueous phase, using adsorbate concentrations below the water solubility limits. Equilibrium was reached in under 20 min and the adsorption capacities were 87 mg/g for benzene and 223 mg/g for toluene, while the individual uptake of both organics, at $C \frac{1}{4} 0.1C_{\text{SAT}}$, was found to be less than 10 mg/L (Wang et al., 2011). Recently aerogels obtained from MTMS as a precursor and dried supercritically were shown to uptake more than 50 mg/g of benzene at a concentration of 50 mg/L of aqueous benzene, which is a significant result at such a low concentration (Perdigoto et al., 2012).

The results discussed above suggest that hydrophobic silica aerogels could be potential adsorbents for the treatment of oil spills. Hence, previous research has focussed markedly on hydrophobic media, with no known studies specifically related to the uptake of aqueous phase BTEX organics using hydrophilic silicas; consequently, many studies have focussed on improving the hydrophobicity of these materials. Hydrophobization of the inner surfaces of aerogels not only improves affinity to organic adsorbates, but it also helps to prevent long-term deterioration of the structure, due to the absorption of water; if water fills the pores of an aerogel and subsequently evaporates, then this acts as a second drying cycle and the structure can collapse, at least partially (Venkateswara Rao et al., 2011). The need to recycle hydrophilic silicas may be considered irrelevant if the absence of functionalising agents and the use of cheaper precursors and synthesis make the production and waste management of these materials economically suitable for a single adsorption cycle, hence, removing regeneration costs and associated issues. Such gains may be achieved by using simpler, less energy intensive processing methods and low cost synthetic routes using ambient pressure drying are already known to produce silica aerogels, from waterglass, with excellent mechanical properties (Zong et al., 2015).

In this paper, we propose a study of hydrophilic silicas that have been seemingly overlooked for organics removal from aqueous systems in the past. Hence, we characterise both hydrophilic and hydrophobic amorphous silicas, determining and comparing their kinetics and capacities of adsorption to selected organic species from aqueous media at a range of different concentrations below the solubility limit. Thus, allowing evaluation of the feasibility of the use of these materials as sorbents for produced water treatment.

Experimental

Adsorbents

Four Quartzene based sorbents were used in the study, namely: ND, Z1, Z1HPO and CMS types, all supplied by Svenska Aerogel AB (SvAAB). The structure of Quartzene and its properties are comparable to silica aerogels but the former is an amorphous silica material. Both have skeletal structures composed of porous silica, very low densities, and very low thermal conductivities. The only significant physical difference is that Quartzene is produced as a powder, not as a gel from a sol-gel process. Its chemical properties, in terms of hydrophilicity/hydrophobicity, can be tailored to fit a specific application and the porous structure can also be controlled, notably without the need of a surfactant. Unlike traditional aerogels, Quartzene is an environmentally friendly material, which is significantly cheaper to produce, as a result of the ambient pressure and temperature conditions used in its manufacture. *ND type Quartzene*: prepared via the precipitation of sodium silicate with sodium chloride (NaCl) at ambient temperature. A defined amount of dilute active aqueous sodium silicate solution ($\text{SiO}_2:\text{Na}_2\text{O} \text{ } \frac{1}{4} \text{ } 3.35$) was prepared, representing solution A, while solution B was composed of aqueous NaCl. Solutions A and B were mixed under rapid stirring and the resulting precipitate mixed with a defined amount of tap water, before vacuum filtration through a filter paper until a paste, comprising up to 85% water, was obtained and dried via spray drying. *Z1 type Quartzene samples*: prepared using a method analogous to that for ND but with a different level of activation of the silica source (Twumasi Afriyie et al., 2014). Furthermore, a methylated version of Z1, herein called Z1HPO, was developed by SvAAB, allowing direct comparison of adsorption uptakes and kinetics between hydrophilic and

hydrophobic versions of the same base material. *CMS type Quartzene*: prepared by adding calcium and magnesium sources at concentrations of 1:2 to the silica source (Waterglass $\text{SiO}_2/\text{Na}_2\text{O}$ ¼ 3.35). A 500 mL salt solution, consisting of MgCl_2 hexahydrate and CaCl_2 dihydrate was prepared at a ratio of 68 mol% Mg and 32 mol% Ca; 500 mL salt solution, was poured onto 1.5 M (with respect to SiO_2) sodium silicate solution (500 mL), and the resulting mixture agitated at room temperature. Subsequent coagulation occurred, as previously described (Twumasi Afriyie et al., 2013), and the obtained gel was washed, filtered and dried in the same manner as ND.

ND and CMS type samples used in this study were powders, with particle sizes between 2 and 150 μm , and D_{v90} (particle size below which 90% of the sample falls) equal, respectively, to 46 and 75 μm , measured with a Malvern Hydro 2000S. Granules of Z1 and Z1HPO were also used, with particle sizes between 1 and 1.5 mm.

Characterization of adsorbents

Samples were dried for 2 h at 358 K prior to coating with a thin layer (1.5 nm) of gold for FE-SEM analysis using a HITACHI SU-6600 (2010) Field Emission Scanning Electron Microscope. The instrument is equipped with Energy Dispersive Spectroscopy (EDS), Oxford Inca 350 with 20 mm X-Max detector and Wavelength Dispersive Spectroscopy (WDS), and uses Oxford Inca Wave 700 Microanalysis System with Energy μ Software.

Surface chemical functionalities of adsorbent materials are known to determine their hydrophilic or hydrophobic nature and this is also true of silicas (El Rassy and Pierre, 2005). FT-IR analysis, obtained using an ABB MB 3000 spectrophotometer with Horizon MBTM FTIR software, were used to determine surface functionalities of samples (dried at 248 K for 2 h) prepared as hydrophilic.

Nitrogen sorption measurements were performed at 77 K using a Micromeritics ASAP 2420, on samples accurately weighed between 0.15 and 0.5 g and degassed at 393 K, for 3.5 h. Degassing at low temperatures requires longer treatment times but has the benefit that the structure of the material is preserved. Forty adsorption points and 30 desorption points were collected per isotherm, spanning the relative pressure range 0–0.99. BET analysis (Brunauer et al., 1938) was used to interpret the data obtained.

A film of adsorbate is known to cover an adsorbent with a defined density profile but, by assuming that the film thickness is uniform, it is possible to obtain a 'statistical thickness' (t) from gas sorption isotherms, such as the nitrogen sorption analysis used here. The Harkins–Jura thickness equation, derived from Lippens and De Boer's analysis for non-porous siliceous materials characterised by nitrogen adsorption at 77 K (Lippens and De Boer, 1965), can be employed as a reference, to estimate surface area, average pore size and pore volume of materials with similar composition and BET C constants, using the t -plot analysis method. An assumption of the t -plot method is the uniformity of the thickness of the adsorbent layer, hence, adsorption on a mesoporous surface is considered similar to adsorption on a flat surface; however, the adsorbed thickness on small mesopores is not constant, but varies as a function of the pore diameter. Consequently, this method, when applied to nitrogen adsorption, should be used with caution in the presence of mesopores with diameters <3.5 nm (Galarneau et al., 2014), which, in this study, includes ND samples. Furthermore, it is essential that the reference surface should be energetically and structurally similar to the porous solid surface under analysis, as both factors affect the level of adsorbate loading at a given relative pressure; however, the BET C value does not guarantee a similar

surface structure, so it is not sufficient basis for selection of a reference isotherm (Biggs et al., 2004).

For these reasons, surface areas and pore volumes reported in this study were estimated using a-plot analysis, as this is considered more reliable than the t-plot method.

Parameters of the reference adsorbent Lichrospher-1000 were applied in the following equation (Gregg and Sing, 1982):

$$a(x) = a + K_{st} S_{ext} \alpha_s (p/p_0)$$

where a is the intercept with the y-axis, related to the adsorption in saturated micropores; $K_{st} \frac{1}{4} a_{st}(x \frac{1}{4} 0.4) / S_{st}$, where S_{st} is the specific surface area of the reference material; $a_s \frac{1}{4} a_{st}(p/p_0) / a_{st}(p/p_0 \frac{1}{4} 0.4)$; and $S_{ext} \frac{1}{4}$ external surface area of the adsorbent analysed.

Adsorptives

Benzene and toluene were used in this study as representative components of dissolved oils in produced water from the BTEX family; the organics were purchased from Sigma Aldrich as chromatography grade reagents (HPLC, >99.9%). Benzene is more representative of dissolved oil, as the most difficult of the BTEX group to adsorb from solution, due to the fact that the adsorption potential of the solute in the liquid carrier decreases with increasing solubility of the adsorbate. Since, the solubility of the monoaromatics in the BTEX group decreases with molecular weight, their adsorption potential increases with the molecular weight (Wang et al., 2011), hence, the lowest molecular weight species (benzene) is the most difficult to adsorb.

Adsorption experiments

Borosilicate glass bottles were used for all adsorption studies, and bottle volumes were selected in order to reduce headspace within the vessel. Mixtures of water and benzene were stirred in filled bottles for 1 h using a magnetic stirrer to solubilize the organic, before samples were extracted with a micropipette, then mixed with methanol and internal standard before injection, using a microsyringe, into the port of a Shimadzu GC 2014 gas chromatograph equipped with FID detectors to determine the concentration present. Pre-determined amounts of adsorbent were added to prepared bottles of aqueous phase organics to study adsorption characteristics. Kinetic tests were conducted at pre-determined intervals, over 24 h, to determine times for maximum equilibria to be achieved for each sample; the aqueous concentrations of benzene and toluene were respectively ~1 g/L and ~0.35 g/L. All measurements were conducted at 293 K.

Adsorption tests involved the addition of benzene, at concentrations in the range 0–1100 ppm, to 110 mL of distilled water mixed with 100–500 mg of adsorbent, equilibrated for 24 h before analysis. An analogous procedure was used for toluene but using aqueous concentrations in the range 0–400 ppm.

The adsorption behaviour of hydrophobic Z1HPO was only tested using aqueous benzene, agitated using a rotary shaker to guarantee sorbent contact with the aqueous phase, which could not be guaranteed by use of a magnetic stirrer, as used for the hydrophilic materials, due to the fact that the light hydrophobic material floats in water. All procedures were performed at 293 K using sealed cups with minimal headspace, as outlined above, to reduce volatilisation losses. Lower temperatures were not investigated

as the reduction in temperature significantly impacts on kinetic performance by increasing the time required for equilibration and making kinetic measurements impractical. Blank tests, conducted without sorbent, demonstrated that volatilisation rates were negligible for both kinetic and adsorption measurements. The stirring rates used were constant, at 200 r/min for magnetic stirring and 20 r/min for rotary stirring. Sampling was performed at various depths within a selected test vessel to verify the absence of concentration gradients within the bulk.

Measurement of organic concentrations: Gas chromatography

Gas chromatography, using a Shimadzu GC 2014 gas chromatograph equipped with FID detectors was used to measure the concentrations of organic species in the aqueous systems studied. A fused silica chromatographic capillary column (5% diphenyl/95% dimethyl siloxane phase), 25 m \times 0.32 mm, was used. The column was purchased from Sigma Aldrich and conditioned at 553 K for 3 h before first use. Samples were extracted and placed in sealed vials, to which the solvent (methanol) and internal standard were also added; from these vials, 1 mL was removed, by microsyringe, and injected into the chromatograph sample port, piercing a rubber septum. Toluene was used as the internal standard for benzene, and vice versa; the construction of a calibration curve allowed direct comparison of peak ratios, thus, the determination of the concentration of the organic species in the test system. Column flows, oven and detector temperatures were evaluated to optimise peak resolution; parameters used in this study were: carrier gas: helium; injection: splitless; injector temperature: 523 K; detector temperature: 523 K; column flow:

1.5 mL/min; purge flow: 2.5 mL/min; oven program: 4 min at 323 K, ramp to 453 K at 10 K/min, ramp to 673 K at 10 K/min, with final holding time of 5 min. Analyses were run in duplicate to ensure equipment precision; additional experiments were conducted on different days, both within a continuous series of analyses, and once on cold start-up, to verify reproducibility of results.

Result and discussion

Characterization results

The results of FE-SEM analysis are presented in Figure 1 and it is evident that the observed networks are quite different despite the similarity of their synthetic processes.

The obtained FTIR spectra (Figure 2) show the presence of silanol polar groups (Si-OH), in the range 2700–3650 cm^{-1} , for all materials studied, with Z1 and ND showing similar surface chemistries, while CMS exhibits more refined Si-OH bond peaks; consequently, these Quartzene materials can be categorised as hydrophilic in nature. The FTIR spectra of Z1HPO show a small peak around 1250 cm^{-1} , attributed to the Si-CH₃ bonds, formed as consequence of the functionalization process. The presence of CO₂ can produce an absorption peak at \sim 2300 cm^{-1} , however, immediately prior background measurements were used to account for its atmospheric presence and as the peak observed for Si-H occurs for all samples, this provides evidence of such functionality in the materials used.

Figure 3 shows the a-plot analysis of the nitrogen adsorption isotherm obtained at 77 K for Quartzene ND. The gradient of the solid line provides an estimation of the total specific surface area, while the gradient of the upper dashed line corresponds to the surface area external to the primary mesopores, which is ascribed as the surface area of any large

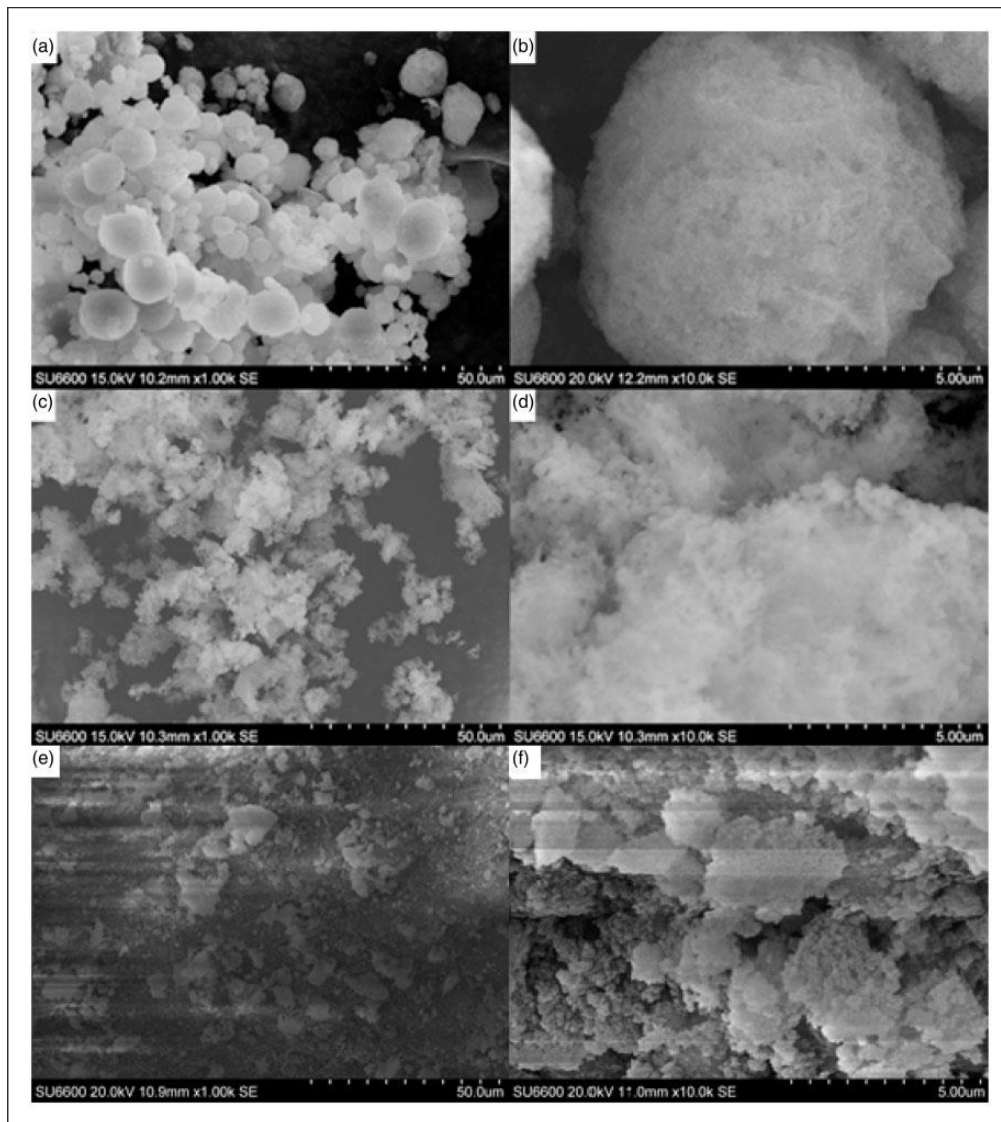


Figure 1. FE-SEM analysis of Quartzene samples: CMS (a: ~1 k, b: ~10 k), ND (c: ~1 k, d: ~10 k) and ZI (e: ~1 k, f: ~10 k).

mesopores and macropores present in the material. The intercept of the dashed line provides an evaluation of the already filled small mesopores, i.e. the small mesopore volume.

The surface areas obtained for the four samples studied here show good agreement between the two methods (BET and a_s), except in the case of ND, which exhibits small mesopores (Table 1), thereby suggesting the value obtained using the a -plot method would be more accurate. Pore sizes determined for CMS, ZI and Z1HPO samples are widely distributed between 2 and 80 nm, while ND exhibits a discrete pore size distribution

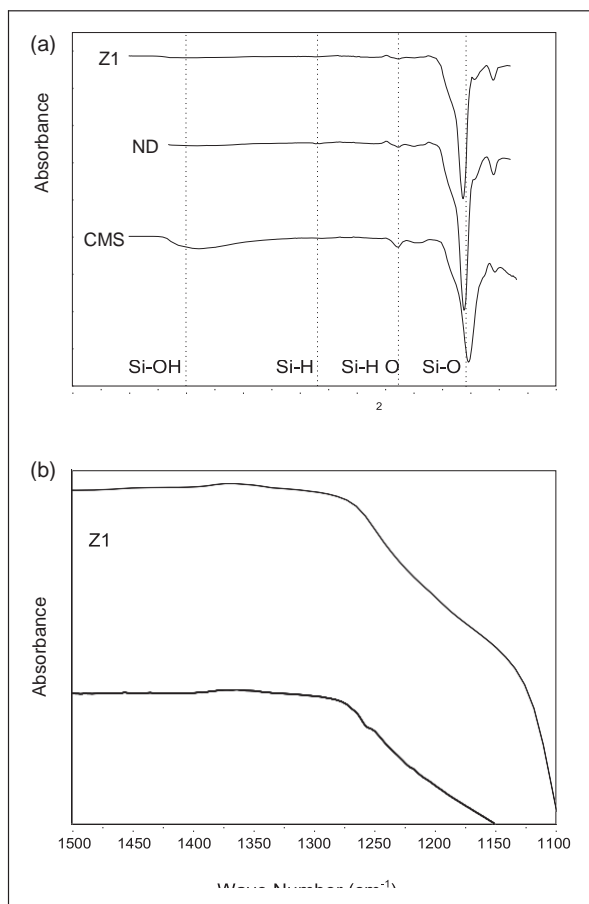


Figure 2. FT-IR spectra of silica samples: (a) Z1, ND and CMS and (b) comparison between the FT-IR spectra of Z1 and hydrophobic Z1HPO. The presence of Si-CH₃ bonds in the sample Z1HPO is confirmed by the small peak around 1250 cm⁻¹.

centred around 3.3 nm (Table 1). Consequently, ND is the only material with a small mesopore contribution but it is notable that all samples exhibit significant total pore volume. The low flow used for the carrier gas in the chromatography analyses was imperative to allow separation of the solvent and benzene peaks (Figure 4). The larger peak, beginning at 4.3 min, is due to the solvent (methanol), followed by the benzene peak (elution time: 6.5 min) and finally the toluene peak (elution time: 8.3 min).

Kinetic analysis and isotherms of the hydrophilic materials

Kinetic data were obtained as outlined above and the results show a logarithmic relationship for the first 6 h of data, in which 84–90% of adsorption take place on CMS and ND samples (Figure 5). The full equilibration time is less than 24 h, for both benzene and toluene uptake. Quartzene Z1 shows slower kinetics, with <80% of toluene and <70% of benzene adsorbed after 24 h. Hydrophobic silica aerogels have been shown to reach their full

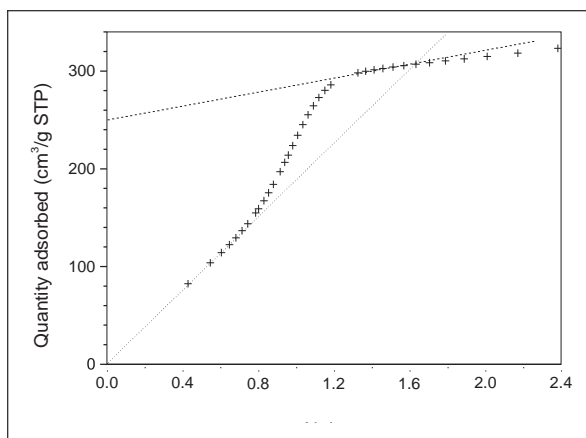


Figure 3. a-plot analysis of ND nitrogen adsorption isotherm measured at 77 K (dotted line fit of low pressure data, dashed line fit of high pressure data).

Table 1. Surface areas and porosities of samples used in this study.

Sample name	ZI	ZIHPO	CMS	ND ^c
$S_{BET}/m^2 g^{-1a}$	325	186	158	597
$S_{as}/m^2 g^{-1}$	331	186	161	546
Average pore width/nm	20.3	17.4	14.6	3.3
Total pore volume/ $cm^3 g^{-1}$	1.03	0.97	0.50	0.54
Small mesopore volume/ $cm^3 g^{-1b}$	–	–	–	0.40
Meso- and macro-pore volume/ $cm^3 g^{-1b}$	1.03	0.97	0.50	0.14

^aBET linearization ($p/[n_s \cdot (p^0 - p)]$ vs. p/p^0) was performed over the relative pressure range 0.05–0.3.

^bPore volume contributions were determined using the a_s method.

^ca-plot for ND exhibits two ranges of mesoporosity (Figure 3); surface area of small mesopores is estimated as 524 m^2/g .

adsorption capacities in <1 h (Perdigoto et al., 2012) or even <30 min (Standeker et al., 2007), the materials tested here show good short time performance but it should be noted that full equilibration takes several hours.

The Freundlich adsorption model (Freundlich and Hatfield, 1926) has been used extensively to determine adsorption capacities, mainly due to the fact that it considers the heterogeneity of real surfaces:

$$q = k \cdot C_e^{1/n}$$

where q is equilibrium uptake (mg adsorbate/g adsorbent); C_e is the equilibrium concentration of the solute (mg/L); k is the unitless constant of adsorption, indicating capacity; $1/n$ is a unitless constant related to the intensity of adsorption. Higher values of k indicate higher maximum adsorption capacity; while higher $1/n$ values (>1) denote unfavourable adsorption. The $1/n$ values obtained in this study are all more than unity,

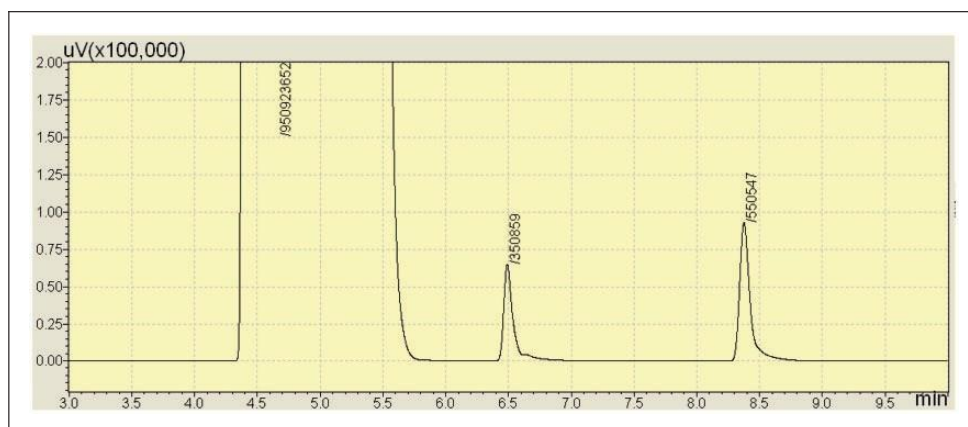


Figure 4. Gas chromatograph analysis of aqueous benzene, with toluene as internal standard and methanol as solvent. x-axis: time/min; y-axis: signal/ μV k, where k is the magnification factor.

hence, adsorption for all materials with both adsorbates is dominated by physical sorption, as opposed to chemical sorption (Jiang et al., 2002).

Aerogels studied previously show higher uptakes for toluene compared to benzene, however, it is important to note that such results are based on adsorption isotherms obtained for two adsorbatives with disparate solubility limits; consideration of the parameters obtained by the Freundlich analysis show that, while k values support this observation, the $1/n$ values demonstrate the theoretical maxima would be greater for benzene, in agreement with previous findings (Standeker et al., 2007; Wang et al., 2011). Such high concentration behaviour is observed as a possible consequence of the delocalisation of the ring in benzene, which is reduced for toluene; also the functional group of toluene may cause associated packing effects, reducing the effective adsorption capacity, hence the maximum adsorption uptake, but only at high theoretical maximum concentrations. It can be seen, from Table 2 and Figure 6, that the ND and CMS samples perform best from the three sorbents studied in the range of concentrations used, as supported by the k values obtained from the Freundlich analysis, with maximum adsorption capacities for ND estimated as close to the adsorbate solubility limits:

78.8 mg/g and 264 mg/g for toluene and benzene, respectively. The higher adsorption of Quartzene ND is ascribed, not only to the comparatively high surface area of this material but also, to its discrete pore size distribution centred around 3.3 nm, which provides good access for the organic molecules of interest while also being sufficiently narrow to prevent the molecular repulsion that can be observed with large adsorbate clusters. The results obtained for Z1 show a greater $1/n$ value for toluene compared to benzene, which is contrary to previous findings and the other data reported here. Z1, which was the only original material used in granular form, underwent significant mechanical degradation during stirred reaction experiments. Z1 is produced with a different level of activation of the silica source with respect to ND, resulting in low surface area, porosity, and subsequent adsorption capacity. While mechanical degradation, due to the stirring procedure, is expected to occur also for the granular forms of ND and CMS (here tested as powders), the lower adsorption of Z1, which is

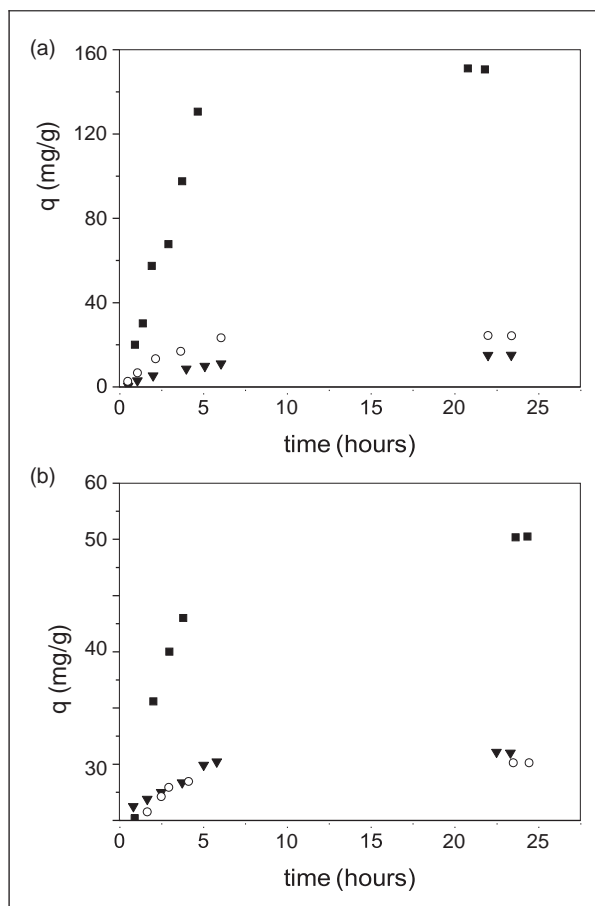


Figure 5. Kinetic profiles of (a) benzene and (b) toluene adsorption on ZI (filled triangle), ND (filled square) and CMS (empty circle) at 293 K.

Table 2. The Freundlich adsorption model parameters calculated using data obtained for adsorption of toluene and benzene of samples used in this study, measured at 293 K. Maximum uptakes are determined from extrapolative interpolation to either a benzene solubility of 1.763 g/L or a toluene solubility of 0.57 g/L (Stephen and Stephen, 1963).

Adsorbate	Sample	K	1/n	Adj. R ²	Max uptake/mg g ⁻¹
Benzene	ZI	26.44	1.23	0.9954	53.25
	ND	102.23	1.67	0.9950	264.03
	CMS	41.42	1.73	0.9820	110.48
Toluene	ZI	120.81	1.68	0.9861	46.91
	ND	141.15	1.04	0.9890	78.82
	CMS	120.09	1.51	0.9995	51.36

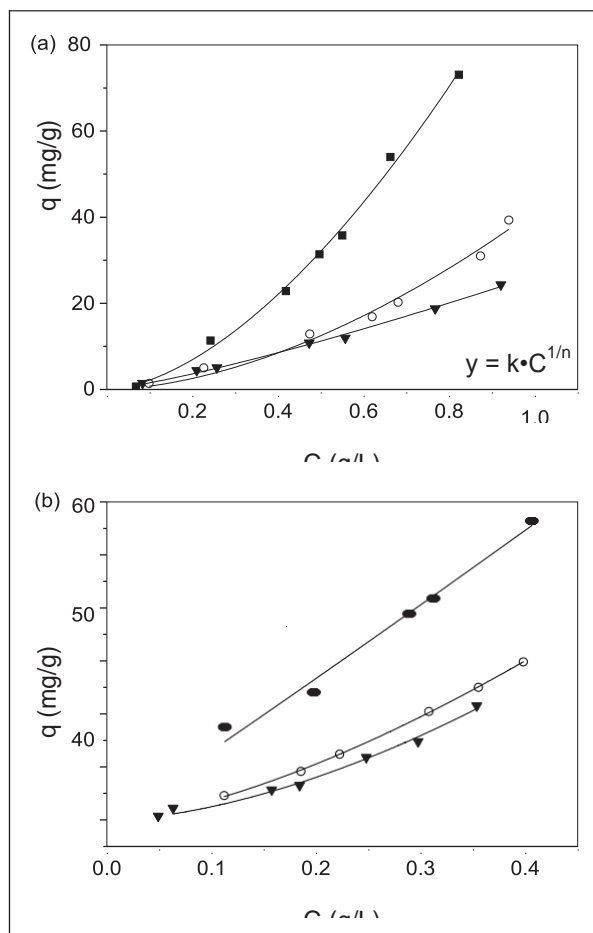


Figure 6. Adsorption isotherms for benzene (a) and toluene (b) on Z1 (filled triangles), ND (filled squares) and CMS (empty circles) at 293 K.

also lower than for CMS, is likely due to the collapse of the pore structure of Z1 after immersion in water. Indeed, the level of activation of the silica source is expected to influence the silica xerogel and aerogel network strength.

Comparison of hydrophilic and hydrophobic version of Z1

Only aqueous benzene concentrations below 0.25 ppm were explored in the comparison of adsorption characteristics the hydrophilic and hydrophobic versions of Z1. Adsorption was faster and a higher quantity of benzene was adsorbed for Z1HPO (Figure 7); furthermore, this material showed no significant mechanical degradation even after five days of rotary stirring at 20r/min.

Equilibrium was reached in less than 3 h for Z1HPO, while previously studied hydrophobic aerogels, particle size <250 nm, were found to reach full adsorption capacity in less than 1 h, adopting a similar method and rate of stirring (Perdigoto et al., 2012); this

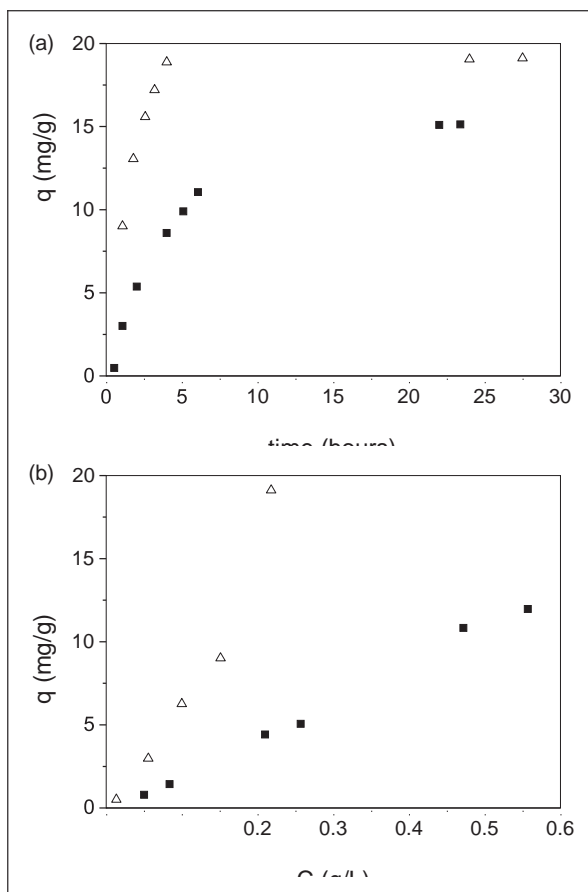


Figure 7. Kinetics (a) and isotherms (b) obtained for benzene adsorption by granular forms of Quartzene ZI (filled squares) and ZIHPO (empty triangles) at 293 K.

difference is likely due to differences in particle size, with a much larger particle size studied here. Testing the granular form of sorbents, as opposed to powders, provides greater insight in to material performance within a filter configuration, which is the most probable layout in a tertiary process dedicated to organics separation from water. The comparison of adsorption behaviour for hydrophilic ZI and hydrophobic ZIHPO confirms that hydrophobicization is fundamental to multiple cycle use of a material. At high benzene concentrations, adsorption on ZIHPO is significantly higher than for ZI, but the difference in terms of uptake between the two adsorbents is reduced with decreasing organic concentration. Hence, at very low aqueous concentrations of organics, the effect of hydrophobicization on pollutant access to the internal porosity of the material may be not great enough to justify the expense of the functionalization process. Recently, it was proposed that organics dissolved in aqueous media in very diluted systems are unable to access the interior porosity of functionalized silica aerogels as a consequence of their inherent hydrophobic nature, suggesting that only the external surfaces are available for adsorption (Shi et al., 2014). These findings suggests a necessity to test adsorption

performances of both hydrophilic and hydrophobic materials, especially when target organic pollutant concentrations are low enough as to make the economic profit of cyclic use, and associated regeneration costs, questionable given the expense of sorbent functionalization.

Conclusions

Novel hydrophilic amorphous silicas were synthesized at low temperature and ambient pressure. Two samples with varied levels of silica source activation, and one sample prepared via the addition of calcium and magnesium sources (ratio of 1:2) were tested for the adsorption of aqueous phase organics (benzene and toluene), at concentrations below their solubility limits. Kinetic tests reveal up to 90% of benzene and toluene is adsorbed in the first 6 h of treatment, and up to 50% in the first 2 h. There are no significant differences between the rates of adsorption for either benzene or toluene. The adsorption mechanism is favourable and described fully by the Freundlich model, with $1/n > 1$ and higher for both adsorbates, while the adsorption capacity, at low concentrations, is higher for toluene, as expected from the literature (Love et al., 2003; Standeker et al., 2007).

Quartzene ND outperforms the other material tests and shows adsorption capacities of 264 mg/g for benzene (solution concentration of 1.76 g/L) and 78 mg/g for toluene (solution concentration of 0.57 g/L). By testing materials in a granular, the results provided a clearer indication of how the material can be expected to perform in a filter configuration, which is the most likely tertiary treatment process layout for organics separation from water. The comparison between hydrophilic Z1 and hydrophobic Z1HPO demonstrated that hydrophobicization is required to impart the mechanical longevity required for cyclic use, and leads to increased adsorption of benzene from aqueous phase concentrations >50 ppm. It is notable that the observed differences in uptake between the two forms of Z1 are reduced as organic concentration decreases. This finding supports the hypothesis that, at very low aqueous phase organic concentrations, the effect of hydrophobicization on access of the pollutants to the internal porosity of the material may be not great enough to justify the expense of the functionalization process. Hence, tuning the hydrophobicity of sorbents to perform multiple adsorption cycles, with the added costs of regeneration should be fully evaluated via a cost analysis to determine whether the actual pollutant concentrations are significantly high to justify the expense of a functionalization process.

The adsorption results presented in this paper suggest that amorphous silica, such as Quartzene based materials, are a promising family of sorbent materials for application in the final stages of produced water treatment. To establish their full capabilities, defined ranges of pollutant concentration should be identified to allow selection of the most appropriate hydrophilic or hydrophobic material type, with additional lifetime cycling measurements to assess the economic feasibility of their use in water treatment plants.

Acknowledgements

The authors kindly thank Svenska Aerogel AB for providing adsorbent materials and associated particle size distribution data.

Declaration of Conflicting Interests

The author(s) declared no potential conflicts of interest with respect to the research, authorship, and/or publication of this article.

Funding

The author(s) received no financial support for the research, authorship, and/or publication of this article.

References

- Adebajo MO, Frost RL, Klopogge TJ, et al. (2003) Porous materials for oil spill cleanup: A review of synthesis and absorbing properties. *Journal of Porous Materials* 10: 159–170.
- Biggs MJ, Buts A and Williamson D (2004) Absolute assessment of adsorption-based porous solid characterization methods: Comparison methods. *Langmuir* 20: 7123–7138.
- Brunauer S, Emmett PH and Teller E (1938) Adsorption of gases in multimolecular layers. *Journal of the American Chemical Society* 60: 309–319.
- El Rassy H and Pierre AC (2005) NMR and IR spectroscopy of silica aerogels with different hydrophobic characteristics. *Journal of Non-Crystalline Solids* 351: 1603–1610.
- Freundlich H and Hatfield H (1926) *Colloid and Capillary Chemistry*. London: Methuen.
- Galarneau A, Villemot F, Rodriguez J, et al. (2014) Validity of the t-plot method to assess microporosity in hierarchical micro/mesoporous materials. *Langmuir* 30: 13266–13274.
- Gregg SJ and Sing KSW (1982) *Adsorption, Surface Area, and Porosity*. London: Academic Press.
- Hrubesh LW, Coronado PR and Satcher JH (2001) Solvent removal from water with hydrophobic aerogels. *Journal of Non-Crystalline Solids* 285: 328–332.
- Jiang J-Q, Cooper C and Ouki S (2002) Comparison of modified montmorillonite adsorbents: Part I: Preparation, characterization and phenol adsorption. *Chemosphere* 47: 711–716.
- Lippens BC and De Boer JH (1965) Studies on pore systems in catalysts: V. The t method. *Journal of Catalysis* 4: 319–323.
- Love A, Hanna ML and Reynolds JG (2003) Engineering surface functional groups on silica aerogel for enhanced cleanup of organics from produced water. *Separation Science and Technology* 40: 311–320.
- Olalekan AP, Dada AO and Adesina OA (2014) Review: Silica aerogel as a viable absorbent for oil spill remediation. *Journal of Encapsulation and Adsorption Sciences* 4: 122–131.
- Perdigoto MLN, Martins RC, Rocha N, et al. (2012) Application of hydrophobic silica based aerogels and xerogels for removal of toxic organic compounds from aqueous solutions. *Journal of Colloid and Interface Science* 380: 134–140.
- Reynolds JG, Coronado PR and Hrubesh LW (2001) Hydrophobic aerogels for oil-spill clean up – Synthesis and characterization. *Journal of Non-Crystalline Solids* 292: 127–137.
- Shi H-X, Cui J-T, Shen H-M, et al. (2014) Preparation of silica aerogel and its adsorption performance to organic molecule. *Advances in Materials Science and Engineering* 2014: 8 pp. <https://www.hindawi.com/journals/amse/2014/850420/>.
- Simpson EJ, Abukhadra RK, Koros WJ, et al. (1993) Sorption equilibrium isotherms for volatile organics in aqueous-solution – Comparison of headspace gas-chromatography and online UV stirred cell results. *Industrial & Engineering Chemistry Research* 32: 2269–2276.
- Standeker S, Novak Z and Knez Z (2007) Adsorption of toxic organic compounds from water with hydrophobic silica aerogels. *Journal of Colloid and Interface Science* 310: 362–368.
- Stephen H and Stephen T (1963) *Solubilities of Inorganic and Organic Compounds*. New York: Macmillan.
- Twumasi Afriyie E, Karami P, Norberg P, et al. (2014) Textural and thermal conductivity properties of a low density mesoporous silica material. *Energy and Buildings* 75: 210–215.

Twumasi Afriyie E, Norberg P, Sjöström C, et al. (2013) Preparation and characterization of double metal-silica sorbent for gas filtration. *Adsorption* 19: 49–61.

Venkateswara Rao A, Marcel Pajonk G, Bangi UKH, et al. (2011) Sodium silicate based aerogels via ambient pressure drying. In: MA Aegerter, NK Leventis and M Matthias (Eds.), *Aerogels Handbook*. New York, Dordrecht, Heidelberg, London: Springer.

- Wang D, McLaughlin E, Pfeffer R, et al. (2011) Adsorption of organic compounds in vapor, liquid, and aqueous solution phases on hydrophobic aerogels. *Industrial & Engineering Chemistry Research* 50: 12177–12185.
- Wang D, McLaughlin E, Pfeffer R, et al. (2012) Adsorption of oils from pure liquid and oil-water emulsion on hydrophobic silica aerogels. *Separation and Purification Technology* 99: 28–35.
- Wang J, Zhang Y, Wei Y, et al. (2015) Fast and one-pot synthesis of silica aerogels via a quasi-solvent- exchange-free ambient pressure drying process. *Microporous and Mesoporous Materials* 218: 192–198.
- Zong SK, Wei W, Jiang ZF, et al. (2015) Characterization and comparison of uniform hydrophilic/ hydrophobic transparent silica aerogel beads: Skeleton strength and surface modification. *RSC Advances* 5: 55579–55587.

9.1.2 Papers submitted

State of the Art of the Environmental Behaviour and Removal Techniques of the Endocrine Disruptor 3,4-dichloroaniline

Andrea Luca Tasca* and Ashleigh Fletcher

Department of Chemical and Process Engineering, University of Strathclyde, Glasgow G1 1XJ, United Kingdom.

* andrea.tasca@mail.strath.ac.uk

ABSTRACT

In recent years, the presence of Endocrine Disrupting Chemicals (EDCs) in wastewater discharges from agricultural and industrial sources [11], fresh- and estuarine-waters, as well as soils, has been reported in the literature [12]. Studies of adverse changes in wildlife, linked to environmental exposure to these substances, and the suggestion that humans could also be at similar risk of adverse health effects [23, 54, 56], have raised concern for urgent action to understand and reduce such risks. 3,4-Dichloroaniline (3,4-DCA) has been recognized as an EDC, with regards to endocrine disruption data for both wildlife populations and human health [23].

3,4-DCA is present in the environment as a product of the biodegradation of phenylurea and phenylcarbamate pesticides [26, 27]; furthermore, it can be introduced by industrial and municipal wastewater that is insufficiently purified, or via accidental spills [28-30]. Increasing concentrations of 3,4-DCA in soil and water, are the result of its high persistence and accumulation, as well as its low biodegradability [24, 32]. Hence, remediation techniques, require indepth study, especially when considering the low removal achieved by traditional activated sludge treatments, and the generation of carcinogenic trihalomethanes as a consequence of the chlorine oxidation methods frequently used in drinking water plants [33]. $\text{Fe}^0/\text{H}_2\text{O}_2$ systems, photodegradation using doped TiO_2 and the use of dielectric barrier discharge reactors, seem to be the most promising techniques for the removal of 3,4-DCA from water.

KEYWORDS

3,4-DCA; water; environment; pollution; adsorption; electrochemistry

INTRODUCTION

Global annual production of 3,4-DCA was ~42000-47000 tonnes prior to 1986 [34], while in the period 1996-1998, the EU production was still around 13,500-15,500 tonnes annum⁻¹ [35]. 3,4-DCA, a derivative of aniline, is an intermediate for the chemical synthesis of 3,4-dichlorophenylisocyanate, for phytosanitary products, such as propanil, linuron, diuron, and neburon [35-37], used to treat crops including rice, potatoes, beans or tobacco [38]. It is also employed in the synthesis of azo dyes for polyester fabrics [37] and pharmaceuticals [23]. Although there is no exposure risk for vulnerable groups from direct use of 3,4-DCA, indirect contact is expected via food, primarily fruit and vegetables [23], as a result of the hydrolysis and biological degradation of phenylurea, phenylcarbamates and acylchloroanilide pesticides present in soils [39-47], by field waters and plant enzymes [48]. Furthermore, industrial wastewater [32] may contain 3,4-DCA, mainly from microbial conversion of 3,4-dichloro-1-nitrobenzol within water treatment plants [23, 48].

In this manuscript, we summarize the current knowledge concerning the introduction, the movement, and the fate of 3,4-dichloroaniline (3,4-DCA) in the environment. We discuss the state-of-the-art remediation technologies in use, as well as those under development, with reference to their effectiveness for pollutant removal from soil and water systems.

TOXICITY

In humans, EDCs are known to affect male and female reproduction, thyroid metabolism [15-17], breast development and cancer, prostate cancer, neuroendocrinology, obesity [18] and cardiovascular endocrinology [19]. Little is known about the mechanisms of action of these substances, nor their physical and chemical diversity, hence, additional research into EDCs is required, especially the cumulative impact of EDC mixtures, which may be additive or synergistic [19, 20], even when individual chemicals are present below the threshold of detectable effects [21]. Consequently, the current lack of knowledge regarding exposure scenarios hinders the assessment of human health risk and impact [22].

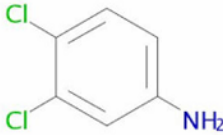
Chloroanilines can negatively affect soil microflora, and the presence of phenylamide herbicide degradation products has been shown to inhibit *Nitrosomonas*, hence, soil nitrification [49]. 3,4-DCA primarily acts by polar narcosis on aquatic organisms [50, 51]; and fish and crustaceans are most

sensitive with respect to water column exposure, while annelids are greatly affected by exposure in the sediment [37]. Tests have demonstrated the relatively low acute toxicity of 3,4-DCA on marine and fresh water animals, as well as unicellular algae, but there are significant chronic effects [52, 53] with consequences for marine life reproduction [54], including changes in secondary sex characteristics [55]; while rats have shown significant hormonal effects [56]. Subsequently, Predicted No-Effect Concentrations (PNECs) have been proposed, at $0.2 \mu\text{g L}^{-1}$ for freshwater and seawater bodies, and 0.1 mg kg^{-1} dry weight (0.04 mg kg^{-1} wet weight) by mass [37].

ENVIRONMENTAL BEHAVIOUR AND FATE

Chloroanilines are known to diffuse easily within the natural environment [11, 34], and are very difficult to remediate, hence, their concentration in soils and waters is increasing due to their high persistence, accumulation, [24, 32] low biodegradation [58] and low leaching potentials [59]. By contrast, 3,4-DCA is barely measured in water bodies [23] and it occurs in higher aqueous concentrations than the parent herbicide diuron [61]. It has been detected in European surface waters [36, 60], and migration is determined by transport and retention mechanisms [62]. Hydrolysis of 3,4-DCA is not considered a mitigating mechanism due to aromatic stabilisation effects [63], and, as a result of its relatively low Henry's law constant (K_H), it is not expected to volatilise from water columns [37, 63]. Rather, as the physical properties data presented in Table 1 suggest, 3,4-DCA losses from natural waters occur via photochemical degradation or adsorption on sediment and dissolved humic materials [64]. To this end, photo-transformation is the major degradation pathway of 3,4-DCA in environmental waters [36], maximised at 300 nm, well within the solar spectrum observed at sea level [54].

Table 1: Properties of 3,4-dichloroaniline.

Property	Value	Ref.
Molecular formula	$\text{C}_6\text{H}_5\text{Cl}_2\text{N}$	-
Molecular structure		[35]
Appearance	Solid at 293 K	[35]
Molecular weight	162 g mol^{-1}	[35]

Molecular size	0.35 nm ²	[66]
Henry's law constant	0.05 Pa m ³ mol ⁻¹	[35]
Solubility in water	580 mg L ⁻¹ at 293 K	[35]
Octanol-water partition coefficient (log K _{ow})	2.7 (shake flask method)	[23, 36]
Estimated surface waters half life	18 days	[35]
Measured rates of loss in outdoor water systems	0.11 - 0.17 day ⁻¹	[54]
	0.06 - 0.14 day ⁻¹	[64]
Estimated atmospheric half life	9 hours	[35]
Estimated half-life in soil and sediment	470 - 1500 days	[67]

It is known that the soil mobility and bioavailability of pollutants, and their degradation products depend on a combination of sorption/desorption by soil components [62]. The binding effect of soil generally increases with the time, leading to a decrease of the pollutant bioavailability and toxicity due to meteoric leaching [68]. Hence, the majority of 3,4-DCA released into the environment accumulates, over time, on the organic fraction of sediments and soils [35]. On the other hand, sorption to dissolved macromolecules and colloidal particles is able to promote the transport in subsurface environments [69]. When chloroanilines are released to the soil with herbicides, only a small portion of the former is mineralized, consequently, many chloroanilines persist for years [70], often immobilized by interaction with humic substances, as mentioned above [28, 39, 71, 72]. Therefore, it is only a small fraction of liberated chloroanilines that undergo dimerization or polymerization, by microbial oxidases and peroxidases, forming stable azo compounds [62, 73]. Surface adsorption due to van der Waals' forces or electrostatic interactions is often the initial phase of binding pollutants on soil, while stronger bonds may arise over time [11]. Consequently, the soluble fraction of soil organic matter, i.e. fulvic and humic acids, play a significant role in the binding of xenobiotics, such as chloroanilines, from aqueous media, via functional substituents including hydroxyl, carboxylic acid, ketone, amino acid, saccharide and aminosaccharide groups [74, 75]. Aniline sorption to soil involves stronger interactions, starting with hydrophobic partitioning and cation exchange, before continuing with covalent bonding due to the contribution of limited energy or availability of sorption sites. Such initial reversible equilibrium followed by a slower irreversible mechanism is well described by a biphasic kinetic model [76, 77]. Similar information on the sorption mechanisms of 3,4-DCA is fundamental to the development of remediation strategies. What is currently known is that 3,4-DCA adsorbs onto sediment [64] and soil particles, building stable, most probably, covalent bonds with organic substances [36, 37]. In laboratory experiments more than 70% of radio labelled 3,4-DCA was found, as stated above, to bind to sediment and suspended matter in a water column [78];

kinetically ~80% of radioactivity was removed from the water column within 8 days, and ~99% after 90 days [79], suggesting an initially quick process that then takes significant time to reach equilibrium. As a consequence of the proposed interaction between 3,4-DCA and organic material, the interactions between dissolved organic matter from soil, organic contaminants and other soil components strongly affect the fate of 3,4-DCA in soil and water systems [80-83]. So increasing soil organic carbon content via organic matter amendments to a soil sample, which may also introduce dissolved organic matter, can potentially enhance sorption, and decrease leaching, of pollutants [84, 85], including 3-4-DCA [64]; notably, similar results have been observed for organic matter amendment of inorganic soils [30, 62].

A study into the interaction of various humic fractions and the herbicide diuron [86], showed that the main degradation product, 3,4-DCA, was irreversibly bound on humic acids within days of formation. As a result, the risk of pollutant leaching is expected to be low for soils with high humic or fulvic acid contents. The irreversible sorption observed in these systems was described using a Freundlich isotherm model:

$$C_s = K_f C_e^n \quad \text{Equation 1}$$

where C_s is the concentration of 3,4-DCA sorbed ($\mu\text{g g}^{-1}$), C_e is the equilibrium solution concentration of 3,4-DCA ($\mu\text{g mL}^{-1}$) and K_f (mL g^{-1}) expresses the soil sorption capacity. The exponent n is related to the degree of isotherm nonlinearity, and provides an indication of the favourability of the sorption process [245].

The results of Freundlich analysis indicated that humic fractions have a sorptive capacity ten times that of their fulvic counterparts, due to the preferential reaction of amino groups of 3,4-DCA with carboxyl and carbonyl groups of soil humic fractions, leading to the formation of soil bound residues [87, 88], as confirmed by high adsorption and small desorption constants [64]. Hence, the sorption of 3,4-DCA in soil can be described as a physicochemical process in which a fraction of the pollutant physically binds to organic and inorganic soil components, while another fraction strongly adsorbs on the organic component [58]. Similarly, soil samples, agitated in aqueous solutions of 3,4-DCA, have shown significant pollutant removal within 15 minutes of exposure and full equilibration, demonstrating up to 70% removal, after 50 hours. The authors report the presence of two associated processes, firstly a physical reaction seemingly followed by chemical bond formation between 3,4-DCA and organic matter within the soil, giving biphasic kinetics with rate constants of 4.9 hour^{-1} , for physical accumulation, and 0.03 hour^{-1} , for chemisorption [64]. Similar

kinetic performance has been observed for different agricultural soils and 3,4-DCA [58], with sorption equilibrium reached within 48 hours regardless of initial pollutant concentration, up to $16.2 \mu\text{g mL}^{-1}$. Again, the data was described well by the Freundlich equation, and the amount sorbed was higher for the sandy clay loam soil used in the study ($K_f = 52 \text{ mL g}^{-1}$), as a consequence of its higher organic matter content compared to the other soils studied and the fact that it creates a slightly acidic pH within the sorption system; by contrast the lowest sorption capacity was obtained for calcareous silty clay soil and sand.

As initial adsorbate concentration increases, availability of adsorption sites decreases, as confirmed by n values lower than 1; such sorption behaviour is expressed by L-type isotherms [89]. K_{oc} values, representing the sorption constant per gram of organic carbon in the soil sample studied, shows significant probability for 3,4-DCA contamination of ground-water in areas with less sorptive soils [59]. This is a consequence of the sorption capacity exhibiting a strong relationship with the organic matter content of samples, and the fact there is less impact with respect to clay content or a material's cation exchange capacity. It is also noteworthy that consideration of soil organic content alone is not sufficient to determine expected sorption behaviour; for example, less sorption of diuron would be expected on clay-rich soils, most likely as a result of a reduction in available binding sites in humic substances, due to the positive interactions between humic materials and clay [86]. Soil pH may be another factor that impacts sorption of 3,4-DCA, as demonstrated by a reduction of K_f values by ~50% after liming of aqueous solutions [58]. Such a trend probably results from aniline functionalities within soils, which are normally protonated species under the usually acidic conditions in such media, becoming neutral species as pH increases [76, 90, 91]. Samples of calcareous soil mixed with aqueous 3,4-DCA, allowed to equilibrate fully [62] showed high values for the Freundlich coefficient (K_f), which denotes that adsorption is concentration dependent [92], validating the assumption that adsorption on such solid media occurs primarily via hydrophobic interactions due to the neutralisation of aniline functional groups at high soil pH [88, 93]. Additional confirmation is provided by further consideration of the sorption equilibria of 3,4-DCA; K_{ow} is known to be high [28, 94] and combined with K_{oc} (338.6 L kg^{-1}), which is equal to $K_d/[\text{organic content}] \times 100$, where K_d reflects the distribution ratio of organic molecules between the sorbed phase and solution, its low water solubility suggests that 3,4-DCA has a low potential for groundwater contamination in calcareous soils with high organic matter content.

Dissolved organic matter has been proven to compete with organic pollutants for the sorption sites on soil surfaces [95, 96], as well as in the building of stable bonds between pollutant and soil [97]; this enhances the apparent solubility of

organic pollutants, thereby reducing sorption and increasing their mobility [83, 98]. In contrast, dissolved organic materials applied in soils may actually be adsorbed to soil surfaces, increasing sorption of hydrophobic organic compounds [99], especially when tannic acid is added [30]. Inclusion of dissolved organic carbon extracts, derived from both a commercial peat and high-purity tannic acid, with a soil sample showed significant impact on the sorption of 3,4-DCA [62]. The coefficient $K_{d,DOC}$, defined as X_{doc}/C_{doc} where X_{doc} is mg L^{-1} of dissolved organic carbon and C_{doc} is the corresponding equilibrium concentration, is consistently higher than K_d values obtained for undoctored soil, thereby confirming the influence of dissolved organic carbon on 3,4-DCA sorption. Further confirmation was provided by the observation of an increase in 3,4-DCA sorption in the presence of an environmental matrix, including inorganic ions and organic matter [100]. Sorption on sedimentary material, hosted in a sediment extract media, was found to be increased in comparison to pure or run-off waters, likely facilitated by previously sorbed dissolved organic content on the sediment surface, present as a result of physical interactions between the two species [88].

REMEDICATION TECHNOLOGIES

Many remediation technologies have been developed for destruction of chloroanilines present in wastewaters; those methods specific to the treatment of 3,4-DCA can be classified as physicochemical, chemical (oxidation) or biological and are discussed in detail below. In essence, physicochemical methods utilise either adsorption, ion exchange, electrolysis or photodegradation, chemical processes require a chemical reaction with a selected additive, while biological degradation involves aerobic or anaerobic microorganisms.

BIOREMEDIATION

Bacteria

3,4-DCA is not readily biodegradable [37]; the process being particularly slow in aqueous media. Incubation of pond water, and pond water containing sewage sludge inoculum, in a dark environment showed that, after a period of 2 weeks, 97% of 3,4-DCA was recovered from the former sample and marginally less (94%) was recovered for the sewage containing sample, indicating little

biodegradation of the pollutant [111]. Similarly, no biodegradation was reported, over the same time period, for an OECD 301 C test [251] with activated sludge [112], nor after 4 weeks for an OECD 301 D test on activated sludge, and less than 5% degradation was observed after 29 days for an OECD 303 A test [251], again using activated sludge [37]. Researchers also observed no discernible removal of 3,4-DCA from contaminated North Sea water samples [113], while only primary degradation occurred after one month using river water as inoculum [114].

Usually, xenobiotics need to be in a solution phase in order to allow bacterial degradation to occur. The '*bioaccessible fraction*' of a pollutant is given by the sum of its concentration in pure water, known as the '*bioavailable fraction*', plus the '*potentially available fraction*', which is the material reversibly sorbed on any material surfaces. The addition of fulvic and humic acids to inoculated soils was seen to decrease the rate of diuron degradation, reducing bioavailability but not bioaccessibility, hence, lengthening the treatment time required; so it was only after 32 days that all diuron was degraded to 3,4-DCA [86]. Hence, bioaccessibility is a better indicator, than bioavailability, of the long-term influence of humic substances on diuron degradation. The mineralisation rate of 3,4-DCA in soils is low, and it decreases as pollutant concentration increases [35]; only 3.9-11.9% mineralisation of 1 mg kg⁻¹ radio labelled 3,4-DCA was recorded after 16 weeks in various soil types [67]. Degradation of 50% of 3,4-DCA was observed in soil slurries with indigenous soil populations, and this was only marginally influenced by the addition of buffer, mineral salts and acetate [57]. In non-acclimated sediments, dechlorination of applied 3,4-DCA started after 20 days, with anaerobic conversion to 3-chloroaniline (44%) and 4-chloroaniline (33%) within two months; these metabolites were not further degraded [115].

The microbial strains *Pseudomonas acidovorans* [116] and *Pseudomonas diminuta* [117] are able to use chlorinated anilines as a sole source of carbon and energy ; the latter are also able to grow on 3,4-DCA [118]. Addition of *Pseudomonas acidovorans* to 3,4-DCA enriched soil slurries enhanced pollutant mineralization, leading to complete elimination of chloride after 10 days [57]. Up to 250 mg L⁻¹ of the pollutant and its intermediates were anaerobically degraded in less than 7 days by a strain of *Pseudomonas fluorescens*. Without added glucose and nitrogen sources, degradation was slower, with 40% of toxicant removal in the first 15 days at an initial concentration of 75 mg L⁻¹ [119]. *Pseudomonas diminuta* was proven to dechlorinate up to 50 µg mL⁻¹ of 3,4-DCA within its growth process; increasing the ratio of degradation in water samples from natural water reservoirs [120] and in fish ponds, where the significant degradation of reversibly sorbed pollutant was observed within the first 12 days.

It is also notable that an appreciable decrease in the irreversibly sorbed fraction occurred in the first 5 days [121].

Microorganisms, from Cuban soils, were grown in two culture media, using 3,4-DCA firstly as the sole source of carbon and secondarily as the sole source of carbon and nitrogen [122]. The pollutant was completely consumed within 3 weeks with species of *Pseudomonas*, *Arthrobacter*, *Aspergillus*, *Penicillium*, and *Fusarium* isolated in the first medium, while species of *Bacillus*, *Arthrobacter*, *Cunninghamella*, *Trichoderma*, and *Fusarium* were isolated in the second system, demonstrating myriad bacterial growth from 3,4-DCA as a feedstock. The biodegradation pathway of 3,4-DCA, and other substituted anilines, involves conversion by oxygenase to the corresponding catechol, which is then metabolised via the ortho-cleavage pathway [123]. Two modes of dioxygenation have been determined, utilising degrading bacteria obtained by genetic exchange between two strains of *Pseudomonas*, and leading to the formation of 3- and 4-chlorocatechol from 3-chloroaniline. In contrast, only 4-chlorocatechol was generated from dioxygenation of 4-chloroaniline [117]. When bacterial strains of *Pseudomonas acidovorans* were used for the degradation of 3-chloroaniline and 4-chloroaniline, the rate-limiting degradation steps were found to be the first attack of the substrate, and conversion to chlorocatechols [116].

Degradation of 3,4-DCA by *Pseudomonas* sp. showed that catechol 2,3-dioxygenase is integral to process efficiency [118]; activity toward 4-methylcatechol, 3-methylcatechol and 4-chlorocatechol was found to be 60, 27 and 13%, respectively, of the activity toward catechol 2,3-dioxygenase. Further tests confirmed catechol 2,3-dioxygenase activity using a strain of *Pseudomonas fluorescens*; the presence of 3-chloro-4-hydroxyaniline as a metabolite suggesting a pathway including dehalogenation and hydroxylation of the aromatic ring, followed by ring cleavage by catechol 2,3-dioxygenase [119].

Recent work has shown *Micrococcus* sp. to degrade 96% of diuron within 30 hours of incubation, at a concentration of 250 ppm, and with the addition of non-ionic detergent (0.01%) [124]. The researchers proposed a mechanism involving removal of the methyl group followed by a hydrolysis step, leading to the accumulation of 3,4-DCA, which undergoes conversion to 4,5-dichlorobenzene-1,2-diol, and further intermediates, within 24 hours of test commencement (Figure 1). Diuron mineralization has also been confirmed by the metabolic cooperation of *Arthrobacter* sp. and *Achromobacter* sp., with CO₂ as only final product [125].

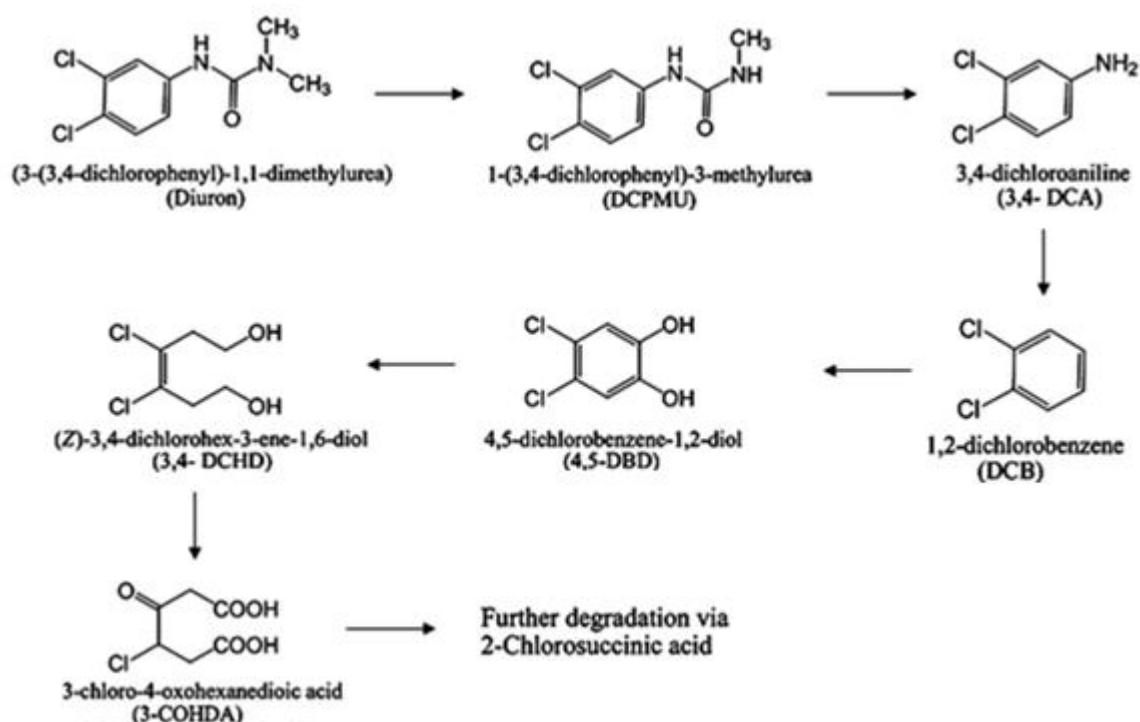


Fig 1: Degradation pathway of diuron by *Micrococcus* sp, confirmed by FTIR spectra and HPLC [124].

Strains of *Aquaspirillum itersonii*, *Aquaspirillum* sp. and *Paracoccus denitrificans* were shown to successfully use 3,4-DCA as the only source of carbon and nitrogen [126]; the latter was able to metabolize the pollutant at concentrations up to 150 mg L⁻¹, through oxidation to *o*-diphenol, intradiol cleavage of 4,5- dichloropyrocatechol and further stages of preparatory metabolism associated with dehalogenation. A study of microorganisms isolated from Cuban soils, treated with Propanide, showed a *Paracoccus denitrificans* strain to be the most efficacious for 3,4-DCA [66] degradation. The cleavage of the aromatic ring via the ortho- or meta-pathways, following formation of 4,5- dichloropyrocatechol, allows full decomposition; hence, successful adsorptive bioremediation from introduction of activated carbons and bacteria to polluted soils [127]. Activated carbon acts as buffer, which keeps the pollutant concentration in the soil solution below the toxicity threshold for the bacteria as shown by a study of three types of activated carbon saturated with 3,4-DCA and placed in a mineral medium with a *Paracoccus denitrificans* strain [66]. The pollutant was reversibly sorbed and available, at a limited concentration, for the bacteria population to process. Different degradation rates, varying from 2 to 10 weeks, suggested that facile desorption and more rapid decomposition are linked to a reduced micropore volume. This is due to the fact that *Paracoccus denitrificans* is only able to penetrate into the

macroporous structure, thus pollutant desorption from the smaller carbon pores is necessary for the bacteria to process any 3,4-DCA sorbed therein; this bacterium seems able to accelerate desorption by acidifying the medium or via excretion of surface-active substances.

Biological studies have also shown microbial consortia to be successfully in the removal of propanil and 3,4-DCA in repeated batch suspended cell cultures [128], as well as in biofilm reactors for agricultural wastewater treatment [129]. In the latter case, the porous volcanic stone tezontle was used as a support for a biofilm in a continuous process able to degrade propanil and metabolic intermediates at rates up to $24.9 \text{ mg L}^{-1} \text{ h}^{-1}$, without the need for co-substrates. *Pseudomonas* sp., *Acinetobacter calcoaceticus*, *Rhodococcus* sp., *Xanthomonas* sp. and *Kokuria* strains can also grow individually in 3,4-DCA, while other strains found in the biofilm, not able to degrade propanil metabolites directly, are probably involved in the metabolization of herbicide adjuvants or in the maintenance of biofilm integrity. Resultantly, the removal of chloroanilines from sewage treatment plant streams could be improved by promoting the growth of indigenous bacterial communities and through the introduction of adapted laboratory strains. The addition of readily degradable aniline and non-toxic haloaromatics may, respectively, improve the breakdown of chloroanilines and the chlorocatechol potential [117].

Uptake by fungi and cultivated plants

When free chloroanilines are released as herbicide metabolites they can be incorporated in the plant 'insoluble' residue fraction; degradation experiments have proposed lignin as a primary binding site [130, 131]. Immersion of the bivalve *Corbicula fluminea* in cages both upstream and downstream of conventional rice fields, in the region of Camargue [43], showed the concentration of 3,4-DCA measured downstream of the rice plantations to be approximately half that in the *Corbicula* caged upstream, suggesting a potential partial bioaccumulation of 3,4-DCA in rice plants. Tomato plants, oat, barley and wheat, grown in nutrient solutions with 4-chloroaniline and 3,4-DCA showed that 90-95% of the chloroanilines incorporated were found in the roots, with uptake proportional to the amount applied. In contrast, distribution of the same chemicals in carrots was approximately equally divided between the roots and the upper part of the vegetables [132]. These results suggest a potential risk of chronic toxicity due to the assumption of 3,4-DCA contained in foods.

Some lignin degraders are able to metabolize chloroanilines and the lignin conjugates of chloroanilines; experiments have shown that chloroanilines appear to be bioavailable to the white rot fungus *Phanerochaete chrysosporium*

once they were mineralized as lignin [133]. More than 50% of the available [ring-U- 14C] -3,4-DCA was mineralized after 33 days of sample incubation and free 3,4-DCA was deemed a superior substrate for mineralization than free 4-chloroaniline. Different metabolites were formed, but chloroanilines were not found, neither were their azo and azoxy derivatives. Hence, lignin incorporation and fungal oxidation can lead to a complete removal of 3,4-DCA from the environment; however, fungi is also known to adsorb less chloro-substituted anilines per biomass unit than bacteria [14], and the degradation pathway of white-rot fungi could lead to the formation of toxic tetrachloroazobenzenes [134].

ADSORPTION AND LIGAND EXCHANGE

Adsorption technologies offer effective removal of many organic pollutants from aqueous media [135], and various adsorbents have been studied for removal of chloroanilines from wastewaters. Batch adsorption experiments, conducted with an acid activated halloysite, using aqueous solutions at pH ~5 [24], gave experimental data that followed a pseudo-second order kinetic model [196]:

$$\frac{t}{q_t} = \frac{1}{(k_2 q_e^2)} + \frac{1}{q_e t} \quad \text{Equation 2}$$

where: q_t is the amount of chloroaniline adsorbed (mg g^{-1}) at time t (s), k_2 is the rate constant of pseudo-second order adsorption ($\text{g mg}^{-1} \text{min}^{-1}$) and q_e is the amount of chloroaniline adsorbed at equilibrium (mg g^{-1}). A 'Weber–Morris' plot of q_t versus $t^{0.5}$ confirmed that chloroaniline removal occurred first by fast diffusion of 3,4-DCA to the surface of the clay mineral, over the first 180 minutes, and continues as slower interparticle diffusion. The adsorption capacity of halloysite was found lower for 3,4-DCA than for 3-DCA and 4-DCA.

Equilibrium isotherm data was effectively described by the semi-empirical Langmuir equation:

$$\frac{C_e}{q_e} = \frac{1}{(K_L q_m)} + \frac{C_e}{q_m} \quad \text{Equation 3}$$

where: q_m is the monolayer adsorption capacity (mg g^{-1}), q_e is the sorption uptake at equilibrium (mg g^{-1}) and K_L is a coefficient related to the affinity between the adsorbent and the adsorbate (L g^{-1}). Similar adsorption experiments have been performed with kaolinite (KGa-1) and montmorillonite (SWy-1), using standard solutions of 3,4-DCA and other chloroanilines at pH ~5

and ~9, respectively [11, 90]; the pH conditions chosen so as to produce neutral organic pollutants species. Kinetic evaluation indicated an initial, rapid surge in chloroaniline removal, with equilibrium achieved in less than 4 days. Langmuir and Freundlich equations both provided adequate descriptions of the data [90]; however, the Langmuir plot showed a marginally better fit for montmorillonite, hence adsorption on this clay is likely to decrease as surface sorption sites are saturated. The chloroanilines studied would be mainly sorbed on the mineral surface of kaolinite, while the structure of montmorillonite allows swelling via sorption in the interlayer [197], as confirmed by studying the dehydrated clay [11]; post heat-treatment the distance between equivalent atomic planes (d_{001}) collapsed from 11 to 9.7 Å. Further evidence was provided by X-ray spectra of the montmorillonite/3,4-DCA system. This contrast in sorption mechanism is reflected in desorption measurements, where kaolinite was shown to retain the pollutant, while montmorillonite showed a higher level of desorption when reversing the sorption process at an earlier point in the isotherm, [90].

While clay materials offer surface sites for adsorption, the main surface area of other well-known sorbents, activated carbons, is ascribed to microporous character; surface hydrophobicity determines the sorptive capacity of many organic molecules, which have molecular sizes small enough to penetrate into the micropores. Highly microporous activated carbons, obtained from coal and peat, were confirmed as better sorbents than mesoporous carbons, obtained from raw plant materials. Increased iron content and other ash elements may positively influence the maximum uptake, by enhancing chemisorption of active organic compounds, such as 3,4-DCA [66].

Studies of aqueous solutions of various pesticides agitated with 10 mg L⁻¹ of powdered activated carbon (surface area ~1000 m² g⁻¹; particle size 40 µm) for 5 minutes, showed 70% removal efficiency for 3,4-DCA (initial concentration: 658 ng L⁻¹), while complete removal was achieved via preoxidation with ozone [126].

Fitting of room temperature sorption isotherms, obtained using suspensions of activated carbon in aqueous solutions of 3,4-DCA [66], using the Langmuir isotherm model (Equation 3), shows monolayer filling of the sorptive surface with 'L-type' isotherms, indicating strong interactions between adsorbate and adsorbent [194].

Sugar beet pulp, corncob, corncob char, perlite, vermiculite and sand have recently been studied for sorption of 3,4-DCA from aqueous solutions at pH 4.8 [100]. These sorbents may be used in field conditions, so it is essential to understand their sorption behaviour in different matrices. However, using liquid

matrices containing cations and organic matter, except for corncob, no significant differences were observed in the maximum uptake of 3,4-DCA from pure water and run-off water. The mechanism of sorption was satisfactorily described by the Freundlich isotherm model, with the highest sorption uptakes obtained at 99% removal from water for corncob char, and, 86% removal for sand. Of the sorbents studied, it is also known that vermiculite has a good resistance to mechanical abrasion [252]. Further investigations would be required to verify the adsorption capacity of low cost materials in field conditions, but it is encouraging that sorbents such as sand could present appreciable capacities capable of removing > 50% of 3,4-DCA, even from sediment extract media (Table 2).

Table 2: Surface area, pore size and adsorption data of different material tested for the removal of 3,4-DCA from water. The parameters q_m and b refer to the Langmuir model (Equation 3)

Adsorbent	Surface area ($\text{m}^2 \text{g}^{-1}$)	Pore volume ($\text{cm}^3 \text{g}^{-1}$)	q_m (mg g^{-1})	B (mL mg^{-1})	Equilibrium time (h)	Stirring method
Halloysite [24]	76.6	0.039	0.078	2.726	> 3	Rotary stirrer
Kaolinite [90]	-	-	0.311	9	> 96	Electromagn.
Montmorillonite [90]	-	-	0.077	23	> 96	Electromagn.
Activated carbon AG [66]	963	0.55	583	-	48	-
Activated carbon SKT [66]	1028	0.53	480	-	0.5	-
Activated carbon RS [66]	410	0.5	364	-	0.5	-

Within ligand exchange processes, polymeric chelating resins are able to selectively remove target contaminants; however, eluate recycle, regeneration of depleted adsorbent, and the high cost of transition metals used as ligand complexing ions are still significant obstacles towards commercial application of such processes in wastewater treatment. Currently, there are no studies on the application of ligand exchange processes for 3,4-DCA removal, but seems possible in light of the recovery of aromatic amines from water, at low concentration, demonstrated with chelating resin-bound cobalt ion [224]. A mini-column apparatus with Co(II)-CDAE-sporopollenin resin was also tested for adsorption of chlorinated anilines, found to be described by a Langmuir model, and effective for 2-chloroaniline, 4-chloroaniline and 2,5-dichloroaniline [26]. The study showed similar values for the maximum adsorption capacity (q_m) for

binding of 2-chloroanilines and 4-chloroanilines, which were consistently lower than those for 3-dichloroaniline and 2,5 dichloroaniline onto the Co^{2+} matrix, suggesting that both electrical forces and steric hindrance are involved in the sorption process. This conclusion is supported by consideration of the inductive effects of *ortho*-Cl and *para*-Cl atoms, as well as the nature of these ligands, which contain charged groups and may offer steric hindrance. Moreover, steric hindrance around the amino nitrogen weakens binding to metal ions, causing faster migration of the aforementioned pollutants [225]. The adsorption of 3-chloroaniline was better represented by a Freundlich model, possibly as a result of a more complex type of binding than the independent and univalent binding described by a Langmuir model.

CHLORINATION, OZONISATION, CHEMICAL PRECIPITATION AND $\text{Fe}^0/\text{H}_2\text{O}_2$ SYSTEMS

A common sequence of operations adopted in many drinking water plants is that of (i) preoxidation, (ii) adsorption, and (iii) coagulation. Preoxidation of an aqueous sample with a concentration of 658 ng L^{-1} of 3,4-DCA, performed using sodium hypochlorite, demonstrated 100% pollutant removal [33]; however, such peroxidizing chemicals have associated risks of carcinogenic trihalomethanes by-products. Hence, researchers have considered other oxidative species and ozonolysis of a sample, again with a concentration of 658 ng L^{-1} of 3,4-DCA, showed 85% pollutant removal; however, the subsequent coagulation and flocculation steps were found to be ineffective, while further adsorption treatment, with activated carbons, led to complete pollutant removal [33].

The oxidizing potential of Fe^0 towards different organic compounds is well known [136]; $\text{Fe}^0/\text{H}_2\text{O}_2$ systems can be used to reduce levels of diuron, and other pesticides in polluted environments, as well as agricultural waste. Fe^0 promotes the reduction of H_2O_2 to hydroxyl radicals, generating Fe^{2+} , which, in turn, also produces hydroxyl radicals via further H_2O_2 reduction. A 10 mg L^{-1} diuron solution, with 2 mmol L^{-1} of H_2O_2 and H_3PO_4 , flowed through a glass tube packed with 2 g of iron wool, showed that pH strongly affected the degradation process, allowing process optimisation. At pH 2.5 more than 99.9% of the pesticide was removed after ten minutes, with only $1 \text{ } \mu\text{g L}^{-1}$ of 3,4-DCA found remaining in the effluent [137].

ELECTROCHEMICAL AND ELECTROHYDRAULIC METHODS

An electrohydraulic discharge (EHD) method for the oxidative degradation of 3,4-DCA was tested by exposing wastewaters to pulsed electrical discharges generated via submerged electrodes [138]. UV radiation is produced by a plasma channel created with the EHD, thereby, generating a shockwave as it expands against the water. The degradation rate is expressed by:

$$\frac{dC}{dN} = -k_1 C_i - k_0 \quad \text{Equation 4}$$

where dC/dN is the change in concentration per discharge, C_i is the initial substrate concentration, k_0 is the zero-order term (an expression of direct photolysis) and k_1 is the first-order term related to oxidation in the plasma channel region.

As part of an Advanced Oxidation Process (AOP), photocatalysis can be employed (i) for water treatment in slurry reactors, where an additional step is required for the separation of any suspended catalysts, or (ii) into reactors, where the catalysts are immobilized on adsorbents or on membranes. Using sols of vanadium pentoxide and cerium oxide, added to a titanium dioxide sol, allowed preparation of Ti–V and Ti–Ce catalysts, respectively; 0.1 g L⁻¹ of each powdered catalyst were added to agitated aqueous solutions of 3,4-DCA, irradiated in an annular reactor at 140 mW cm⁻², and the Ti–V catalyst gave a higher degradation than Ti–Ce, due to its band gap energy (which is more towards the visible region) and smaller particle size. The kinetic plot suggested bi-phase kinetics, with a sharp increase in rate after 45 minutes; further bench scale reactor experiments showed 85% degradation in 106 minutes [32] and Figure 2 shows the intermediate species formed.

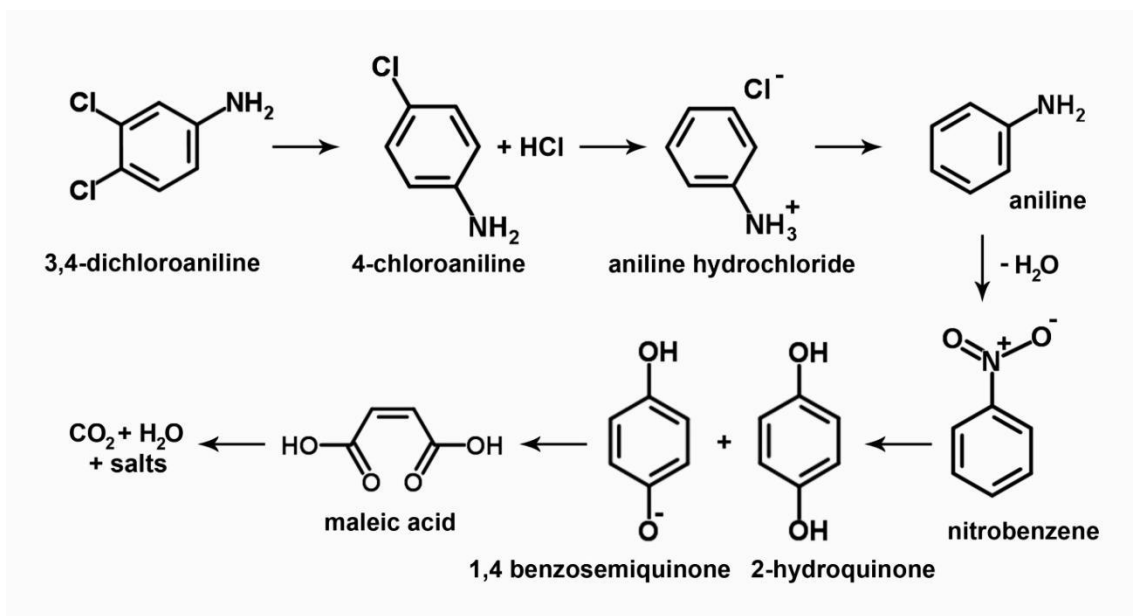


Fig 2: Intermediates formed during photo-degradation of 3,4-DCA using Ti-V (sol) catalyst, confirmed by HPLC and GC-MS analysis [32].

Biphasic kinetics were also observed in the photocatalytic degradation of 3,4-DCA using Ti-N and Ti-S catalysts [48]; the former showing higher surface area, lower particle size and band-gap energy. Higher specific surface area results in a higher degree of contact of the pollutant with the catalyst surface, while smaller particle size means a reduced degradation time, due to shorter distances between the charge carrier and the surface, where the reaction occurs. 3,4-DCA was fully degraded using Ti-N catalyst in 120 min with the best degradation obtained at pH = 6. At higher catalyst dosages ($> 0.1 \text{ g L}^{-1}$) the reaction rate starts to decrease, due to the deactivation of molecules that collide with ground state molecules, and subsequent agglomeration of catalyst particles. Meanwhile, at 3,4-DCA concentrations higher than 10 mg L^{-1} , the degradation efficiency starts to decrease, as the number of collisions between the 3,4-DCA molecules increases, while there is a reduction in collisions between pollutant molecules and $\cdot\text{OH}$ radicals [139].

Degradation of aqueous 3,4-DCA was recently performed using a dielectric barrier discharge (DBD) plasma reactor [140]; where generated ozone interacts with the pollutant directly or by the generation of hydroxyl radicals, which results in a faster rate of reaction than for molecular ozone alone [141]. The process involved flowing a water film between the discharge zone created by two aluminium electrodes, and the degradation process was well described by pseudo-first order kinetics, with higher efficiency reached under acidic conditions, increasing the input power and adding Fe^{2+} or Fe^{3+} . The main

pathways involved were deamination, hydroxylation, dechlorination, and hydroxylation and oxidation, followed by the generation of organic acids, via aromatic ring opening. Mineralization into CO₂ and H₂O was only partially achieved, as confirmed by the lower rate of removal for total organic carbon than for DCA, and by degradation intermediates identified using GC-MS analysis. Solution pH decreased during DCA degradation, as observed in previous work [142], where aqueous 3,4-DCA was degraded by a wire-cylinder DBD reactor, with an efficiency that was observed to increase when the input power was increased to 90 W, but decreased at powers above that; aqueous ozone concentration was seen to follow the same trend. It was also noted that, similar to other systems, the process was pH dependent with a lower degradation rate obtained under neutral conditions than at acidic or basic levels.

CONCLUSIONS

Myriad technologies have been developed for the degradation of pesticides; however, attention has to be mainly focussed on the fate of metabolites. 3,4-DCA is a degradation product generally more toxic than its parent substances; if it is covalently bound to humic substances within soil, the risk of groundwater contamination via leaching is low, but it also has an extremely low rate of mineralization [86] making it a significant environmental issue.

Lignin incorporation and fungal oxidation are able to effect complete removal of 3,4-DCA from the environment [133], while the use of bacteria and porous materials can be successful in bioreactors, as well as for in-situ bioremediation techniques. Bioremediation has been successfully demonstrated, introducing activated carbons and bacteria to polluted soils [66], and the biological removal of 3,4-DCA from sewage can be enhanced by the growth of indigenous communities, and through the introduction of adapted laboratory strains [117]; however, the technical and economic feasibility of such process also need to be considered. Further investigations are required to confirm the adsorption capacity of promising low cost materials such as activated carbons, corncob char and sand, especially within field conditions [100]. The possibility of recovering aromatic amines from low concentration water streams has been already demonstrated using chelating resin-bound cobalt ions [224], as well as for Co(II)-CDAE-sporopollenin resin [26], but there have been no specific studies related to the application of such technologies to 3,4-DCA removal.

Fe⁰/H₂O₂ systems could be developed for the degradation of 3,4-DCA in agricultural soils and waste [137], while photodegradation using doped TiO₂ has

been successfully performed and degradation kinetics are available for the scale up of reactors [32]. Low toxicity and cost, combined with good chemical stability and high natural abundance [253] make this catalyst potentially suitable for the environmentally friendly removal of 3,4-DCA from water. While, effective degradation is also observed for the use of dielectric barrier discharge reactors, further studies are required to reach the complete mineralization of 3,4-DCA [140].

Hence, there is significant scope for the application of existing technologies to the issue of 3,4-DCA removal from aqueous streams, some of which have timely potential for implementation; however, there is a need for more data to be acquired to permit economic and environmental impact of these proposed systems to be fully addressed.

REFERENCES

1. Angioi, S., et al., *Sorption studies of chloroanilines on kaolinite and montmorillonite*. Environmental Pollution, 2005. **134**(1): p. 35-43.
2. Bevan, R., et al., *A review of latest endocrine disrupting chemicals research implications for drinking water*. 2012.
3. Cook, J.C., et al., *Investigation of a mechanism for leydig-cell tumorigenesis by linuron in rats*. Toxicology and Applied Pharmacology, 1993. **119**(2): p. 195-204.
4. Crossland, N.O. and J.M. Hillaby, *Fate and effects of 3,4-dichloroaniline in the laboratory and in outdoor ponds .2. Chronic toxicity to daphnia spp and other invertebrates*. Environmental Toxicology and Chemistry, 1985. **4**(4): p. 489-499.
5. Groshart and Okkerman, *Towards the establishment of a priority list of substances for further evaluation of their role in endocrine disruption*. 2000, European Commission.
6. Ucan, M. and A. Ayar, *Sorption equilibria of chlorinated anilines in aqueous solution on resin-bound cobalt ion*. Colloids and Surfaces a-Physicochemical and Engineering Aspects, 2002. **207**(1-3): p. 41-47.
7. Muller, L., E. Fattore, and E. Benfenati, *Determination of aromatic amines by solid-phase microextraction and gas chromatography mass spectrometry in water samples*. Journal of Chromatography A, 1997. **791**(1-2): p. 221-230.

8. Flores-Céspedes, F., et al., *Cosorption study of organic pollutants and dissolved organic matter in a soil*. Environmental Pollution, 2006. **142**(3): p. 449-456.
9. Parris, G.E., *Covalent binding of aromatic-amines to humates .1. Reactions with carbonyls and quinones* Environmental Science & Technology, 1980. **14**(9): p. 1099-1106.
10. Park, J.W., et al., *Effect of humic constituents on the transformation of chlorinated phenols and anilines in the presence of oxidoreductive enzymes or birnessite*. Environmental Science & Technology, 1999. **33**(12): p. 2028-2034.
11. Padmini, E. and L.R. Miranda, *Nanocatalyst from sol-sol doping of TiO₂ with Vanadium and Cerium and its application for 3,4 Dichloroaniline degradation using visible light*. Chemical Engineering Journal, 2013. **232**: p. 249-258.
12. Szczepanik, B., et al., *Adsorption of chloroanilines from aqueous solutions on the modified halloysite*. Applied Clay Science, 2014. **101**: p. 260-264.
13. Ormad, M.P., et al., *Pesticides removal in the process of drinking water production*. Chemosphere, 2008. **71**(1): p. 97-106.
14. Livingston, A.G. and A. Willacy, *Degradation of 3,4-dichloroaniline in synthetic and industrially produced wastewaters by mixed cultures freely suspended and immobilized in a packed-bed reactor* Applied Microbiology and Biotechnology, 1991. **35**(4): p. 551-557.
15. Bureau, E.C., *European Union Risk Assessment Report*. 2006.
16. Gülden, M., A. Turan, and H. Seibert, *Endocrinically active chemicals and their occurrence in surface waters: research report 10204279*. 1998.
17. Sorokin, N., et al., *Proposed EQS for Water Framework Directive Annex VIII substances: 3,4- dichloroaniline*. 2008.
18. Tomlin, C., *The Pesticide Manual, British Crop Protection Council, Surrey, UK (1999)*. 1999.
19. Roche, H., et al., *Rice fields regulate organochlorine pesticides and PCBs in lagoons of the Nature Reserve of Camargue*. Chemosphere, 2009. **75**(4): p. 526-533.
20. Hsu, T.S. and R. Bartha, *Hydrolyzable and nonhydrolyzable 3,4-dichloroaniline humus complexes and their respective rates of biodegradation* Journal of Agricultural and Food Chemistry, 1976. **24**(1): p. 118-122.
21. Pothuluri, J.V., J.A. Hinson, and C.E. Cerniglia, *Propanil - toxicological characteristics, metabolism, and biodegradation potential in soil* Journal of Environmental Quality, 1991. **20**(2): p. 330-347.

22. Cullington, J.E. and A. Walker, *Rapid biodegradation of diuron and other phenylurea herbicides by a soil bacterium*. *Soil Biology & Biochemistry*, 1999. **31**(5): p. 677-686.
23. Bartha, R. and D. Pramer, *Pesticide transformation to aniline and azo compounds in soil* *Science*, 1967. **156**(3782): p. 1617-&.
24. Di Corcia, A., et al., *Quantification of phenylurea herbicides and their free and humic acid-associated metabolites in natural waters*. *Journal of Chromatography A*, 1999. **852**(2): p. 465-474.
25. Gosetti, F., et al., *Sun light degradation of 4-chloroaniline in waters and its effect on toxicity. A high performance liquid chromatography – Diode array – Tandem mass spectrometry study*. *Environmental Pollution*, 2010. **158**(2): p. 592-598.
26. Loos, R., G. Hanke, and S.J. Eisenreich, *Multi-component analysis of polar water pollutants using sequential solid-phase extraction followed by LC-ESI-MS*. *Journal of Environmental Monitoring*, 2003. **5**(3): p. 384-394.
27. Norberg, J., A. Zander, and J.A. Jonsson, *Fully automated on-line supported liquid membrane liquid chromatographic determination of aniline derivatives in environmental waters*. *Chromatographia*, 1997. **46**(9-10): p. 483-488.
28. Ellappan, P. and L.R. Miranda, *Two-regime kinetic study and parameter optimization of degradation of 3,4-dichloroaniline using TI-N/S catalyst under visible light*. *Desalination and Water Treatment*, 2016. **57**(5): p. 2203-2216.
29. Vastermark, A., et al., *Polymorphic variation in the androgen receptor gene: Association with risk of testicular germ cell cancer and metastatic disease*. *European Journal of Cancer*, 2011. **47**(3): p. 413-419.
30. Swedenborg, E., et al., *Endocrine disruptive chemicals: mechanisms of action and involvement in metabolic disorders*. *Journal of Molecular Endocrinology*, 2009. **43**(1-2): p. 1-10.
31. Rüegg, J., et al., *Receptors mediating toxicity and their involvement in endocrine disruption*, in *Molecular, Clinical and Environmental Toxicology: Volume 1: Molecular Toxicology*, A. Luch, Editor. 2009, Birkhäuser Basel: Basel. p. 289-323.
32. Newbold, R.R., *Impact of environmental endocrine disrupting chemicals on the development of obesity*. *Hormones-International Journal of Endocrinology and Metabolism*, 2010. **9**(3): p. 206-217.
33. Diamanti-Kandarakis, E., et al., *Endocrine-Disrupting Chemicals: An Endocrine Society Scientific Statement*. *Endocrine Reviews*, 2009. **30**(4): p. 293-342.
34. Koppe, J.G., et al., *Exposure to multiple environmental agents and their effect*. *Acta Paediatrica*, 2006. **95**: p. 106-113.

35. Brian, J.V., et al., *Evidence of estrogenic mixture effects on the reproductive performance of fish*. Environmental Science & Technology, 2007. **41**(1): p. 337-344.
36. Kortenkamp, A., et al., *Low-Level Exposure to Multiple Chemicals: Reason for Human Health Concerns?* Environmental Health Perspectives, 2007. **115**(Suppl 1): p. 106-114.
37. Corke, C.T. and F.R. Thompson, *Effects of some phenylamide herbicides and their degradation products on soil nitrification* Canadian Journal of Microbiology, 1970. **16**(7): p. 567-&.
38. Bearden, A.P. and T.W. Schultz, *Structure-activity relationships for Pimephales and Tetrahymena: A mechanism of action approach*. Environmental Toxicology and Chemistry, 1997. **16**(6): p. 1311-1317.
39. Argese, E., et al., *Assessment of chloroaniline toxicity by the submitochondrial particle assay*. Environmental Toxicology and Chemistry, 2001. **20**(4): p. 826-832.
40. Hooftman, R.N. and G.J. Vink, *The determination of toxic effects of pollutants with the marine polychaete worm ophryotrocha-diadema* Ecotoxicology and Environmental Safety, 1980. **4**(3): p. 252-262.
41. Adema, D.M. and I.G. Vink, *A comparative-study of the toxicity of 1,1,2-trichloroethane, dieldrin, pentachlorophenol and 3,4 dichloroaniline for marine and fresh-water organisms* Chemosphere, 1981. **10**(6): p. 533-554.
42. Allner, *Toxikokinetik von 3,4-Dichloranilin beim dreistachligen Stichling (Gasterosteus aculeatus) unter besonderer Berücksichtigung der Fortpflanzungsphysiologie*. 1997, Joannes Gutenberg Universitat.
43. Droulia, F.E., V. Kati, and C.N. Giannopolitis, *Sorption of 3,4-dichloroaniline on four contrasting Greek agricultural soils and the effect of liming*. Journal of Environmental Science and Health Part B-Pesticides Food Contaminants and Agricultural Wastes, 2011. **46**(5): p. 404-410.
44. Fava, L., et al., *Pesticide metabolites as contaminants of groundwater resources: assessment of the leaching potential of endosulfan sulfate, 2,6-dichlorobenzoic acid, 3,4-dichloroaniline, 2,4-dichlorophenol and 4-chloro-2-methylphenol*. Microchemical Journal, 2005. **79**(1-2): p. 207-211.
45. Claver, A., et al., *Study of the presence of pesticides in surface waters in the Ebro river basin (Spain)*. Chemosphere, 2006. **64**(9): p. 1437-1443.
46. Wegman, R.C.C. and G.A.L. De Korte, *Aromatic amines in surface waters of The Netherlands*. Water Research, 1981. **15**(3): p. 391-394.
47. Gonzalez-Pradas, E., et al., *Effects of dissolved organic carbon on sorption of 3,4-dichloroaniline and 4-bromoaniline in a calcareous soil*. Chemosphere, 2005. **59**(5): p. 721-728.

48. Crossland, N.O., *A review of the fate and toxicity of 3,4-dichloroaniline in aquatic environments* Chemosphere, 1990. **21**(12): p. 1489-1497.
49. Beyerlepfur, R. and J.P. Lay, *Adsorption and desorption of 3,4-dichloroaniline on soil* Chemosphere, 1990. **21**(9): p. 1087-1094.
50. Bakhaeva, L.P., et al., *Microbial degradation of 3,4-dichloroaniline sorbed by activated carbon*. Microbiology, 2001. **70**(3): p. 277-284.
51. Süß, Z. *Pflanzenernähr. Bodenk*, 1978. **141**(57-66).
52. Reid, B.J., K.C. Jones, and K.T. Semple, *Bioavailability of persistent organic pollutants in soils and sediments - a perspective on mechanisms, consequences and assessment*. Environmental Pollution, 2000. **108**(1): p. 103-112.
53. Bengtsson, G., R. Lindqvist, and M.D. Piwoni, *Sorption of trace organics to colloidal clays, polymers, and bacteria* Soil Science Society of America Journal, 1993. **57**(5): p. 1261-1270.
54. Freitag, D., et al., *Long-term fate of 4-chloroaniline-c-14 in soil and plants under outdoor conditions - a contribution to terrestrial ecotoxicology of chemicals* Journal of Agricultural and Food Chemistry, 1984. **32**(2): p. 203-207.
55. Li, H., et al., *Effect of substitution on irreversible binding and transformation of aromatic amines with soils in aqueous systems*. Environmental Science & Technology, 2000. **34**(17): p. 3674-3680.
56. Li, H. and L.S. Lee, *Sorption and abiotic transformation of aniline and alpha-naphthylamine by surface soils*. Environmental Science & Technology, 1999. **33**(11): p. 1864-1870.
57. Corke, C.T., et al., *Diazonium cations as intermediates in the microbial transformation of chloroanilines to chlorinated biphenyls, azo-compounds, and triazenes* Journal of Agricultural and Food Chemistry, 1979. **27**(3): p. 644-646.
58. Albers, C.N., et al., *Characterization and structural modelling of humic substances in field soil displaying significant differences from previously proposed structures*. European Journal of Soil Science, 2008. **59**(4): p. 693-705.
59. Stevenson, F.J., *Humus Chemistry: Genesis, Composition, Reactions*. 1994, New York: Wiley & Sons.
60. Weber, E.J., D. Colon, and G.L. Baughman, *Sediment-associated reactions of aromatic amines. 1. Elucidation of sorption mechanisms*. Environmental Science & Technology, 2001. **35**(12): p. 2470-2475.
61. Weber, E.J., D.L. Spidle, and K.A. Thorn, *Covalent binding of aniline to humic substances .1. Kinetic studies*. Environmental Science & Technology, 1996. **30**(9): p. 2755-2763.

62. Nagel, R., *Bioakkumulation und Verteilung von Umweltchemikalien in aquatischen Laborsystemen zur realitätsnahen Prognose der Umweltgefährlichkeit*, ed. U.F.-V. 10603106/01. 1997, Berlin.
63. Heim, K., I. Schuphan, and B. Schmidt, *Behavior of c-14 4-nitrophenol and c-14 3,4-dichloroaniline in lab sediment-water systems .1. Metabolic-fate and partitioning of radioactivity* Environmental Toxicology and Chemistry, 1994. **13**(6): p. 879-888.
64. Dunnivant, F.M., et al., *Cotransport of cadmium and hexachlorobiphenyl by dissolved organic-carbon through columns containing aquifer material* Environmental Science & Technology, 1992. **26**(2): p. 360-368.
65. Huang, X.J. and L.S. Lee, *Effects of dissolved organic matter from animal waste effluent on chlorpyrifos sorption by soils*. Journal of Environmental Quality, 2001. **30**(4): p. 1258-1265.
66. Li, K., B.S. Xing, and W.A. Torello, *Effect of organic fertilizers derived dissolved organic matter on pesticide sorption and leaching*. Environmental Pollution, 2005. **134**(2): p. 187-194.
67. Chiou, C.T., et al., *Water solubility enhancement of some organic pollutants and pesticides by dissolved humic and fulvic-acids* Environmental Science & Technology, 1986. **20**(5): p. 502-508.
68. Guo, L., et al., *Sorption and movement of alachlor in soil modified by carbon-rich wastes* Journal of Environmental Quality, 1993. **22**(1): p. 186-194.
69. Johnson, A.C., et al., *The potential of incorporated organic matter to reduce pesticide leaching*. Toxicological & Environmental Chemistry, 1997. **58**: p. 47-61.
70. Albers, C.N., et al., *Effect of Different Humic Substances on the Fate of Diuron and Its Main Metabolite 3,4-Dichloroaniline in Soil*. Environmental Science & Technology, 2008. **42**(23): p. 8687-8691.
71. Freundlich, H. and H. Hatfield, *Colloid and Capillary Chemistry*. 1926, London: Methuen.
72. Hsu, T.S. and R. Bartha, *Interaction of pesticide-derived chloroaniline residues with soil organic-matter* Soil Science, 1973. **116**(6): p. 444-452.
73. Saxena, A. and R. Bartha, *Microbial mineralization of humic-acid 3,4-dichloroaniline complexes* Soil Biology & Biochemistry, 1983. **15**(1): p. 59-62.
74. Giles, C.H., et al., *Studies in adsorption .11. A system of classification of solution adsorption isotherms, and its use in diagnosis of adsorption mechanisms and in measurement of specific surface areas of solids* Journal of the Chemical Society, 1960(OCT): p. 3973-3993.
75. Polati, S., et al., *Sorption and desorption behavior of chloroanilines and chlorophenols on montmorillonite and kaolinite*. Journal of Environmental

- Science and Health Part B-Pesticides Food Contaminants and Agricultural Wastes, 2006. **41**(6): p. 765-779.
76. Bouras, O., et al., *Adsorption of diuron and its degradation products from aqueous solution by surfactant-modified pillared clays*. Applied Clay Science, 2007. **37**(3-4): p. 240-250.
 77. Hance, R.J., *Adsorption–desorption phenomena*, in *Interactions between Herbicides and the Soil*. 1980, Academic Press.
 78. Sheng, G.Y., S.H. Xu, and S.A. Boyd, *Mechanism(s) controlling sorption of neutral organic contaminants by surfactant-derived and natural organic matter*. Environmental Science & Technology, 1996. **30**(5): p. 1553-1557.
 79. Gonzalez-Pradas, E., et al., *Sorption and leaching of diuron on natural and peat-amended calcareous soil from Spain*. Water Research, 1998. **32**(9): p. 2814-2820.
 80. Celis, R., E. Barriuso, and S. Houot, *Sorption and desorption of atrazine by sludge-amended soil: Dissolved organic matter effects*. Journal of Environmental Quality, 1998. **27**(6): p. 1348-1356.
 81. Nelson, S.D., et al., *Stability and mobility of napropamide complexed with dissolved organic matter in soil columns*. Journal of Environmental Quality, 2000. **29**(6): p. 1856-1862.
 82. Lee, D.Y. and W.J. Farmer, *Dissolved organic matter interaction with napropamide and four other nonionic pesticides*. Journal of Environmental Quality, 1989. **18**: p. 468-474.
 83. Graber, E.R., et al., *Enhanced transport of atrazine under irrigation with effluent (vol 59, pg 1513, 1995)*. Soil Science Society of America Journal, 1996. **60**(2): p. 424-424.
 84. Totsche, K.U., J. Danzer, and I. KogelKnabner, *Dissolved organic matter-enhanced retention of polycyclic aromatic hydrocarbons in soil miscible displacement experiments*. Journal of Environmental Quality, 1997. **26**(4): p. 1090-1100.
 85. Huguenot, D., et al., *Selection of low cost materials for the sorption of copper and herbicides as single or mixed compounds in increasing complexity matrices*. Journal of Hazardous Materials, 2010. **182**(1-3): p. 18-26.
 86. Lyons, C.D., S.E. Katz, and R. Bartha, *Persistence and mutagenic potential of herbicide-derived aniline residues in pond water* Bulletin of Environmental Contamination and Toxicology, 1985. **35**(5): p. 696-703.
 87. OECD, *OECD guidelines for testing of chemicals*. 1992.
 88. CITI, *Data of existing chemicals based on the CSCL Japan*. 1992. **10-26**: p. 32,33.

89. Kuiper, J. and A.O. Hanstveit, *Fate and effects of 3,4-dichloroaniline (dca) in marine plankton communities in experimental enclosures* Ecotoxicology and Environmental Safety, 1984. **8**(1): p. 34-54.
90. Bayer, A., *Internal examination on the biological degradation of 2,4-, 2,5- and 3,4-dichloroaniline in samples of Rhine-water.* 1992.
91. Brunsbach, F.R. and W. Reineke, *Degradation of chloroanilines in soil slurry by specialized organisms* Applied Microbiology and Biotechnology, 1993. **40**(2-3): p. 402-407.
92. Struijs, J. and J.E. Rogers, *Reductive dehalogenation of dichloroanilines by anaerobic microorganisms in fresh and dichlorophenol-acclimated pond sediment* Applied and Environmental Microbiology, 1989. **55**(10): p. 2527-2531.
93. Loidl, M., et al., *Degradation of aniline and monochlorinated anilines by soil-born pseudomonas-acidovorans strains* Archives of Microbiology, 1990. **155**(1): p. 56-61.
94. Latorre, J., W. Reineke, and H.J. Knackmuss, *Microbial-metabolism of chloroanilines - enhanced evolution by natural genetic exchange* Archives of Microbiology, 1984. **140**(2-3): p. 159-165.
95. Kim, Y.-M., et al., *Isolation and characterization of 3,4-dichloroaniline degrading bacteria.* Korean Journal of Microbiology and Biotechnology, 2007. **35**(3): p. 245-249.
96. Travkin, V.M., et al., *Degradation of 3,4-dichloro- and 3,4-difluoroaniline by Pseudomonas fluorescens 26-K.* Journal of Environmental Science and Health Part B-Pesticides Food Contaminants and Agricultural Wastes, 2003. **38**(2): p. 121-132.
97. Surovtseva, E.G., et al., *Chlorinated anilines as a source of carbon nitrogen and energy for pseudomonas-diminuta* Mikrobiologiya, 1985. **54**(6): p. 948-952.
98. Sergeeva, N.R., M.S. Sokolov, and G.K. Vasil'eva, *Using bacteria to accelerate the decomposition of 3,4-dichloroaniline in fish ponds.* Agrokhimiya, 1998. **0**(4): p. 84-90.
99. Martinez Viera, R., M.M. Alfonso Hernandez, and R.F. Castaneda Ruiz, *Decomposition of 3 4 dichloroaniline by microorganisms from two cuban soils* Ciencias de la Agricultura, 1984(20): p. 117-124.
100. Wasserfallen, A., J. Zeyer, and K.N. Timmis, *Bacterial metabolism and toxicity of halogenated anilines* Experientia, 1986. **42**(1): p. 106-106.
101. Sharma, P., et al., *Efficient biotransformation of herbicide diuron by bacterial strain Micrococcus sp. PS-1.* Biodegradation, 2010. **21**(6): p. 979-987.
102. Devers-Lamrani, M., et al., *Evidence for cooperative mineralization of diuron by Arthrobacter sp. BS2 and Achromobacter sp. SP1 isolated*

- from a mixed culture enriched from diuron exposed environments. *Chemosphere*, 2014. **117**: p. 208-215.
103. Surovtseva, E.G., et al., *Degradation of chlorinated anilines by certain representatives of the genera Aquaspirillum and Paracoccus*. *Microbiology*, 1996. **65**(5): p. 553-559.
 104. Vasilyeva, G.K., L.P. Bakhaeva, and E.G. Surovtseva, *The Use of In Situ Soil Adsorptive Bioremediation Following an Accidental Spill of Propanil in the Krasnodar Region of Russia*. *Land Contam. Reclam.*, 1996. **4**: p. 263-268.
 105. Carvalho, G., et al., *Biological treatment of propanil and 3,4-dichloroaniline: Kinetic and microbiological characterisation*. *Water Research*, 2010. **44**(17): p. 4980-4991.
 106. Emmanuel Herrera-Gonzalez, V., et al., *Biodegradation of the herbicide propanil, and its 3,4-dichloroaniline by-product in a continuously operated biofilm reactor*. *World Journal of Microbiology & Biotechnology*, 2013. **29**(3): p. 467-474.
 107. Yih, R.Y., D.H. McRae, and H. Wilson, *Science*. Vol. 161. 1968, Washington D.C.
 108. Still, G., *Science*. Vol. 159. 1968, Washington D.C.
 109. Fuchsbichler, G., A. Suss, and P. Wallnofer, *Uptake of 4-chloro-chloraniline and 3,4-dichloroaniline by cultivated plants* *Zeitschrift Fur Pflanzenkrankheiten Und Pflanzenschutz-Journal of Plant Diseases and Protection*, 1978. **85**(5): p. 298-307.
 110. Arjmand, M. and H. Sandermann, *Mineralization of chloroaniline lignin conjugates and of free chloroanilines by the white rot fungus phanerochaete-chrysosporium* *Journal of Agricultural and Food Chemistry*, 1985. **33**(6): p. 1055-1060.
 111. Funtikova, N.S. and E.G. Surovtseva, *Adsorption of herbicides derivatives of phenyl urea and chloro substituted anilines by microorganisms* *Mikrobiologiya*, 1979. **48**(6): p. 1086-1092.
 112. Pieper, D.H., R. Winkler, and H. Sandermann, *Formation of a toxic dimerization product of 3,4-dichloroaniline by lignin peroxidase from phanerochaete-chrysosporium* *Angewandte Chemie-International Edition in English*, 1992. **31**(1): p. 68-70.
 113. Pavlovic, I., et al., *Adsorption of acidic pesticides 2,4-D, Clopyralid and Picloram on calcined hydrotalcite*. *Applied Clay Science*, 2005. **30**(2): p. 125-133.
 114. Ho, Y.S. and G. McKay, *The kinetics of sorption of basic dyes from aqueous solution by sphagnum moss peat*. *Canadian Journal of Chemical Engineering*, 1998. **76**(4): p. 822-827.

115. Meier, L.P., R. Nueesch, and F.T. Madsen, *Organic Pillared Clays*. Journal of Colloid and Interface Science, 2001. **238**(1): p. 24-32.
116. Bansal, R.C., J.-B. Donnet, and F. Stoeckli, *Active Carbon*. 1988, New York.
117. Malandrino, M., et al., *Adsorption of heavy metals on vermiculite: Influence of pH and organic ligands*. Journal of Colloid and Interface Science, 2006. **299**(2): p. 537-546.
118. Chanda, M., O'Driscoll, and G.L. Rempel, *Reactive Polymers*. 1984
119. Davankov, V.A., J.D. Navratil, and H.F. Walton, *Ligand Exchange Chromatography*. 1988, US: CRC Press.
120. Joo, S.H., et al., *Quantification of the oxidizing capacity of nanoparticulate zero-valent iron*. Environmental Science & Technology, 2005. **39**(5): p. 1263-1268.
121. Cabrera, L.C., et al., *Degradation of Herbicide Diuron in Water Employing the Fe-0/H₂O₂ System*. Journal of the Brazilian Chemical Society, 2010. **21**(12): p. 2347-2352.
122. Willberg, D.M., et al., *Degradation of 4-chlorophenol, 3,4-dichloroaniline, and 2,4,6-trinitrotoluene in an electrohydraulic discharge reactor*. Environmental Science & Technology, 1996. **30**(8): p. 2526-2534.
123. Lodha, S., et al., *Photocatalytic degradation of Phenol Red using complexes of some transition metals and hydrogen peroxide*. Journal of the Serbian Chemical Society, 2008. **73**(6): p. 631-639.
124. Feng, J., et al., *Degradation of aqueous 3,4-dichloroaniline by a novel dielectric barrier discharge plasma reactor*. Environmental Science and Pollution Research, 2015. **22**(6): p. 4447-4459.
125. Haag, W.R. and C.C.D. Yao, *Rate constants for reaction of hydroxyl radicals with several drinking-water contaminants* Environmental Science & Technology, 1992. **26**(5): p. 1005-1013.
126. Feng, J.-w., et al., *Degradation of aqueous 3, 4-dichloroaniline by wire-cylinder dielectric barrier discharge reactor*, in *Advances in Environmental Science and Engineering, Pts 1-6*, R. Iranpour, et al., Editors. 2012. p. 1729-1732.
127. Ambrus, Z., et al., *Low temperature synthesis, characterization and substrate-dependent photocatalytic activity of nanocrystalline TiO₂ with tailor-made rutile to anatase ratio*. Applied Catalysis A: General, 2008. **340**(2): p. 153-161.

9.1.3 Invited papers

The paper: “Quartzene® process: From synthesis to commercial scale of a green nanoporous silica material”, is not presented in this manuscript, as still in draft form.

Organics adsorption on novel amorphous silica and silica xerogels: Micro Column Rapid Breakthrough test coupled with Sequential Injection Flow-based Techniques

Andrea Luca Tasca*, Ashleigh J. Fletcher^a, Fernando Maya Alejandro^b, Gemma Turnes Palomino^b, Farnaz Ghajeri^c

^a Department of Chemical and Process Engineering, University of Strathclyde, Glasgow G1 1XJ, United Kingdom

^b Department of Chemistry, Faculty of Sciences, University of the Balearic Islands, Carretera de Valldemossa km 7.5, E-07122 Palma de Mallorca, Illes Balears, Spain

^c Department of Engineering Sciences, Applied Materials Science, Uppsala University, Uppsala, Sweden

Abstract

The adsorption capacities of a novel amorphous silica, and silica xerogels, for aromatic compounds were investigated under batch conditions and using Micro Column Rapid Breakthrough tests coupled with Sequential Injection Flow-based automated instrumentation, in order to evaluate their operative feasibility under conditions typically used in water treatment facilities. Extraction columns were fabricated using stereolithographic 3D printing. Sorbent reusability was also investigated using automated flow-based techniques. Benzene was selected as target dissolved organic compound usually present in produced waters from the oil and gas sector, continuously increasing. 3,4-dichloroaniline (3,4-DCA) was selected as part of Endocrine Disrupting Chemicals, which are becoming source of major concern for human and wildlife toxicity. Novel amorphous silicas were synthesised at low temperature and under ambient pressure from a sodium metasilicate precursor, and were subject to post-synthetic methylation. Silica xerogels were prepared via acid catalysis of a sodium metasilicate solution and functionalised with trimethylchlorosilane, at low temperature and under ambient pressure. The removal efficiency of the silica xerogels tested was found equal greater than 22.62 mg/g for benzene at a flow rate of 0.6 mL/min, while the uptake of 3,4-DCA was found >4.63 mg/g and >7.17 mg/g, respectively at flow rates of 1.8 mL/min and 0.6 mL/min.

Keywords

Introduction

Global demand on clean water supplies is becoming increasingly intensive, thus the need for innovative and cost effective water treatment technologies is rising, including those designed to treat produced water from oil exploration activities. Produced water is the largest by-product generated by oil and gas extraction; hence, there are significant quantities of contaminated water that require remediation. Additional stress has been placed on this valuable resource by the presence of further organics known as Endocrine Disrupting Chemicals (EDCs), which have been detected at increasing levels in various sewage discharges, fresh- and estuarine-waters in recent years, and are, therefore of increasing concern for water agencies [12, 22].

Membranes are a promising but expensive technology for water remediation, however, the use of an adsorption media as a prior treatment could make them a potentially cost-effective option. Within the range of available solid sorbents, hydrophobic aerogels and xerogels exhibit very attractive properties for oil spill remediation [212-215, 254]. However, very few studies have investigated the adsorption performance of hydrophobic gels at the low organic concentrations typical of water treatment applications [192, 217, 255], while the costs associated with functionalisation of these materials currently hinder their use as sorbents in the final stages of produced water treatments. It is also notable that the majority of previous work on organics adsorption from aqueous phase has been limited to batch tests, which fails to assess the feasibility of the materials developed as sorbents in apparatus commonly used in water treatment plants.

Column breakthrough experiments are crucial in identifying sorbent capacity, allowing estimation of material utilisation rate and treatment costs. The first recorded breakthrough experiments employed non-sieved sorbents and high flow rates in order to guarantee the same empty bed contact times (EBCT) employed in treatment facilities, where long exposure times and large sample volumes are required. Such experimental regimes have not always been practicable, hence, advanced studies were subsequently performed using small (>100 g), mini (>5 g) and then micro (<2 g) columns. [226], while Rapid Small Scale Column Tests (RSSCT) were specifically developed to provide an estimate of the operative capacities of granular activated carbons [227]. The underlying theory behind RSSCT and all Micro-Column Breakthrough (MCRB) techniques is the appropriate scaling of hydrodynamic and mass transfer characteristics to small scale flow test column dimensions, assuming that the breakthrough curves would be similar to those of a pilot scale plant. Such tests mean that only minimal quantities of water and time are required to simulate pilot scale studies.

Recent improvements to MCRB methods were introduced by Chang *et al.*, who proposed a further simplification to the procedure, by use of low cost sampler, piping, fittings, and pumps, to obtain data on the adsorption of phenol, methyl tert-butyl ether, and other organic pollutants on carbon [226]. In tandem with these improvements, sequential-injection analysis

(SIA) has been shown to overcome the some limitations of classic flow-injection analysis (FIA), mainly related to complex manifold operations. As such, SIA simplifies the sample manipulation required before measurement steps, and includes in-line sample dilution, dialysis and gas diffusion, enzymatic and immunological testing, as well as extraction [230]. Additional gains in ease of analysis can be made by avoiding traditional solid-phase extraction, which is time-consuming, reagent intensive and produces significant waster, instead using automated solid phase extraction, which is quicker, requires little manipulation by the analyst, reduces reagent consumption and, consequently, minimises waste generation [256].

This work uses advanced adsorption methods to study the uptake of benzene, as representative of dissolved oil species in produced water, on hydrophilic and hydrophobic amorphous silica and silica xerogels, synthesised under ambient pressure and at low temperature conditions. Results are also presented for adsorption of 3,4-dichloroaniline on the aforementioned materials, using both batch and MCRB tests coupled with SIA. Additional automated solid-phase extraction was used for desorbing the organics from the materials.

Materials and methods

3D printing of the column

To design the column was used the 3D modelling tool for designers Rhinoceros 5, developed by Robert McNeel & Associates. The inside components of the column were created one by one and combined using Boolean operators. The model of the column was then extracted as a Stereolithography file (.STL file) and loaded in the software preForm, provided by FormLabs. A Form1+ 3D printer from FormLabs (tech specs) was used to printing the model on clear methacrylate photopolymer, while a CL-1000 ultraviolet crosslinker was adopted to finish the cure process.

Adsorbent synthesis

Quartzene

Quartzene is a novel amorphous silica; samples used in this study were supplied by Svenska Aerogel AB (SvAAB) and offered a range of silicas with hydrophilic nature (ND, Z1 and CMS), and their hydrophobic analogues (NDH, Z1H and CMSH). Hydrophilicity and hydrophobicity of Quartzene can be tailored to suit the desired application, and its porous structure can also be controlled, notably without the addition of any surfactant. Unlike traditional aerogels, the material is cheap to produce and is prepared via an environmentally friendly synthetic procedure, by virtue of the temperature and pressure conditions used. The synthetic procedure for Quartzene has been reported previously [1]; in summary, ND type Quartzene was prepared via the precipitation of sodium metasilicate ($\text{SiO}_2:\text{Na}_2\text{O} = 3.35$) with sodium chloride, where after, the precipitate was mixed with tap water, before vacuum filtration, and the resulting paste, comprising up to 85% water, was spray-dried. Z1 samples using a method

analogous to that for ND, but with a different level of activation of the silica source [232]. CMS samples were prepared by mixing magnesium chloride hexahydrate (68 mol% Mg) and calcium chloride dihydrate (32 mol% Ca) before adding to a sodium metasilicate solution, at a concentration ratio of 1:2. Coagulation occurred, as previously described [233], and the resulting gel was washed, filtered and dried, as described for ND samples. Hydrophobic NDH, Z1H and CMSH were prepared, by SvAAB, via methylation of the hydrophilic analogues.

Silica xerogels

Silica xerogels were synthesised using diluted solutions of sodium metasilicate, as inspired by the work of Bangi *et al.* [1]; the commercial solution has formulation $(\text{NaOH})_x(\text{Na}_2\text{SiO}_3)_y \cdot z\text{H}_2\text{O}$, $\geq 10\% \text{NaOH}$ basis and $\geq 27\% \text{SiO}_2$ basis, and was diluted with distilled water to produce $\text{H}_2\text{O}:\text{Na}_2\text{SiO}_3$ molar ratios from 80 to 200. Acid catalysis was performed by dropwise addition of citric acid (3 M), to 40 mL of 10%vol diluted sodium silicate solution placed in a 400 mL cylindrical glass container and manually stirred during the addition. Containers were subsequently placed in oven at 323 K, partially covered, for gelation and a first drying phase to occur. Consecutive washing, solvent exchange, and hydrophobisation were chosen to minimize consumption of the hydrophobisation agent. 24 h post acid addition, the dried gels were washed 3 times in 24 h, after first being cut into small pieces (~1 cm cubes) in order to speed up the exchange of sodium ions with distilled water. Water was then exchanged with methanol, prior to functionalisation with a mixture of 1:1:1 volume of hexane, TMCS and methanol. Samples were placed in the oven at 323 K during washing, methanol exchange and functionalisation. Finally, curing for 1 d at room temperature and 1 h in an oven at 473 K completed the synthesis. Similar gels were synthesised without functionalisation.

Adsorbent characterisation

Samples were dried for 2 h at 358K prior to coating with a thin layer (1.5 nm) of gold for Field Emission Scanning Electron Microscopy analysis (FE-SEM). A HITACHI SU-6600 (2010) microscope was used; the instrument is equipped with Energy Dispersive Spectroscopy (EDS), Oxford Inca 350 with 20 mm X-Max detector, Wavelength Dispersive Spectroscopy (WDS), and Oxford Inca Wave 700 Microanalysis System with Energy + Software. Surface areas, average pore sizes and pore size distributions were determined by nitrogen sorption measurements, performed at 77 K using a Micromeritics ASAP 2420. Samples were degassed at 393 K for 3-5 h, prior to analysis. Brunauer-Emmet-Teller (BET) [177] and Barret-Joyner-Halenda (BJH) methods [234] were used to interpret the data obtained.

Adsorption studies

Batch adsorption

Virgin xerogels, fully functionalised xerogels and partially functionalised xerogels (obtained with 0.5 TMCS:Na₂SiO₃ ratio with respect to the fully functionalised samples) with ratios H₂O:Na₂SiO₃ between 138 and 154, were synthesised and used for batch adsorption tests with aqueous solutions of benzene and 3,4-DCA. Samples were ground to obtain particles with dimensions between 0.5 and 1.4 mm, prior to addition to glass bottles containing either aqueous benzene or aqueous 3,4-DCA; all solutions were previously equilibrated for 3 h with magnetic stirring. Bottles were subsequently placed in a Gerhardt® rotary stirrer for the determination of adsorption isotherms, and associated kinetics, as well as verification of the mechanical resistance of the materials. Adsorption batch tests on the amorphous silica Quartzene have been detailed in a previous work [255].

Breakthrough curves

Samples were ground to obtain a particle size suitable for adsorption studies. Quartzene particles with average size of 140 µm and silica xerogel particles between 60 and 140 µm were used. A cylindrical column (length 80 mm, width 6 mm) was filled with adsorbent material and stoppered (pore size range 10 to 100 µm). UV-vis spectrophotometry was used for species detection, hence, the adsorption apparatus was positioned between a rotary valve and a UV-Vis detector, as presented in Figure 1.

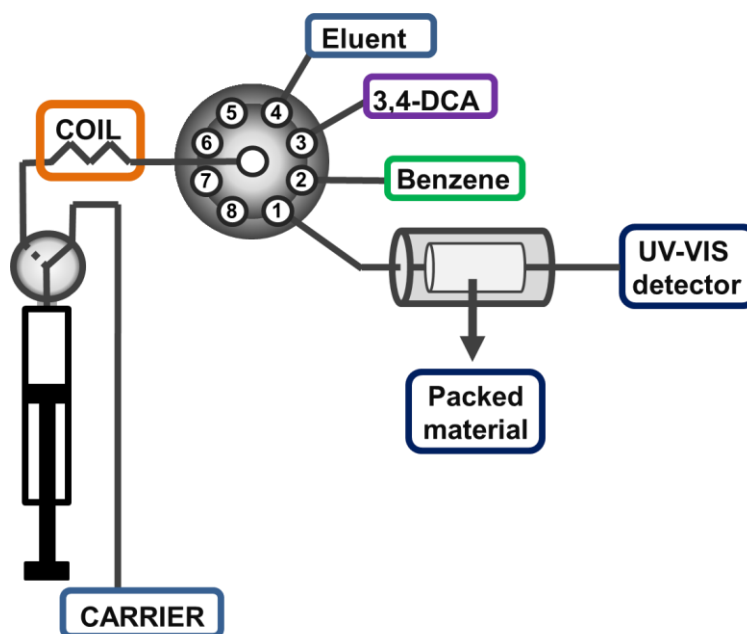


Figure 1: Sequential injection analysis manifolds connected to the adsorption column with a packed material and an on-line UV-Vis detector for adsorption tests on silica samples used in this study.

Compared to FIA, SIA employs a simpler, single-channel manifold for sample introduction, even with multi-component chemical systems; additionally, more accurate, robust syringe pumps are used in place of multi-channel peristaltic pumps. Through single-channel operation, the same manifold can be used to implement a wide range of assays and the rotary

valve enables automated calibration. Moreover, sample and reagent use are significantly reduced [230]. In this study, using the aforementioned valve and a bidirectional syringe pump, water samples containing the target analyte were inserted into a loading coil (between the syringe and the central port of the valve), and subsequently injected towards the column. At the same time the detector begins recording the signal, in order to determine whether the analyte was fully retained in the column. Breakthrough curves are thus obtained, in order to establish both the volume and capacity of saturation. Automated solid-phase extraction was here used to desorb the analytes from the exhausted adsorbents; whereby the procedure outlined above to obtain breakthrough curves was modified slightly, such that instead of loading a sample, methanol was loaded to promote desorption of the analyte once it was known to be fully retained within the column.

Results and discussion

3D printing of the column

Designing the model

Through the 3D modelling tool all the inside components of the column were individually created. Working from the top of the column to the bottom they comprise:

- a 7 mm diameter cylinder of 7 mm length;
- a 1 mm diameter cylinder of 1 mm length;
- a truncated cone with 1 mm diameter top (to fit the previous tube) and 12.5 mm diameter base, with 5.75 mm height (to obtain the required 45° angle);
- a 12.5 mm diameter cylinder of 40 mm length (the inner column);
- a reverse truncated cone with 12.5 mm diameter base, height of 1 mm (to obtain the 20° angle) and 7 mm diameter base;
- a 7 mm diameter cylinder of 7 mm length.

A Boolean union was used to combine the objects listed above into one solid piece; this command trims the shared areas of selected surfaces, creating a single polysurface from the unshared areas. The so-created inner part of the column (Figure 2b) was then fitted into a cylinder of 25 mm diameter and height equal to the sum of the heights of the previous parts (Figure 2a).

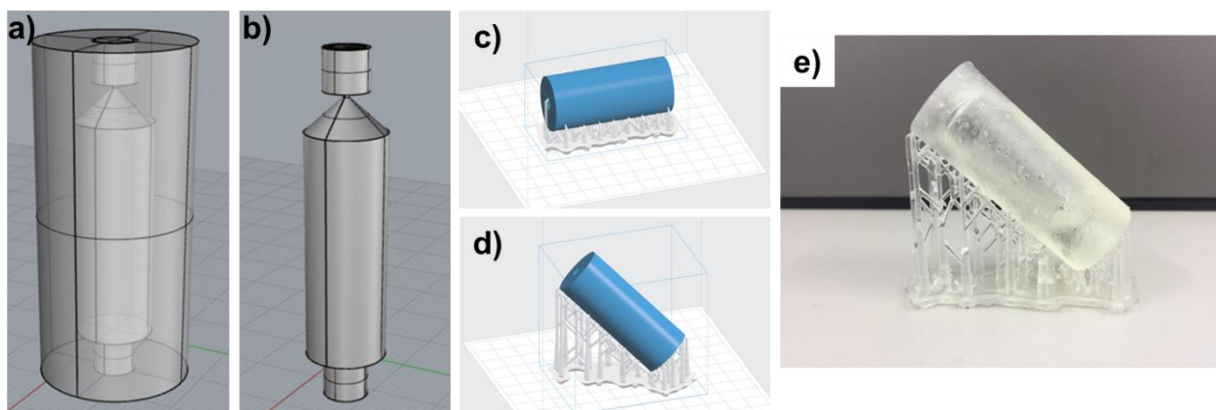


Figure 2: Inner column (b) and its fitting into the external cylinder(a). Models of the microcolumn and related supports (c,d), as shown by the software preform (FormLabs) and printed column on its supports, prior to smoothing (e).

Using a Boolean difference, which trims the shared areas of selected polysurfaces with another set of polysurfaces, the volume of the inside part of the model was extracted from the outside cylinder. Spirals were then designed in the inner part of the upper and lower cylinders of 7 mm diameter and 7 mm height, to permit fitting of the required connections. Once complete, the model was extracted as a .STL file which stands for Stereolithography file and sent to the 3D printer.

Printing the model

The STL file created as described in Chapter [above] was loaded in the software preForm, provided by FormLabs. The model was printed on clear methacrylate photopolymer resin by a Form1+ 3D printer from FormLabs (tech specs). After loading, two different orientations of the model, horizontal and inclined at 45°, were chosen, and related supports were added for correct printing. Figures 2c and 2d show the model in both orientations ready for printing.

The printing time for the model showed in Figure 2d was 4 h, requiring 31.41 ml of resin, while the model in Figure 2c required 1 h 38 min and 30.99 ml of resin due to the lower number of layers used in the print. The thickness of each layer was 0.1 mm. When each print was complete, the model was taken out of the printer, the supports were removed with a cutting tool, and the column was washed in isopropyl alcohol to eliminate any remaining liquid resin.

The penultimate processing step involved a CL-1000 ultraviolet crosslinker, used to cure the resin and remove the residual surface residue of methacrylate photopolymer and the associated 'tacky' sensation; finally a lathe was used to smooth the surface of the model.

Adsorbent characterisation

Quartzene

The structure of Quartzene and its properties are analogous to silica aerogels; all have porous skeletal silica structures, very low densities, and extremely low thermal conductivities. The major physical difference is that Quartzene is produced as a powder, not as a gel from a sol-gel process. FE-SEM analysis of ND and CMS samples are shown in Figure 3. Z1 samples show similar surface topography to ND samples.

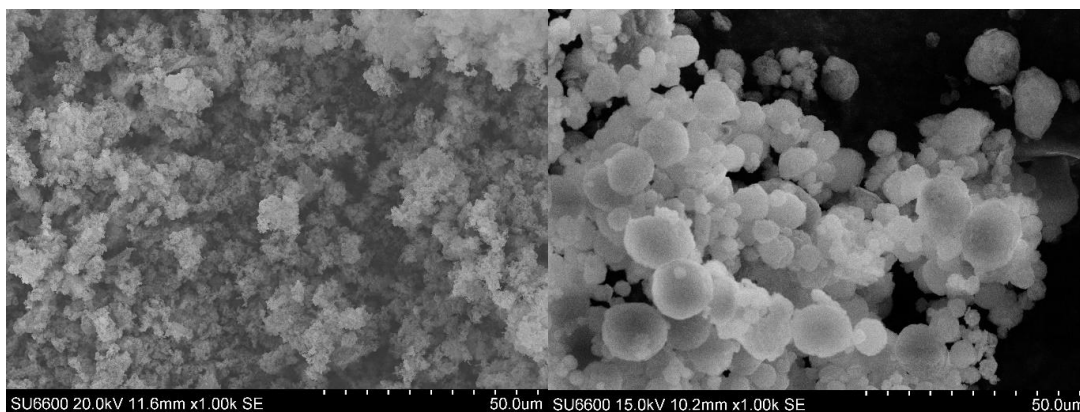


Figure 3: FE-SEM analysis of Quartzene ND (left) and CMS (right). Magnification: x1k.

Detailed surface area and pore size analysis of Quartzene have been reported previously [255]; by comparison ND samples exhibit a higher surface area ($546 \text{ m}^2/\text{g}$) and a narrower pore size distribution, with an average pore width of 3.3 nm. Samples CMS and Z1 have smaller surface areas, at $325 \text{ m}^2/\text{g}$ and $158 \text{ m}^2/\text{g}$, respectively, and larger average pore widths of 20.3 nm and 14.6 nm, respectively.

Silica xerogels

FE-SEM analysis of virgin (non-functionalised) and functionalised silica xerogels are shown in Figure 4.

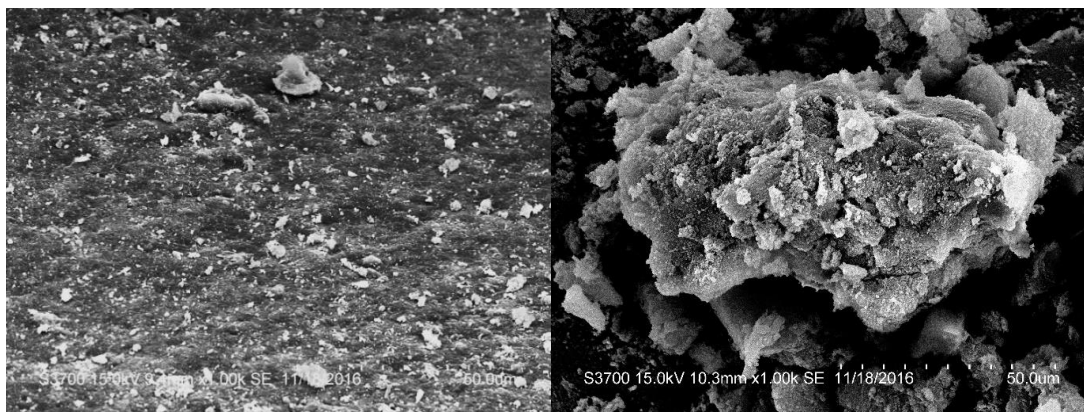


Figure 4: FE-SEM analysis of virgin xerogel (left) and functionalised xerogel (right) samples.

Magnification: x1k.

Nitrogen sorption isotherms and the associated pore size distribution of the functionalised xerogel sample, obtained using $\text{H}_2\text{O}:\text{Na}_2\text{SiO}_3$ ratio equal to 148, are presented in Figure 5. The cooling time used after the last drying procedure was found to significantly affecting the porosity of the materials obtained; indeed, a rate of 10 K/min was initially used, while a gradient of 1 K/min was later found to increase the total pore volume of the samples, and was used in subsequent syntheses.

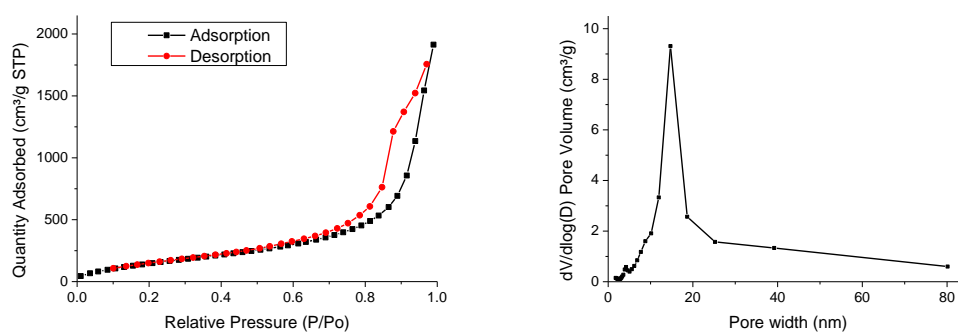


Figure 5: Adsorption isotherm (left) and pore size distribution (right) of functionalised xerogel sample.

Results for surface area and pore size analysis of functionalised xerogel samples obtained for $\text{H}_2\text{O}:\text{Na}_2\text{SiO}_3$ ratios between 80 and 154 are shown in Table 1; gels resulting from ratios ≥ 175 , were too weak to undergo washing, as they dissolved in water. It is also notable that the main pore size distribution is considerably narrower for the lowest ratio examined.

Table 1: Surface area and porosity of xerogels obtained through citric acid catalysis, with different H₂O / Na₂SiO₃ ratios, fully functionalised.

Sample	Ratio n H ₂ O/n Si ₂ O ₃	Surface Area m ² /g	Pore Volume cm ³ /g	Pore Size nm	Pore size distribution nm
CF80	80	449.53	1.22	10.77	6.4 - 18
CF108	108	473.47	2.16	17.98	8.1 - 65
CF138	138	654.04	3.27	16.80	7-70
CF154	154	669.40	3.24	15.65	6.5 - 70

Adsorption studies

Batch adsorption

Quartzene

Results from batch adsorption studies using Quartzene ND, CMS, Z1 and Z1H have been discussed recently [255]. The majority of adsorption (84–90%) was observed to take place in the first 6 h of organics contact for CMS and ND samples, while Z1, tested in granular form, showed slower adsorption kinetics. The Freundlich adsorption model [245] fitted the data well and maximum adsorption capacity for ND was estimated as close to the adsorptive solubility limits at 264 mg/g for benzene. Under batch conditions, higher adsorption capacity was determined for the hydrophobic version of Z1 compared with its hydrophilic analogue (Z1H), however, the difference between the samples was seen to decrease with decreasing organic concentration. It was also noted that only hydrophobic samples showed no significant mechanical degradation post testing. The observations for Z1 are supported by batch results for CMS, which similarly showed a better performance for the hydrophilic version (CMSH) over all concentrations studied.

Silica xerogels

Kinetic tests on functionalised xerogels showed that they required long equilibrium times; only 50% of adsorption capacity was measured within 5 h, while full equilibrium required 2 d, for both benzene and 3,4-DCA. Non-functionalised samples of xerogel, catalysed synthetically using citric acid, were unable to show sufficient mechanical resistance during the required tests, and were recovered as powder. Same problem was observed with samples catalysed with TMCS/sodium silicate ratios with respect to the full functionalised samples. It can, therefore, be concluded that sodium silicate xerogels synthesised under ambient pressure and at low temperature with low TMCS/Na₂SiO₃ ratio cannot be used for the uptake of organics in water in a filter configuration. Adsorption of benzene on functionalised xerogel samples

exhibits Langmuir-Freundlich behaviour [257] at concentrations >130 mg/L, while a Langmuir trend [245] can be used to describe the first adsorption points (Figure 6). A similar trend was recently observed for adsorption on mesoporous silica by Maretto *et al.* [1], who suggested a hybrid isotherm model, similar to that obtained by Lee *et al.* [2] for the adsorption of gaseous hydrocarbons on mesoporous silica MCM-48, in which the organic uptake at low concentrations is described by a Langmuir isotherm before shifting to Langmuir-Freundlich behaviour at concentrations >75 mg/L. As suggested for this gas adsorption system, the first step could be related to adsorption on the wall of the mesoporous channel until monolayer formation, in agreement with the Langmuir model, with subsequent adsorption and formation of successive layers in agreement with the Langmuir-Freundlich model, until filling of the entire mesoporous channel occurs. Here, the results fit two separate models within specific concentration ranges better than the hybrid model proposed by Maretto *et al.*, which was based on adsorption data <150 mg/L and it is likely to underestimate the adsorption capacity of the silica xerogels beyond that threshold.

Adsorption tests with functionalised xerogels in an aqueous solution of 3,4-DCA confirmed Langmuir-Freundlich behaviour for concentrations >40 mg/L (Figure 6).

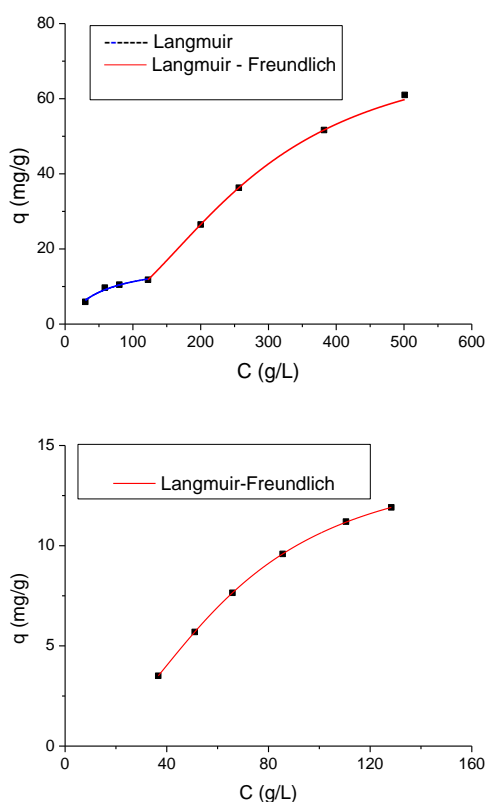


Figure 6: Adsorption isotherms for benzene (left) and 3,4-DCA (right) on xerogels with $\text{H}_2\text{O}:\text{Na}_2\text{SiO}_3$ ratio = 148.

The adsorption capacity of 3,4-DCA (12 mg/L) was found to be similar to benzene at concentrations of 130 mg/L but lower than benzene uptake at lower concentrations.

Considering the solubility of 3,4-DCA and benzene at 293 K: 0.58 g/L and 1.77 g/L, respectively; it can be concluded that the adsorption trend of 3,4-DCA is similar to that obtained for benzene at concentrations between 130-600 mg/L, shifted to a lower range of concentrations (40-125 mg/L) as 3,4-DCA has a lower solubility limit. Indeed, 90% of the estimated maximum uptake is achieved at 130 mg/L for 3,4-DCA and at 600 mg/L for benzene; thereby following the same adsorption trend from concentrations above ~8% of their solubility limits.

Table 2: Parameters of isotherms models.

	Langmuir			R²
	q_{max}(mg/g)	b (L/mg)		
Benzene (<130 mg/L)	19.41	0.0155		0.9823
	Langmuir-Freundlich			
	Q_m(mg/g)	k_s (L/mg)	n	R²
Benzene (>130 mg/L)	74.03	0.0038	2.1956	0.9997
3,4-DCA (≥ 40 mg/L)	14.43	0.0016	2.1462	0.9990

The intercept of the Langmuir-Freundlich plot of the data obtained for 3,4-DCA adsorption would be far from zero (Figure 6). Thus, further analyses could be useful to verify the presence of a two-step adsorption mechanism for the uptake of 3,4-DCA, as the one observed with benzene. Adsorption capacity of silica xerogels of 3,4-DCA was found greater than the uptake measured on the silicate minerals Halloysite [24] Kaolinite and montmorillonite [11] in previous studies; difference is likely more related to the greater pore volume of xerogels and to its main role in the physical adsorption mechanism.

Breakthrough curves

30 mm x 7 mm and 40 mm x 10 mm columns were used and preliminary tests were conducted to evaluate the flow rate applicable without incurring overpressure (with consequent partial return of the flow in the sample container). Overpressure problems were experienced with the smaller column. Furthermore, channelling was less likely in the larger column, so the data reported here refer to the 3D printed 40 mm x 10 mm column. The materials were slightly swollen after flowing with methanol, with the increased volume notably maintained after washing with water. The sample solution organic concentration was determined, both during and at the end of the test, to confirm the absence of losses. For the same reason, the sample was flowed through the system after disconnecting the column and again no significant losses were recorded. Hence, it can be assumed that the difference between the concentration of the organic in the solution before and after passing through the column it is due to adsorption on the packed material. Adsorption capacities were estimated by excluding the first 2 mL of sample flowed to wash the column from the water previously introduced and were limited to the uptake corresponding to the last point measured, so ~90% of the ratio C/C_0 , where C is the initial concentration of the organic in the solution flowed and C is the concentration of the organic in the solution leaving the column.

Amorphous silica

230 mg of NDH, provided with a particle size between 75 and 200 μm , were packed into the fabricated microcolumn, and a solution of 73.3 mg/g benzene in water was flowed through it at 1 mL/min. The flow rate selected equates to an EBCT_s of 1.47 min and EBCT_L of 19.5 min, for a particle size of 0.5 mm to be employed in the bench scale reactor. The removal efficiency at $0.9 \cdot C/C_0$ was found to be 5.85 mg/g, i.e. insufficient to support scale up of the reactor.

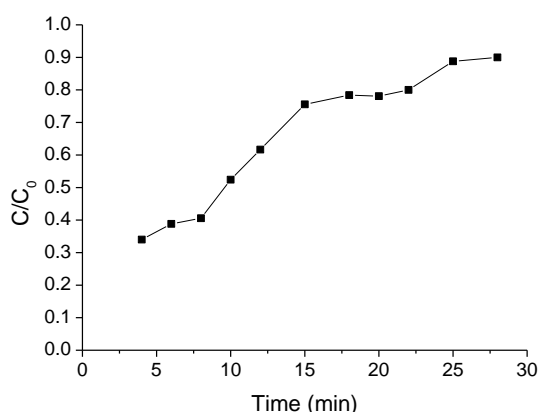


Figure 7: Breakthrough curve of benzene solution, 73.3 mg/L, flowed through microcolumn packed with 230 mg of NDH at 1 mL/min.

The analyte was successfully desorbed by the use of automated solid-phase extraction. Higher flow rates were not investigated, as even lower adsorption capacities would be expected, as contact time would be reduced. Higher removal efficiencies, coupled with no increase in EBCT_L would be required for the adsorbent tested to be used for treatment of produced water prior to a membrane configuration, especially in offshore facilities.

Table 3: Parameters related to microcolumn tests with sample NDH (average particle size R_{sc} assumed equal to 0.014 mm and assuming 0.050 mm as particle size of the large column).

Adsorbent	Pollutant	Concentration	R_{sc}	EBCT_{sc}	EBCT_{LC}	Flowrate	Uptake
		mg/L	Mm	Min	Min	mL/min	mg/g
NDH	Benzene	73.3	0.14	1.47	19.5	1	5.85

Silica xerogels

110 mg of silica xerogel, catalysed with citric acid and with $\text{H}_2\text{O}/\text{Na}_2\text{SiO}_3$ ratio = 148, were packed into a capillary microcolumn. The material was crushed and sieved to obtain particle sizes between 60 and 140 μm . A 105.12 mg/L benzene solution was flowed into the column at 0.6 mL/min; the related breakthrough curve is shown in Figure 8. The column was then packed

with the same amount of adsorbent and solutions of 20 mg/L and 16 mg/L of 3,4-DCA were flowed at rates of 0.6 mL/min and 1.8 mL/min, respectively. Both the analytes were then successfully desorbed by the use of automated solid-phase extraction.

The uptake of benzene at $0.9 \cdot C/C_0$ was 22.62 mg/g, and this significant removal efficiency is related to long EBCT_s, thus, long EBCT_L, during flow. Benzene adsorption was tested at selected concentrations, which were higher than those used for 3,4-DCA and in keeping with the range of interest for the offshore oil & gas sector probed in the present work. The sorbents studied here would not be competitive with hydrocyclones or flotators at concentrations of BTEX >100 mg/L, nor would they be competitive with nutshell or membrane for BTEX concentrations <20 mg/L.

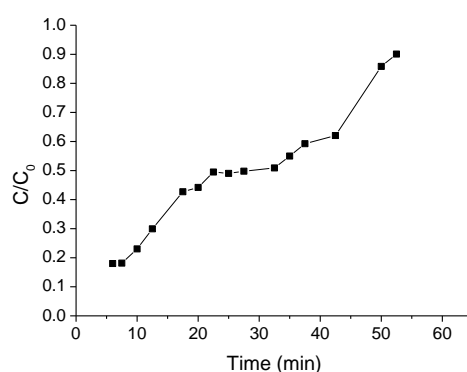


Figure 8: Breakthrough curve of benzene 105.12 mg/L at 0.6 mL/min, flowed through microcolumn packed with 110 mg of silica xerogels catalysed with citric acid and with H_2O/Na_2SiO_3 ratio = 148.

Greater flow rates, despite the corresponding reduction in adsorption capacity, could lead to a positive evaluation of the material for the use in a bench scale reactor; 1.8 mL/min was tested, but was judged unsuitable, as breakthrough curves started with values of 0.5 C/C_0 . Silica xerogels synthesized here could then find an application for the adsorption of benzene, but only in systems for which fast adsorption rate is not a priority.

The uptake of 3,4-DCA was found to be >4.63 mg/g and >7.17 mg/g at flowrates of 1.8 mL/min and 0.6 mL/min, respectively; the breakthrough curves of the two runs are shown in Figure []. The flowrate of 1.8 mL/min gives an EBCT_L of 20.5 min, considering 0.5 mm particles to be employed in the full scale reactor. The rate of adsorption, and the adsorption capacity of these silica xerogels, could be promising for a large scale application, as filling of filters, cartridges or permeable reactive barriers.

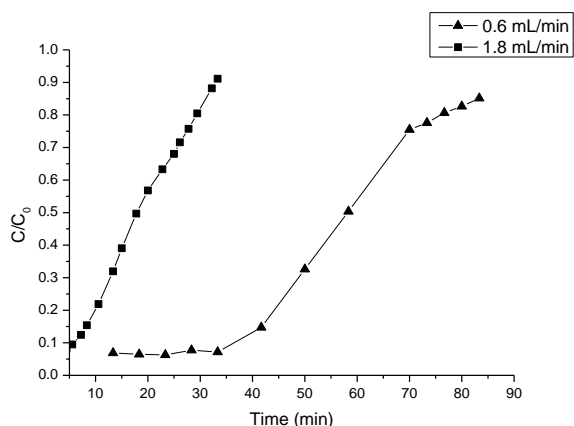


Figure 9: Breakthrough curves of 3,4-DCA adsorption on 110 mg of silica xerogels catalysed with citric acid and with H₂O/Na₂SiO₃ ratio = 148, 16 mg/L at 1.8 mL/min; 20 mg/L at 0.6 mL/min.

It is interesting to note that both the adsorption capacities obtained with column tests exceed those verified through batch test. This could be due to interparticle retention of the organic molecules and/or methanol conditioning prior to column packing.

Table 4: Parameters related to microcolumn tests using silica xerogels catalysed by citric acid (ratio H₂O/acid =148), with average particle size R_{sc} of 0.01 mm and assuming 0.050 mm as particle size of large column.

Adsorbent	Pollutant	Concentration mg/L	R _{sc} mm	EBCT _{sc} Min	EBCT _{LC} Min	Flowrate mL/min	Uptake mg/g
Silica xerogel	benzene	105.1	0.1	2.44	61	0.6	5.85
	3,4-DCA	20	0.1	2.44	61	0.6	7.17
	3,4-DCA	16	0.1	0.83	20.7	1.8	4.63

Conclusions

The MCRB test coupled with Sequential Injection Analysis and automated solid-phase extraction have employed to identify the best sorbents among those studied here, to assess their treatment effectiveness, to estimate the capacity utilisation rate and regeneration options.

The developed materials could find application in filtration vessels in oil and gas plants for removal of dissolved oils or as filling of cartridges for the same purpose, as stand-alone technology, or prior to a membrane configuration, extending the membrane lifetime. Functionalised silica could also be used for the removal of 3,4-DCA and other EDCs in drinking water treatment facilities, as well as sorbents for the in-situ remediation of pesticides-polluted groundwater as part of permeable reactive barriers.

Acknowledgements

The authors would like to thank Svenska Aerogel AB for providing the adsorbent material Quartzene.

References

1. Bevan, R., et al., *A review of latest endocrine disrupting chemicals research implications for drinking water*. 2012.
2. Kortenkamp, A., et al., *Low-Level Exposure to Multiple Chemicals: Reason for Human Health Concerns?* Environmental Health Perspectives, 2007. **115**(Suppl 1): p. 106-114.
3. Reynolds, J.G., P.R. Coronado, and L.W. Hrubesh, *Hydrophobic aerogels for oil-spill clean up – synthesis and characterization*. Journal of Non-Crystalline Solids, 2001. **292**(1–3): p. 127-137.
4. Reynolds, J.G., P.R. Coronado, and L.W. Hrubesh, *Hydrophobic aerogels for oil-spill cleanup - Intrinsic absorbing properties*. Energy Sources, 2001. **23**(9): p. 831-843.
5. Adebajo, M.O., et al., *Porous Materials for Oil Spill Cleanup: A Review of Synthesis and Absorbing Properties*. Journal of Porous Materials, 2003. **10**(3): p. 159-170.
6. Wang, D., et al., *Adsorption of oils from pure liquid and oil-water emulsion on hydrophobic silica aerogels*. Separation and Purification Technology, 2012. **99**: p. 28-35.
7. Olalekan, A.P., A.O. Dada, and O.A. Adesina, *Review: Silica Aerogel as a Viable Absorbent for Oil Spill Remediation*. Journal of Encapsulation and Adsorption Sciences, 2014. **4**: p. 122-131.
8. Simpson, E.J., et al., *Sorption Equilibrium Isotherms for Volatile Organics in Aqueous-Solution - Comparison of Headspace Gas-Chromatography and Online Uv Stirred Cell Results*. Industrial & Engineering Chemistry Research, 1993. **32**(10): p. 2269-2276.
9. Wang, D., et al., *Adsorption of Organic Compounds in Vapor, Liquid, and Aqueous Solution Phases on Hydrophobic Aerogels*. Industrial & Engineering Chemistry Research, 2011. **50**(21): p. 12177-12185.
10. Tasca, A.L., F. Ghajeri, and A.J. Fletcher, *Novel hydrophilic and hydrophobic amorphous silica: Characterization and adsorption of aqueous phase organic compounds*. Adsorption Science & Technology, 2017.
11. Chang, Q.G., et al., *Efficient micro carbon column rapid breakthrough technique for water and wastewater treatability studies*. Environmental Progress, 2007. **26**(3): p. 280-288.
12. *Standard Practice for the Prediction of Contaminant Adsorption On GAC In Aqueous Systems Using Rapid Small-Scale Column Tests*.
13. Economou, A., *Sequential-injection analysis (SIA): A useful tool for on-line sample-handling and pre-treatment*. TrAC Trends in Analytical Chemistry, 2005. **24**(5): p. 416-425.
14. Rodríguez, R., et al., *Strategies for automating solid-phase extraction and liquid-liquid extraction in radiochemical analysis*. TrAC Trends in Analytical Chemistry, 2016. **76**: p. 145-152.
15. Bangi, U.K.H., et al., *Physico-chemical properties of ambiently dried sodium silicate based aerogels catalyzed with various acids*. Journal of sol-gel science and technology, 2009. **50**: p. 87-97.

16. Twumasi Afriyie, E., et al., *Textural and thermal conductivity properties of a low density mesoporous silica material*. Energy and Buildings, 2014. **75**: p. 210-215.
17. Twumasi Afriyie, E., et al., *Preparation and Characterization of Double Metal-Silica Sorbent for Gas Filtration*. Adsorption, 2013. **19**(1): p. 49-61.
18. Brunauer, S., P.H. Emmett, and E. Teller, *Adsorption of Gases in Multimolecular Layers*. Journal of the American Chemical Society, 1938. **60**(2): p. 309-319.
19. Barrett, E.P., L.G. Joyner, and P.P. Halenda, *The determination of pore volume and area distributions in porous substances .1. Computations from nitrogen isotherms*. Journal of the American Chemical Society, 1951. **73**(1): p. 373-380.
20. Freundlich, H. and H. Hatfield, *Colloid and Capillary Chemistry*. 1926, London: Methuen.
21. Turiel, E., C. Perez-Conde, and A. Martin-Esteban, *Assessment of the cross-reactivity and binding sites characterisation of a propazine-imprinted polymer using the Langmuir-Freundlich isotherm*. Analyst, 2003. **128**(2): p. 137-141.
22. Szczepanik, B., et al., *Adsorption of chloroanilines from aqueous solutions on the modified halloysite*. Applied Clay Science, 2014. **101**: p. 260-264.
23. Angioi, S., et al., *Sorption studies of chloroanilines on kaolinite and montmorillonite*. Environmental Pollution, 2005. **134**(1): p. 35-43.

9.2 Pending patent of Quartzene

1

A filter apparatus and a method for removing dissolved organic compounds from a water based liquid

TECHNICAL FIELD

5

The present invention relates to a filter apparatus according to the preamble of claim 1 and to a method for removing dissolved organic compounds from a water based liquid. The invention also relates to use of an amorphous precipitated silica material and to

10 use of a filter apparatus.

By "produced water" is herein intended any water that comes out of an oil or gas reservoir as part of an oil or gas production process. Sources of produced water include connate water present in the reservoir prior to production, condensed water from

15 produced gas, and injected water derived from injection wells.

BACKGROUND AND PRIOR ART

20 Produced water is the largest by-product generated by oil and gas extraction, hence, there are significant quantities requiring remediation, of which the removal of dissolved organic compounds in low concentrations is the final step.

25 Produced water, at the refining stage, contains only low concentrations of dissolved oil droplets, mainly pollutants in the form of benzene, toluene, ethylbenzene and xylene (BTEX group). The concentrations of these pollutants are typically well below the solubility limits.

30

Multilayer filters comprising filtration media in the form of e.g. anthracite, sand, garnet, gravel and rock have commonly been used for removal of such pollutants from produced water. Also walnut shells are commonly used as a filtration media. However,

35 multilayer filters comprising sand are heavy and the abrasive sand particles reduces the lifetime of the filter components. The

5 fine sand particles may also cause an elevated pressure loss across the filter bed, thus reducing the efficiency of the filter. The expected lifetime of filtration media is relatively low, with replacement required frequently, depending on media type and feed water quality.

10 Another technique for treatment of produced water is adsorption using a variety of materials including zeolites, organoclays, activated alumina, and activated carbon. However, the adsorption material eventually becomes consumed with contaminants and must be disposed or regenerated using chemicals. Furthermore, activated carbon is associated with relatively slow kinetics and large volumes are needed, thus requiring space consuming vessels. Organoclays, on the other hand, are relatively
15 expensive.

20 Currently used techniques for removal of dissolved organic compounds in produced water also include use of a porous polymeric bed impregnated with an organic surfactant. However, this method is relatively costly and is therefore less suitable for large scale filtration of produced water.

SUMMARY OF THE INVENTION

25 It is an objective of the present invention to achieve an in at least some aspect improved technique for removal of dissolved organic compounds from water based liquids such as produced water.

30 This and other objectives are according to a first aspect of the present invention achieved by means of the initially defined filter apparatus, which is characterised in that the filter bed comprises at least one layer of an adsorbent comprising an amorphous precipitated silica material.

35 According to another aspect of the invention, the above defined objective is achieved by means of use of the proposed filter

apparatus for removing dissolved organic compounds from a water based liquid. The dissolved organic compounds may typically be present at a concentration of 200 ppm or less.

5 According to another aspect of the invention, the above defined objective is achieved by means of a method for removing dissolved organic compounds from a water based liquid, comprising passing the water based liquid through the proposed filter apparatus.

10

Amorphous precipitated silica material, which is a mesoporous, low density material having a relatively large surface area, has according to the present disclosure been found to be efficient for the removal of dissolved organic compounds from water based liquids at low concentrations, typical for produced water. The filter apparatus according to the invention is therefore suitable for the final step of cleaning of produced water. The adsorption of dissolved organic compounds on amorphous precipitated silica has been found to be a predominantly physical process, in which organic compounds are adsorbed on the surfaces of the adsorbent due to primary adsorption interactions with the surface and thereafter cooperative multilayer formation.

15

20

Low cost synthetic routes for producing amorphous precipitated silica using ambient pressure drying are already known to produce suitable amorphous precipitated silica materials from waterglass, having excellent mechanical properties. The amorphous precipitated silica material can be produced in a cost efficient manner by mixing alkali silicate with a salt solution, e.g. such as previously described in WO2006/071183.

25

30

The low density of the adsorbent makes the filter apparatus light-weight.

35 According to one embodiment, the amorphous precipitated silica material has a porosity with an average pore width within the

range of 1–50 nm. Thereby, the organic compounds which are to be adsorbed can gain good access to the pores of the adsorbent, while as molecular repulsion that can be observed with large adsorbate clusters can be avoided. In particular, an average pore width within the range of 1–10 nm may be advantageous.

According to one embodiment, the amorphous precipitated silica material has been prepared via the precipitation of sodium silicate with sodium chloride by mixing an aqueous sodium silicate solution with aqueous sodium chloride. Such an adsorbent has proved to exhibit desirable adsorption properties.

According to one embodiment, the amorphous precipitated silica material has a BET surface area of at least 100 m²/g. The surface area is thereby sufficiently large to achieve efficient adsorption of organic compounds. Preferably, the amorphous precipitated silica material has a BET surface area of at least 300 m²/g, providing optimum conditions for adsorption. Even more preferably, the BET surface area is at least 500 m²/g. The BET surface area may be up to 700 m²/g or larger, depending on the conditions of preparation.

According to one embodiment, the amorphous precipitated silica material has a total pore volume within the range of 0.50–1.2 cm³/g. The relatively large total pore volume results in enhanced adsorption.

According to one embodiment, the amorphous precipitated silica material has a density within the range of 0.06–0.1 g/cm³. The relatively low density makes it possible to provide a light weight filter which can e.g. be transported in an energy efficient manner.

According to one embodiment, the amorphous precipitated silica material has a hydrophilic surface. This generally removes the need for functionalising agents and enables use of cheaper precursors, thereby reducing the cost of synthesis of the

adsorbent. The production and waste management of these materials thereby becomes economically suitable for a single adsorption cycle, hence, removing filter regeneration costs and associated issues. This embodiment is particularly suitable for filtering of water based liquid containing organic compounds at very low concentrations, such as at concentrations up to 200 ppm.

According to one embodiment, the adsorbent has been functionalised using at least one type of functional group to obtain a hydrophobic surface. The functionalization, in which for example methyl groups are used to achieve hydrophobicity, improves the affinity to organic adsorbates and can thereby increase adsorption. It also helps to prevent long-term deterioration of the structure due to the absorption of water. Regeneration of the adsorbent thereby becomes possible, enabling reuse of the adsorbent.

According to one embodiment, the adsorbent is in the form of granules having an average particle size within the range of 0.5–2 mm. By using granules within this size range, regeneration of the adsorbent is facilitated in comparison with smaller powder particles. The flow resistance of the filter bed may be adapted by adjusting the size of the granules, and the size may therefore be selected on the basis of the desired flow resistance. Flow resistance is generally inversely proportional to particle size. Too large granules will thereby offer too little flow resistance and the adsorption will be less efficient.

According to one embodiment, the filter apparatus comprises at least two filter units connected in series, so that the water based liquid can be passed through the filter bed of each filter unit successively. The filter apparatus may comprise several filter units connected in series and/or in parallel, depending on the needs. This allows a more efficient large scale filtration.

According to one embodiment, the filter apparatus further comprises bypass means for selectively bypassing at least one of said filter units. Thus, it is possible to bypass one or more of the filter units while it is being regenerated. Bypass conduits as well
5 as pumps and valves may of course be provided in order to achieve an efficient flow of liquid and bypass of filter units that are to be regenerated.

The invention also relates to use of an amorphous precipitated silica material as an adsorbent for removing dissolved organic
10 compounds from a water based liquid. Preferred embodiments of such an amorphous precipitated silica material appear from the above description of the adsorbent.

15 Further advantages as well as advantageous features of the present invention will appear from the following detailed description.

20 BRIEF DESCRIPTION OF THE DRAWINGS

Embodiments of the invention will in the following be described with reference to the appended drawings, in which:

- 25 Fig. 1 schematically shows a cross sectional view of a filter apparatus according to a first embodiment,
Fig. 2a shows absorbance spectra of three different adsorbents,
Fig. 2b shows absorbance spectra of a hydrophilic and a
30 hydrophobic adsorbent,
Fig. 3a shows kinetic profiles of benzene adsorption on the adsorbents of fig. 2a,
Fig. 3b shows kinetic profiles of toluene adsorption on the adsorbents of fig. 2a,
35 Fig. 4a shows adsorption isotherms for benzene on the adsorbents of fig. 2a,

- Fig. 4b shows adsorption isotherms for toluene on the adsorbents of fig. 2a,
Fig. 5a shows kinetic profiles of benzene adsorption on the adsorbents of fig. 2b,
5 Fig. 5b shows adsorption isotherms for benzene on the adsorbents of fig. 2b, and
Fig. 6 schematically shows a filter apparatus according to a second embodiment.

10

DETAILED DESCRIPTION OF EMBODIMENTS OF THE INVENTION

15 A filter apparatus 1 according to a first embodiment of the invention is schematically shown in fig. 1. The filter apparatus comprises a filter unit 2 in the form of a container 3, in which an inlet 4 and an outlet 5 is provided for passage of water based liquid such as produced water. A filter bed 6 comprising an adsorbent is arranged in the container 3, between the inlet 4 and
20 the outlet 5 so that the liquid may pass through the filter bed. The filter apparatus may of course comprise several filter units 2 arranged in series and/or in parallel, with conduits for passage of liquid, valves and one or more pumps being provided between the filter units. Bypass arrangements may be provided such that one
25 or some of the filter units can be bypassed during regeneration of the bypassed filter unit/units.

30 During use, water based liquid containing dissolved organic compounds is introduced into the filter unit 2 via the inlet 4, is passed through the filter bed 6 and is discharged via the outlet 5. Organic compounds within the water based liquid are thereby adsorbed by the adsorbent of the filter bed 6.

35 A filter apparatus 11 according to a second embodiment is schematically shown in fig. 6. The filter apparatus 11 comprises a first filter unit 12 in the form of a container 13 having an inlet

- 14 connected to a supply pipe 15. The first filter unit 12 has two outlets 16, 17, of which a first one 16 is connected to a collecting pipe 18 and a second one 17 is connected to a transfer pipe 19 leading to a second filter unit 20 in the form of a container 21.
- 5 The second filter unit 20 has a first inlet 22 connected to the supply pipe 15 and a second inlet 23 connected to the transfer pipe 19. The second filter unit 20 has an outlet 24 connected to the collecting pipe 18. In both filter units, a filter bed 25 comprising a layer of an adsorbent is provided. A split valve 26 is provided in the supply pipe 15, by means of which a flow of liquid
- 10 can be controlled to the first filter unit 12 or to the second filter unit 20. A valve 27 is also provided in the first outlet 16 of the first filter unit 12, by means of which the first outlet 16 can be opened or closed. Another valve 28 is provided in the second outlet 17 of
- 15 the first filter unit 12, for closing and opening of the second outlet 17. A pump (not shown) is provided in the transfer pipe 19 for pumping liquid from the first filter unit 12 to the second filter unit 20.
- 20 When the filter apparatus 11 is in use, the split valve 26 is first open so that liquid is passed via the supply pipe 15, the open split valve 26 and the inlet 14 to the first filter unit 12, in which it is passed through the filter bed 25. The valve 27 is initially closed while the valve 28 is open, so the liquid, after passing through the
- 25 filter bed 25, is pumped via the transfer pipe 19 to the second filter unit 20, where it passes through the filter bed 25 and into the collecting pipe 18 via the outlet 24. When a need to regenerate the first filter unit 12 arises, i.e. when the adsorbent in the filter bed 25 has reached its full adsorption capacity, the
- 30 split valve 26 is closed so that liquid is passed directly to the second filter unit 20 via the first inlet 22. Liquid then passes through the filter bed 25 and into the collecting pipe 18 via the outlet 24. Once the first filter unit 12 is regenerated, the split valve 26 is opened again and liquid flows once again into the first filter
- 35 unit 12. For regeneration of the second filter unit 20, the valve 17 is closed so that the second outlet 17 is blocked, and the valve

27 is opened. Liquid thereby flows via the first outlet 16 to the collecting pipe 18.

5 Of course, it is also possible to provide a second transfer pipe from the second filter unit to the first filter unit, so that liquid may be passed either via the first filter unit to the second filter unit, or via the second filter unit to the first filter unit. In this way, the filtering process can always be started in the currently more exhausted filter unit.

10 In both embodiments shown, the filter bed 6, 25 comprises a layer of adsorbent in the form of an amorphous precipitated silica material. The adsorbent can be prepared by preparing two solutions, solution A and solution B. Solution A is a dilute aqueous
15 alkali silicate solution, comprising silica (SiO_2) and an alkali metal oxide, e.g. sodium oxide (Na_2O) or potassium oxide (K_2O). Solution B is a concentrated or even saturated salt solution, such as a sodium chloride (NaCl) solution. Solution B may also
20 comprise metal salts, such as magnesium or calcium salts. Also salts based on other metals may be used. An activation level of the silica source can be selected such as to obtain desired properties in terms of surface area, pore size distribution, density, total pore volume, etc.

25 Solutions A and B are mixed under rapid stirring and coagulates immediately. The resulting precipitate is rinsed, before dewatering using e.g. vacuum filtration or centrifugal filtration until a paste is obtained. The paste is dried via spray drying or via other techniques, such as in a rotary drier, or using pressure
30 gradients such as described in WO2015/104317.

WO2006/071183 discloses a method for preparing an amorphous precipitated silica material which has, within the frame of the present disclosure, been found to be useful as an adsorbent for
35 removing dissolved organic compounds from a water based liquid, such as produced water. The material is formed as a precipitate

by mixing alkali silicate with a salt solution. The precipitate is thereafter processed in various ways to obtain an end product having desired properties in terms of pore size, particle size, surface area, density, etc.

5

The filter bed may also comprise several layers, e.g. of different types of amorphous precipitated silica materials, different particle sizes, different functionalization, etc.

10

EXAMPLES

Four different types of amorphous precipitated silica materials were prepared, namely ND, Z1, Z1HPO and CMS types. The silica materials are sold under the trade name Quartzene®.

15

ND type silica was prepared via the precipitation of sodium silicate with sodium chloride at ambient temperature. A defined amount of dilute active aqueous sodium silicate solution ($\text{SiO}_2:\text{Na}_2\text{O} = 3.35$) was prepared, representing solution A, while solution B was composed of aqueous sodium chloride (NaCl). Solutions A and B were mixed under rapid stirring and the resulting precipitate was mixed with a defined amount of tap water, before vacuum filtration through a filter paper until a paste, comprising up to 85% water, was obtained and dried via spray drying.

20

25

Z1 type silica samples were prepared using a method analogous to that for ND, but with a different level of activation of the silica source.

30

A methylated version of Z1, herein called Z1HPO, was also prepared, i.e. a Z1 type silica functionalised using methyl groups to obtain a hydrophobic surface.

35

CMS type silica was prepared by adding calcium and magnesium sources at concentrations of 1:2 to the silica source (waterglass $\text{SiO}_2:\text{Na}_2\text{O} = 3.35$). A 500 ml salt solution, consisting of MgCl_2 hexahydrate and CaCl_2 dihydrate was prepared at a ratio of 68 mol% Mg and 32 mol% Ca; 500 ml salt solution, was poured onto 1.5 M (with respect to SiO_2) sodium silicate solution (500 ml), and the resulting mixture agitated at room temperature. Subsequent coagulation occurred, and the obtained gel was washed, filtered and dried in the same manner as ND.

10

The ND and CMS type samples were powders, with particle sizes within the range of 2–150 μm . The D_{v90} of the ND and CMS type silica materials, i.e. the 90th percentile of the particle size distribution by volume, was determined to be 46 and 75 μm , respectively. The Z1 and Z1HPO samples were in the form of granules with particle sizes between 1 and 1.5 mm.

15

Surface chemical functionalities of adsorbent materials are known to determine the hydrophilic or hydrophobic nature of a material. FT-IR analysis was used to determine surface functionalities of the samples (dried at 248 K for 2 h) prepared as hydrophilic. The obtained spectra shown in fig. 2a show the presence of silanol polar groups (Si-OH), in the range of 2700–3650 cm^{-1} , for all materials studied, with Z1 and ND showing similar surface chemistries, while CMS exhibits more refined Si-OH bond peaks; consequently, the ND, CMS and Z1 type materials can be categorised as hydrophilic in nature. Fig. 2b shows a comparison between the hydrophilic Z1 and the hydrophobic Z1HPO materials.

20

25

30

Nitrogen sorption measurements were performed at 77 K using a Micromeritics ASAP 2420, on samples accurately weighed between 0.15 and 0.5 g and degassed at 393 K. 40 adsorption points and 30 desorption points were collected per isotherm, spanning the relative pressure range 0 - 0.99. Degassing at low temperatures requires longer treatment times but has the benefit

35

that the structure of the material is preserved. Brunauer–Emmett–Teller (BET) analysis was used to interpret the data obtained.

5 Surface areas and pore volumes were also estimated using α -plot analysis of a nitrogen adsorption isotherm obtained at 77 K. Such α -plot analysis is for small pore sizes generally considered more reliable.

10 The surface areas obtained for the four samples show good agreement between the two methods (BET and α -plot), except in the case of ND, which exhibits small mesopores (Table I), thereby suggesting that the value obtained using the α -plot method would be more accurate. Pore sizes determined for CMS, Z1 and Z1HPO samples are widely distributed between 2 and 80 nm, while ND
15 exhibits a discrete pore size distribution centred on 3.3 nm (Table I). Consequently, ND is the only material with a small mesopore contribution but it is notable that all samples exhibit significant total pore volume.

Sample name	S_{BET} [m ² /g]	S_{α} [m ² /g]	Average pore width [nm]	Total pore volume [cm ³ /g]	Small mesopore volume [cm ³ /g]	Meso- and macro-pore volume [cm ³ /g]
Z1	325	331	20.3	1.03	-	1.03
Z1HPO	186	186	17.4	0.97	-	0.97
CMS	158	161	14.6	0.50	-	0.50
ND	597	546	3.3	0.54	0.40	0.14

20 *Table I*

Benzene and toluene were used as representative components of dissolved oils in produced water. The organics were purchased from Sigma Aldrich as chromatography grade reagents (HPLC, \geq 99.9%). Benzene is more representative of dissolved oil, as it is
25 the most difficult organic compound from the BTEX group to adsorb from solution, due to the fact that the adsorption potential of the solute in the liquid carrier decreases with increasing

solubility of the adsorbate. Since the solubility of the monoaromatics in the BTEX group decreases with molecular weight, their adsorption potential increases with the molecular weight, hence, the lowest molecular weight species (benzene) is the most difficult to adsorb.

Borosilicate glass bottles were used for all adsorption studies, and bottle volumes were selected in order to reduce headspace within the vessel. Mixtures of water and benzene were stirred in filled bottles for 1 h using a magnetic stirrer to solubilize the organic, before samples were extracted with a micropipette, then mixed with methanol and internal standard before injection, using a microsyringe, into the port of a gas chromatograph equipped with FID detectors to determine the concentration present. Pre-determined amounts of adsorbent were added to prepared bottles of aqueous phase organics to study adsorption characteristics; kinetic tests were conducted at pre-determined intervals, over 24 h, to determine times for maximum equilibria to be achieved for each sample. All measurements were conducted at 293 K.

Adsorption tests involved the addition of benzene, at concentrations in the range 0–1100 ppm, to 110 ml of distilled water mixed with 100–500 mg of adsorbent, equilibrated for 24 h before analysis. An analogous procedure was used for toluene but using aqueous concentrations in the range of 0–400 ppm. However, the adsorption behaviour of hydrophobic Z1HPO was only tested using aqueous benzene, agitated using a rotary shaker to guarantee sorbent contact with the aqueous phase since the Z1HPO material floats in water.

All procedures were performed at 293 K using sealed cups with minimal headspace, as outlined above, to reduce volatilisation losses. Blank tests, conducted without sorbent, demonstrated that volatilisation rates were negligible for both kinetic and adsorption measurements. The stirring rates used were constant, 200 rpm for magnetic stirring and 20 rpm for rotary stirring.

Sampling was performed at various depths within a selected test vessel to verify the absence of concentration gradients within the bulk.

- 5 Gas chromatography was used to measure the concentrations of organic species in the aqueous systems studied.

Kinetic profiles of benzene and toluene adsorption on Z1, ND and CMS samples are shown in figs. 3a and 3b, respectively, showing
10 equilibrium uptake q (mg adsorbate per g adsorbent) as a function of time. 84–90% of adsorption takes place on CMS and ND samples within the first six hours, with a full equilibrium time of less than 24 hours. For Z1, less than 80% of toluene and less than 70% of benzene is adsorbed after 24 hours.

15 The Freundlich adsorption model was used to determine adsorption capacities of the samples. According to this model,

$$q = k \cdot C_e^{1/n},$$

20 wherein C_e is the equilibrium concentration of the solute (mg/l), k is the unitless constant of adsorption, indicating capacity, and $1/n$ is a unitless constant related to the intensity of adsorption.

- 25 Adsorption isotherms for benzene and toluene adsorption on Z1, ND and CMS samples are shown in figs. 4a and 4b, respectively.

Table 2 shows maximum uptakes of the samples Z1, ND and CMS type as calculated using data obtained for adsorption of benzene and toluene, determined from extrapolative interpolation to a
30 benzene solubility of 1.763 g/l or a toluene solubility of 0.57 g/l. The maximum uptake is shown in terms of mg adsorbate per gram adsorbent.

Sample	Adsorbate	Max. uptake [mg/g]
Z1	Benzene	53.25
	Toluene	46.91
CMS	Benzene	110.48
	Toluene	51.36
ND	Benzene	264.03
	Toluene	78.82

Table II

5 It can be seen from Table II that the ND and CMS samples perform better than the Z1 from the three sorbents studied in the range of concentrations used, with maximum adsorption capacities for ND estimated as close to the adsorbate solubility limits. The higher adsorption of ND is ascribed not only to the comparatively high surface area of this material, but also to its
10 discrete pore size distribution centred around 3.3 nm, which provides good access for the organic molecules of interest while also being sufficiently narrow to prevent the molecular repulsion that can be observed with large adsorbate clusters. Z1, which was the only original material used in granular form, however
15 underwent mechanical degradation during stirred reaction experiments.

Aqueous benzene concentrations below 0.25 ppm were explored in the comparison of adsorption characteristics of the hydrophilic
20 Z1 and the hydrophobic Z1HPO. Adsorption was faster and a higher quantity of benzene was adsorbed for Z1HPO as shown in figs. 5a and 5b, showing kinetic profiles and isotherms, respectively. Furthermore, Z1HPO showed no significant mechanical degradation even after five days of rotary stirring at
25 20 rpm. Equilibrium was reached in less than three hours for Z1HBO.

The comparison of adsorption behaviour for hydrophilic Z1 and hydrophobic Z1HBO indicates that hydrophobicity is

- advantageous if multiple cycle use of the adsorbent is desired. At concentrations of approximately 200 ppm, benzene adsorption on Z1HBO is four times higher than for Z1, but the difference in terms of uptake between the two adsorbents is reduced with decreasing organic concentration. Hence, at very low aqueous concentrations of organics, functionalization to achieve hydrophobicity may have negligible effect on the organic compound's access to the internal porosity of the material.
- 5
- 10 The invention is of course not in any way restricted to the embodiments described above. On the contrary, many possibilities to modifications thereof will be apparent to a person with ordinary skill in the art without departing from the basic idea of the invention such as defined in the appended claims.

15

CLAIMS

1. A filter apparatus (1, 11) for removing dissolved organic compounds from a water based liquid, the filter apparatus (1, 11) comprising at least one filter unit (2, 12, 20) in the form of a container (3, 13, 21) in which at least one inlet (4, 14, 22, 23) and at least one outlet (5, 16, 17, 24) are provided, a filter bed (6, 25) being arranged in the at least one container (3, 13, 21) between the at least one inlet (4, 14, 22, 23) and the at least one outlet (5, 16, 17, 24), so that water based liquid can pass into the container (3, 13, 21) via the at least one inlet (4, 14, 22, 23), through the filter bed (6, 25), and out via the at least one outlet (5, 16, 17, 24),
- characterised in*
- that the filter bed (6, 25) comprises at least one layer of an adsorbent comprising an amorphous precipitated silica material.
2. The filter apparatus according to claim 1, wherein the amorphous precipitated silica material has a porosity with an average pore width within the range of 1–50 nm.
3. The filter apparatus according to claim 1, wherein the amorphous precipitated silica material has a porosity with an average pore width within the range of 1–10 nm.
4. The filter apparatus according to any one of the preceding claims, wherein the amorphous precipitated silica material has been prepared via the precipitation of sodium silicate with sodium chloride by mixing an aqueous sodium silicate solution with aqueous sodium chloride.
5. The filter apparatus according to any one of the preceding claims, wherein the amorphous precipitated silica material has a BET surface area of at least 100 m²/g, preferably at least of 300 m²/g.

6. The filter apparatus according to any one of the preceding claims, wherein the amorphous precipitated silica material has a total pore volume within the range of 0.50–1.2 cm³/g.
- 5 7. The filter apparatus according to any one of the preceding claims, wherein the amorphous precipitated silica material has a density within the range of 0.06–0.1 g/cm³.
8. The filter apparatus according to any one of the preceding claims, wherein the amorphous precipitated silica material has a hydrophilic surface.
- 10 9. The filter apparatus according to any one of claims 1–7, wherein the adsorbent has been functionalised using at least one type of functional group to obtain a hydrophobic surface.
- 15 10. The filter apparatus according to any one of the preceding claims, wherein the adsorbent is in the form of granules having an average particle size within the range of 0.5–2 mm.
- 20 11. The filter apparatus according to any one of the preceding claims, comprising at least two filter units (12, 20) connected in series, so that the water based liquid can be passed through the filter bed (25) of each filter unit (12, 20) successively.
- 25 12. The filter apparatus according to claim 11, further comprising bypass means for selectively bypassing at least one of said filter units (12, 20).
- 30 13. Use of an amorphous precipitated silica material as an adsorbent for removing dissolved organic compounds from a water based liquid.
- 35 14. Use of a filter apparatus according to any one of claims 1–12 for removing dissolved organic compounds from a water based liquid.

15. A method for removing dissolved organic compounds from a water based liquid, comprising passing the water based liquid through a filter apparatus (1) according to any one of claims 1–12.

ABSTRACT

5 A filter apparatus (11) for removing dissolved organic compounds
from a water based liquid, comprising at least one filter unit (12,
20) in the form of a container (13, 21) in which an inlet (14, 22,
23) and an outlet (16, 17, 24) is provided, a filter bed (25) being
arranged in the at least one container between the inlet and the
outlet, the filter bed comprising at least one layer of an adsorbent
10 comprising an amorphous precipitated silica material.
(Fig. 6)

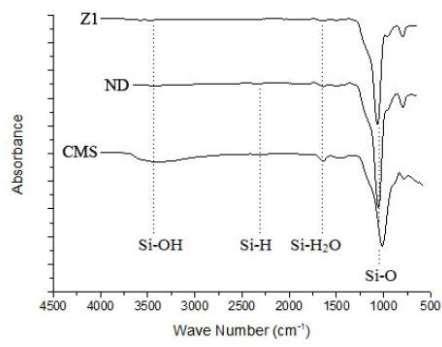
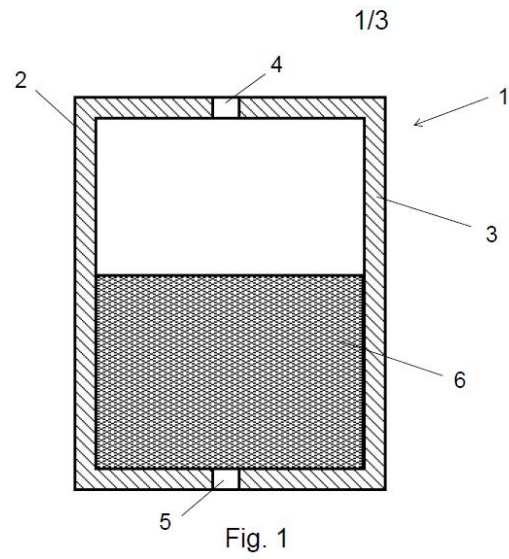


Fig. 2a

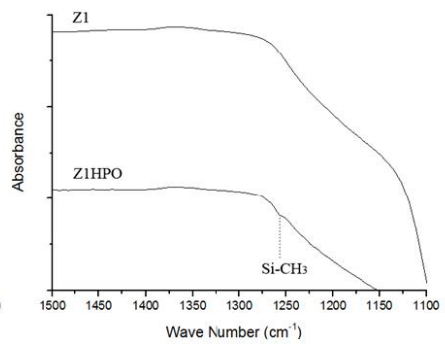


Fig. 2b

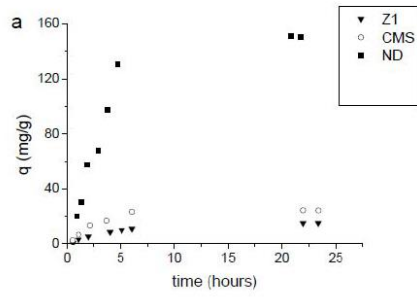


Fig. 3a

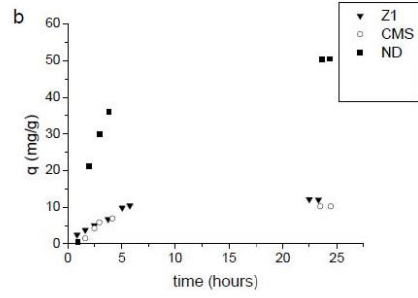


Fig. 3b

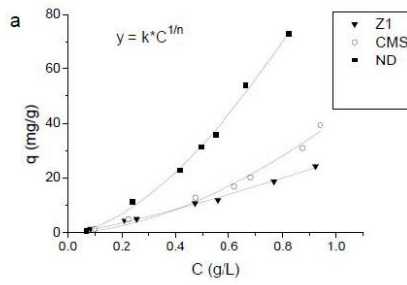


Fig. 5a

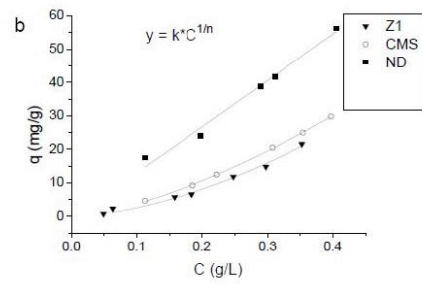
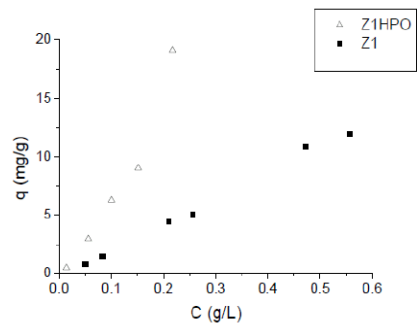
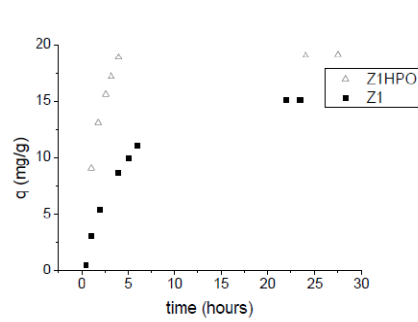


Fig. 5b



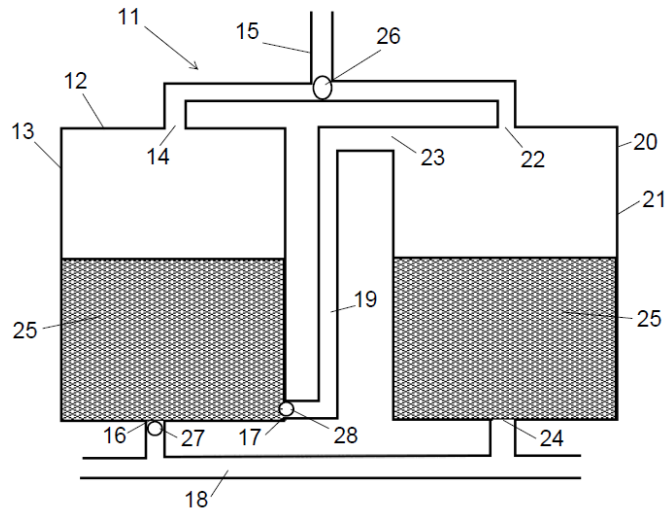


Fig. 6

10 References

1. Bangi, U.K.H., et al., *Physico-chemical properties of ambiently dried sodium silicate based aerogels catalyzed with various acids*. Journal of sol-gel science and technology, 2009. **50**: p. 87-97.
2. Perego, C., et al., *Zeolites and related mesoporous materials for multi-talented environmental solutions*. Microporous and Mesoporous Materials, 2013. **166**(0): p. 37-49.
3. DESA, U., *World Population Prospects, The 2000 Revision: Highlights*. 2001: New York.
4. Falkenmark, M. and C. Widstrand, *Population and water-resources - a delicate balance*. Population Bulletin, 1992. **47**(3): p. 2-36.
5. FAO. *Total renewable resources per inhabitant in 2014 (m³/year)*. 2015; Available from: http://www.fao.org/nr/water/aquastat/maps/TRWR.Cap_eng.pdf.
6. UNESCO, *The United Nations World Water Development Report 2016* 2016.
7. FAO, *Proportion of renewable water resources withdrawn: MDG Water Indicator*. 2015.
8. United Nations Educational, S.a.C.O.U., *The United Nations World Water Development Report 4: Managing Water under Uncertainty and Risk*. 2009: Paris.
9. Richey, A.S., et al., *Quantifying renewable groundwater stress with GRACE*. Water Resources Research, 2015. **51**(7): p. 5217-5238.
10. IFPRI, V.a., *The Murky Future of Global Water Quality. A White Paper by Veolia & IFPR*. 2015.
11. Angioi, S., et al., *Sorption studies of chloroanilines on kaolinite and montmorillonite*. Environmental Pollution, 2005. **134**(1): p. 35-43.
12. Bevan, R., et al., *A review of latest endocrine disrupting chemicals research implications for drinking water*. 2012.
13. Commission, E. *Priority list*. 2002; Available from: http://ec.europa.eu/environment/chemicals/endocrine/strategy/substances_en.htm#priority_list.
14. Funtikova, N.S. and E.G. Surovtseva, *Adsorption of herbicides derivatives of phenyl urea and chloro substituted anilines by microorganisms* Mikrobiologiya, 1979. **48**(6): p. 1086-1092.
15. Vastermark, A., et al., *Polymorphic variation in the androgen receptor gene: Association with risk of testicular germ cell cancer and metastatic disease*. European Journal of Cancer, 2011. **47**(3): p. 413-419.
16. Swedenborg, E., et al., *Endocrine disruptive chemicals: mechanisms of action and involvement in metabolic disorders*. Journal of Molecular Endocrinology, 2009. **43**(1-2): p. 1-10.
17. Rüegg, J., et al., *Receptors mediating toxicity and their involvement in endocrine disruption*, in *Molecular, Clinical and Environmental Toxicology: Volume 1: Molecular Toxicology*, A. Luch, Editor. 2009, Birkhäuser Basel: Basel. p. 289-323.

18. Newbold, R.R., *Impact of environmental endocrine disrupting chemicals on the development of obesity*. Hormones-International Journal of Endocrinology and Metabolism, 2010. **9**(3): p. 206-217.
19. Diamanti-Kandarakis, E., et al., *Endocrine-Disrupting Chemicals: An Endocrine Society Scientific Statement*. Endocrine Reviews, 2009. **30**(4): p. 293-342.
20. Koppe, J.G., et al., *Exposure to multiple environmental agents and their effect*. Acta Paediatrica, 2006. **95**: p. 106-113.
21. Brian, J.V., et al., *Evidence of estrogenic mixture effects on the reproductive performance of fish*. Environmental Science & Technology, 2007. **41**(1): p. 337-344.
22. Kortenkamp, A., et al., *Low-Level Exposure to Multiple Chemicals: Reason for Human Health Concerns?* Environmental Health Perspectives, 2007. **115**(Suppl 1): p. 106-114.
23. Groshart and Okkerman, *Towards the establishment of a priority list of substances for further evaluation of their role in endocrine disruption*. 2000, European Commission.
24. Szczepanik, B., et al., *Adsorption of chloroanilines from aqueous solutions on the modified halloysite*. Applied Clay Science, 2014. **101**: p. 260-264.
25. Kijima, K., H. Kataoka, and M. Makita, *Determination of aromatic amines as their N-dimethylthiophosphoryl derivatives by gas chromatography with flame photometric detection*. Journal of Chromatography A, 1996. **738**(1): p. 83-90.
26. Ucan, M. and A. Ayar, *Sorption equilibria of chlorinated anilines in aqueous solution on resin-bound cobalt ion*. Colloids and Surfaces a-Physicochemical and Engineering Aspects, 2002. **207**(1-3): p. 41-47.
27. Muller, L., E. Fattore, and E. Benfenati, *Determination of aromatic amines by solid-phase microextraction and gas chromatography mass spectrometry in water samples*. Journal of Chromatography A, 1997. **791**(1-2): p. 221-230.
28. Parris, G.E., *Covalent binding of aromatic-amines to humates .I. Reactions with carbonyls and quinones* Environmental Science & Technology, 1980. **14**(9): p. 1099-1106.
29. Park, J.W., et al., *Effect of humic constituents on the transformation of chlorinated phenols and anilines in the presence of oxidoreductive enzymes or birnessite*. Environmental Science & Technology, 1999. **33**(12): p. 2028-2034.
30. Flores-Cespedes, F., et al., *Cosorption study of organic pollutants and dissolved organic matter in a soil*. Environmental Pollution, 2006. **142**(3): p. 449-456.
31. Szczepanik, B., et al., *Adsorption of chloroanilines from aqueous solutions on the modified halloysite*. Applied Clay Science, 2014. **101**: p. 260-264.
32. Padmini, E. and L.R. Miranda, *Nanocatalyst from sol-sol doping of TiO₂ with Vanadium and Cerium and its application for 3,4 Dichloroaniline degradation using visible light*. Chemical Engineering Journal, 2013. **232**: p. 249-258.
33. Ormad, M.P., et al., *Pesticides removal in the process of drinking water production*. Chemosphere, 2008. **71**(1): p. 97-106.
34. Livingston, A.G. and A. Willacy, *Degradation of 3,4-dichloroaniline in synthetic and industrially produced wastewaters by mixed cultures freely suspended and immobilized in a packed-bed reactor* Applied Microbiology and Biotechnology, 1991. **35**(4): p. 551-557.
35. Bureau, E.C., *European Union Risk Assessment Report*. 2006.

36. Gülden, M., A. Turan, and H. Seibert, *Endocrinically active chemicals and their occurrence in surface waters: research report 10204279*. 1998.
37. Sorokin, N., et al., *Proposed EQS for Water Framework Directive Annex VIII substances: 3,4-dichloroaniline*. 2008.
38. Tomlin, C., *The Pesticide Manual, British Crop Protection Council, Surrey, UK (1999)*. 1999.
39. Hsu, T.S. and R. Bartha, *Hydrolyzable and nonhydrolyzable 3,4-dichloroaniline humus complexes and their respective rates of biodegradation* Journal of Agricultural and Food Chemistry, 1976. **24**(1): p. 118-122.
40. Pothuluri, J.V., J.A. Hinson, and C.E. Cerniglia, *Propanil - toxicological characteristics, metabolism, and biodegradation potential in soil* Journal of Environmental Quality, 1991. **20**(2): p. 330-347.
41. Cullington, J.E. and A. Walker, *Rapid biodegradation of diuron and other phenylurea herbicides by a soil bacterium*. Soil Biology & Biochemistry, 1999. **31**(5): p. 677-686.
42. Bartha, R. and D. Pramer, *Pesticide transformation to aniline and azo compounds in soil* Science, 1967. **156**(3782): p. 1617-&.
43. Roche, H., et al., *Rice fields regulate organochlorine pesticides and PCBs in lagoons of the Nature Reserve of Camargue*. Chemosphere, 2009. **75**(4): p. 526-533.
44. Di Corcia, A., et al., *Quantification of phenylurea herbicides and their free and humic acid-associated metabolites in natural waters*. Journal of Chromatography A, 1999. **852**(2): p. 465-474.
45. Gosetti, F., et al., *Sun light degradation of 4-chloroaniline in waters and its effect on toxicity. A high performance liquid chromatography – Diode array – Tandem mass spectrometry study*. Environmental Pollution, 2010. **158**(2): p. 592-598.
46. Loos, R., G. Hanke, and S.J. Eisenreich, *Multi-component analysis of polar water pollutants using sequential solid-phase extraction followed by LC-ESI-MS*. Journal of Environmental Monitoring, 2003. **5**(3): p. 384-394.
47. Norberg, J., A. Zander, and J.A. Jonsson, *Fully automated on-line supported liquid membrane liquid chromatographic determination of aniline derivatives in environmental waters*. Chromatographia, 1997. **46**(9-10): p. 483-488.
48. Ellappan, P. and L.R. Miranda, *Two-regime kinetic study and parameter optimization of degradation of 3,4-dichloroaniline using TI-N/S catalyst under visible light*. Desalination and Water Treatment, 2016. **57**(5): p. 2203-2216.
49. Corke, C.T. and F.R. Thompson, *Effects of some phenylamide herbicides and their degradation products on soil nitrification* Canadian Journal of Microbiology, 1970. **16**(7): p. 567-&.
50. Bearden, A.P. and T.W. Schultz, *Structure-activity relationships for Pimephales and Tetrahymena: A mechanism of action approach*. Environmental Toxicology and Chemistry, 1997. **16**(6): p. 1311-1317.
51. Argese, E., et al., *Assessment of chloroaniline toxicity by the submitochondrial particle assay*. Environmental Toxicology and Chemistry, 2001. **20**(4): p. 826-832.

52. Hooftman, R.N. and G.J. Vink, *The determination of toxic effects of pollutants with the marine polychaete worm ophryotrocha-diadema* Ecotoxicology and Environmental Safety, 1980. **4**(3): p. 252-262.
53. Adema, D.M. and I.G. Vink, *A comparative-study of the toxicity of 1,1,2-trichloroethane, dieldrin, pentachlorophenol and 3,4 dichloroaniline for marine and fresh-water organisms* Chemosphere, 1981. **10**(6): p. 533-554.
54. Crossland, N.O. and J.M. Hillaby, *Fate and effects of 3,4-dichloroaniline in the laboratory and in outdoor ponds .2. Chronic toxicity to daphnia spp and other invertebrates.* Environmental Toxicology and Chemistry, 1985. **4**(4): p. 489-499.
55. Allner, *Toxikokinetik von 3,4-Dichloranilin beim dreistachligen Stichling (Gasterosteus aculeatus) unter besonderer Berücksichtigung der Fortpflanzungsphysiologie.* 1997, Joannes Gutenberg Universitat.
56. Cook, J.C., et al., *Investigation of a mechanism for leydig-cell tumorigenesis by linuron in rats.* Toxicology and Applied Pharmacology, 1993. **119**(2): p. 195-204.
57. Brunsbach, F.R. and W. Reineke, *Degradation of chloroanilines in soil slurry by specialized organisms* Applied Microbiology and Biotechnology, 1993. **40**(2-3): p. 402-407.
58. Droulia, F.E., V. Kati, and C.N. Giannopolitis, *Sorption of 3,4-dichloroaniline on four contrasting Greek agricultural soils and the effect of liming.* Journal of Environmental Science and Health Part B-Pesticides Food Contaminants and Agricultural Wastes, 2011. **46**(5): p. 404-410.
59. Fava, L., et al., *Pesticide metabolites as contaminants of groundwater resources: assessment of the leaching potential of endosulfan sulfate, 2,6-dichlorobenzoic acid, 3,4-dichloroaniline, 2,4-dichlorophenol and 4-chloro-2-methylphenol.* Microchemical Journal, 2005. **79**(1-2): p. 207-211.
60. Wegman, R.C.C. and G.A.L. De Korte, *Aromatic amines in surface waters of The Netherlands.* Water Research, 1981. **15**(3): p. 391-394.
61. Claver, A., et al., *Study of the presence of pesticides in surface waters in the Ebro river basin (Spain).* Chemosphere, 2006. **64**(9): p. 1437-1443.
62. Gonzalez-Pradas, E., et al., *Effects of dissolved organic carbon on sorption of 3,4-dichloroaniline and 4-bromoaniline in a calcareous soil.* Chemosphere, 2005. **59**(5): p. 721-728.
63. Crossland, N.O., *A review of the fate and toxicity of 3,4-dichloroaniline in aquatic environments* Chemosphere, 1990. **21**(12): p. 1489-1497.
64. Beyerlepfnur, R. and J.P. Lay, *Adsorption and desorption of 3,4-dichloroaniline on soil* Chemosphere, 1990. **21**(9): p. 1087-1094.
65. Chemspider. 2015; Available from: <http://www.chemspider.com/Chemical-Structure.13860720.html>.
66. Bakhaeva, L.P., et al., *Microbial degradation of 3,4-dichloroaniline sorbed by activated carbon.* Microbiology, 2001. **70**(3): p. 277-284.
67. Süß, Z. *Pflanzenernähr. Bodenk*, 1978. **141**(57-66).
68. Reid, B.J., K.C. Jones, and K.T. Semple, *Bioavailability of persistent organic pollutants in soils and sediments - a perspective on mechanisms, consequences and assessment.* Environmental Pollution, 2000. **108**(1): p. 103-112.

69. Bengtsson, G., R. Lindqvist, and M.D. Piwoni, *Sorption of trace organics to colloidal clays, polymers, and bacteria* Soil Science Society of America Journal, 1993. **57**(5): p. 1261-1270.
70. Freitag, D., et al., *Long-term fate of 4-chloroaniline-c-14 in soil and plants under outdoor conditions - a contribution to terrestrial ecotoxicology of chemicals* Journal of Agricultural and Food Chemistry, 1984. **32**(2): p. 203-207.
71. Li, H. and L.S. Lee, *Sorption and abiotic transformation of aniline and alpha-naphthylamine by surface soils*. Environmental Science & Technology, 1999. **33**(11): p. 1864-1870.
72. Li, H., et al., *Effect of substitution on irreversible binding and transformation of aromatic amines with soils in aqueous systems*. Environmental Science & Technology, 2000. **34**(17): p. 3674-3680.
73. Corke, C.T., et al., *Diazonium cations as intermediates in the microbial transformation of chloroanilines to chlorinated biphenyls, azo-compounds, and triazines* Journal of Agricultural and Food Chemistry, 1979. **27**(3): p. 644-646.
74. Albers, C.N., et al., *Characterization and structural modelling of humic substances in field soil displaying significant differences from previously proposed structures*. European Journal of Soil Science, 2008. **59**(4): p. 693-705.
75. Stevenson, F.J., *Humus Chemistry: Genesis, Composition, Reactions*. 1994, New York: Wiley & Sons.
76. Weber, E.J., D.L. Spidle, and K.A. Thorn, *Covalent binding of aniline to humic substances .1. Kinetic studies*. Environmental Science & Technology, 1996. **30**(9): p. 2755-2763.
77. Weber, E.J., D. Colon, and G.L. Baughman, *Sediment-associated reactions of aromatic amines. 1. Elucidation of sorption mechanisms*. Environmental Science & Technology, 2001. **35**(12): p. 2470-2475.
78. Nagel, R., *Bioakkumulation und Verteilung von Umweltchemikalien in aquatischen Laborsystemen zur realitätsnahen Prognose der Umweltgefährlichkeit*, ed. U.F.-V. 10603106/01. 1997, Berlin.
79. Heim, K., I. Schuphan, and B. Schmidt, *Behavior of c-14 4-nitrophenol and c-14 3,4-dichloroaniline in lab sediment-water systems .1. Metabolic-fate and partitioning of radioactivity* Environmental Toxicology and Chemistry, 1994. **13**(6): p. 879-888.
80. Dunnivant, F.M., et al., *Cotransport of cadmium and hexachlorobiphenyl by dissolved organic-carbon through columns containing aquifer material* Environmental Science & Technology, 1992. **26**(2): p. 360-368.
81. Huang, X.J. and L.S. Lee, *Effects of dissolved organic matter from animal waste effluent on chlorpyrifos sorption by soils*. Journal of Environmental Quality, 2001. **30**(4): p. 1258-1265.
82. Li, K., B.S. Xing, and W.A. Torello, *Effect of organic fertilizers derived dissolved organic matter on pesticide sorption and leaching*. Environmental Pollution, 2005. **134**(2): p. 187-194.
83. Chiou, C.T., et al., *Water solubility enhancement of some organic pollutants and pesticides by dissolved humic and fulvic-acids* Environmental Science & Technology, 1986. **20**(5): p. 502-508.
84. Guo, L., et al., *Sorption and movement of alachlor in soil modified by carbon-rich wastes* Journal of Environmental Quality, 1993. **22**(1): p. 186-194.

85. Johnson, A.C., et al., *The potential of incorporated organic matter to reduce pesticide leaching*. Toxicological & Environmental Chemistry, 1997. **58**: p. 47-61.
86. Albers, C.N., et al., *Effect of Different Humic Substances on the Fate of Diuron and Its Main Metabolite 3,4-Dichloroaniline in Soil*. Environmental Science & Technology, 2008. **42**(23): p. 8687-8691.
87. Hsu, T.S. and R. Bartha, *Interaction of pesticide-derived chloroaniline residues with soil organic-matter* Soil Science, 1973. **116**(6): p. 444-452.
88. Saxena, A. and R. Bartha, *Microbial mineralization of humic-acid 3,4-dichloroaniline complexes* Soil Biology & Biochemistry, 1983. **15**(1): p. 59-62.
89. Giles, C.H., et al., *Studies in adsorption .11. A system of classification of solution adsorption isotherms, and its use in diagnosis of adsorption mechanisms and in measurement of specific surface areas of solids* Journal of the Chemical Society, 1960(OCT): p. 3973-3993.
90. Polati, S., et al., *Sorption and desorption behavior of chloroanilines and chlorophenols on montmorillonite and kaolinite*. Journal of Environmental Science and Health Part B-Pesticides Food Contaminants and Agricultural Wastes, 2006. **41**(6): p. 765-779.
91. Bouras, O., et al., *Adsorption of diuron and its degradation products from aqueous solution by surfactant-modified pillared clays*. Applied Clay Science, 2007. **37**(3-4): p. 240-250.
92. Hance, R.J., *Adsorption-desorption phenomena*, in *Interactions between Herbicides and the Soil*. 1980, Academic Press.
93. Sheng, G.Y., S.H. Xu, and S.A. Boyd, *Mechanism(s) controlling sorption of neutral organic contaminants by surfactant-derived and natural organic matter*. Environmental Science & Technology, 1996. **30**(5): p. 1553-1557.
94. Gonzalez-Pradas, E., et al., *Sorption and leaching of diuron on natural and peat-amended calcareous soil from Spain*. Water Research, 1998. **32**(9): p. 2814-2820.
95. Celis, R., E. Barriuso, and S. Houot, *Sorption and desorption of atrazine by sludge-amended soil: Dissolved organic matter effects*. Journal of Environmental Quality, 1998. **27**(6): p. 1348-1356.
96. Nelson, S.D., et al., *Stability and mobility of napropamide complexed with dissolved organic matter in soil columns*. Journal of Environmental Quality, 2000. **29**(6): p. 1856-1862.
97. Lee, D.Y. and W.J. Farmer, *Dissolved organic matter interaction with napropamide and four other nonionic pesticides*. Journal of Environmental Quality, 1989. **18**: p. 468-474.
98. Graber, E.R., et al., *Enhanced transport of atrazine under irrigation with effluent (vol 59, pg 1513, 1995)*. Soil Science Society of America Journal, 1996. **60**(2): p. 424-424.
99. Totsche, K.U., J. Danzer, and I. KogelKnabner, *Dissolved organic matter-enhanced retention of polycyclic aromatic hydrocarbons in soil miscible displacement experiments*. Journal of Environmental Quality, 1997. **26**(4): p. 1090-1100.

100. Huguenot, D., et al., *Selection of low cost materials for the sorption of copper and herbicides as single or mixed compounds in increasing complexity matrices*. Journal of Hazardous Materials, 2010. **182**(1-3): p. 18-26.
101. Igunnu, E.T. and G.Z. Chen, *Produced water treatment technologies*. International Journal of Low Carbon Technologies, 2012.
102. Ahmadun, F.R., et al., *Review of technologies for oil and gas produced water treatment*. Journal of Hazardous Materials, 2009. **170**(2-3): p. 530-551.
103. Chowdhury, W.E.a.R.K., ed. *Water treatment*. Vol. 1. 2013, InTech. 392.
104. Bakke, T., J. Klungsoyr, and S. Sanni, *Environmental impacts of produced water and drilling waste discharges from the Norwegian offshore petroleum industry*. Marine Environmental Research, 2013. **92**: p. 154-169.
105. Hale, S.E., et al., *The role of passive sampling in monitoring the environmental impacts of produced water discharges from the Norwegian oil and gas industry*. Marine Pollution Bulletin, 2016. **111**(1-2): p. 33-40.
106. OSPAR. *Joint Assessment & Monitoring Programme (JAMP) 2014*; Available from: <http://www.ospar.org/work-areas/cross-cutting-issues/jamp>.
107. Union, T.E.p.a.t.c.o.t.E., *EU Marine Strategy Framework Directive (MSFD)*, in 2008/56/EC, O.J.o.t.E. Communities, Editor. 2008.
108. Union, E.P.a.C.o.t.E., *Water framework directive 2000/60/EC*, in 2000/60/EC, O.J.o.t.E. Communities, Editor. 2000.
109. Group, N.T., *Introduction to Produced Water Treatment*. Nature Technology Solutions, 2005: p. 2-18.
110. GOV.UK. *Oil and gas: field data*. 2014; Available from: <https://www.gov.uk/oil-and-gas-uk-field-data#oil-discharged-with-produced-water>.
111. Lyons, C.D., S.E. Katz, and R. Bartha, *Persistence and mutagenic potential of herbicide-derived aniline residues in pond water* Bulletin of Environmental Contamination and Toxicology, 1985. **35**(5): p. 696-703.
112. CITI, *Data of existing chemicals based on the CSCL Japan*. 1992. **10-26**: p. 32,33.
113. Kuiper, J. and A.O. Hanstveit, *Fate and effects of 3,4-dichloroaniline (dca) in marine plankton communities in experimental enclosures* Ecotoxicology and Environmental Safety, 1984. **8**(1): p. 34-54.
114. Bayer, A., *Internal examination on the biological degradation of 2,4-, 2,5- and 3,4-dichloroaniline in samples of Rhine-water*. 1992.
115. Struijs, J. and J.E. Rogers, *Reductive dehalogenation of dichloroanilines by anaerobic microorganisms in fresh and dichlorophenol-acclimated pond sediment* Applied and Environmental Microbiology, 1989. **55**(10): p. 2527-2531.
116. Loidl, M., et al., *Degradation of aniline and monochlorinated anilines by soil-born pseudomonas-acidovorans strains* Archives of Microbiology, 1990. **155**(1): p. 56-61.
117. Latorre, J., W. Reineke, and H.J. Knackmuss, *Microbial-metabolism of chloroanilines - enhanced evolution by natural genetic exchange* Archives of Microbiology, 1984. **140**(2-3): p. 159-165.

118. Kim, Y.-M., et al., *Isolation and characterization of 3,4-dichloroaniline degrading bacteria*. Korean Journal of Microbiology and Biotechnology, 2007. **35**(3): p. 245-249.
119. Travkin, V.M., et al., *Degradation of 3,4-dichloro- and 3,4-difluoroaniline by Pseudomonas fluorescens 26-K*. Journal of Environmental Science and Health Part B-Pesticides Food Contaminants and Agricultural Wastes, 2003. **38**(2): p. 121-132.
120. Surovtseva, E.G., et al., *Chlorinated anilines as a source of carbon nitrogen and energy for pseudomonas-diminuta* Mikrobiologiya, 1985. **54**(6): p. 948-952.
121. Sergeeva, N.R., M.S. Sokolov, and G.K. Vasil'eva, *Using bacteria to accelerate the decomposition of 3,4-dichloroaniline in fish ponds*. Agrokhimiya, 1998. **0**(4): p. 84-90.
122. Martinez Viera, R., M.M. Alfonso Hernandez, and R.F. Castaneda Ruiz, *Decomposition of 3 4 dichloroaniline by microorganisms from two cuban soils* Ciencias de la Agricultura, 1984(20): p. 117-124.
123. Wasserfallen, A., J. Zeyer, and K.N. Timmis, *Bacterial metabolism and toxicity of halogenated anilines* Experientia, 1986. **42**(1): p. 106-106.
124. Sharma, P., et al., *Efficient biotransformation of herbicide diuron by bacterial strain Micrococcus sp. PS-1*. Biodegradation, 2010. **21**(6): p. 979-987.
125. Devers-Lamrani, M., et al., *Evidence for cooperative mineralization of diuron by Arthrobacter sp. BS2 and Achromobacter sp. SPI isolated from a mixed culture enriched from diuron exposed environments*. Chemosphere, 2014. **117**: p. 208-215.
126. Surovtseva, E.G., et al., *Degradation of chlorinated anilines by certain representatives of the genera Aquaspirillum and Paracoccus*. Microbiology, 1996. **65**(5): p. 553-559.
127. Vasilyeva, G.K., L.P. Bakhaeva, and E.G. Surovtseva, *The Use of In Situ Soil Adsorptive Bioremediation Following an Accidental Spill of Propanide in the Krasnodar Region of Russia*. Land Contam. Reclam., 1996. **4**: p. 263-268.
128. Carvalho, G., et al., *Biological treatment of propanil and 3,4-dichloroaniline: Kinetic and microbiological characterisation*. Water Research, 2010. **44**(17): p. 4980-4991.
129. Emmanuel Herrera-Gonzalez, V., et al., *Biodegradation of the herbicide propanil, and its 3,4-dichloroaniline by-product in a continuously operated biofilm reactor*. World Journal of Microbiology & Biotechnology, 2013. **29**(3): p. 467-474.
130. Yih, R.Y., D.H. McRae, and H. Wilson, *Science*. Vol. 161. 1968, Washington D.C.
131. Still, G., *Science*. Vol. 159. 1968, Washington D.C.
132. Fuchsbichler, G., A. Suss, and P. Wallnofer, *Uptake of 4-chloro-chloraniline and 3,4-dichloroaniline by cultivated plants* Zeitschrift Fur Pflanzenkrankheiten Und Pflanzenschutz-Journal of Plant Diseases and Protection, 1978. **85**(5): p. 298-307.
133. Arjmand, M. and H. Sandermann, *Mineralization of chloroaniline lignin conjugates and of free chloroanilines by the white rot fungus phanerochaete-chrysosporium* Journal of Agricultural and Food Chemistry, 1985. **33**(6): p. 1055-1060.

134. Pieper, D.H., R. Winkler, and H. Sandermann, *Formation of a toxic dimerization product of 3,4-dichloroaniline by lignin peroxidase from phanerochaete-chrysosporium* *Angewandte Chemie-International Edition in English*, 1992. **31**(1): p. 68-70.
135. Pavlovic, I., et al., *Adsorption of acidic pesticides 2,4-D, Clopyralid and Picloram on calcined hydrotalcite*. *Applied Clay Science*, 2005. **30**(2): p. 125-133.
136. Joo, S.H., et al., *Quantification of the oxidizing capacity of nanoparticulate zero-valent iron*. *Environmental Science & Technology*, 2005. **39**(5): p. 1263-1268.
137. Cabrera, L.C., et al., *Degradation of Herbicide Diuron in Water Employing the Fe-0/H₂O₂ System*. *Journal of the Brazilian Chemical Society*, 2010. **21**(12): p. 2347-2352.
138. Willberg, D.M., et al., *Degradation of 4-chlorophenol, 3,4-dichloroaniline, and 2,4,6-trinitrotoluene in an electrohydraulic discharge reactor*. *Environmental Science & Technology*, 1996. **30**(8): p. 2526-2534.
139. Lodha, S., et al., *Photocatalytic degradation of Phenol Red using complexes of some transition metals and hydrogen peroxide*. *Journal of the Serbian Chemical Society*, 2008. **73**(6): p. 631-639.
140. Feng, J., et al., *Degradation of aqueous 3,4-dichloroaniline by a novel dielectric barrier discharge plasma reactor*. *Environmental Science and Pollution Research*, 2015. **22**(6): p. 4447-4459.
141. Haag, W.R. and C.C.D. Yao, *Rate constants for reaction of hydroxyl radicals with several drinking-water contaminants* *Environmental Science & Technology*, 1992. **26**(5): p. 1005-1013.
142. Feng, J.-w., et al., *Degradation of aqueous 3, 4-dichloroaniline by wire-cylinder dielectric barrier discharge reactor*, in *Advances in Environmental Science and Engineering, Pts 1-6*, R. Iranpour, et al., Editors. 2012. p. 1729-1732.
143. Judd, S., et al., *The size and performance of offshore produced water oil-removal technologies for reinjection*. *Separation and Purification Technology*, 2014. **134**: p. 241-246.
144. Srinivasan, A. and T. Viraraghavan, *Removal of oil by walnut shell media*. *Bioresource Technology*, 2008. **99**(17): p. 8217-8220.
145. Srinivasan, A. and T. Viraraghavan, *Oil removal from water using biomaterials*. *Bioresource Technology*, 2010. **101**(17): p. 6594-6600.
146. Stevenson, J., *Organoclay absorption media excels in produced water polishing*. *Filtration + Separation*, 2012. **49**(1): p. 30-31.
147. Dejak, M. *Spectrum™ Micro Media Filters* http://eco-tec.com/wp-content/uploads/2013/04/Spectrum-Next_Generation_Filtration.pdf. Available from: http://eco-tec.com/wp-content/uploads/2013/04/Spectrum-Next_Generation_Filtration.pdf.
148. Younker, J.M. and M.E. Walsh, *Bench-scale investigation of an integrated adsorption-coagulation-dissolved air flotation process for produced water treatment*. *Journal of Environmental Chemical Engineering*, 2014. **2**(1): p. 692-697.
149. Plebon, M.J., et al., *De-oiling of produced water from offshore oil platforms using a recent commercialized technology which combines adsorption,*

- coalescence and gravity separation*, in *Proceedings of the Sixteenth*, J.S. Chung, et al., Editors. 2006. p. 503-507.
150. Veolia®. *MPPE technologies*. Available from: <http://technomaps.veoliawatertechnologies.com/mppe/en/technology.htm>.
 151. *Preliminary Studies on the Application of Ceramic Membranes for Oilfield Produced Water Management*. 2013.
 152. Alzahrani, S. and A.W. Mohammad, *Challenges and trends in membrane technology implementation for produced water treatment: A review*. Journal of Water Process Engineering, 2014. **4**(0): p. 107-133.
 153. Rangarajan T. Duraisamy, A.H.B.a.A.H., *State of the Art Treatment of Produced Water*, in *Water treatment*, W.E.a.R.K. Chowdhury, Editor. 2013.
 154. Zhang, M., et al., *Effects of hydrophilicity/hydrophobicity of membrane on membrane fouling in a submerged membrane bioreactor*. Bioresource Technology, 2015. **175**: p. 59-67.
 155. Maguire-Boyle, S.J. and A.R. Barron, *A new functionalization strategy for oil/water separation membranes*. Journal of Membrane Science, 2011. **382**(1-2): p. 107-115.
 156. Li, Y.S., et al., *Treatment of oily wastewater by organic-inorganic composite tubular ultrafiltration (UF) membranes*. Desalination, 2006. **196**(1-3): p. 76-83.
 157. Duong, P.H.H. and T.-S. Chung, *Application of thin film composite membranes with forward osmosis technology for the separation of emulsified oil–water*. Journal of Membrane Science, 2014. **452**(0): p. 117-126.
 158. Mi, B.X. and M. Elimelech, *Organic fouling of forward osmosis membranes: Fouling reversibility and cleaning without chemical reagents*. Journal of Membrane Science, 2010. **348**(1-2): p. 337-345.
 159. Cui, J.Y., et al., *Preparation and application of zeolite/ceramic microfiltration membranes for treatment of oil contaminated water*. Journal of Membrane Science, 2008. **325**(1): p. 420-426.
 160. Wen, Q., et al., *Zeolite-coated mesh film for efficient oil-water separation*. Chemical Science, 2013. **4**(2): p. 591-595.
 161. Abousnina, R.M. and L.D. Nghiem, *Removal of dissolved organics from produced water by forward osmosis*. Desalination and Water Treatment, 2014. **52**(4-6): p. 570-579.
 162. Phuntsho, S., et al., *A novel low energy fertilizer driven forward osmosis desalination for direct fertigation: Evaluating the performance of fertilizer draw solutions*. Journal of Membrane Science, 2011. **375**(1-2): p. 172-181.
 163. Motta, A., et al., *Oil Produced Water treatment for oil removal by an integration of coalescer bed and microfiltration membrane processes*. Journal of Membrane Science, 2014. **469**(0): p. 371-378.
 164. Abbasi, M., et al., *Integrated membrane pilot plant for refinery wastewater treatment in order to produce boiler feedwater*. Desalination and Water Treatment, 2013. **51**(13-15): p. 2543-2553.
 165. Xue, Z., et al., *Special wettable materials for oil/water separation*. Journal of Materials Chemistry A, 2014. **2**(8): p. 2445-2460.
 166. Howarter, J.A. and J.P. Youngblood, *Amphiphile grafted membranes for the separation of oil-in-water dispersions*. Journal of Colloid and Interface Science, 2009. **329**(1): p. 127-132.

167. Yang, J., et al., *Superhydrophilic-superoleophobic coatings*. Journal of Materials Chemistry, 2012. **22**(7): p. 2834-2837.
168. Zhang, L.B., Z.H. Zhang, and P. Wang, *Smart surfaces with switchable superoleophilicity and superoleophobicity in aqueous media: toward controllable oil/water separation*. Npg Asia Materials, 2012. **4**.
169. Kota, A.K., G. Kwon, and A. Tuteja, *The design and applications of superomniphobic surfaces*. Npg Asia Materials, 2014. **6**.
170. Kwon, G., et al., *On-Demand Separation of Oil-Water Mixtures*. Advanced Materials, 2012. **24**(27): p. 3666-3671.
171. Malato, S., et al., *Enhancement of the rate of solar photocatalytic mineralization of organic pollutants by inorganic oxidizing species*. Applied Catalysis B-Environmental, 1998. **17**(4): p. 347-356.
172. Adams, M., I. Campbell, and P.K.J. Robertson, *Novel Photocatalytic Reactor Development for Removal of Hydrocarbons from Water*. International Journal of Photoenergy, 2008.
173. Rouquerol, F., et al., *1 - Introduction*, in *Adsorption by Powders and Porous Solids (Second Edition)*. 2014, Academic Press: Oxford. p. 1-24.
174. Maurin, G., *Modelling of Physisorption in Porous Solids*, in *Adsorption by Powders and Porous Solids (Second Edition)*. 2014, Academic Press: Oxford. p. 191-235.
175. Rouquerol, J., et al., *RECOMMENDATIONS FOR THE CHARACTERIZATION OF POROUS SOLIDS*. Pure and Applied Chemistry, 1994. **66**(8): p. 1739-1758.
176. Humpola, P.D., et al., *Thermodynamic analysis of adsorption models of phenol in liquid phase on different activated carbons*. Journal of the Chilean Chemical Society, 2013. **58**(1): p. 1541-1544.
177. Brunauer, S., P.H. Emmett, and E. Teller, *Adsorption of Gases in Multimolecular Layers*. Journal of the American Chemical Society, 1938. **60**(2): p. 309-319.
178. Gregg, S.J. and K.S.W. Sing, *Adsorption, surface area, and porosity*. 1982, London: Academic Press.
179. Thommes, M., et al., *Physisorption of gases, with special reference to the evaluation of surface area and pore size distribution (IUPAC Technical Report)*. Pure and Applied Chemistry, 2015. **87**(9-10): p. 1051-1069.
180. Sing, K.S.W., *7 - Assessment of Surface Area by Gas Adsorption*, in *Adsorption by Powders and Porous Solids (Second Edition)*. 2014, Academic Press: Oxford. p. 237-268.
181. Dubinin, M.M. and V.A. Astakhov, *Development of the concepts of volume filling of micropores in the adsorption of gases and vapors by microporous adsorbents*. Bulletin of the Academy of Sciences of the USSR, Division of chemical science, 1971. **20**(1): p. 3-7.
182. STOECKLI, F., et al., *Extension of Dubinin's theory to adsorption from aqueous solutions*, in *Recent advances in Adsorption Processes for Environmental protection and Security*. 2006, Springer.
183. Woodruff, D.P., *The Chemical Physics of Solid Surfaces*. 2007.
184. Bonn, D., et al., *Wetting and spreading*. Reviews of Modern Physics, 2009. **81**(2): p. 739-805.

185. Kern, K.D., R; Palmer, R L; Cosma, G, *Complete Wetting on 'Strong' Substrates: Xe/Pt(111)*. Physical Review Letters, 1986. **56**: p. 2823–2826.
186. Sing, K.S.W., *Adsorption by active carbons*, in *Adsorption by Powders and Porous Solids (Second Edition)*. 2014, Academic Press: Oxford.
187. Velasco, L.F. and C.O. Ania, *Understanding phenol adsorption mechanisms on activated carbons*. Adsorption, 2011. **17**(1): p. 247-254.
188. Derylo-Marczewska, A., et al., *Studies of adsorption equilibria and kinetics of o-, m-, p-nitro- and chlorophenols on microporous carbons from aqueous solutions*. Adsorption, 2010. **16**(4): p. 359-375.
189. Stoeckli, F., M.V. Lopez-Ramon, and C. Moreno-Castilla, *Adsorption of phenolic compounds from aqueous solutions, by activated carbons, described by the Dubinin-Astakhov equation*. Langmuir, 2001. **17**(11): p. 3301-3306.
190. C. Moreno-Castillo, M.A.F.-C., M.A. Alvarez-Merino, M.V. Lopez-Ramon, F. Carrasco-Marin, Adsorption, 2011. **17**: p. 413.
191. F. Zeinali, A.A.G. and G.N. , *Adsorption of Volatile Organic Compounds from Aqueous Solution*
by Granular Activated Carbon (GAC) in Batch System. Iranian Journal of Chemical Engineering, 2011. **8**.
192. Simpson, E.J., et al., *Sorption Equilibrium Isotherms for Volatile Organics in Aqueous-Solution - Comparison of Headspace Gas-Chromatography and Online Uv Stirred Cell Results*. Industrial & Engineering Chemistry Research, 1993. **32**(10): p. 2269-2276.
193. H. Sontheimer, J.C.C., R. Scott Summers, *Activated carbon for water treatment*. 1988, Karlsruhe, Germany : DVGW-Forschungsstelle, Engler-Bunte-Institut, Universitat Karlsruhe (TH).
194. Bansal, R.C., J.-B. Donnet, and F. Stoeckli, *Active Carbon*. 1988, New York.
195. IHRD. *The role of clays and shales in low resistivity log response*. Available from: https://www.ihrdc.com/els/ipims-demo/t26/offline_IPIMS_s23560/resources/data/G4105.htm.
196. Ho, Y.S. and G. McKay, *The kinetics of sorption of basic dyes from aqueous solution by sphagnum moss peat*. Canadian Journal of Chemical Engineering, 1998. **76**(4): p. 822-827.
197. Meier, L.P., R. Nueesch, and F.T. Madsen, *Organic Pillared Clays*. Journal of Colloid and Interface Science, 2001. **238**(1): p. 24-32.
198. Croissant, J.G., et al., *Syntheses and applications of periodic mesoporous organosilica nanoparticles*. Nanoscale, 2015. **7**(48): p. 20318-20334.
199. Ma, X.B., et al., *Hollow periodic mesoporous organosilica nanospheres by a facile emulsion approach*. Journal of Colloid and Interface Science, 2016. **475**: p. 66-71.
200. Moura, C.P., et al., *Adsorption of BTX (benzene, toluene, o-xylene, and p-xylene) from aqueous solutions by modified periodic mesoporous organosilica*. Journal of Colloid and Interface Science, 2011. **363**(2): p. 626-634.
201. Cooney, D.O., *Adsorption Design for Wasterwater Treatment*. 1999, London: Lewis Publishers

202. Febrianto, J., et al., *Equilibrium and kinetic studies in adsorption of heavy metals using biosorbent: A summary of recent studies*. Journal of Hazardous Materials, 2009. **162**(2-3): p. 616-645.
203. Maretto, M., et al., *Microporous and mesoporous materials for the treatment of wastewater produced by petrochemical activities*. Journal of Cleaner Production, 2014. **77**: p. 22-34.
204. Carati, A., et al., *Preparation and characterisation of mesoporous silica-alumina and silica-titania with a narrow pore size distribution*. Catalysis Today, 2003. **77**(4): p. 315-323.
205. Lee, J.W., et al., *Adsorption of chlorinated volatile organic compounds on MCM-48*. Journal of Chemical and Engineering Data, 2003. **48**(2): p. 381-387.
206. Germanus, A., et al., *INTRACRYSTALLINE SELF-DIFFUSION OF BENZENE, TOLUENE AND XYLENE ISOMERS IN ZEOLITES NA-X*. Zeolites, 1985. **5**(2): p. 91-95.
207. Wang, J., et al., *Fast and one-pot synthesis of silica aerogels via a quasi-solvent-exchange-free ambient pressure drying process*. Microporous and Mesoporous Materials, 2015. **218**: p. 192-198.
208. Husing, N., et al., *Formation and structure of porous gel networks from Si(OMe)(4) in the presence of A(CH₂)_nSi(OR)(3) (A = functional group)*. Chemistry of Materials, 1998. **10**(10): p. 3024-3032.
209. Bernik, D.L., *Silicon Based Materials for Drug Delivery Devices and Implants*. Recent Patents on Nanotechnology, 2007. **1**(3): p. 186-192.
210. Gurav, J.L., et al., *Silica Aerogel: Synthesis and Applications*. Journal of Nanomaterials, 2010.
211. Alain C.Pierre, A.R., *SiO₂ aerogels* in *Aerogels Handbook*, M.A. Aegerter, Leventis, N. K., Matthias M. , Editor. 2011.
212. Wang, D., et al., *Adsorption of oils from pure liquid and oil-water emulsion on hydrophobic silica aerogels*. Separation and Purification Technology, 2012. **99**: p. 28-35.
213. Reynolds, J.G., P.R. Coronado, and L.W. Hrubesh, *Hydrophobic aerogels for oil-spill clean up – synthesis and characterization*. Journal of Non-Crystalline Solids, 2001. **292**(1–3): p. 127-137.
214. Adebajo, M.O., et al., *Porous Materials for Oil Spill Cleanup: A Review of Synthesis and Absorbing Properties*. Journal of Porous Materials, 2003. **10**(3): p. 159-170.
215. Olalekan, A.P., A.O. Dada, and O.A. Adesina, *Review: Silica Aerogel as a Viable Absorbent for Oil Spill Remediation*. Journal of Encapsulation and Adsorption Sciences, 2014. **4**: p. 122-131.
216. Hrubesh, L.W., P.R. Coronado, and J.H. Satcher, *Solvent removal from water with hydrophobic aerogels*. Journal of Non-Crystalline Solids, 2001. **285**(1–3): p. 328-332.
217. Wang, D., et al., *Adsorption of Organic Compounds in Vapor, Liquid, and Aqueous Solution Phases on Hydrophobic Aerogels*. Industrial & Engineering Chemistry Research, 2011. **50**(21): p. 12177-12185.
218. Standeker, S., Z. Novak, and Z. Knez, *Adsorption of toxic organic compounds from water with hydrophobic silica aerogels*. Journal of Colloid and Interface Science, 2007. **310**(2): p. 362-368.

219. Perdigoto, M.L.N., et al., *Application of hydrophobic silica based aerogels and xerogels for removal of toxic organic compounds from aqueous solutions*. Journal of Colloid and Interface Science, 2012. **380**(1): p. 134-140.
220. Tang, Q. and T. Wang, *Preparation of silica aerogel from rice hull ash by supercritical carbon dioxide drying*. Journal of Supercritical Fluids, 2005. **35**(1): p. 91-94.
221. Li, T. and T. Wang, *Preparation of silica aerogel from rice hull ash by drying at atmospheric pressure*. Materials Chemistry and Physics, 2008. **112**(2): p. 398-401.
222. Tadjarodi, A., M. Haghverdi, and V. Mohammadi, *Preparation and characterization of nano-porous silica aerogel from rice husk ash by drying at atmospheric pressure*. Materials Research Bulletin, 2012. **47**(9): p. 2584-2589.
223. Venkateswara Rao, A., et al., *Sodium Silicate Based Aerogels via Ambient Pressure Drying*
- in *Aerogels Handbook*, M.A. Aegerter, Leventis, N. K., Matthias M. , Editor. 2011.
224. Chanda, M., O'Driscoll, and G.L. Rempel, *Reactive Polymers*. 1984
225. Davankov, V.A., J.D. Navratil, and H.F. Walton, *Ligand Exchange Chromatography*. 1988, US: CRC Press.
226. Chang, Q.G., et al., *Efficient micro carbon column rapid breakthrough technique for water and wastewater treatability studies*. Environmental Progress, 2007. **26**(3): p. 280-288.
227. *Standard Practice for the Prediction of Contaminant Adsorption On GAC In Aqueous Systems Using Rapid Small-Scale Column Tests*.
228. Crittenden, J.C., et al., *PREDICTING GAC PERFORMANCE WITH RAPID SMALL-SCALE COLUMN TESTS*. Journal American Water Works Association, 1991. **83**(1): p. 77-87.
229. Lawrence K. Wang, Y.-T.H., Nazih K. Shammam, *Psicochemical Treatment Processes*. 2007, Springer Science & Business Media.
230. Economou, A., *Sequential-injection analysis (SIA): A useful tool for on-line sample-handling and pre-treatment*. TrAC Trends in Analytical Chemistry, 2005. **24**(5): p. 416-425.
231. Robinson, D., *Oil and gas: Treatment and discharge of produced waters offshore*. Filtration + Separation, 2013. **50**(2): p. 20-23.
232. Twumasi Afriyie, E., et al., *Textural and thermal conductivity properties of a low density mesoporous silica material*. Energy and Buildings, 2014. **75**: p. 210-215.
233. Twumasi Afriyie, E., et al., *Preparation and Characterization of Double Metal-Silica Sorbent for Gas Filtration*. Adsorption, 2013. **19**(1): p. 49-61.
234. Barrett, E.P., L.G. Joyner, and P.P. Halenda, *The determination of pore volume and area distributions in porous substances .1. Computations from nitrogen isotherms*. Journal of the American Chemical Society, 1951. **73**(1): p. 373-380.
235. Seymour Lowell, J.E.S., Martin A. Thomas, Matthias Thommes, *Characterization of Porous Solids and Powders: Surface Area, Pore Size and Density*. 2004.
236. Lippens, B.C. and J.H. De Boer, *Studies on pore systems in catalysts: V. The t method*. Journal of Catalysis, 1965. **4**(3): p. 319-323.

237. de Boer, J.H., et al., *The t-curve of multimolecular N₂-adsorption*. Journal of Colloid and Interface Science, 1966. **21**(4): p. 405-414.
238. Galarneau, A., et al., *Validity of the t-plot Method to Assess Microporosity in Hierarchical Micro/Mesoporous Materials*. Langmuir, 2014. **30**(44): p. 13266-13274.
239. Heckel, B. *Classic Michelson Interferometer*
- Available from:
<https://www.learner.org/courses/physics/visual/visual.html?shortname=michelson>
240. Instruments, N. *SEM technology*. Available from:
<http://www.nanoscience.com/technology/sem-technology/>.
241. University, S.H. *Gas Chromatography*. Available from:
<http://teaching.shu.ac.uk/hwb/chemistry/tutorials/chrom/gaschrom.htm>.
242. Shewale, P.M., et al., *Synthesis and characterization of low density and hydrophobic silica aerogels dried at ambient pressure using sodium silicate precursor*. Journal of Porous Materials, 2009. **16**(1): p. 101-108.
243. Biggs, M.J., A. Buts, and D. Williamson, *Absolute assessment of adsorption-based porous solid characterization methods: Comparison methods*. Langmuir, 2004. **20**(17): p. 7123-7138.
244. El Rassy, H. and A.C. Pierre, *NMR and IR spectroscopy of silica aerogels with different hydrophobic characteristics*. Journal of Non-Crystalline Solids, 2005. **351**(19–20): p. 1603-1610.
245. Freundlich, H. and H. Hatfield, *Colloid and Capillary Chemistry*. 1926, London: Methuen.
246. Jiang, J.-Q., C. Cooper, and S. Ouki, *Comparison of modified montmorillonite adsorbents: Part I: preparation, characterization and phenol adsorption*. Chemosphere, 2002. **47**(7): p. 711-716.
247. Stephen, H. and T. Stephen, *Solubilities of Inorganic and Organic Compounds*. Vol. 1. 1963, New York: Macmillan.
248. Scientific, R. *Vacuum filtration system*. 2017; Available from:
<http://www.rocker.com.tw/product-1.asp?ser=Laboratory%20Filtration>.
249. Shi, H.-x., et al., *Preparation of Silica Aerogel and Its Adsorption Performance to Organic Molecule*. Advances in Materials Science and Engineering, 2014. **2014**.
250. Love, A., M.L. Hanna, and J.G. Reynolds, *Engineering surface functional groups on silica aerogel for enhanced cleanup of organics from produced water*. Separation Science and Technology, 2003. **40**: p. 311-320.
251. OECD, *OECD guidelines for testing of chemicals*. 1992.
252. Malandrino, M., et al., *Adsorption of heavy metals on vermiculite: Influence of pH and organic ligands*. Journal of Colloid and Interface Science, 2006. **299**(2): p. 537-546.
253. Ambrus, Z., et al., *Low temperature synthesis, characterization and substrate-dependent photocatalytic activity of nanocrystalline TiO₂ with tailor-made rutile to anatase ratio*. Applied Catalysis A: General, 2008. **340**(2): p. 153-161.

254. Reynolds, J.G., P.R. Coronado, and L.W. Hrubesh, *Hydrophobic aerogels for oil-spill cleanup - Intrinsic absorbing properties*. Energy Sources, 2001. **23**(9): p. 831-843.
255. Tasca, A.L., F. Ghajeri, and A.J. Fletcher, *Novel hydrophilic and hydrophobic amorphous silica: Characterization and adsorption of aqueous phase organic compounds*. Adsorption Science & Technology, 2017.
256. Rodríguez, R., et al., *Strategies for automating solid-phase extraction and liquid-liquid extraction in radiochemical analysis*. TrAC Trends in Analytical Chemistry, 2016. **76**: p. 145-152.
257. Turiel, E., C. Perez-Conde, and A. Martin-Esteban, *Assessment of the cross-reactivity and binding sites characterisation of a propazine-imprinted polymer using the Langmuir-Freundlich isotherm*. Analyst, 2003. **128**(2): p. 137-141.